

National Institute of Materials Physics

---

(Institutul Național de Cercetare-Dezvoltare pentru Fizica Materialelor)

# National Institute of Materials Physics

---

(Institutul Național de Cercetare-Dezvoltare pentru Fizica Materialelor)

## DIRECTORATE

Director: Dr. Ionut Enculescu

Scientific Director: Dr. Florin Vasiliu

## ADDRESS

P.O. BOX MG – 7

Bucharest – Magurele / ROMANIA

Tel. (+4) 021 369 01 85

Fax (+4) 021 369 01 77

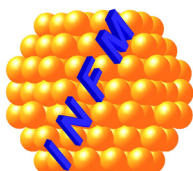
## E-Mail

I. Enculescu: [encu@infim.ro](mailto:encu@infim.ro)

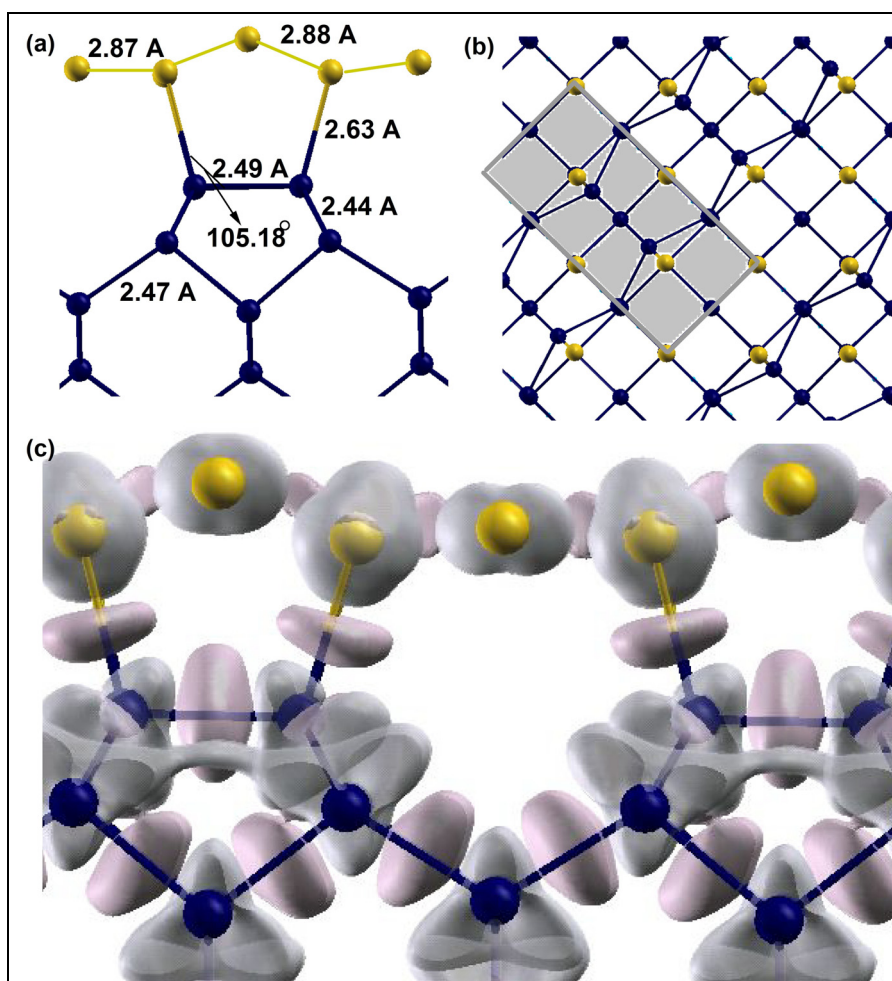
F. Vasiliu: [fvasiliu@infim.ro](mailto:fvasiliu@infim.ro)

## WWW

[http: // www.infim.ro](http://www.infim.ro)



# NATIONAL INSTITUTE OF MATERIALS PHYSICS



## ANNUAL REPORT 2013

---

## Contents

Preface . . . . .	5
Laboratories . . . . .	7
Personnel . . . . .	13
List of Personnel . . . . .	14
Visiting Guests . . . . .	21
Ph. D. Theses . . . . .	23
Awards . . . . .	24
Honorary Membership . . . . .	25
Publications and Presentations . . . . .	27
Books . . . . .	28
Journals . . . . .	29
Conference Proceedings . . . . .	45
Contributed Presentations . . . . .	50
Invited Lectures . . . . .	67
Selected Results . . . . .	71
Condensed Matter Physics at Mesoscale . . . . .	71
Nanoscale Physics . . . . .	105
Potential Applications . . . . .	125
Patents and Patent Requests . . . . .	141
Events . . . . .	143
International Cooperation . . . . .	147
Funding . . . . .	155

**Cover image:** *Side view of the Au-covered Ge(001) surface (a); the top view of the relaxed structure (b); the deformation density isosurface of the relaxed Au-covered Ge(001) surface(c).*  
[D.G. Popescu, M.A. Husanu, *Phys. Status Solidi – Rapid Res. Lett.* 7, 274 (2013)]

---

## PREFACE

In the year 2013, National Institute for Materials Physics (NIMP) has published 168 papers in ISI journals which correspond to a cumulated impact factor of 361,73 which is a similar figure as compared to the previous year. We must mention that in next couple of months, some other publications will be added at this record (taking into account some delayed journal issues) and also that now other 19 papers are already published or accepted for 2014.

The cumulated impact factors obtained by NIMP in last three years prove the consolidation of the scientific performance especially by comparison with years 2009, 2010 when the impact factor was roughly half from the nowadays value.

A very important observation is related to the recent tendency of our researchers to publish in journals having an increased impact factor. Thus, in Fig. 1, an impact factor distribution for papers published by NIMP researchers between 2009-2013 is shown. As compared to the years 2010, 2011, an increase of about 25% of papers published in journals with  $FI > 3$  can be observed. Moreover, if we consider the papers published in journals with  $4 < FI < 8$ , an increase of four times is registered as compared to 2010 and of 50% to the previous year. Therefore, in spite a slight reduction of paper number, their quality is on constant rise.

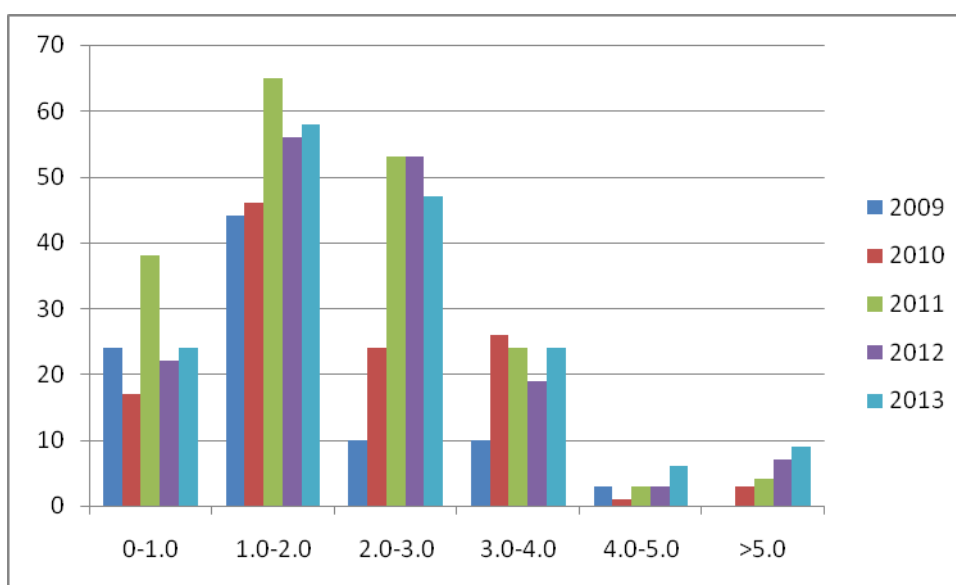


Fig. 1

---

The cummulated AIS values have for the last three years values between 100-120 whereas the percentage of papers having as first or corresponding author a researcher from our institute can vary between 65-75%.

The number of citations in ISI journals in 2013 reached about 2760 (Web of Science, for papers published in the period 2009-2013) and about 9400 (Scopus, for papers published in the period 1996-2013).

In the framework of various international conferences and congresses, our researchers have presented 168 scientific communications.

In 2013 two patents have been obtained and three patent requests have been registered. Eight new products and nine material technologies have been elaborated on the basis of current institute research whereas 19 services have been offered by contracts with economical agents.

Two events with international participation were organized in the last year: the workshop "Biomimetic sensing using nano-objects (BioSuN)" (17 – 19 June 2013), with participation of 10 foreign invited guests and 7 Romanian lecturers, and "New trends in the research of carbon based nanomaterials" (22-23 April 2013) with participation of 8 foreign invited guests and 6 Romanian lecturers.

In December 2013, a Catalogue for services and products of NIMP 2014, containing useful information for economical environment, concerning the preparation and characterization methods available in our Institute and also the materials and products developed by applied research, has been released.

Research work was dedicated to a high number of projects such as: 3 CORE projects, 3 projects UEFISCDI Module III, 17 IDEAS-PCE projects, 12 HUMAN RESOURCES projects, 2 IDEAS-PCCE projects as coordinator, 2 IDEAS-PCCE projects as partner, 3 IFA-CEA projects, 7 EURATOM projects, 4 ROSA projects, 4 PARTNERSHIP projects as coordinator and other 13 as partner.

NIMP continued to develop new international collaborations with research institutions from whole world. In 2013 NIMP has continued or started 2 FP7 projects, 2 projects Romanian Swiss Research Program RSRP, 3 projects with Commissariat de l'Energie Atomique (CEA), 1 project with Agence Nationale de Recherche (ANR), other 8 European-funded projects, 5 inter-governmental agreements and 17 bilateral cooperation with foreign institutes or universities.

We hope to obtain also in the year 2014 very good results in scientific research in the fields of condensed matter physics and materials science, in spite of some recent financial difficulties.

Dr. Ionut Enculescu  
General Director

# Laboratories

## 10. Laboratory of Multifunctional Materials and Structures

Currently the laboratory is divided in two research groups:

- The group of functional nanostructures: works on preparation and characterization of different nano-objects (nanotubes, nanowires, nanorods, etc.) with potential of applications in micro-, nano- and opto-electronics (field effect transistors, organic and hybrid LED and photovoltaic cells, photodiodes, etc.), sensors (with focus on bio-sensors), renewable energy sources.
- The group of complex heterostructures and perovskite oxides: works on preparation and characterization of oxide materials with dielectric, ferroelectric, multiferroic, semiconductor properties with potential of applications in micro- and nano-electronics (non-volatile memories, transparent electronics), telecommunications and security (microwave devices), sensors (pyroelectric, photoconductive cells), solar cells (based on photovoltaic effect in ferroelectrics or other perovskite materials).

The human resources is formed by 4 CS1 (equivalent professor), 4 CS2 (equivalent assistant professor), 10 CS3 (equivalent lectureship), 7 CS (junior researchers), 12 ACS (equivalent assistant junior researcher), 2 sub-engineers, 5 technicians and 2 workers. The infrastructure comprises modern equipments for preparation and characterization such as: PLD workstation; RF sputtering; SEM; micro-fluorescence microscope; cryostations with vertical and horizontal magnetic fields; network analyzers up to 325 GHz; THz spectrometer; ellipsometer; magnetic dichroism, etc.

## 20. Laboratory of Magnetism and Superconductivity

The laboratory is devoted to research in the field of materials with magnetic or superconducting properties and related electronic phenomena. The research process covers all the steps from preparation (powder, bulk, ribbons, thin films or nanostructures), going through basic physical characterizations, and ending with in-depth analysis of the magnetic dependent and superconducting properties. The laboratory is composed by two groups of specific activities related to electronic correlations and magnetism and respectively, superconductivity. As main research directions are to be mentioned: size effects and interactions in nanoparticulate systems and nanocomposites, interfacial interactions and surface electronic/spin configurations in layered nanosystems, molecular magnets, phase transitions and electron correlations in functional materials, vortex dynamics in high- $T_c$  superconductors, MgB<sub>2</sub> for practical applications, composite superconductors, exotic superconductors (iron-based pnictides, non-centro-symmetric superconductors). The presently available experimental facilities allow the complex processing and investigation of the mentioned systems as well as the understanding the basic interaction mechanisms at the microscopic level, by using first principles atomistic modeling and simulation of materials within the Density Functional Theory (DFT) framework, on specially assigned computer clusters.

The magnetic and superconducting structures are prepared by various technologies, like mechanical attrition, melt spinning, microwave annealing, spark plasma & hot press sintering, radiofrequency sputtering, chemical routes, etc. Subsequent processing via thermal treatments (assisted or not by applied magnetic fields) or via gas reaction control can be also managed.

The structural and morphological characterization of the samples and a large field of magnetic, thermodynamic and transport properties are studied by Physical Properties and Magnetic Properties Measurement systems (PPMS, MPMS-SQUID), Vibrating Sample and Magneto-Optic Kerr effect magnetometry (VSM and MOKE), DSC/DTA as well as Laser Flash Calorimetry. The declared purpose of understanding and controlling the electronic phenomena and spin configurations is enhanced by the whole range of Mössbauer spectroscopies (the only institute in Romania), from temperature /field dependent Mossbauer spectroscopy, to the surface/ interface sensitive Conversion Electron Mössbauer Spectroscopy (CEMS).



*Spark Plasma Sintering (left), MPMS (middle) and PPMS (right) systems*

## 30. Laboratory of Nanoscale Condensed Matter

There are 3 research groups in the laboratory of Nanoscale Condensed Matter Physics: SITSC-XESD team (Surfaces, interfaces, thin films and single crystals. X-ray / electron spectroscopies and diffraction), Si- and Ge-based nanomaterials and Nanostructures team and the Theoretical Physics group.

The main activities of the SITSC-XESD group are centred on the development and complex studies of new materials, heterostructures, surfaces and interfaces. The group utilizes and maintains several widely used installations of NIMP: (i) a surface and interface science cluster composed by a molecular beam epitaxy (MBE), a scanning tunneling microscopy (STM) and a spin- and angle-resolved photoelectron spectroscopy (SARPES). A non-negligible amount of activity is dedicated to the development of analysis methods, starting from the theory of quantitative assessment to the adjustment of the experimental conditions. The group also provides unique expertise at national level in two very demanded fields: X-ray diffraction and X-ray photoelectron spectroscopy. Also, this is practically the unique group in the country concentrated on surface and interface science, working in real ultrahigh vacuum (UHV,  $10^{-10}$  to  $10^{-11}$  mbar). An MBE setup is installed and works currently.

The X-ray diffraction expertise is also boosted by novel developments in the XRD basic theory and data analysis, often implemented in widely used XRD analysis codes, which emerged also from the SITSC-XESD group.

The Si- and Ge-based nanomaterials team is working in the field of nanostructured semiconductors with applications in nanoelectronics, photovoltaics and sensors. The group studies:

- Films of Si nanodots embedded in amorphous  $\text{SiO}_2$  matrix: (i) preparation; (ii) investigation of microstructure, electrical transport, phototransport, and photoluminescence with the aim of capturing quantum confinement effects; (iii) modelling of nanoparticle energy structure.
- GeSiO-based nanostructures: (i) preparation of Ge nanoparticles embedded in a- $\text{SiO}_2$  matrix, by magnetron sputtering and sol-gel methods; (ii) investigation of electrical behaviour and phototransport (experiment and modelling), photoluminescence and Hall effect.
- Electrical processes in carbon nanotubes based structures.
- Percolation phenomena: evidenced in carbon nanotubes based structures, Si nanodots embedded in amorphous  $\text{SiO}_2$  matrix and nanocrystalline porous Si.
- Trapping phenomena in Si-based nanostructures: stress-induced traps.
- The Theoretical Physics Group studies quantum transport phenomena in mesoscopic systems and provides phenomenological models and reliable descriptions of various effects observed in transport measurements. The main research topics cover several timely and challenging issues of mesoscopic transport: the transient transport regime in nano-devices, the mesoscopic Kondo and Fano-Kondo effects, controlled and intrinsic dephasing in mesoscopic interferometers, Coulomb drag and quantum ratchet effects in parallel quantum dots, spin interference in Rashba rings.

## 40. Laboratory of Optical Process in Nanostructured Materials

This laboratory is focused on the study and characterization by optical methods of the nanocomposites and nanostructured materials. Other research topics regard the preparation and characterization of semiconducting nanometric structures, of electrochemical synthesis of polymers with special properties as well as the synthesis and characterization of calcogenide glasses. The main equipment's used to optical characterization of investigated materials are: UV – VIS-NIR spectrometer (Lambda 950 model, Perkin Elmer), FTIR spectrophotometer (Vertex 70, Bruker), FTIR imaging microscope (Perkin Elmer), FT-Raman spectrometer (RFS 100/S model, Bruker), confocal Raman spectrometer (T64000 model, Horiba Jobin Yvon) equipped with Ar and Kr lasers, Scanning Near-Field Optical Microscope and Atomic Force Microscope (Nanonics), a fluorolog for emission study in VIS and NIR range (3.2.2.1 model, Horiba Jobin Yvon), thermoluminescence reader (TLD 3500 model, Harshaw), experimental setup for photoconductivity studies and solar simulator (LOT Oriel).



Other equipment's used to characterization and/or preparation of materials are: broadband dielectric spectroscopy system (Novocontrol), drop shape analysis (DSA 100 model, Kruss), the film evaporation system for organic materials research "Spectros", Langmuir–Blodgett systems (KSV 5000 model), spin coater (KW-4A model, Chemat) and potentiostats/galvanostats (Voltalab 80 model, Radiometer Analytical and Orignalys) for the synthesis of composite materials and their testing as electrode materials in battery and supercapacitors.

## 50. Laboratory of Atomic Structures and Defects in Advanced Materials

This laboratory is mainly committed to structural investigations by advanced characterization methods such as analytical transmission electron microscopy (TEM), electron paramagnetic resonance (EPR), Mössbauer spectroscopy. The research activity includes, also, synthesis of nanostructured materials by the hydrothermal or co-precipitation methods. Other important research subjects are related to the gas sensing and photocatalysis fields.

Among the important research equipments we mention: two analytical transmission electron microscopes, a SEM-FIB dual analytical system, five EPR spectrometers operating in several microwave bands and working modes down to liquid He temperature, three Mössbauer spectrometers, XRD installations, complex gas mixing station for electrical measurements under controlled gas atmosphere for gas sensing, specialized equipments for hydrothermal and co-precipitation synthesis.

A new atomic resolution TEM has been installed in 2011. The instrument is provided with probe  $C_s$  corrector of the spherical aberration, EDS and EELS microanalytical facilities. Another newly acquired equipment is the analytical SEM-FIB dual system which has been installed in a cleanroom next to equipments for photolithography and nanolithography.

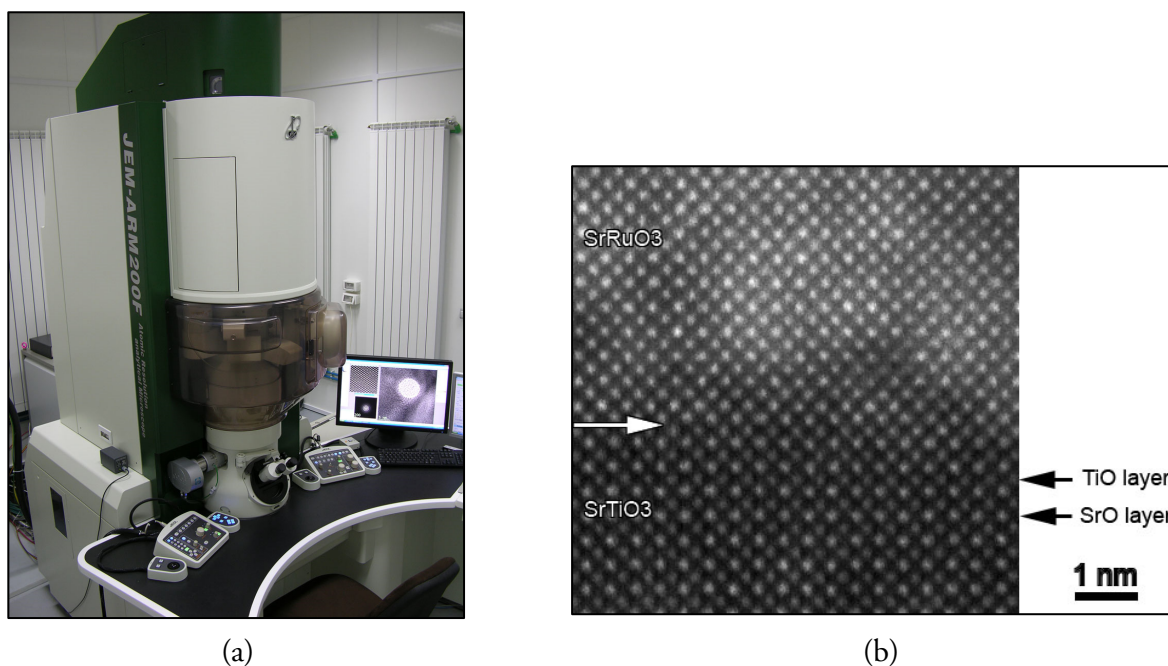


*Figure 1. (a) The atomic resolution TEM, JEM ARM 200F, recently installed at NIMP; (b) HAADF-STEM image of the  $SrRuO_3$ - $SrTiO_3$  interface obtained with the JEM ARM 200F microscope installed at NIMP.*

The research activity of the scientists working in this laboratory is focused on the physical properties of advanced materials (structure, optical, electrical properties), resulting either as size effects (nanostructures, thin films) or by structural defect engineering. The scientific concerns are mainly directed towards the discovery, investigation and manipulation of physical properties at nanometric and atomic scale for the development and characterization of new materials (dielectrics, semiconductors, alloys, ceramics) to be used in various applications (semiconductor technology, gas sensing, radiation detectors, telecommunications).

# Personnel

# List of Personnel

## Lab. 10 – Laboratory of Multifunctional Materials and Structures

**HEAD:** Dr. Lucian PINTILIE  
E-mail: pintilie@infim.ro  
Tel : (+4) 021 369 01 85  
Fax: (+4) 021 369 01 77

1. Dr. Gabriel BANCIU	senior researcher I
2. Dr. Cornel MICLEA	senior researcher I
3. Dr. Ioana PINTILIE	senior researcher I
4. Dr. Daniela PREDOI	senior researcher I
5. Dr. Marin CERNEA	senior researcher II
6. Dr. Monica ENCULESCU	senior researcher II
7. Dr. Corneliu Florin MICLEA	senior researcher II
8. Dr. Silviu POLOSAN	senior researcher II
9. Dr. Luminita AMARANDE	senior researcher III
10. Dr. Lucian Dragos FILIP	senior researcher III
11. Dr. Aurelian GALCA	senior researcher III
12. Dr. Luminita HRIB	senior researcher III
13. Dr. Alin IUGA	senior researcher III
14. Dr. Elena MATEI	senior researcher III
15. Dr. Liviu NEDELCU	senior researcher III
16. Dr. Iuliana PASUK	senior researcher III
17. Dr. Nicoleta PREDA	senior researcher III
18. Dr. George STAN	senior researcher III
19. Dr. Viorica STANCU	senior researcher III
20. Dr. Lucian TRUPINA	senior researcher III
21. Georgia BONI	researcher
22. Cristina BESLEAGA STAN	researcher
23. Dr. Cristina BUSUIOC	researcher
24. Dr. Cristina CHIRILA	researcher
25. Dr. Marius CIOANGHER	researcher
26. Dr. Carmen CIOBANU	researcher
27. Mihaela BOTEA	assistant researcher
28. Constantin CIOBOTARU	assistant researcher
29. Corina CIOBOTARU	assistant researcher
30. Andreea COSTAS	assistant researcher
31. Constantin DUTU	assistant researcher
32. Alexandru EVANGHELIDES	assistant researcher
33. Camelia FLORICA	assistant researcher
34. Irina GHITA	assistant researcher
35. Simona ICONARU	assistant researcher

36. Mihaela OANCEA	assistant researcher
37. Claudiu POPA	assistant researcher
38. Cristina POPA	assistant researcher
39. Roxana RADU	assistant researcher
40. Andrei Gabriel TOMULESCU	assistant researcher
41. Liliana TRANCA	assistant researcher
42. Alexandru GAVRILA	engineer
43. Vasilica TOMA	engineer

## Lab. 20 – Laboratory of Magnetism and Superconductivity

**HEAD:** Dr. Victor Eugen KUNCSEER

E-mail: kuncser@infim.ro

Tel.: (+4) 021 369 01 85

Fax: (+4) 021 369 01 77

- |   |  |
|---|--|
| 1. Dr. Gheorghe Virgil ALDICA           | senior researcher I                          |
| 2. Dr. Petre BADICA                     | senior researcher I                          |
| 3. Dr. Ovidiu CRISAN                    | senior researcher I                          |
| 4. Dr. George FILOTI                    | senior researcher I (associate collaborator) |
| 5. Dr. Andrei GALATANU                  | senior researcher I                          |
| 6. Dr. Lucica MIU                       | senior researcher I                          |
| 7. Dr. Neculai PLUGARU                  | senior researcher I                          |
| 8. Dr. Viorel Constantin SANDU          | senior researcher I                          |
| 9. Dr. Mihaela VALEANU                  | senior researcher I                          |
| 10. Dr. Alina CRISAN                    | senior researcher III                        |
| 11. Dr. Valentina MIHALACHE             | senior researcher III                        |
| 12. Dr. Petru PALADE                    | senior researcher III                        |
| 13. Ancuta BARSAN                       | researcher                                   |
| 14. Dr. Ion IVAN                        | researcher                                   |
| 15. Dr. Carmen PLAPCIANU                | researcher                                   |
| 16. Dr. Bogdan POPESCU                  | researcher                                   |
| 17. Dr. Gabriel SCHINTEIE               | researcher                                   |
| 18. Dr. Mihaela SOFRONIE                | researcher                                   |
| 19. Dr. Felicia TOLEA                   | researcher                                   |
| 20. Dr. Maria-Cristina VALSANGIACOM     | researcher                                   |
| 21. Mihai Burdusel                      | assistant researcher                         |
| 22. Magda GALATANU                      | assistant researcher                         |
| 23. Simona Gabriela GRECULEASA          | assistant researcher                         |
| 24. Marilena Alina IONESCU              | assistant researcher                         |
| 25. Aurel LECA                          | engineer                                     |
| 26. Dr. Adrian Ioan CRISAN <sup>1</sup> | senior researcher I                          |
| 27. Dr. Adrian JIANU <sup>2</sup>       | senior researcher I                          |
| 28. Dr. Marilena TOMUT <sup>3</sup>     | senior researcher III                        |

<sup>1</sup> Univ. Birmingham, Dept. Met & Mat., Birmingham, England.

<sup>2</sup> Institute for Pulsed Power and Microwave Technology, Forschungszentrum Karlsruhe.

<sup>3</sup> GSI / KP2 Nuclear Structure and Nuclear Chemistry, Darmstadt.

## Lab. 30 – Laboratory of Nanoscale Condensed Matter

**HEAD:** Dr. Valeriu MOLDOVEANU

E-mail: valim@infim.ro

Tel.: (+4) 021 369 01 85

Fax: (+4) 021 369 01 77

1. Dr. Alexandru Emil ALDEA	senior researcher I
2. Dr. Magdalena Lidia CIUREA	senior researcher I
3. Dr. Paul GARTNER	senior researcher I
4. Dr. Sorina LAZANU	senior researcher I
5. Dr. Dan MACOVEI	senior researcher I
6. Dr. Nicolae POPA	senior researcher I
7. Dr. Cristian-Mihail TEODORESCU	senior researcher I
8. Dr. Gheorghe IORDACHE	senior researcher II
9. Dr. Nicoleta APOSTOL	senior researcher III
10. Dr. Maria-Ruxandra COSTESCU	senior researcher III
11. Dr. Ion Viorel DINU	senior researcher III
12. Dr. Rodica GHITA	senior researcher III
13. Dr. Marius Adrian HUSANU	senior researcher III
14. Dr. Ana Maria LEPADATU	senior researcher III
15. Dr. Constantin Catalin NEGRILA	senior researcher III
16. Dr. Marian NITA	senior researcher III
17. Dr. Ionel STAVARACHE	senior researcher III
18. Dr. Mihaela STEGARESCU	senior researcher III
19. Dr. Mugurel TOLEA	senior researcher III
20. George-Adrian LUNGU	researcher
21. Dr. Dana Georgeta POPESCU	researcher
22. Adrian SLAV	researcher
23. Laura Elena ABRAMIUC	assistant researcher
24. Amelia Elena BOCARNEA	assistant researcher
25. Radu DRAGOMIR	assistant researcher
26. Bogdan OSTAHIE	assistant researcher
27. Catalin PALADE	assistant researcher
28. Nicoleta RADUTOIU	assistant researcher
29. Liviu Cristian TANASE	assistant researcher
30. Ioana Cristina BUCUR	engineer
31. Cristian TACHE	engineer
32. Dr. Nicolae BARSAN <sup>1</sup>	senior researcher I
33. Dr. Andrei MANOLESCU <sup>2</sup>	senior researcher I
34. Dr. Paul RACEC <sup>3</sup>	senior researcher III
35. Dr. Toma STOICA <sup>4</sup>	senior researcher I

<sup>1</sup> Institute of Physical and Theoretical Chemistry, University of Tübingen

<sup>2</sup> School of Science and Engineering, Reykjavik, Iceland

<sup>3</sup> Institut für Theoretische Physik, Universität Bremen, Germany

<sup>4</sup> Forschungszentrum Jülich, Peter Grunberg Institut, Jülich, Germany

## Lab. 40 – Laboratory of Optical Processes in Nanostructured Materials

**HEAD:** Dr. Mihaela BAIBARAC  
E-mail: barac@infim.ro  
Tel.: (+4) 021 369 01 77  
Fax: (+4) 021 369 01 77

1. Dr. Ioan BALTOG	senior researcher I
2. Dr. Ligia FRUNZA	senior researcher I
3. Dr. Stefan FRUNZA	senior researcher I
4. Dr. Mihai POPESCU	senior researcher I
5. Dr. Mihai SECU	senior researcher I
6. Dr. Marian SIMA	senior researcher II
7. Dr. Anca STANCULESCU	senior researcher II
8. Dr. Florin COTOROBAI	senior researcher III
9. Dr. Adam LORINCZI	senior researcher III
10. Lucian MIHUT	senior researcher III
11. Dr. Corina SECU	senior researcher III
12. Dr. Marcela SOCOL	senior researcher III
13. Dr. Alin VELEA	senior researcher III
14. Timucin VELULA	senior researcher III
15. Dr. Irina Ionela ZGURA	senior researcher III
16. Paul Constantin GANEA	researcher
17. Dr. Florentina NEATU	researcher
18. Dr. Oana RASOGA	researcher
19. Dr. Florinel SAVA	researcher
20. Dr. Mariana SIMA	researcher
21. Carmen BREAZU	assistant researcher
22. Monica DAESCU	assistant researcher
23. Ioana DUMITRESCU	assistant researcher
24. Mirela ILIE	assistant researcher
25. Adelina MATEA	assistant researcher
26. Daniel-Iosif SIMANDAN	assistant researcher
27. Ion SMARANDA	assistant researcher
28. Malvina SCOCIOREANU	assistant researcher

## Lab. 50 – Laboratory of Atomic Structures and Defects in Advanced Materials

**HEAD:** Dr. Corneliu GHICA  
E-mail: cghica@infim.ro  
Tel.: (+4) 021 369 01 85  
Fax: (+4) 021 369 01 77

- |                                   |                       |
|-----------------------------------|-----------------------|
| 1. Dr. Ion BIBICU                 | senior researcher I   |
| 2. Dr. Lucian DIAMANDESCU         | senior researcher I   |
| 3. Dr. Nicoleta Maria GRECU       | senior researcher I   |
| 4. Dr. Leona Cristina NISTOR      | senior researcher I   |
| 5. Dr. Sergiu Vasile NISTOR       | senior researcher I   |
| 6. Dr. Corneliu SARBU             | senior researcher I   |
| 7. Dr. Valentin Serban TEODORESCU | senior researcher I   |
| 8. Dr. Adelina STANOIU            | senior researcher II  |
| 9. Dr. Mariana STEFAN             | senior researcher II  |
| 10. Dr. Alina BANUTA              | senior researcher III |
| 11. Dr. Marcel FEDER              | senior researcher III |
| 12. Dr. Daniela GHICA             | senior researcher III |
| 13. Dr. Mihai VLAICU              | senior researcher III |
| 14. Dr. Cristian Eugen SIMION     | researcher            |
| 15. Alexandra Camelia JOITA       | assistant researcher  |
| 16. Andrei Cristian KUNCSEK       | assistant researcher  |
| 17. Raluca NEGREA                 | assistant researcher  |
| 18. Andreea Alexandra NILA        | assistant researcher  |
| 19. Traian POPESCU                | assistant researcher  |
| 20. Ioana VLAICU                  | assistant researcher  |
| 21. Dr. Valentin Adrian MARALOIU  | assistant researcher  |
| 22. Dr. Ionel Florinel MERCIONIU  | engineer              |
| 23. Dr. Manuela STIR <sup>1</sup> | assistant researcher  |

---

<sup>1</sup> EMPA Materials Research and Technology, Thun, Switzerland

**MAAS Laboratory for X-Ray Photoelectron Spectroscopy (XPS) Analysis**

- |                                 |                      |
|---------------------------------|----------------------|
| 1. Dr. Mihail Florin LAZARESCU  | senior researcher I  |
| 2. Dr. Constantin LOGOFATU      | senior researcher I  |
| 3. Dr. Stefan Adrian MANEA      | senior researcher I  |
| 4. Dr. Costel COTIRLAN-SIMIONUC | assistant researcher |
| 5. Florica FRUMOSU              | assistant researcher |

## Visiting Guests

**Prof. Evangelos Hristoforou, Technical University Athens, Greece, 31.01.2013:** Magnetism against tumor

**Dr. Gopi Krishnan, Zernike Institute for Advanced Materials, University of Groningen, Olanda:** Joint TEM characterization of bimetallic nanoparticles (Mg-Cu, Mg-Ni, & Mo-Cu) synthesized by Gas-Phase method.

Working Stage (22-26.04.2013) in Laboratory 50 – Electron Microscopy Group (Dr. C. Ghica)

**Dr. Manuel Bibes, CNRS-THALES group, Palaiseau, France 13.06.2013:** Ferroelectric tunnel junctions for electronics and spintronics

**Mr. Marwene Oumezzine, Ph.D. student, Laboratoire de Physico-chimie des Matériaux, Département de Physique, Faculté des Sciences, Université de Monastir, Tunisia**

Working Stage in Laboratory 10 – Heterostructures Group (Dr. A. C. Galca)

**Mrs. Dovilė Meškauskaitė, Master student, Faculty of Physics, Vilnius University, Vilnius, Lithuania**

Working Stage (Erasmus Programme) – July-October 2013 – in Laboratory 10 – Heterostructures Group (Dr. I. Pintilie)

**Prof. Dr. Seizi Nishizawa, University of Fukui, Fukui City, Japan**

Working Stage in Laboratory 10 – Heterostructures Group, September 2013, (Dr. G.M. Banciu)

**Prof. Dr. Gerald Lucovsky, North Carolina State University, USA**

Receiving of “Prize for Excellence in Amorphous Chalcogenides” for the year 2012

Invited lectures :

- 09 September 2013, 11:00: "Medium range order in oxide glasses: IR, RAMAN and X-ray Diffraction".
- 09 September 2013, 12:00: "Medium range order in nc-Si: IR, ESR, RAMAN, Photoconductivity".
- 10 September 2013, 12:00: "Band edge and band-gap electronic structure and intrinsic bonding defects: nc-Si and nc-SiO<sub>2</sub>".
- 10 September 2013, 13:00: "Band edge and band-gap electronic structure and intrinsic bonding defects: nc-Chalcogenides and nano-grain transition metal oxides".

**Dr. Piotr Klimczyk, Institute of Advanced Manufacturing Technology, Krakow, Poland**

Working Stage (14-25.10.2013) in the framework of FP7 REGPOT SINTERCER project in Laboratory 50 –Electron Microscopy Group (Dr. I. Mercioniu)

**Dr. Till Hoschen, Max-Planck-Institut für Plasmaphysik IPP, Garching bei München, Germany, 12-13.11.2013,** Euratom project, TEM characterization of electron beam surface annealed Eurofer 97 samples. Working visit in Lab. 50 at the invitation of Dr. C. Ghica

**Prof. JiaCai Nie, Drd. YinLong Han, Beijing Normal University**  
Working Stage (Nov. 2013) in Laboratory 20 (Dr. P. Badica)

**Prof. JiaCai Nie, Beijing Normal University, 26.11.2013:**What is the Key to Formation of Two-Dimensional Electron Gas at  $\text{LaAlO}_3 / \text{SrTiO}_3$  Interfaces

**Prof. Dr. Masahiko Tani, University of Fukui, Fukui City, Japan**  
Working Stage (December 2013) in Laboratory 10 – Heterostructures Group (Dr. G.M. Banciu)

## Ph. D. Theses

**Cristina Besleaga Stan**

Wide band semiconductors with application in transparent electronics

May 2013

**Ana-Maria Lepadatu**

The study of electrical properties of some nanostructures materials based on group IV elements

June 2013

**Nicoleta G. Apostol**

Surfaces of elemental and oxidic semiconductors and their interfaces with metals deposited by molecular beam epitaxy

October 2013

**Dana G. Popescu**

Contributions to the development of methods and techniques for analysis and characterization of photonic crystal devices

October 2013

**Bogdan Popescu**

Study of some magnetic materials exhibiting magnetoresistive effect. Ferromagnetic Kondo systems

November 2013

## Awards

Florica C: Winner of BEST ORAL AWARD for symposium K-ZnO material science from researches to electronic applications, E-MRS Fall Meeting, Warsaw, Poland, 16-20 September 2013, paper "Tunable electrical properties of field effect transistors based on electrodeposited ZnO nanowires"

Galatanu A, Popescu B, Galatanu M, Bartha C, Palade P, Enculescu M:  
Gold medal at the international exhibition "Proinvent 2013", Cluj-Napoca, for works on:  
"Refractory materials for fusion reactor DEMO"

Lepadatu A.M., Secu E. C., Stavarache I.: Romanian Academy Prize „Radu Grigorovici” for the group of papers entitled: „Physical properties of some nanostructured materials”

Lepadatu AM: Best Poster presented during EMRS 2013, Spring Meeting, Strasbourg, Franta, 27-31 mai 2013, Symposium J

Stanculescu A, Galca AC: Romanian Academy Prize „Radu Grigorovici” for the group of papers entitled: “Optical properties of some oxidized systems”.

# Honorary Membership

NIMP is honorary membership in various prestigious professional societies and associations, such as:

- American Chemical Society
- German Physical Society
- European Society of Applied Superconductivity
- Japanese Applied Physics Society (former)
- Cryogenic Society of Japan (former)
- Alumni JSPS, Romania (founding member)

3 NIMP distinguished researchers are Editor-in-chief or Co-Editor for 8 ISI journals. Finally, 16 researchers are members in Editorial Board and Advisory Board for 11 ISI journals (6 edited in Romania).

Also, NIMP is present in following databases:

- **MyNet Research Empowering Collaboration** ([www.mynetresearch.com](http://www.mynetresearch.com)) – international resource for innovation centers in Eastern Europe and Central Asia. The top five Romanian institutions in terms of research productivity are:
  - Univ Bucharest
  - Univ Babes Bolyai
  - Romanian Acad
  - Inst Atom Phys
  - Natl Inst Mat Phys
- The **CEEC IST NET** portal ([www.eu-istcommunity.net](http://www.eu-istcommunity.net)) – is a support instrument for partners search and consortia creation in the field of research and innovation concerning the information society technologies
- **Europartners Search** ([www.europartnersearch.net](http://www.europartnersearch.net))
- **Resource Guide to Nanotechnology and Nanomaterials Services (NanoPerspective)**  
This guide includes a list of more 1000 organizations active in the field of Nanotechnology and Nanomaterials.
  - <http://wikimapia.org/19116027/INCDFM-National-RD-Institute-of-Materials-Physics-NIMP>
  - [http://cercetare.ccib.ro/intranetHTML/infoFILES/infoHTML/File/2012\\_03\\_22\\_prezentareINCDFM.pdf](http://cercetare.ccib.ro/intranetHTML/infoFILES/infoHTML/File/2012_03_22_prezentareINCDFM.pdf)
  - <http://www.ancs.ro/ro/articol/1325/de-cercetare-incd-institute-nationale-de-cercetare-dezvoltare-incd-in-coordonarea-ancs-institutul-national-de-cercetare-dezvoltare-pentru-fizica-materialelor-incdfm-bucuresti>
  - [http://www.infocercetare.ro/ro/Listeaza-Institutie/Ilfov-84\\_Localitate\\_Magurele-86\\_Institutie\\_INCDFM-pentru-Fizica-Materialelor-INCDFM-253](http://www.infocercetare.ro/ro/Listeaza-Institutie/Ilfov-84_Localitate_Magurele-86_Institutie_INCDFM-pentru-Fizica-Materialelor-INCDFM-253)

## Memberships in National Research Policy and Evaluation Organizations

- President of Consulting College for Research, Development and Innovation, Dr. A. Aldea
- Member in National Council for Development and Innovation (CNDI), Dr. O. Crisan
- Members in Chemistry Board of National Council of Academic Titles, Diplomas and Certificates (CNATDCU):
  - Dr. L. Frunza

- **Expert evaluators and monitoring for FP 7 and various programmes:**
  - Dr. L. Pintilie
  - Dr. O. Crisan
  - Dr. A. Stanculescu
  - Dr. F. Vasiliu
  - Dr. L. Frunza

### Membership in Other International Organizations

**Badica Petre:** member of American Chemical Society and German Physical Society

**Banciu Marian Gabriel:** member of IEEE: Microwave Theory and Techniques Society, Antennas and Propagation Society

**Bibicu Ion:** member of European Physical Society

- member of Academy of Technical sciences from Romania

**Ciurea Magdalena Lidia:** member of European Physical Society

**Crisan Ovidiu:** member of Institute of Nanotechnology, UK

**Diamandescu Lucian:** member of “American Nano Science”

- Romanian Representative in International Board on the Applications of Mössbauer Effect - IBAME (2011-2017)
- member in Editorial Board of “ISRN Nanomaterials” (SUA)

**Frunza Ligia:** member of American Chemical Society and of Romanian Society of Catalysis

**Ghica Corneliu:** member of European Materials Research Society

**Ghica Daniela:** member of European Materials Research Society

**Grecu Maria Nicoleta:** member of AMPERE Group

**Maraloiu Valentin Adrian:** member of Société Française des Microscopies

**Nistor Sergiu Vasile:** member of American Physical Society

**Pintilie Lucian:** member of European Physical Society

**Popescu Mihai:** member of NACNOG (North Atlantic Consortium on Non-Oxide Glasses, 19 countries from Europe, Canada and USA)

- member of VIP (Virtual Institute of Physics): <http://www.infim.ro/-inst>

**Predoi Daniela:** member of Romanian Society of Catalysis

**Sandu Viorel:** member of American Physical Society and Material Research Society Singapore

**Sarbu Corneliu:** member of Microscopical Society of America

**Socol Marcela:** member of International Organization on Crystal Growth

**Stanculescu Anca:** member of International Organization on Crystal Growth

- member of SPIE

# **Publications and Presentations**

**Books**

1. *Ciurea ML, Lepadatu AM, Stavarache I*  
Book Chap. 3: Quantum Well Solar Cells- Physics, Materials and Technology  
In: Advanced Solar Cell Materials, Technology, Modeling and Simulation, Fara L and Yamaguchi M (eds.), Publisher: IGI Global, pp. 33 – 47, ISBN: 978-1-4666-1927-2 (2013)
2. *Kuncser V, Crisan O, Schinteie G, Tolea F, Palade P, Valeanu M, Filoti G*  
Book chapter: Magnetic Nanophases: From exchange coupled multilayers to nanopowders and nanocomposites  
In: Modern Trends in Nanoscience, Eds M. Balasoiu and G.M. Arzumarian, Editura Academiei Romane, Bucharest, pp. 197-222, ISBN:978-973-27-2230-5 (2013)
3. *Nistor SV, Stefan M, Nistor LC, Ghica D, Mateescu CD, Barascu JN*  
Book chapter: Preparation and properties of mesoporous cubic ZnS doped with Mn<sup>2+</sup> activating ions  
In: Modern Trends in Nanoscience, Eds M. Balasoiu and G.M. Arzumarian, Editura Academiei Romane, Bucharest, pp. 143-155, ISBN 978-973-27-2230-5 (2013)

**Papers in ISI Ranked Journals (with Impact Factor)**

1. *Aldica G, Popa S, Enculescu M, Badica P*  
Te and SiC co-doped MgB<sub>2</sub> obtained by an ex situ spark plasma sintering technique  
*Scripta Materialia*, (2013), 68, pp.428-431, **2.699**, **1.204**
2. *Angelescu DG, Munteanu G, Anghel DF, Peretz S, Maraloiu AV, Teodorescu VS*  
Formation mechanism of CdS nanoparticles with tunable luminescence via a non-ionic microemulsion route  
*Journal of Nanoparticle Research*, (2013), 15, pp.1376-1391, **3.287**, **0.929**
3. *Apostol NG, Stoflea LE, Lungu GA, Tanase LC, Chirila C, Frunza L, Pintilie L Teodorescu CM*  
Band bending in Au/Pb(Zr,Ti)O<sub>3</sub> investigated by X-ray photoelectron spectroscopy: Dependence on the initial state of the film  
*Thin Solid Films*, (2013), 545, pp.13-21, **1.89**, **0.595**
4. *Apostol NC, Stoflea LE, Lungu GA, Chirila C, Trupina L, Negrea RF, Ghica C, Pintilie L, Teodorescu CM*  
Charge transfer and band bending at Au/Pb(Zr,Ti)O<sub>3</sub> interfaces investigated by photoelectron spectroscopy  
*Applied Surface Science*,(2013), 273, pp. 415-425, **2.103**, **0.549**
5. *Apostol NC, Stoflea LE, Lungu GA, Tache CA, Pintilie L, Teodorescu CM*  
Band bending at free Pb(Zr,Ti)O<sub>3</sub> surfaces analyzed by X-ray photoelectron spectroscopy  
*Materials Science Engineering B*, (2013), 178, pp. 1317-1322, **1.518**, **0.533**
6. *Baibarac M, Baltog I, Mihut L, Pasuk I, Lefrant S*  
Casimir effect demonstrated by Raman spectroscopy on trilayer grapheme intercalated into stiff layered structures of surfactant  
*Carbon*, (2013), 51, pp.134-142, **5.868**, **1.595**
7. *Baibarac M, Baltog I, Frunza S, Magrez A, Schur D, Zaginaichenk S Yu*  
Single-walled carbon nanotubes functionalized with polydiphenylamine as active materials for applications in the supercapacitors field  
*Diamond and Related Materials*, (2013), 32, pp.72-82, **1.913**, **0.528**
8. *Baschir L, Antohe S, Radu A, Constantineanu R, Iftimie S, Simandan ID, Popescu M*  
Effect of cnts and metal-phthalocyanines adding on the photo-electrical behavior of the photovoltaic structures based on polymeric blends  
*Digest Journal of Nanomaterials and Biostructures*, (2013), 8, pp.1645-1651, **1.2**
9. *Bibicu I*  
Comments on <sup>151</sup>Eu surface Mössbauer Spectroscopy  
*European Physical Journal Applied Physics*, (2013), 62, 11302, **0.771**, **0.264**
10. *Birsan A, Palade P*  
Band structure calculations of Ti<sub>2</sub>FeSn: A new half-metallic compound  
*Intermetallics*, (2013), 36, pp.86-89, **1.649**, **0.635**

11. **Birsan A, Palade P, Kuncser V**  
Prediction of half metallic properties in  $\text{Ti}_2\text{CoSi}$  Heusler alloy based on density functional theory  
*Journal of Magnetism and Magnetic Materials*, (2013), 331, pp.109-112, **1.78**, **0.475**
12. **Blagoeva DT, Opschoor J, Pintsuk G, Sarbu C**  
Development and qualification of tungsten and tungsten alloys for fusion  
*Fusion Science and Technology*, (2013), 64, pp.203-210, **1.12**, **0.299**
13. **Blagoeva DT, Opschoor J, Van der Laan JG, Sarbu C, Pintsuk G, Jong M, Bakker T, ten Pierick P, Nolles H**  
Development of tungsten alloys for DEMO divertor applications via MIM technology  
*Journal of Nuclear Materials*, (2013), 442, pp.S198-S203, **2.052**, **0.585**
14. **Bogomol I, Badica P, Shen YQ, Nishimura T, Loboda P, Vasylykiv O**  
Room and high temperature toughening in directionally solidified  $\text{B}_4\text{C-TiB}_2$  eutectic composites by Si doping  
*Journal of Alloys and Compounds*, (2013), 570, pp.94-99, **2.289**, **0.507**
15. **Boni AG, Pintilie I, Pintilie L, Preziosi D, Deniz H, Alexe M**  
Electronic transport in  $(\text{La,Sr})\text{MnO}_3$ -ferroelectric- $(\text{La,Sr})\text{MnO}_3$  epitaxial structures  
*Journal of Applied Physics*, (2013), 113, 10.1063/1.4808335, **2.168**, **0.834**
16. **Botea M, Iuga A, Pintilie L**  
Giant pyroelectric coefficient determined from the frequency dependence of the pyroelectric signal generated by epitaxial  $\text{Pb}(\text{Zr}_{0.2}\text{Ti}_{0.8})\text{O}_3$  layers grown on single crystal  $\text{SrTiO}_3$  substrates  
*Applied Physics Letters*, (2013), 103, 232902, **3.844**, **1.384**
17. **Brasoveanu M, Craciun G, Manaila E, Ighigeanu D, Nemtanu MR, Grecu MN**  
Evolution of the levels of free radicals generated on wheat flour and wheat bran by electron beam  
*Cereal Chemistry*, (2013), 90, pp.469-473, **1.452**, **0.372**
18. **Bucur C, Badea M, Chifiriuc MC, Bleotu C, Iorgulescu EE, Badea I, Grecu MN, Lazar V, Patriciu OI, Marinescu D, Olar R**  
Studies on thermal, spectral, magnetic and biological properties of new Ni(II), Cu(II) and Zn(II) complexes with a bismacrocyclic ligand bearing an aromatic linker  
*Journal of Thermal Analysis and Calorimetry*, (2013), DOI: 10.1007/s10973-013-3460-1, **1.604**, **0.239**
19. **Bucur C, Korosec RC, Badea M, Calu L, Chifiriuc MC, Grecu MN, Stanica N, Marinescu D, Olar R**  
Investigation of thermal stability, spectral, magnetic, and antimicrobial behavior for new complexes of Ni(II), Cu(II), and Zn(II) with a bismacrocyclic ligand  
*Journal of Thermal Analysis and Calorimetry*, (2013), 113, pp.1287-1295, **1.604**, **0.239**
20. **Burdusel M, Aldica G, Popa S, Enculescu M, Pasuk I, Badica P**  
 $\text{MgB}_2$  with addition of  $\text{Bi}_2\text{O}_3$  obtained by spark plasma sintering technique  
*Journal of Superconductivity and Novel Magnetism*, (2013), 26, pp.1553-1556, **0.65**, **0.237**

21. *Cernea M, Vasiliu F, Plapcianu C, Bartha C, Mercioniu I, Pasuk I, Lowndes R, Trusca R, Aldica GV, Pintilie L*  
Preparation by sol-gel and solid state reaction methods and properties investigation of double perovskite  $\text{Sr}_2\text{FeMoO}_6$   
*Journal of the European Ceramic Society*, (2013), 33, pp.2483-2490, **2.353**, **0.689**
22. *Cernea M, Trupina L, Vasile BS, Trusca R, Chirila C*  
Nanotubes of piezoelectric BNT-BT0.08 obtained from sol-gel precursor  
*Journal of Nanoparticle Research*, (2013), 15, pp.1787-1793, **3.287**, **0.929**
23. *Cernea M, Sandu SG, Galassi C, Radu R, Kuncser V*  
Magnetic properties of  $\text{Ba}_x\text{Sr}_{1-x}\text{Fe}_{12}\text{O}_{19}$  ( $x=0.05-0.35$ ) ferrites prepared by different methods  
*Journal of Alloys and Compounds*, (2013), 561, pp.121-128, **2.289**, **0.507**
24. *Cernea M, Pintilie L, Trupina L, Vasile BS, Chirila C, Pasuk I*  
BNT-BT0.08 wires derived from sol-gel precursor and their piezoelectric behavior  
*Journal of Nanoparticle Research*, (2013), 15, pp.1668-1673, **3.287**, **0.929**
25. *Cernea M, Secu CE, Vasile BS, Secu M*  
Structural and optical characterization of sol-gel derived Tm-doped  $\text{BaTiO}_3$  nanopowders and ceramics  
*Current Applied Physics*, (2013), 13, 1, pp.137-141, **1.9**, **0.502**
26. *Chiriac A, Stan GE, Iliescu B, Poata I*  
The influence of host bone substrate in titanium mesh cranioplasty  
*Digest Journal of Nanomaterials and Biostructures*, (2013), 8, pp.729-735, **1.2**
27. *Chirila C, Ibanescu G, Hrib L, Negrea R, Pasuk I, Kuncser V, Pintilie I, Pintilie L*  
Structural, electric and magnetic properties of  $\text{Pb}(\text{Zr}_{0.2}\text{Ti}_{0.8})\text{O}_3\text{CoFe}_2\text{O}_4$  heterostructures  
*Thin Solid Films*, (2013), 545, pp. 2-7, **1.89**, **0.595**
28. *Chivu AE, Ciuca S, Bojin D, Stan GE, Gebert A, Eckert J*  
Electrochemical deposited hydroxyapatite on pre-treated CP-Ti surfaces  
*Metalurgia International*, (2013), 18, pp.34-38, **0.084**
29. *Choina J, Kosslick H, Fischer C, Flechsig GU, Frunza L, Schulz A*  
Photocatalytic decomposition of pharmaceutical ibuprofen pollutions in water over titania catalyst  
*Applied Catalysis B-Environmental*, (2013), 129, pp.589-598, **5.625**, **1.421**
30. *Ciobanu CS, Iconaru SL, Chapon P, Predoi D*  
Antimicrobial activity of silver doped hydroxyapatite thin films  
*Febs Journal*, (2013), 280, pp.359-360, **3.79**, **1.182**
31. *Ciobanu CS, Andronescu E, Prodan AM, Pall L, Costescu A, Le Coustumer P, Huneau F, Marutescu L, Ene NI, Trusca R, Barna ES, Iconaru SL*  
Physico-chemical and antibacterial studies on silver doped nano-hydroxyapatite  
*Journal of Optoelectronics and Advanced Materials*, (2013), 15, pp.918-922, **0.457**, **0.11**
32. *Ciobanu CS, Iconaru SL, Pasuk I, Vasile BS, Lupu AR, Hermenean A, Dinischiotu A, Predoi D*  
Structural properties of silver doped hydroxyapatite and their biocompatibility  
*Materials Science & Engineering C-Materials for Biological Applications*, (2013), 33, pp.1395-1402, **2.686**, **0.605**

33. *Ciobanu CS, Iconaru SL, Chifiriuc MC, Costescu A, Le Coustumer P, Predoi D*  
Synthesis and antimicrobial activity of silver-doped hydroxyapatite nanoparticles  
*Biomed Research International*, (2013), vol. 2013, pp.1-10, **2.88**
34. *Ciobanu CS, Iconaru SL, Le Coustumer P, Predoi D*  
Vibrational investigations of silver-doped hydroxyapatite with antibacterial properties  
*Journal of Spectroscopy*, (2013), vol. 2013, pp.1-5, **0.53**
35. *Ciurea ML*  
Effect of stress on trapping phenomena in silicon: from single crystal to nanostructures  
*Romanian Reports in Physics*, (2013), 65, pp.841-856, **0.5, NU**
36. *Comorosan S, Polosan S, Popescu I, Stamatina I, Ionescu E, Avramescu S, Cune LC, Apostol M*  
Optical manipulation of complex molecular systems by high density green photons:  
experimental and theoretical evidence  
*European Physical Journal B*, (2013), 86:232 DOI:10.1140/epjb/e2013-40049-8, **1.534, 0.684**
37. *Costescu A, Ciobanu CS, Iconaru SL, Ghita RV, Chifiriuc CM, Marutescu LG, Predoi D*  
Fabrication, characterization, and antimicrobial activity, evaluation of low silver concentrations  
in silver-doped hydroxyapatite nanoparticles  
*Journal of Nanomaterials*, (2013), 194854/1-9, **1.376, 0.471**
38. *Covaliu CI, Paraschiv G, Biris SS, Jitaru I, Vasile E, Diamandescu L, Velickovic TC, Krstic M, Ionita V, Iovu H, Matei E*  
Maghemite and poly-DL-alanine based core-shell multifunctional nanohybrids for  
environmental protection and biomedicine applications  
*Applied Surface Science*, (2013), 285, pp. 86-95, **2.103, 0.549**
39. *Covaliu CI, Jitaru I, Paraschiv G, Vasile E, Biris SS, Diamandescu L, Ionita V, Iovu H*  
Core-shell hybrid nanomaterials based on  $\text{CoFe}_2\text{O}_4$  particles coated with PVP or PEG  
biopolymers for applications in biomedicine  
*Powder Technology*, (2013), 237, pp.415-426, **2.08, 0.615**
40. *Cristescu R, Popescu C, Dorcioman G, Miroiu FM, Socol G, Mihailescu IN, Gittard SD, Miller PR, Narayan RJ, Enculescu M, Chrissey DB*  
Antimicrobial activity of biopolymer-antibiotic thin films fabricated by advanced pulsed laser  
methods  
*Applied Surface Science*, (2013), 278, pp.211-213, **2.103, 0.549**
41. *Culita DC, Patron L, Oprea O, Bartha C, Palade P, Teodorescu VS, Filoti G*  
Detailed characterization of functionalized magnetite and ascertained effects  
*Journal of Nanoparticle Research*, (2013), 15:1916:DOI10.1007/s11051-013-1916-7, **3.287, 0.929**
42. *D'Acapito F, Pochet P, Somma F, Aloe P, Montereali RM, Vincenti MA, Polosan S*  
Lead incorporation mechanism in LiF crystals  
*Applied Physics Letters*, (2013), 102, 081, **3.844, 1.384**
43. *Dascalu G, Popescu T, Feder M, Caltun OF*  
Structural, electric and magnetic properties of  $\text{CoFe}_{1.8}\text{RE}_{0.2}\text{O}_4$  (RE=Dy, Gd, La) bulk materials  
*Journal of Magnetism and Magnetic Materials*, (2013), 333, pp. 69-74, **1.78, 0.475**

44. *Del Pino AP, Gyorgy E, Logofatu C, Duta A*  
Study of the deposition of graphene oxide by matrix-assisted pulsed laser evaporation,  
*Journal of Physics D: Applied Physics*, (2013), 46, 505309, **2.544**, **0.898**
45. *Diacon A, Rusen E, Mocanu A, Nistor LC*  
Polymer photonic crystal band-gap modulation using PbS quantum dots  
*Journal of Materials Chemistry C*, (2013), 1, pp. 4350-4357, **5.968**, **1.571**
46. *Dias M, Mateus R, Catarino N, Franco N, Nunes D, Correia JB, Carvalho PA, Hanada K, Sarbu C, Alves E*  
Synergistic helium and deuterium blistering in tungsten-tantalum composites  
*Journal of Nuclear Materials*, (2013), 442, pp.69-74, **2.052**, **0.585**
47. *Dorolti E, Trifu AV, Isnard O, Chicinas I, Tolea F, Valeanu M, Pop V*  
Influence of mechanical milling on the physical properties of SmCo<sub>5</sub>/Fe<sub>65</sub>Co<sub>35</sub> type hard/soft magnetic nanocomposite  
*Journal of Alloys and Compounds*, (2013), 560, pp.189-194, **2.289**, **0.507**
48. *Dumbrava A, Olar R, Badea M, Grecu MN, Patrascu F, Marutescu L, Stanica N*  
Synthesis and characterisation of Ni(II), Cu(II), and Zn(II) complexes with an acyclic Mannich base functionalised with thioglycolate moiety  
*Journal of Thermal Analysis and Calorimetry*, (2013), DOI:10.1007/s10973-013-3437-0, **1.604**, **0.239**
49. *Dumitru R, Papa F, Balint I, Culita DC, Munteanu C, Stanica N, Ianculescu A, Diamandescu L, Carp, O*  
Mesoporous cobalt ferrite: A rival of platinum catalyst in methane combustion reaction  
*Applied Catalysis A-General*, (2013), 467, pp.178-186, **3.903**, **0.929**
50. *Dumitru V, Costea S, Brezeanu M, Stan GE, Besleaga C, Galca AC, Ionescu G, Ionescu O*  
InN based water condensation sensors on glass and flexible plastic substrates  
*Sensors*, (2013), 13, pp. 16940-16949, 10.3390/s131216940, **1.953**
51. *Duta L, Oktar FN, Stan GE, Popescu-Pelin G, Serban N, Luculescu C, Mihailescu IN*  
Novel doped hydroxyapatite thin films obtained by pulsed laser deposition  
*Applied Surface Science*, (2013), 265, pp.41-49, **2.103**, **0.549**
52. *Feraru I, Vasiliu IC, Iordanescu R, Elisa M, Bartha C*  
Structural characterization of CdSe-doped sol-gel silicophosphate films  
*Surface Engineering and Applied Electrochemistry*, (2013), 49(6), pp.493-499, **0.332**
53. *Fernandes S, Pellemoine F, Tomut M, Avilov M, Bender M, Boulesteix M, Krause M, Mittig W, Schein M, Severin D, Trautmann C*  
In-situ electric resistance measurements and annealing effects of graphite exposed to swift heavy ions  
*Nuclear Instruments & Methods in Physics Research Section B-Beam Interactions with Materials and Atoms*, (2013), 314, pp.125-129, **1.211**, **0.364**
54. *Filip LD, Pintilie I, Nistor LC, Svensson BG*  
Evidence for resonant tunneling from interface states in as-grown n-4H-SiC/SiO<sub>2</sub> capacitors  
*Thin Solid Films*, (2013), 545, pp.22-28, **1.89**, **0.595**

55. Filip V, Filip LD, Okuyama F  
Miniature x-ray tubes: current state and future prospects  
*Journal of Instrumentation*, (2013), 8, T03005, **1.869**, **0.807**
56. Filipescu M, Stokker-Cheregi F, Colceag D, Nedelcea A, Birjega R, Nistor LC, Dinescu M  
Morphological and structural characterization of SiC based composite nanostructures  
*Applied Surface Science*, (2013), 278, pp.96-100, **2.103**, **0.549**
57. Fleaca CT, Dumitrache F, Morjan I, Alexandrescu R, Luculescu C, Niculescu A, Vasile E, Kuncser V  
Novel Fe@C-TiO<sub>2</sub> and Fe@C-SiO<sub>2</sub> water-dispersible magnetic nanocomposites  
*Applied Surface Science*, (2013), 278, pp.284-288, **2.103**, **0.549**
58. Florea M, Alifanti M, Kuncser V, Parvulescu VI  
Structural changes during toluene complete oxidation on supported EuFeO<sub>3</sub> monitored by in situ Eu-151 and Fe-57 Mossbauer spectroscopy  
*Catalysis Today*, (2013), 208, pp.56-59, **3.407**, **0.919**
59. Florian M, Gartner P, Gies C, Jahnke F  
Phonon-mediated off-resonant coupling effects in semiconductor quantum-dot lasers  
*New Journal of Physics*, (2013), 15, 035019, **4.177**, **2.097**
60. Frunza L, Preda N, Matei E, Frunza S, Ganea CP, Vlaicu AM, Diamandescu L, Dorogan A  
Synthetic fabrics coated with zinc oxide nanoparticles by electroless deposition: Structural characterization and wetting  
*Journal of Polymer Science Part B-Polymer Physics*, (2013), 51, pp.1427-1437, **1.531**, **0.57**
61. Galatanu M, Popescu B, Enculescu M, Tiseanu I, Craciunescu T, Galatanu A  
Direct sintering of SiC-W composites with enhanced thermal conductivity  
*Fusion Engineering and Design*, (2013), 88, pp.2598-2602, **1.49**, **0.374**
62. Galca AC, Socol G, Trinca LM, Craciun V  
Stoichiometry dependence of the optical properties of amorphous-like In<sub>x-w</sub>Ga<sub>w</sub>Zn<sub>1-x</sub>O<sub>1+0.5x</sub>-delta thin films  
*Applied Surface Science*, (2013), 281, pp.96-99, **2.103**, **0.549**
63. Ganea CP  
Electrode polarization and interface effects in liquid crystal systems with mobile ions: development of a model of bipolar diffusion  
*Central European Journal of Physics*, (2013), 11, pp.497-511, **0.909**, **0.268**
64. Georgescu S, Voiculescu AM, Matei C, Secu CE, Negrea RF, Secu M  
Ultraviolet and visible up-conversion luminescence of Er<sup>3+</sup>/Yb<sup>3+</sup> co-doped CaF<sub>2</sub> nanocrystals in sol-gel derived glass-ceramics  
*Journal of Luminescence*, (2013), 143, pp.150-156, **2.102**, **0.502**
65. Gheorghe NG, Lungu GA, Husanu MA, Costescu RM, Macovei D, Teodorescu CM  
Structure, reactivity, electronic configuration and magnetism of samarium atomic layers deposited on Si(001) by molecular beam epitaxy  
*Applied Surface Science*, (2013), 267, pp.106-111, **2.103**, **0.549**
66. Gherendi F, Nistor M, Antohe S, Ion L, Enculescu I, Mandache NB  
Self-assembled homojunction In<sub>2</sub>O<sub>3</sub> transparent thin-film transistors  
*Semiconductor Science and Technology*, (2013), 28, 085002, **1.723**, **0.569**

67. *Ghica D, Nistor SV*  
High thermal stability of the off-center paramagnetic  $\text{Fe}^{3+}$  ions in chlorinated  $\text{SrCl}_2:\text{Fe}^{2+}$  crystals  
*Romanian Reports in Physics*, (2013), 65, pp.825-831, **0.5**
68. *Ghita RV, Negrila CC, Cotirlan C, Logofatu C*  
On the passivation of gas surface by sulfide compounds  
*Digest Journal of Nanomaterials and Biostructures*, (2013), 8, pp.1335-1344, **1.2**
69. *Ghitulica C, Cernea M, Vasile BS, Andronescu E, Vasile OR, Dragoi C, Trusca R*  
Structural and electrical properties of NBT-BT0.08 ceramic prepared by the pyrosol method  
*Ceramics International*, (2013), 39, pp.5925-5930, **1.751, 0.533**
70. *Gingasu D, Mindru I, Patron L, Culita DC, Calderon-Moreno JM, Diamandescu L, Feder M, Oprea O*  
Precursor method-A nonconventional route for the synthesis of  $\text{ZnCr}_2\text{O}_4$  spinel  
*Journal of Physics and Chemistry of Solids*, (2013), 74, pp.1295-1302, **1.632, 0.431**
71. *Girtan M, Vlad A, Mallet R, Bodea MA, Pedarnig JD, Stanculescu A, Mardare D, Leontie L, Antohe S*  
On the properties of aluminium doped zinc oxide thin films deposited on plastic substrates from ceramic targets  
*Applied Surface Science*, (2013), 274, pp.306-313, **2.103, 0.549**
72. *Greuc MN, Macovei D, Ghica D, Logofatu C, Valsan S, Apostol NG, Lungu GA, Negrea RF, Piticescu RR*  
Co environment and magnetic defects in anatase  $\text{Co}_x\text{Ti}_{1-x}\text{O}_2$  nanopowders  
*Applied Physics Letters*, (2013), 102, 161909, **3.844, 1.384**
73. *Hrib LM, Boni AG, Chirila C, Pasuk I, Pintilie I, Pintilie L*  
Electrode interface control of the Schottky diode-like behavior in epitaxial  $\text{Pb}(\text{Zr}_{0.2}\text{Ti}_{0.8})\text{O}_3$  thin films: A critical analysis  
*Journal of Applied Physics*, (2013), 113, 214108, **2.168, 0.834**
74. *Iancu V, Baia M, Diamandescu L, Pap Z, Vlaicu AM, Danciu V, Baia L*  
Weighting the influence of  $\text{TiO}_2$  anatase/brookite ratio in  $\text{TiO}_2\text{-Ag}$  porous nanocomposites on visible photocatalytic performances  
*Materials Chemistry and Physics*, (2013), 141, pp.234-239, **2.234, 0.628**
75. *Iconaru SL, Ciobanu CS, Le Coustumer P, Predoi D*  
Structural characterization and magnetic properties of iron oxides biological polymers  
*Journal of Superconductivity and Novel Magnetism*, (2013), 26, pp.851-855, **0.65, 0.237**
76. *Iconaru SL, Motelica-Heino M, Predoi D*  
Study on europium-doped hydroxyapatite nanoparticles by Fourier transform infrared spectroscopy and their antimicrobial properties  
*Journal of Spectroscopy*, (2013), vol.2013, pp.1-10, **0.53**
77. *Iconaru SL, Prodan AM, Le Coustumer P, Predoi D*  
Synthesis and antibacterial and antibiofilm activity of iron oxide glycerol nanoparticles obtained by coprecipitation method  
*Journal of Chemistry*, (2013), vol.2013, pp. 1-6, **0.484**

78. *Iliut M, Gabudean AM, Leordean C, Simon T, Teodorescu CM, Astilean S*  
Riboflavin enhanced fluorescence of highly reduced graphene oxide  
*Chemical Physics Letters*, (2013), 586, pp.127-131, [2.337](#), [0.694](#)
79. *Khanal M, Vausselin T, Barras A, Bande O, Turcheniuk K, Benazza M, Zaitsev V, Teodorescu CM, Boukherroub R, Siriwardena A, Dubuisson J, Szunerits S*  
Phenylboronic-acid-modified nanoparticles: potential antiviral therapeutics  
*ACS Applied Materials & Interfaces*, (2013), 5, pp.12488-12498, [4.525](#), [1.274](#)
80. *Klanner R, Fretwurst E, Pintilie I, Schwandt J, Zhang JG*  
Study of high-dose X-ray radiation damage of silicon sensors  
*Nuclear Sociated Equipment*, (2013), 732, pp.117-121, [1.207](#)
81. *Klanner R, Becker J, Fretwurst E, Pintilie I, Pohlsen T, Schwandt J, Zhang JG*  
Challenges for silicon pixel sensors at the European XFEL  
*Nuclear Instruments & Methods in Physics Research Section A-Accelerators Spectrometers Detectors and Associated Equipment*, (2013), 730, pp.2-7, [1.207](#), [0.361](#)
82. *Lazanu I, Ciurea ML, Lazanu S*  
Analysis of defect formation in semiconductor cryogenic bolometric detectors created by heavy dark matter  
*Astroparticle Physics*, (2013), 44, pp.9-14, [3.216](#), [1.266](#)
83. *Lepadatu AM, Stoica T, Stavarache I, Teodorescu VS, Buca D, Ciurea ML*  
Dense Ge nanocrystal layers embedded in oxide obtained by controlling the diffusion-crystallization process  
*Journal of Nanoparticle Research*, (2013), 15, 1981, [3.287](#), [0.929](#)
84. *Li SY, Morasch J, Klein A, Chirila C, Pintilie L, Jia LC, Ellmer K, Naderer M, Reichmann K, Grotting M, Albe K*  
Influence of orbital contributions to the valence band alignment of  $\text{Bi}_2\text{O}_3$ ,  $\text{Fe}_2\text{O}_3$ ,  $\text{BiFeO}_3$ , and  $\text{Bi}_{0.5}\text{Na}_{0.5}\text{TiO}_3$   
*Physical Review B*, (2013), 88, 045428, [3.691](#), [1.426](#)
85. *Lungu GA, Apostol NC, Stoflea LE, Costescu RM, Popescu DG, Teodorescu CM*  
Room temperature ferromagnetic, anisotropic, germanium rich FeGe(001) alloys  
*Materials*, (2013), 6, pp. 612-625, [1.677](#), [0.494](#)
86. *Lupu AR, Popescu T*  
The noncellular reduction of MTT tetrazolium salt by  $\text{TiO}_2$  nanoparticles and its implications for cytotoxicity assays  
*Toxicology in Vitro*, (2013), 27, pp.1445-1450, [2.775](#), [0.636](#)
87. *Marcu A, Enculescu I, Vizireanu S, Birjega R, Porosnicu C*  
Single crystal ZnO nanowire luminescence shifting by nanostructured ZnO layers  
*Digest Journal of Nanomaterials and Biostructures*, (2013), 8, pp.597-605, [1.2](#)
88. *Matei E, Enculescu I, Toimil-Molares ME, Leca A, Ghica C, Kuncser V*  
Magnetic configurations of Ni-Cu alloy nanowires obtained by the template method  
*Journal of Nanoparticle Research*, (2013), 15, UNSP1863, [3.287](#), [0.929](#)

89. *Matei E, Enculescu M, Enculescu I*  
Single bath electrodeposition of samarium oxide/zinc oxide nanostructured films with intense, broad luminescence  
*Electrochimica Acta*, (2013), 95, pp.170-178, **3.832**, **0.981**
90. *Mazur M, Barras A, Kuncser V, Galatanu A, Zaitzev V, Turcheniuk KV, Woisel P, Lyskawa J, Laure W, Siriwardena A, Boukherroub R, Szunerits S*  
Iron oxide magnetic nanoparticles with versatile surface functions based on dopamine anchors  
*Nanoscale*, (2013), 5, pp.2692-2702, **5.914**, **1.561**
91. *Miclea CF, Hochheimer HD, Martin B, Miclea C, Ohtani T*  
Superconductivity and charge density wave formation in  $\text{Tl}_x\text{V}_6\text{S}_8$   
*New Journal of Physics*, (2013), 15, 083008, **4.177**, **2.097**
92. *Mihailescu CN, Pasuk I, Athanasopoulos GI, Luculescu C, Socol M, Saint-Martin R*  
Growth and structural characterization of orthorhombic and tetragonal  $\text{SrCuO}_2$  thin films  
*Applied Surface Science*, (2013), 278, pp.132-135, **2.103**, **0.549**
93. *Mihaiescu DE, Cristescu R, Dorcioman G, Popescu CE, Nita C, Socol G, Mihailescu IN, Grumezescu AM, Tamas D, Enculescu M, Negrea RF, Ghica C, Chifiriuc C, Bleotu C, Chrisey DB*  
Functionalized magnetite silica thin films fabricated by MAPLE with antibiofilm properties  
*Biofabrication*, (2013), 5, Article Number: 015007, **3.48**, **0.823**
94. *Miu L, Ivan I, Miu D, Mele P, Matsumoto K, Mikheenko P, Dang VS, Crisan A*  
High vortex depinning temperatures in YBCO films with BZO nanorods  
*Journal of Superconductivity and Novel Magnetism*, (2013), 26, pp.1167-1173, **0.65**, **0.237**
95. *Miu D, Ivan I, Crisan A, Mele P, Jakob G, Miu L*  
Inhibition of the detrimental double vortex-kink formation in thick  $\text{YBa}_2\text{Cu}_3\text{O}_7$  films with  $\text{BaZrO}_3$  nanorods  
*Superconductor Science & Technology*, (2013), 26, 045008/1-6, **2.662**, **0.81**
96. *Nagaraj B, Divya TK, Barasa M, Krishnamurthy NB, Dinesh R, Negrila CC, Predoi D*  
Phytosynthesis of gold nanoparticles using caesalpinia pulcherrima (peacock flower) flower extract and evaluation of their antimicrobial activities  
*Journal of Optoelectronics and Advanced Materials*, (2013), 15( 3-4), pp.299-304, **0.457**, **0.11**
97. *Nedelcu L, Scarisoreanu ND, Chirila C, Busuioc C, Banciu MG, Jinga SI, Dinescu M*  
Structural and dielectric properties of  $\text{Ba}(\text{X}_{1/3}\text{Ta}_{2/3})\text{O}_3$  thin films grown by RF-PLD  
*Applied Surface Science*, (2013), 278, pp.158-161, **2.103**, **0.549**
98. *Negoi A, Trotus IT, Steiner OM, Tudorache M, Kuncser V, Macovei D, Parvulescu VI, Coman SM*  
Direct synthesis of sorbitol and glycerol from cellulose over ionic Ru/Magnetite nanoparticles in the absence of external hydrogen  
*Chemosuschem*, (2013), 6, pp.2090-2094, **6.827**, **1.864**
99. *Nistor LC, Ghica C, Kuncser V, Pantelica D, Grob JJ, Epurescu G, Dinescu M*  
Microstructure-related magnetic properties in Co-implanted ZnO thin films  
*Journal of Physics D-Applied Physics*. (2013), 46, 065003, **2.544**, **0.898**

100. *Nistor LC, Nistor SV, Ghica D*  
Low temperature tem investigation of electron beam induced decomposition of nanocrystalline hydrozincite into ZnO  
*Romanian Reports in Physics*, (2013), 65, pp.186-192, **0.5**
101. *Nistor SV, Stefan M, Ghica D, Nistor LC*  
Nanosize induced effects in luminescent ZnS:Mn<sup>2+</sup> quantum dots  
*Radiation Measurements*, (2013), 56, pp.40-43, **1.177, 0.463**
102. *Nistor SV, Ghica D, Stefan M, Vlaicu I, Barascu JN, Bartha C*  
Magnetic defects in crystalline Zn(OH)(2) and nanocrystalline ZnO resulting from its thermal decomposition  
*Journal of Alloys and Compounds*, (2013), 548, pp.222-227, **2.289, 0.507**
103. *Nistor SV, Ghica D, Pintilie I, Manaila E*  
Paramagnetic point defects in pure and C-13 and O-17 implanted silicon for high energy particle detectors  
*Romanian Reports in Physics*, (2013), 65, pp.812-819, **0.5**
104. *Nistor SV, Ghica D, Stefan M, Nistor LC*  
Sequential thermal decomposition of the shell of cubic ZnS/Zn(OH)<sub>2</sub> core-shell quantum dots observed with Mn<sup>2+</sup> probing ions  
*Journal of Physical Chemistry C (Nano)*, (2013), 117, pp.22017-22028, **4.805, 1.339**
105. *Nita M, Ostabie B, Aldea A*  
Spectral and transport properties of the two-dimensional Lieb lattice  
*Physical Review B*, (2013), 87, 125428-1-125428-13, **3.691, 1.426**
106. *Pancotti A, Wang JL, Chen PX, Tortech L, Teodorescu CM, Frantzeskakis E, Barrett N*  
X-ray photoelectron diffraction study of relaxation and rumpling of ferroelectric domains in BaTiO<sub>3</sub>(001)  
*Physical Review B*, (2013), 87, 184116/1-10, **3.691, 1.426**
107. *Pap Z, Radu A, Hidi IJ, Melinte G, Diamandescu L, Popescu T, Baia L, Danciu V, Baia M*  
Behavior of gold nanoparticles in a titania aerogel matrix: Photocatalytic activity assessment and structure investigations  
*Chinese Journal of Catalysis*, (2013), pp.734-740, **1.171, 0.139**
108. *Patrascu F, Badea M, Grecu MN, Stanica N, Marutescu L, Marinescu D, Spinu C, Tigae C, Olar R*  
Thermal, spectral, magnetic and antimicrobial behaviour of new Ni(II), Cu(II) and Zn(II) complexes with a hexaazamacrocyclic ligand  
*Journal of Thermal Analysis and Calorimetry*, (2013), 113, pp.1421-1429, **1.604, 0.239**
109. *Podolean L, Kuncser V, Gheorghe N, Macovei D, Parvulescu VI, Coman SM*  
Ru-based magnetic nanoparticles (MNP) for succinic acid synthesis from levulinic acid  
*Green Chemistry*, (2013), 15, pp.3077-3082, **6.32, 1.497**
110. *Polosan S, Radu IC*  
Mechanisms of the charge transfer in IrQ(ppy)<sub>2</sub>-5Cl dual-emitter compounds  
*Journal of Nnanoscience & Nanotechnology*, (2013), 13(7), pp. 5203-5208, **1.563, 0.29**

111. *Popa AC, Stan GE, Husanu MA, Pasuk I, Popescu ID, Popescu AC, Mihailescu IN*  
Multi-layer haemocompatible diamond-like carbon coatings obtained by combined radio frequency plasma enhanced chemical vapor deposition and magnetron sputtering  
*Journal of Materials Science-Materials in Medicine*, (2013), 24, pp.2695-2707, **2.316**, **0.642**
112. *Popa NC, Lungu GA*  
Dependence of the strain diffraction line broadening on (hkl) and sample direction in textured polycrystals  
*Journal of Applied Crystallography*, (2013), 46, pp.391-395, **5.152**, **2.872**
113. *Popescu AC, Stan GE, Duta L, Dorcioman G, Iordache O, Dumitrescu I, Pasuk I, Mihailescu IN*  
Influence of a hydrophobin underlayer on the structuring and antimicrobial properties of ZnO films  
*Journal of Materials Science*, (2013), 48, pp.8329-8336, **2.015**, **0.583**
114. *Popescu DG, Husanu MA*  
Au-Ge bonding on a uniformly Au-covered Ge(001) surface  
*Physica Status Solidi-Rapid Research Letters*, (2013), 7, pp.274-277, **2.218**, **0.96**
115. *Popescu DG, Sterian P*  
Analysis of even and odd modes of a two-dimensional photonic crystal at Si/SiO<sub>2</sub>/Cu interface  
*Journal Optoelectronics Advanced Materials*, (2013), 15, pp. 610-614, **0.457**, **0.11**
116. *Popescu DG*  
Two dimensional photonic crystals with different symmetries for waveguides and resonant cavities applications  
*University Politehnica of Bucharest Scientific Bulletin-Series A-Applied Mathematics and Physics*, (2013), 75, pp.237-252, **0.300**
117. *Popescu M, Sava F, Lorinczi A, Velea A*  
Disorder in order: silicon versus grapheme  
*Physica Status Solidi B-Basic Solid State Physics*, (2013), 250, pp.1008-1010, **1.316**, **0.503**
118. *Popescu M, Velea A, Miclos S, Savastru D*  
Optics of microlenses created by irradiation of As<sub>2</sub>S<sub>3</sub> amorphous chalcogenide films with femtosecond laser pulses  
*Philosophical Magazine Letters*, (2013), 93, pp.213-220, **1.241**, **0.592**
119. *Popescu T, Lupu AR, Diamandescu L, Tarabasanu-Mihaila D, Teodorescu VS, Raditoiu V, Purcar V, Vlaicu AM*  
Effects of TiO<sub>2</sub> nanoparticles on the NO<sub>2</sub><sup>-</sup> levels in cell culture media analysed by Griess colorimetric methods  
*Journal of Nanoparticle Research*, (2013), 15:1449/17 pp. DOI 10.1007/s11051-013-1449-0, **3.287**, **0.929**
120. *Preda L, Negrila CC, Lazarescu MF, Enache M, Anastasescu M, Toader AM, Ionescu S, Lazarescu V*  
Ga and As competition for thiolate formation at p-GaAs(111) surfaces  
*Electrochimica Acta*, (2013), 104, pp.1-11, **3.832**, **0.981**
121. *Preda N, Enculescu M, Zgura I, Socol M, Matei E, Vasilache V, Enculescu I*  
Superhydrophobic properties of cotton fabrics functionalized with ZnO by electroless deposition  
*Materials Chemistry and Physics* (2013), 138(1), pp.253-261, **2.234**, **0.628**

122. *Preda N, Enculescu M, Enculescu I*  
Polymer sphere array assisted ZnO electroless deposition  
*Soft Materials*, (2013), 11, pp. 457-464, **1.154**, **0.313**
123. *Preda N, Enculescu M, Florica C, Costas A, Evangelidis A, Matei E, Enculescu I*  
Morphology-controlled synthesis of ZnO structures by a simple wet chemical method  
*Digest Journal of Nanomaterials and Biostructures*, (2013), 8, pp.1591-1600, **1.2**
124. *Preda S, Teodorescu VS, Musuc AM, Andronescu C, Zaharescu M*  
Influence of the TiO<sub>2</sub> precursors on the thermal and structural stability of titanate-based nanotubes  
*Journal of Materials Research*, (2013), 28, pp.294-303, **1.434**, **0.583**
125. *Prodan AM, Iconaru SL, Ciobanu CS, Chifiriuc MC, Stoicea M, Predoi D*  
Iron oxide magnetic nanoparticles: Characterization and toxicity evaluation by in vitro and in vivo assays  
*Journal of Nanomaterials*, (2013), vol.2013, pp.1-10, **1.376**, **0.471**
126. *Prodan AM, Iconaru SL, Chifiriuc CM, Bleotu C, Ciobanu CS, Motelica-Heino M, Sizaret S, Predoi D*  
Magnetic properties and biological activity evaluation of iron oxide nanoparticles  
*Journal of Nanomaterials*, (2013), vol.2013, pp.1-7, **1.376**, **0.471**
127. *Radu R, Fretwurst E, Klanner R, Lindstroem G, Pintilie I*  
Radiation damage in n-type silicon diodes after electron irradiation with energies between 1.5 MeV and 15 MeV  
*Nuclear Instruments & Methods in Physics Research Section A-Accelerators Spectrometers Detectors and Associated Equipment*, (2013), 730, pp.84-90, **1.207**
128. *Radutoiu N, Teodorescu CM*  
Satellites in Ce 3d X-ray photoelectron spectroscopy of ceria  
*Digest Journal of Nanomaterials Biostructures*, (2013), 8(4), pp. 1535-1549 , **1.2**
129. *Sandu V, Aldica G, Baibarac M, Enachescu M, Sandu E, Chee CY*  
Effect of tritiation on the superconducting properties of MgB<sub>2</sub>  
*Superconductor Science & Technology*, (2013), 26, 045014/1-8, **2.662**, **0.81**
130. *Sandu V, Aldica G, Damian R, Guo ZC, Suo HL*  
One-step synthesis and sintering of MgB<sub>2</sub> by spark plasma sintering  
*Journal of Superconductivity and Novel Magnetism*, (2013), 26, pp.361-369, **0.65**, **0.237**
131. *Sandu V, Chee CY*  
On the scaling law of the pinning force in MgB<sub>2</sub> superconducting composites with magnetic nano-inclusions  
*Journal of Superconductivity and Novel Magnetism*, (2013), 26, pp.125-131, **0.65**, **0.237**
132. *Sandu V, Nicolescu MS, Banciu MG, Ivan I*  
Synthesis, thermal and magnetic properties of the magnetically frustrated CoNb<sub>2</sub>O<sub>6</sub> compound  
*Advanced Science Letters*, (2013), 19, pp.622-625, **1.253**

133. *Sava F, Lorinczi A, Velea A, Simandan ID, Preda N, Socol G, Mihailescu IN, Zamfira CS, Cretu NC, Popescu M*  
Effect of thermal annealing on the structural and optical properties of Ag/As<sub>2</sub>S<sub>3</sub> multilayers  
*Chalcogenide Letters*, (2013), 10, pp.467-471, **0.834**
134. *Sava F, Popescu M, Lorinczi A, Velea A*  
Possible mechanism of Ag photodiffusion in a-As<sub>2</sub>S<sub>3</sub> thin films  
*Physica Status Solidi B-Basic Solid State Physics*, (2013), 250, pp.999-1003, **1.316, 0.503**
135. *Sava F, Velea A, Popescu M, Lörinczi A, Simandan ID, Vlaicu AM, Socol G, Mihailescu IN, Stefan N*  
Effect of broadband light on Ag/As<sub>2</sub>S<sub>3</sub> multilayers  
*Journal of Non - Crystalline Solids*, (2013), 377, pp.159 – 161, **1.537, 0.459**
136. *Schinteie G, Palade P, Vekas L, Iacob N, Bartha C, Kuncser V*  
Volume fraction dependent magnetic behaviour of ferrofluids for rotating seal applications  
*Journal of Physics D-Applied Physics*, (2013), 46/(39), 395501/8p, **2.544, 0.898**
137. *Schinteie G, Kuncser V, Palade P, Dumitrache F, Alexandrescu R, Morjan I, Filoti G*  
Magnetic properties of iron-carbon nanocomposites obtained by laser pyrolysis in specific configurations  
*Journal of Alloys and Compounds*, (2013), 564, pp.27-34 , **2.289, 0.507**
138. *Scocioreanu M, Mihut L, Baibarac M, Baltog I*  
Photoluminescence decay time studies on ZnS in cubic and hexagonal phase and its mechanic-chemical interaction with polyaniline  
*Physica Status Solidi B-Basic Solid State Physics*, (2013), 250, pp.1426-1431, **1.489, 0.503**
139. *Schub K, Gartner P, Jahnke F*  
Combined influence of carrier-phonon and Coulomb scattering on the quantum-dot population dynamics  
*Physical Review B*, (2013), 87, 035301/1-L, **3.691, 1.426**
140. *Secu M, Secu CE, Sima M, Negrea RF, Bartha C, Dinescu M, Damian V*  
Luminescent Eosin Y-SiO<sub>2</sub> hybrid nano and microrods prepared by sol-gel template method  
*Journal of Luminescence*, (2013), 143, pp.89-92, **2.102, 0.502**
141. *Secu CE, Negrea RF, Secu M*  
Eu<sup>3+</sup> probe ion for rare-earth dopant site structure in sol-gel derived LiYF<sub>4</sub> oxyfluoride glass-ceramic  
*Optical Materials*, (2013), 35, pp.2456-2460, **2.023, 0.562**
142. *Secu CE, Bartha C, Polosan S, Secu M*  
Thermally activated conversion of a silicate gel to an oxyfluoride glass ceramic: optical study using Eu<sup>3+</sup> probe ion  
*Journal of Luminescence*, (2013), 146, pp.543, **2.102, 0.502**
143. *Sima M, Vasile E, Sima A*  
Photoanode for dye-sensitized solar cell based on electrophoretically deposited ZnO layer  
*Digest Journal of Nanomaterials and Biostructures*, (2013), 8, pp.757-763, **1.2**

144. *Sima M, Vasile E, Sima M*  
ZnO films and nanorod/shell arrays electrodeposited on PET-ITO electrodes  
*Materials Research Bulletin*, (2013), 48, pp.1581-1586, [2.105](#), [0.546](#)
145. *Simandan ID, Sava F, Popescu M, Lorinczi A*  
Complex Langmuir-Blodgett films based on barium stearate multilayers with carbon nanotubes and As<sub>2</sub>S<sub>3</sub> nanoparticles  
*Chalcogenide Letters*, (2013), 10, pp.481-484, [0.834](#)
146. *Smaranda I, Baibarac M, Baltog I, Mevellec JY, Lefrant S*  
Spectroelectrochemical properties of the single walled carbon nanotubes functionalized with polydiphenylamine doped with heteropolyanions  
*Journal of Solid State Chemistry*, (2013), 197, pp.352-360, [2.159](#), [0.67](#)
147. *Socol G, Preda N, Socol M, Sima L, Luculescu CR, Sima F, Miroiu M, Axente E, Visan A, Stefan N, Cristescu R, Dorcioman G, Stanculescu A, Radulescu L, Mihailescu IN*  
Maple deposition of plga micro- and nanoparticles embedded into polymeric coatings  
*Digest Journal of Nanomaterials and Biostructures*, (2013), 8(2), pp.621-630, [1.2](#)
148. *Stan GE, Popa AC, Galca AC, Aldica G, Ferreira JMF*  
Strong bonding between sputtered bioglass-ceramic films and Ti-substrate implants induced by atomic inter-diffusion post-deposition heat-treatments  
*Applied Surface Science*, (2013), 280, pp.530-538, [2.103](#), [0.549](#)
149. *Stanoiu A, Simion CE, Somacescu S*  
NO<sub>2</sub> sensing mechanism of ZnO-Eu<sub>2</sub>O<sub>3</sub> binary oxide under humid air conditions  
*Sensors and Actuators B-Chemical*, (2013), 186, pp.687-694, [3.898](#), [0.801](#)
150. *Stavarache I, Lepadatu AM, Stoica T, Ciurea ML*  
Annealing temperature effect on structure and electrical properties of films formed of Ge nanoparticles in SiO<sub>2</sub>  
*Applied Surface Science*, (2013), 285, pp.175-179, [2.103](#), [0.549](#)
151. *Stefan M, Nistor SV, Ghica D*  
Correlation of lattice disorder with crystallite size and the growth kinetics of Mn<sup>2+</sup> doped ZnO nanocrystals probed by electron paramagnetic resonance  
*Crystal Growth & Design*, (2013), 13, pp.1350-1359, [4.72](#), [0.912](#)
152. *Steinke L, Mitsumoto K, Miclea CF, Weickert F, Donni A, Akatsu M, Nemoto Y, Goto T, Kitazawa H, Thalmeier P, Brando M*  
Role of hyperfine coupling in magnetic and quadrupolar ordering of Pr<sub>3</sub>Pd<sub>20</sub>Si<sub>6</sub>  
*Physical Review Letters*, (2013), 111, 077202, [7.37](#), [3.511](#)
153. *Steinhoff A, Kurtze H, Gartner P, Florian M, Reuter D, Wieck AD, Bayer M, Jahnke F*  
Combined influence of Coulomb interaction and polarons on the carrier dynamics in InGaAs quantum dots  
*Physical Review B*, (2013), 88, 205309/1-13, [3.691](#), [1.426](#)
154. *Teodorescu VS, Maraloiu AV, Stavarache I, Lepadatu AM, Ciurea ML*  
Transmission electron microscopy study of ge nanoparticles formed in GeSiO films by annealing in hydrogen  
*Digest Journal of Nanomaterials and Biostructures*, (2013), 8, pp.1771-1780, [1.2](#)

155. *Tiseanu I, Zani L, Craciunescu T, Cotorobai F, Dobrea C, Sima A*  
Characterization of superconducting wires and cables by X-ray micro-tomography  
*Fusion Engineering and Design*, (2013), 88, pp.1613-1618, **1.49**, **0.374**
156. *Trotus IT, Teodorescu CM, Parvulescu VI, Marcu IC*  
Enhancing oxidative dehydrogenation selectivity of ceria-based catalysts with phosphorus as additive  
*Chemcatchem*, (2013), 5, pp.757-765, **5.207**, **1.352**
157. *Tutunaru B, Samide A, Negriila C*  
Thermal analysis of corrosion products formed on carbon steel in ammonium chloride solution  
*Journal of Thermal Analysis and Calorimetry*, (2013), 111, pp.1149-1154, **1.604**, **0.239**
158. *Ulmeanu M, Anghel I, Jipa F, Filipescu M, Enculescu M, Zamfirescu M*  
Silicon bump arrays by near-field enhanced femtosecond laser irradiation in fluorine liquid precursors  
*Applied Surface Science*, (2013), 278, pp.301-304, **2.103**, **0.549**
159. *Ulmeanu M, Anghel I, Filipescu M, Luculescu C, Enculescu M, Zamfirescu M*  
Periodic arrays of nanostructures in silicon and gallium arsenide by near-field enhanced laser irradiation in liquid precursors  
*Colloids and Surfaces A-Physicochemical and Engineering Aspects*, (2013), 418, pp.47-51, **2.236**, **0.587**
160. *Vasilache V, Lungu GA, Logofatu C, Medianu RV, Teodorescu CM*  
Ferromagnetism and reactivity of Fe deposited on GaAs(001) by magnetron sputtering  
*Digest Journal of Nanomaterials and Biostructures*, (2013), 8, pp.255-261, **1.2**
161. *Vasile BS, Andronescu E, Ghitulica C, Vasile OR, Curechiu L, Scurtu R, Vasile E, Trusca R, Pall L, Aldica GV*  
Microstructure and electrical properties of zirconia and composite nanostructured ceramics sintered by different methods  
*Ceramics International*, (2013), 39(3), pp. 2535-2543, **1.751**, **0.533**
162. *Velea A, Popescu M, Lorinczi A, Simandan ID, Vlaicu AM, Socol G, Mihailescu IN, Stefan N*  
Effect of broadband light on Ag/As<sub>2</sub>S<sub>3</sub> multilayers  
*Journal of Non-Crystalline Solids*, (2013), 377, pp.150-161, **1.537**, **0.459**
163. *Vizireanu S, Dinescu G, Nistor LC, Baibarac M, Ruxanda G, Stancu M, Ciuparu D*  
Stability of carbon nanowalls against chemical attack with acid solutions  
*Physica E-Low-Dimensional Systems & Nanostructures*, (2013), 47, pp.59-65, **1.532**, **0.418**
164. *Vlaicu ID, Constand M, Olar R, Marinescu D, Grecu MN, Lazar V, Chifiriuc MC, Badea M*  
Thermal stability of new biologic active copper(II) complexes with 5,6-dimethylbenzimidazole  
*Journal of Thermal Analysis and Calorimetry*, (2013), 113, pp.1369-1377, **1.604**, **0.239**
165. *Voicescu M, Angelescu DG, Ionescu S, Teodorescu VS*  
Spectroscopic analysis of the riboflavin-serum albumins interaction on silver nanoparticles  
*Journal of Nanoparticle Research*, (2013), 15:1555, **3.287**, **0.929**

166. Wu Y, Dujardin C, Granger P, Tiseanu C, Sandu S, Kuncser V, Parvulescu VI  
Spectroscopic investigation of iron substitution in  $\text{EuCoO}_3$  related impact on the catalytic properties in the high-temperature  $\text{N}_2\text{O}$  decomposition  
*Journal of Physical Chemistry C*, (2013), 117, pp.13989-13999, **4.805**, **1.339**
167. Zhao PH, Yan W, Han YL, Shen SC, Aldica G, Sandu V, Badica P, Nie JC  
Enhancement of superconductivity in quenched alpha-FeSe flakes  
*Journal of Superconductivity and Novel Magnetism*, (2013), 26(12), pp.3349-3353, **0.65**, **0.237**
168. Zgura I, Moldovan R, Negrila CC, Frunza S, Cotorobai VF, Frunza L  
Surface free energy of smooth and dehydroxylated fused quartz from contact angle measurements using some particular organics as probe liquids  
*Journal of Optoelectronics and Advanced Materials*, (2013), 15, pp.627-634, **0.457**, **0.11**

**Conference Proceedings**

1. *Apostol I, Damian V, Damian R, Nistor LC, et al.*  
Laser induced breakdown spectroscopy surface analysis correlated with the process of nanoparticle production by laser ablation in liquids  
In: *Conference: 6th International Conference on Laser Probing (LAP) Location: Paris, FRANCE Date: JUN 04-08, 2012*  
Hyperfine Interactions Volume: 216 Issue: 1-3 Pages: 139-143 Published: APR 2013
2. *Bibicu I, Bulea C*  
Investigation of Fe-C steel galvanization by Mössbauer spectroscopy  
In: *International Conference on Applications of Mössbauer Spectroscopy ICAME, Opatija, Croatia, Sep. 1-6, 2013, Book of Abstracts, P10-7, p. 298*
3. *Blagoeva DT, Opschoor J, Pintsuk G, Sarbu C, et al.*  
Development and qualification of tungsten and tungsten alloys for fusion  
In: *Conference: 20th American-Nuclear-Society (ANS) Topical Meeting on the Technology of Fusion Energy (TOFE) Location: Nashville, TN Date: AUG 27-31, 2012*  
Fusion Science and Technology Volume: 64 Issue: 2 Pages: 203-210 Published: AUG 2013
4. *Choina J, Kosslick H, Fischer Ch, Flechsig GU, Schulz A, Frunza L, Frumosu F, Diamandescu L, Frunza S, Ganea CP*  
Titania P25 photocatalyst still a challenge: complex characterization and activity in thabatementof ibuprofen as a model compound  
In: *Intern. Symp. Rom. Catal. Society RomCat 2013, Cluj-Napoca, Romania, May 29-31, 2013, Book of Abstracts pp78-79*
5. *Cristescu R, Popescu C, Dorcioman G, Enculescu M*  
Antimicrobial activity of biopolymer-antibiotic thin films fabricated by advanced pulsed laser methods  
In: *Conference: Spring Meeting of the European-Materials-Research-Society (E-MRS) / Symposium N / Symposium O / Symposium V on Laser Materials Processing for Micro and Nano Applications Location: Strasbourg, FRANCE Date: MAY 14-18, 2012*  
Applied Surface Science Volume: 278 Pages: 211-213 Published: AUG 1 2013
6. *Diamandescu L, Feder M, Popescu T*  
Mössbauer study on the GaFeO<sub>3</sub> formation by high energy ball milling and post annealing pathway  
In: *International Conference on Applications of Mössbauer Spectroscopy ICAME, Opatija, Croatia, Sep. 1-6, 2013, Book of Abstracts, P10-7 p. 298*
7. *Filip LD, Pintilie I, Svensson BG*  
Evidence of tunneling in n-4H-SiC/SiO<sub>2</sub> capacitors at low temperatures  
Edited by: Lebedev, AA; Davydov, SY; Ivanov, PA; et al.  
In: *Conference: 9th European Conference on Silicon Carbide and Related Materials (ECSCRM 2012) Location: St Petersburg, RUSSIA Date: SEP 02-06, 2012*  
Silicon Carbide and Related Materials 2012 Book Series: Materials Science Forum Volume: 740-742 Pages: 557-560 Published: 2013

8. *Filipescu M, Stokker-Cheregi F, Colceag D, Nistor LC et al.*  
**Morphological and structural characterization of SiC based composite nanostructures**  
In: *Conference: Spring Meeting of the European-Materials-Research-Society (E-MRS) / Symposium N / Symposium O / Symposium V on Laser Materials Processing for Micro and Nano Applications Location: Strasbourg, FRANCE Date: MAY 14-18, 2012*  
Sponsor(s): European Mat Res Soc (E-MRS)  
Applied Surface Science Volume: 278 Pages: 96-100 Published: AUG 1 2013
9. *Fleaca C T, Dumitrache F, Morjan Ion, Kuncser V et al.*  
Novel Fe@C-TiO<sub>2</sub> and Fe@C-SiO<sub>2</sub> water-dispersible magnetic nanocomposites  
In: *Conference: Spring Meeting of the European-Materials-Research-Society (E-MRS) / Symposium N / Symposium O / Symposium V on Laser Materials Processing for Micro and Nano Applications Location: Strasbourg, FRANCE Date: MAY 14-18, 2012*  
Sponsor(s): European Mat Res Soc (E-MRS)  
Applied Surface Science Volume: 278 Pages: 284-288 Published: AUG 1 2013
10. *Galatanu M, Popescu B, Enculescu M, Galatanu A, et al.*  
Direct sintering of SiC-W composites with enhanced thermal conductivity  
In: *Conference: 27th Symposium on Fusion Technology (SOFT) Location: Liege, BELGIUM Date: SEP 24-28, 2012*  
Sponsor(s): Trilateral Euregio Cluster; SCK CEN; ERM KMS; FZJ; FOM  
Fusion Engineering and Design Volume: 88 Issue: 9-10 Pages: 2598-2602 Published: OCT 2013
11. *Iconaru SL, Ciobanu CS, Le Coustumer P, Predoi D*  
Structural characterization and magnetic properties of iron oxides biological polymers  
In: *Conference: 3rd International Conference on Superconductivity and Magnetism (ICSM) Location: Istanbul, TURKEY Date: APR 29-MAY 04, 2012*  
Journal of Superconductivity and Novel Magnetism Volume: 26 Issue: 4 Special Issue: SI Pages: 851-855 Published: APR 2013
12. *Klanner R, Fretwurst E, Pintilie I, et al.*  
Study of high-dose X-ray radiation damage of silicon sensors  
In: *Conference 13th Vienna Conference on Instrumentation Location: Tech Univ Vienna, Vienna, AUSTRIA Date: FEB 11-15, 2013*  
Sponsor(s): Austrian Fed Minist Sci & Res; Int Atom Energy Agcy; European Phys Soc; Vienna Convent Bur  
Nuclear Instruments & Methods in Physics Research Section A-Accelerators Spectrometers Detectors and Associated Equipment Volume: 732 Pages: 117-121 Published: DEC 21 2013
13. *Klanner R, Becker J, Fretwurst E, Pintilie I, et al.*  
Challenges for silicon pixel sensors at the European XFEL  
In: *Conference: 9th International Conference on Radiation Effects on Semiconductor Materials, Detectors and Devices (RESMDD) Location: Dipartimento Fis Astronomia, Sezione Astronomia Sci Spazio, Florence, ITALY Date: OCT 09-12, 2012*  
Nuclear Instruments & Methods in Physics Research Section A-Accelerators Spectrometers Detectors and Associated Equipment Volume: 730 Pages: 2-7 Published: DEC 1 2013

14. *Mihailescu CN, Pasuk I, Athanasopoulos GI, et al.*  
Growth and structural characterization of orthorhombic and tetragonal SrCuO<sub>2</sub> thin films  
In: *Conference: Spring Meeting of the European-Materials-Research-Society (E-MRS) / Symposium N / Symposium O / Symposium V on Laser Materials Processing for Micro and Nano Applications* Location: Strasbourg, FRANCE Date: MAY 14-18, 2012  
Applied Surface Science Volume: 278 Pages: 132-135 Published: AUG 1 2013
15. *Miu L, Ivan I, Miu D, et al.*  
High Vortex depinning temperatures in YBCO films with BZO nanorods  
In: *Conference: 3rd International Conference on Superconductivity and Magnetism (ICSM)* Location: Istanbul, TURKEY Date: APR 29-MAY 04, 2012  
Journal of Superconductivity and Novel Magnetism Volume: 26 Issue: 4 Special Issue: SI Pages: 1167-1173 Published: APR 2013
16. *Nedelcu L, Scarisoreanu N D, Chirila C, Busuioc C, Banciu MG, et al.*  
Structural and dielectric properties of Ba(X<sub>1/3</sub>Ta<sub>2/3</sub>) O<sub>3</sub> thin films grown by RF-PLD  
In: *Conference: Spring Meeting of the European-Materials-Research-Society (E-MRS) / Symposium N / Symposium O / Symposium V on Laser Materials Processing for Micro and Nano Applications* Location: Strasbourg, FRANCE Date: MAY 14-18, 2012  
Applied Surface Science Volume: 278 Pages: 158-161 Published: AUG 1 2013
17. *Nistor SV, Stefan M, Ghica D, Nistor LC, et al.*  
Nanosize induced effects in luminescent ZnS: Mn<sup>2+</sup> quantum dots  
In: *Conference: 8th International Conference on Luminescence Detectors and Transformers of Ionizing Radiation (LUMDETR)* Location: Martin Luther Univ Halle Wittenberg, Halle, GERMANY Date: SEP 10-14, 2012  
Radiation Measurements Volume: 56 Special Issue: SI Pages: 40-43 Published: SEP 2013
18. *Palade, Catalin; Lepadatu, Ana-Maria; Stavarache I, Teodorescu VS, Ciurea ML et al.*  
Conduction mechanism versus annealing in SiO<sub>2</sub> films with Ge nanoparticles  
In: *Conference: 36th International Semiconductor Conference (CAS)* Location: Natl Inst Res & Dev Microtechnologies, Sinaia, ROMANIA Date: OCT 14-16, 2013  
International Semiconductor Conference (CAS), VOLS 1-2 Book Series: International Semiconductor Conference Pages: 31-34 Published: 2013
19. *Palade C, Slav A, Ciurea M L, Lazanu S*  
Effect of bismuth irradiation on crystalline silicon  
In: *Conference: 36th International Semiconductor Conference (CAS)* Location: Natl Inst Res & Dev Microtechnologies, Sinaia, ROMANIA Date: OCT 14-16, 2013  
International Semiconductor Conference (CAS), VOLS 1-2 Book Series: International Semiconductor Conference Pages: 73-76 Published: 2013
20. *Polosan S, Radu IC*  
Mechanisms of the charge transfer in IrQ(ppy)(2)-5Cl dual-emitter compound  
In: *Conference: Symposium H on Organic and Hybrid Materials for Flexible Electronics - Properties and Applications at Spring Meeting of the European-Materials-Research-Society (E-MRS)* Location: Strasbourg, FRANCE Date: MAY 14-18, 2012  
Journal of Nanoscience and Nanotechnology Volume: 13 Issue: 7 Pages: 5203-5208 Published: JUL 2013

21. **Radu R, Fretwurst, E, Klanner R, Pintilie I, et al.**  
Radiation damage in n-type silicon diodes after electron irradiation with energies between 1.5 MeV and 15 MeV  
In: *Conference: 9th International Conference on Radiation Effects on Semiconductor Materials, Detectors and Devices (RESMDD) Location: Dipartimento Fis Astronomia, Sezione Astronomia Sci Spazio, Florence, ITALY Date: OCT 09-12, 2012*  
Nuclear Instruments & Methods in Physics Research Section A-Accelerators Spectrometers Detectors and Associated Equipment Volume: 730 Pages: 84-90 Published: DEC 1 2013
22. **Sava F, Lorinczi A, Velea A, et al.**  
Effect of thermal annealing on the structural and optical properties of Ag/As<sub>2</sub>S<sub>3</sub> multilayers  
In: *Conference: 6th International Conference on Amorphous and Nanostructured Chalcogenides Location: Brasov, ROMANIA Date: JUN 24-28, 2013*  
Chalcogenide Letters Volume: 10 Issue: 11 Pages: 467-471 Published: NOV 2013
23. **Simandan I D, Sava F, Popescu M, et al**  
Complex Langmuir-Blodgett films based on barium stearate multilayers with carbon nanotubes and As<sub>2</sub>S<sub>3</sub> nanoparticles  
In: *Conference: 6th International Conference on Amorphous and Nanostructured Chalcogenides Location: Brasov, ROMANIA Date: JUN 24-28, 2013*  
Chalcogenide Letters Volume: 10 Issue: 11 Pages: 481-484 Published: NOV 2013
24. **Tiseanu I, Zani Louis, Craciunescu T, Cotorobai F, et al.**  
Characterization of superconducting wires and cables by X-ray micro-tomography  
In: *Conference: 27th Symposium on Fusion Technology (SOFT) Location: Liege, BELGIUM Date: SEP 24-28, 2012*  
Fusion Engineering and Design Volume: 88 Issue: 9-10 Pages: 1613 1618 Published: OCT 2013
25. **Teodorescu VS, Ghica C, Maraloiu AV, Lepadatu AM, Stavarache I, Ciurea ML, Scarisoreanu ND, Andrei A, Dinescu M**  
Nanoscale fast diffusion in laser irradiated SiGe thin films  
In: *Proc. of NSTI-Nanotech, May 12-16, 2013, Washington, USA, vol.1, pp 109-112*
26. **Teodorescu V S, Maraloiu AV, Blanchin M-G, et al.**  
Structure and dielectric properties of low fluence excimer laser annealing of sol-gel HfO<sub>2</sub> thin films deposited on Si wafer  
In: *Conference: 36<sup>th</sup> International Semiconductor Conference (CAS) Location: Natl Inst Res & Dev Microtechnologies, Sinaia, ROMANIA Date: OCT 14-16, 2013*  
International Semiconductor Conference (CAS), VOLS 1-2 Book Series: International Semiconductor Conference Pages: 77-80 Published: 2013
27. **Ulmeanu M, Anghel I, Jipa F, Filipescu M, Enculescu M, et.al.**  
Silicon bump arrays by near-field enhanced femtosecond laser irradiation in fluorine liquid precursors  
In: *Conference: Spring Meeting of the European-Materials-Research-Society (E-MRS) / Symposium N / Symposium O / Symposium V on Laser Materials Processing for Micro and Nano Applications Location: Strasbourg, FRANCE Date: MAY 14-18, 2012*  
Applied Surface Science Volume: 278 Pages: 301-304 Published: AUG 1 2013

28. *Velea A, Popescu M, Lorinczi A, Simandan ID, Vlaicu AM, et al.*

Effect of broadband light on Ag/As<sub>2</sub>S<sub>3</sub> multilayers

In: *Conference: 18th International Symposium on Non-Oxide and New Optical*

*Glasses Location: Saint Malo, FRANCE Date: JUL 01-05, 2012*

Journal of Non-Crystalline Solids Volume: 377 Special Issue: SI Pages: 159-161

Published: OCT 1 2013

**Contributed Presentations**

1. *Aldea A*  
Topological properties of graphene and other 2D lattices  
Workshop-ul New trends in the research of carbon based nanomaterials, Bucharest, Romania  
22-23 April 2013, Talk
2. *Aldica GV, Kumakura H, Ye S, Badica P*  
Thermal analysis in vacuum and Ar of MgB<sub>2</sub> based tapes  
2<sup>nd</sup> Central and Eastern European Conference on Thermal Analysis and Calorimetry (CEEC-TAC2), Vilnius, Lithuania  
27-30 August 2013, Poster
3. *Aldica GV, Popa S, Enculescu M, Batalu D, Badica P*  
MgB<sub>2</sub> obtained by ex-situ Spark Plasma Sintering: addition of Ho<sub>2</sub>O<sub>3</sub> with different morphology  
EUCAS 2013, Genoa, Italy  
15-19 September 2013, Poster
4. *Apostol NG, Stoflea LE, Lungu GA, Tache CA, Tanase LC, Chirila C, Pintilie L, Teodorescu CM*  
Potential of ferroelectric surfaces for selective adsorption and surface reactions  
10<sup>th</sup> International Symposium of The Romanian Catalysis Society ROMCAT 2013, Cluj-Napoca, Romania  
29-31 May 2013, Talk
5. *Axente E, Socol G, Beldjilali S, Luculescu CR, Galca AC, Ristoscu C, Craciun V, Mihailescu IN, and Hermann J*  
Accurate quantitative laser-induced breakdown spectroscopy analysis applied to IZO combinatorial library thin films  
E-MRS Spring Meeting, Strasbourg, France  
27-31 May 2013, Poster
6. *Axente E, Hermann J, Socol G, Mercadier L, Beldjilali SD, Cirisan M, Luculescu CR, Pantelica D, Ionescu P, Galca AC, Craciun V*  
Accurate analysis of amorphous indium zinc oxide thin films via laser-induced breakdown spectroscopy  
E-MRS Fall Meeting, Warsaw, Poland  
16-20 September 2013, Poster
7. *Axente E, Sima F, Grumezescu V, Nita C, Socol M, Zgura I, Sima L E, Chiritoiu G, Mihailescu IN, Socol G*  
Kinetic release of Lysozyme embedded in biodegradable PCL/PLA and PCL/PLGA composite coatings synthesized by MAPLE technique  
SPRING 13 R: Nano-engineered bioactive interfaces, E-MRS Spring Meeting, Strasbourg, France  
May 27-31 2013, Poster

8. *Bacsei R, Nedelcu L, Alexandru HV*  
Peculiar dielectric characteristic of  $Ba_{1-x}Sr_xTiO_3$  ceramics of technological importance  
International Balkan Workshop on Applied Physics (IBWAP) - 13<sup>th</sup> Edition, Constanta, Romania  
6-8 July 2013, Poster
9. *Badica P, Burdusel M, Aldica GV, Popa S, Enculescu M, Pasuk I*  
BN addition to  $MgB_2$  superconductor obtained by ex-situ spark plasma sintering technique  
EUCAS 2013, Genoa, Italy  
15-19 September 2013, Poster
10. *Baibarac M, Baltog I, Scocioreanu M, Magrez A, Schur D, Zaginaichenko S. Yu*  
Carbon nanotubes functionalized with poly(N-vinyl carbazole) doped with heteropolyanions as electrode materials for supercapacitors  
International Conference on Diamond and Carbon Materials, Riva del Garda, Italy  
2-5 September 2013, Talk
11. *Baibarac M, Baltog I, Scocioreanu M, Velula T, Mevellec JY, Lefrant S*  
Electrochemical functionalization of carbon nanotubes with copolymers based on 2, 2'-bithiophene and pyrene evidenced by Raman scattering and IR spectroscopy  
5th edition ElecNano, Bordeaux, France  
15-17 May 2013, Poster
12. *Baltog I, Baibarac M, Lefrant S, Mevellec JY*  
Electrochemical functionalization of HIPCO SWNTs with poly(3,4-ethylenedioxythiophene) evidenced by anti-Stokes and Stokes SERS studies  
5th edition ElecNano, , Bordeaux, France  
15-17 May 2013, Poster
13. *Baltog I, Baibarac M, Popa C, Scocioreanu M, Mibut L*  
Composite materials based on poly(3,4-ethylenedioxythiophene) and reduced graphene oxide as active material for supercapacitors  
International Conference on Diamond and Carbon Materials, Riva del Garda, Italy  
2-5 September 2013, Poster
14. *Besleaga Stan C, Antohe S, Barquinha P, Fortunato E, Martins R*  
The origins of the electrical instabilities in a-IGZO thin film transistors  
PhD-workshop "Electronically-active Interface", Ameland, Netherland  
16-21 June 2013, Poster
15. *Besleaga Stan C, Antohe S, Stan GE, Galca AC, Barquinha P, Fortunato E, Martins R*  
Fully transparent transistors based on AlN-gate dielectric and IGZO-channel semiconductor  
International Balkan Workshop on Applied Physics (IBWAP) - 13<sup>th</sup> Edition, Constanta, Romania  
4-6 July 2013, Talk
16. *Bibicu I, Bulea C*  
Investigation of Fe-C steel galvanization by Mössbauer spectroscopy  
International Conference on the Applications of the Mössbauer Effect (ICAME 2013), Opatija, Croatia  
1-6 September 2013, Poster

17. *Boni AG, Chirila C, Pintilie I, Pintilie L, Preziosi D, Deniz H, Alexe M*  
Charge transport mechanism in epitaxial  $\text{Pb}(\text{Zr,Ti})\text{O}_3$  films with different electrodes  
PhD-workshop “Electronically-active Interface”, Ameland, Netherlands  
16–21 June 2013, Poster
18. *Boni G A, Pintilie L, Pintilie I, Preziosi D, Alexe M, Hesse D*  
Conduction mechanism in LSMO-ferroelectric-LSMO heterostructures  
EUROMAT, Sevilla, Spain  
8-13 September 2013, Talk
19. *Bradu C, Papa F, Balint I, Olaru EA, Căpăț C, Frunză L*  
Reductive dechlorination of mono- and dichlorophenols in aqueous phase over Pd-Cu nanostructured catalysts  
Conferinta Internationala de Chimie Fizica ROMPHYSICHEM 2013, Academia Romana, Bucharest, Romania  
11-13 September 2013, Poster
20. *Bradu C, Capat C, Ruta F, Olaru EA, Enculescu M, Diamandescu L, Negri CC, Papa F, Balint I, Udrea I*  
Pd and Pd-Cu catalysts supported on a macroporous strong base anion resin for the liquid phase reduction of nitrate  
In XIth European Congress on Catalysis (EUROPACAT XI), Lyon, France  
1-6 September 2013, Poster
21. *Cernea M, Trupina L, Vasile BS, Pasuk I, Pintilie L*  
Nanowires of BNT-BT<sub>0.08</sub> doped with BiFeO<sub>3</sub> derived from sol-gel precursor  
IXVII International Sol-Gel Conference (SG2013), Madrid, Spain  
25-30 August 2013, Poster
22. *Cernea M, Baldisserrri C, Ibanescu AG, Negrea R, Capiani C, Galassi C*  
Barium ferrite doped-SrFe<sub>12</sub>O<sub>19</sub>: sol-gel synthesis and electro-magnetic characterization  
Conference COST MPO904 Action, Faenza, Italy  
22-23 April 2013, Poster
23. *Chirila C, Boni G, Hrib L, Galca AC, Negrea R, Pasuk I, Kuncser V, Ghica C, Pintilie I, Pintile L*  
The influence of CoFe<sub>2</sub>O<sub>4</sub> layer on  $\text{Pb}(\text{Zr}_{0.2}\text{Ti}_{0.8})\text{O}_3$  and BaTiO<sub>3</sub>, Epitaxial thin films deposited by Pulsed Laser Deposition  
International Balkan Workshop on Applied Physics (IBWAP) - 13<sup>th</sup> Edition, Constanta, Romania  
6-8 July 2013, Talk
24. *Choina J, Kosslick H, Fischer Ch, Flechsig GU, Schulz A, Frunza L, Frumosu F, Diamandescu L, Frunza S, Ganea CP*  
Titania P25 photocatalyst still a challenge: complex characterization and activity in the abatement of ibuprofen as a model compound  
Intern. Symp. Rom. Catal. Society RomCat 2013, Cluj-Napoca, Romania  
29-31 May 2013, Poster

25. *Ciobanu CS, Iconaru SL, Chapon P, Predoi D*  
Antimicrobial activity of silver doped hydroxyapatite thin films  
FEBS Congress 2013 St. Petersburg, Russia  
6-11 July 2013, Poster
26. *Ciobanu CS, Iconaru SL, Predoi D*  
Anti-biofilm activity of maghemite nanoparticles coated with dextran  
FEBS Congress 2013 St. Petersburg, Russia  
6-11 July 2013, Poster
27. *Ciobotaru IC, Polosan S*  
New composite material based on IrQ(ppy)<sub>2</sub>-5Cl:PS layer for OLED applications  
Third International Conference on Multifunctional, Hybrid and Nanomaterials, Sorrento, Italy  
3-7 March 2013, Poster
28. *Ciobotaru IC, Polosan S, Enculescu I, Ciobotaru CC, H. Iovu*  
IrQ(ppy)<sub>2</sub> in Poly(methyl methacrylate) matrix for OLED applications  
6th International Symposium on Flexible Organic Electronics (ISFOE13), Thessaloniki, Greece  
8-11 July 2013, Poster
29. *Ciobotaru IC, Polosan S, Ciobotaru CC, H. Iovu*  
New IrQ(ppy)<sub>2</sub> organometallic compound for OLED applications: Synthesis and optical characterization  
The 13th International Balkan Workshop on Applied Physics, Constanta, Romania  
4-6 July 2013, Talk
30. *Ciobotaru IC, Polosan S, Ciobotaru CC, H. Iovu*  
New IrQ(ppy)<sub>2</sub> organometallic compound for OLED applications  
RICCCE XVIII, Sinaia, Romania  
4-7 September 2013, Talk
31. *Ciurea ML, Lepadatu AM, Stavarache I, Stoica T, Teodorescu VS*  
Ge nanocrystal formation versus Ge diffusion in Ge/SiO<sub>2</sub> multilayers  
A 12-a editie a Seminarului National de nanostiinta si nanotehnologie, Biblioteca Academiei  
Romane, Bucuresti, Romania  
16 May 2013, Talk
32. *Costescu A, Andronescu E, Vasile BS, Trusca R, Le Coustumer P, Iconaru SL, Barna E, Ciobanu C*  
Synthesis and characterisation of hydroxyapatite for environmental applications  
International Conference INnovation and Collaboration in Engineering Research  
Bucharest, Romania  
20-22 June 2013, Poster
33. *Craciun F, Dimitriu E, Grigoras M, Lupu N, Cernea M*  
Multiferroic properties of (Sm, Fe)-doped PbTiO<sub>3</sub> perovskite ceramics  
Conference COST MPO904 Action, Faenza, Italy  
22-23 April 2013, Talk
34. *Craciun F, Dimitriu E, Grigoras M, Lupu N, Cernea M*  
Ferroelectricity and magnetism in (Sm, Fe)-doped PbTiO<sub>3</sub> perovskite ceramics  
34<sup>th</sup> International Symposium on Dynamical Properties of Solids, Vienna, Austria  
15-19 September 2013, Poster

35. *Crisan AD, Vasiliu F, Mercioniu I, Crisan O*  
Ag-induced interlayer exchange coupling in FePt-based nanocrystalline melt-spun ribbons  
20th International Symposium on Metastable, Amorphous and Nanostructured Materials – ISMANAM 2013, Torino, Italy  
30 June-5 July 2013, Talk
36. *Crisan AD, Bednarcik J, Michalik Š, Crisan O*  
In-situ monitoring of disorder-order A1 - L10 FePt phase transformation in nanocomposite FePt-based alloys  
20th International Symposium on Metastable, Amorphous and Nanostructured Materials – ISMANAM 2013, Torino, Italy  
30 June-5 July 2013, Poster
37. *Crisan AD*  
RKKY-induced interlayer exchange coupling in nanocomposite FePt-based magnets  
8<sup>th</sup> International Conference on Fine Particle Magnetism, ICFPM – 2013, Perpignan, France  
24-27 June 2013, Talk
38. *Crisan O*  
2D arrays of core-shell magnetic nanoparticles: hybrid magnetoresistive architectures  
International Conference on Fine Particle Magnetism ICFPM 2013, Perpignan, France  
24-27 June 2013, Talk
39. *Crisan O, Crisan AD, Vasiliu F, Mercioniu I, Nicula R*  
Temperature dependent phase transformations and magnetic behaviour of FePt-based nanocomposite magnets  
Joint European Magnetic Symposia 2013 - JEMS 2013, Rhodes, Greece  
25-30 August 2013, Talk
40. *Crisan O, Crisan AD, Vasiliu F, Mercioniu I, Stir M, Nicula R, Hoffmann P*  
Direct formation and thermal stability of exchange-coupled FePt-based nanocomposite magnets  
5th Seeheim Conference on Magnetism, Frankfurt, Germany  
29 september-3 October 2013, Poster
41. *Diamandescu L, Feder M, Popescu T*  
Mössbauer study on the GaFeO<sub>3</sub> formation by high energy ball milling and post annealing pathway  
1-6 September 2013, Poster
42. *Dragomir R*  
Exciton dynamics in optically active quantum dots  
Workshop "New trends in nanophysics and solar energy conversion", Bucharest, Romania  
23-25 September 2013, Talk
43. *Duta L, Popescu AC, Stan GE, Mihailescu IN*  
Finishing treatment of textile materials with ZnO thin films or particles. Boost of antimicrobial efficiency in presence of hydrophobins  
E-MRS Spring Meeting, Strasbourg, France  
27–31 May 2013, Poster

44. *Duta L, Stan GE, Popescu AC, Mihailescu IN, Poeata I, Chiriac A*  
Adherent hydroxyapatite thin films biofunctionalized by Pulsed Laser Deposition onto titanium mesh implants for cranioplasty applications  
E-MRS Spring Meeting, Strasbourg, France  
27–31 May 2013, Poster
45. *Duta L, Stan GE, Oktar FN, Serban N, Mihailescu IN*  
Doped biological hydroxyapatite thin films synthesized by Pulsed Laser Deposition for a new generation of implants  
E-MRS Spring Meeting, Strasbourg, France  
27–31 May 2013, Poster
46. *Duta L, Popescu AC, Dorcioman G, Stan GE, Pasuk I, Dumitrescu I, Mihailescu IN*  
Influence of a hydrophobin buffer layer on the structuring and antimicrobial properties of ZnO thin films synthesized by PLD on textile materials  
International Conference of Physical Chemistry (ROMCHEMPHYS) – 15<sup>th</sup> Edition, Bucharest, Romania  
11–13 September 2013, Talk
47. *Duta L, Stan GE, Popescu AC, Mihailescu IN, Poeata IN, Chiriac A*  
Titanium mesh implants biofunctionalized with hydroxyapatite thin films by Pulsed Laser Deposition  
25<sup>th</sup> Symposium and Annual Meeting of the International Society for Ceramics in Medicine (BIOCERAMICS 25), Bucharest, Romania  
7–10 November 2013, Poster
48. *Elisa M, Sava B, Boroica L, Valeanu M, Kuncser V, Iordanescu R, Feraru I*  
Rare-earth-doped phosphate glasses with interesting magneto-optical properties  
Joint European Magnetic Symposia Rhodos, Greece  
25-30 August 2013, Poster
49. *Enculescu I, Matei E, Florica C, Costas A*  
Electrical properties of ZnO nanowires prepared by templateless electrodeposition  
224<sup>th</sup>ECS Meeting, San Francisco, SUA  
27 October-1 November 2013, Talk
50. *Enculescu I, Matei E, Enculescu M, Florica C, Costas A*  
Influence of electrodeposition conditions on the properties of samaria films  
224<sup>th</sup>ECS Meeting, San Francisco, SUA  
27 October-1 November 2013, Talk
51. *Enculescu M, Matei E, Preda N, Florica C, Enculescu I*  
Influence of nickel nanowires on the optical properties of dye-doped polymer films  
E-MRS 2013 Spring Meeting, Strasbourg, France  
27-31 May 2013, Poster
52. *Enculescu M, Matei E, Preda N, Florica C, Enculescu I*  
Influence of the ZnO nanorods on the emissive properties of dye-doped polymer thin films  
E-MRS 2013 Spring Meeting, Strasbourg, France  
27-31 May 2013, Poster

53. *Enculescu M, Matei E, Florica C, Preda N, Enculescu I*  
Nanowire-based devices for applications  
E-MRS 2013 Fall Meeting, Varsovia, Poland  
16-20 September 2013, Talk
54. *Eraković S, Janković A, Ristoscu C, Duta L, Serban N, Visan A, Stan GE, Luculescu C, Janacković Dj, Mihailescu IN, Mišković-Stanković V*  
Laser assembling of thin bioceramic and biocomposite films on titanium utilizing pulsed laser deposition (PLD) and Matrix-assisted pulsed laser evaporation (MAPLE) techniques  
12<sup>th</sup> Young Researchers' Conference – Materials Science and Engineering, Belgrade, Serbia  
11–13 December 2013, Talk
55. *Eraković S, Janković A, Ristoscu C, Duta L, Serban N, Visan A, Mihailescu IN, Stan GE, Socol M, Iordache O, Dumitrescu I, Luculescu CR, Janacković Dj, Mišković-Stanković V*  
Silver/hydroxyapatite coating on pure and anodized titanium obtained by pulsed laser deposition  
15<sup>th</sup> Annual Conference YUCOMAT, Herceg Novi, Montenegro  
2–6 September 2013, Talk
56. *Florica C, Matei E, Toimil-Molares M E, Enculescu I*  
Fabrication and properties of semiconductor nanowire channel field effect transistors  
International Conference on Materials for Advanced Technologies ICMAT 2013, Suntec, Singapore  
30 June-5 July 2013, Talk
57. *Florica C, Matei E, Toimil Molares M E, Enculescu I*  
Influence of electrodeposition conditions on electrical properties of ZnO nanowires  
E-MRS Spring Meeting, Strasbourg, France  
27-31 May 2013, Poster
58. *Florica C, Matei E, Toimil Molares M E, Enculescu I*  
Tunable electrical properties of field effect transistors based on electrodeposited ZnO nanowires  
E-MRS Fall Meeting, Warsaw, Poland  
16-20 September 2013, Talk
59. *Frunza L, Preda N, Matei E, Frunza S, Ganea P*  
Superhydrophobicity of polyester fabrics by electroless deposition of ZnO nanoparticles  
In Conferinta Internationala de Chimie Fizica ROMPHYSICHEM 2013, Academia Romana, Bucharest, Romania  
11-13 September 2013, Poster
60. *Galatanu A*  
Thermal properties of fusion related composites  
Netzsch Thermal Analysis Seminar, Bucharest November 21<sup>st</sup>. Faculty of Biotechnical Systems Engineering, UPB, Romania  
21 November 2013, Talk

61. *Galatanu M, Enculescu M, Galatanu A*  
Tuning the thermal conductivity in SiC based metal-ceramic composites  
IBWAP 2013, Constanta, Romania  
4-6 July 2013, Poster
62. *Galatanu M, Popescu B, Enculescu M, Galatanu A*  
Cu-W functional gradient materials  
IBWAP 2013, Constanta, Romania  
4-6 July 2013, Talk
63. *Galca AC, Besleaga-Stan C, Secu M*  
Correlations between structural, optical and electrical properties of aluminum doped zinc oxide thin films deposited by rf-magnetron sputtering  
International Conference of Physical Chemistry (ROMCHEMPHYS) – 15<sup>th</sup> Edition, Bucharest, Romania  
11–13 September 2013, Talk
64. *Galca AC, Trinca LM, Socol V, Craciun V*  
Effect of gallium concentration on the optical properties of amorphous IGZO thin films  
International Balkan Workshop on Applied Physics (IBWAP) - 13<sup>th</sup> Edition, Constanta, Romania  
6-8 July 2013, Poster
65. *Galca AC, Trinca LM, Socol V, Craciun V*  
Investigations of the optical, structural and mechanical properties of nanostructured thin SiC films  
E-MRS Fall Meeting, Warsaw, Poland  
16–20 September 2013, Poster
66. *Ghica C*  
Microstructural characterization of multilayered perovskite coatings for artificial multiferroics  
International Multidisciplinary Microscopy Congress INTERM 2013, Antalya, Turkey  
10-13 October 2013, Talk
67. *Ghica C, Negrea RF, Nistor L, Maraloiu VA, Chirila C, Pintilie L*  
HRTEM characterization of strained perovskite coatings  
E-MRS 2013 Spring Meeting, Strasbourg, France  
27 - 31 May 2013, Talk
68. *Ghica D, Stefan M, Ghica C, Stan GE*  
Atomic scale magnetic defects in Mn-doped ZnO films  
E-MRS Spring Meeting, Strasbourg, France  
27–31 May 2013, Talk
69. *Ghica D, Stefan M, Ghica C, Stan GE*  
Atomic scale magnetic defects in Mn-doped ZnO films  
E-MRS 2013 Spring Meeting, Strasbourg, France  
27-31 May 2013, Talk

70. *Ghita RV, Predoi D, Iconaru SL, Ciobanu CS, Chifiriuc CM, Frumosu F, Chapon P*  
Features of hydroxyapatite thin films doped with transition elements  
Synthesis of ceramic composites for environmental applications  
The XVII International Sol-Gel Conference Madrid, Spain  
25-30 August 2013, Poster
71. *Greco MN, Tolea F, Ghica D, Vlaicu AM*  
On the local structure and magnetic behaviour of anatase  $\text{Co}_x\text{TiO}_{1-x}\text{O}_2$  nanoparticles  
Magnetic Resonance Conference (EUROMAR 2013), Crete, Greece  
30 June- 5 July 2013, Poster
72. *Grumezescu AM, Socol G, Grumezescu V, Axente El, Socol M, Ficai A, Andronescu E, Ghitulica CD, Mihailescu I, Bleotu C, Chifiriuc CM*  
Biocompatible magnetic PLGA-PVA thin film fabricated by MAPLE for the design of new surfaces resistant to microbial colonization  
SPRING 13 R: Nano-engineered bioactive interfaces, E-MRS Spring Meeting, Strasbourg, France  
27-31 May 2013, Poster
73. *Iconaru SL, Andronescu E, Ciobanu C, Ghita RV, Prodan AM, Chapon P, Le Coustumer P, Costescu A, Predoi D*  
Preparation of silver doped hydroxyapatite thin films with environmental applications  
5th FESTEEM International Symposium - Trace Elements in Avignon: Bridging between new Advances and Public Health Issues, Bucharest, Romania  
22-24 May 2013, Poster
74. *Iconaru SL, Ciobanu CS, Costescu A, Andronescu E, Motelica-Heino M, Le Coustumer P, Prodan A M, Predoi D*  
Synthesis of ceramic composites for environmental applications  
The XVII International Sol-Gel Conference Madrid, Spain  
25-30 August 2013, Poster
75. *Iconaru SL, Ciobanu C, Costescu A, Motelica M, Le Coustumer P, Predoi D*  
Porous hydroxyapatite with environmental applications  
ICSAAM 2013, The 5th International Conference on Structural Analysis of Advanced Materials, Island of Kos, Greece  
23 - 26 September 2013, Talk
76. *Iconaru SL, Ciobanu CS, Motelica-Heino M, Guegan R, Costescu A, Barna ES, Predoi D*  
Novel hydroxyapatite composites for Pb (II) removal  
ICESE 2013: International Conference on Environmental Science and Engineering, Paris, France  
7-8 October, Talk
77. *Janković A, Duta L, Serban N, Ristoscu C, Eraković S, Visan A, Stan GE, Luculescu C, Chifiriuc MC, Mišković-Stanković V, Mihailescu IN*  
Pure and doped hydroxyapatite thin films synthesized by advanced laser techniques for metal implant coatings  
E-MRS Spring Meeting, Strasbourg, France  
27-31 May 2013, Poster

78. *Kuncser V, Schinteie G, Palade P, Filoti G*  
Distributions of the barriers via temperature dependent Fe-57 Mossbauer  
International Conference on the Applications of the Mossbauer Effect, Opatija, Croatia  
1-6 september, 2013, Talk
79. *Kuncser V, Sandu S, Bartha C, Plapcianu C, Filoti G, Parvulescu V*  
Perovskite based catalysts studied by Mossbauer spectroscopy and magnetic measurements  
International Symposium of the Romanian Catalysis Society, RomCat 2013, Cluj Napoca,  
Romania  
29-31 May, Talk
80. *Kuncser V*  
Research on magnetic nanostructures at NIMP  
HepTech Industry Open Innovation Forum, IFIN-HH, Romania  
8-9 October 2013, Talk
81. *Le Febvrier A, Deputier S, Bouquet V, Demange V, Galca AC, Chirila C, Iuga A, Pintilie I, Pintilie L, Guilloux-Viry M*  
Reduction of the dielectric losses of KTN thin film using MgO doping or multilayer  
heterostructures with BZN  
E-MRS Spring Meeting, Strasbourg, France  
27-31 May 2013, Poster
82. *Lepadatu AM, Stavarache I, Stoica T, Ciurea ML*  
Raman and electrical properties of Ge-SiO<sub>2</sub> films versus annealing temperature  
6-th Edition of the Conference on Amorphous and Nanostructured Chalcogenides, Brasov,  
Romania  
24-28 June 2013, Poster
83. *Lepadatu AM, Stavarache I, Teodorescu VS, Stoica T, Ciurea ML*  
Study of Ge nanocrystals formation in Ge/SiO<sub>2</sub> multilayer structures by TEM and Raman  
spectroscopy  
E-MRS Spring Meeting, Congress Center, Strasbourg, France  
27-31 May 2013, Poster
84. *Matei E, Florica C, Enculescu M, Teodorescu C M, Enculescu I*  
Influence of deposition conditions on the properties of templateless electrodeposited ZnO  
nanowires  
International Conference on Materials for Advanced Technologies ICMAT 2013, Suntec,  
Singapore  
30 June -5 July 2013, Talk
85. *Miroiu F, Socol G, Stefan N, Cristescu R, Visan A, Sima L, Sima F, Grumezescu V, Nita C, Socol M, Rasoga O, Mihailescu I.N*  
Controlled release of proteins embedded in biodegradable silk fibroin - Poly(3-  
hydroxybutyric acid-Co-3-hydroxy-valeric acid) composite coatings  
SPRING 13 V: Laser materials interactions for micro and nano applications, E-MRS Spring  
Meeting, Strasbourg, France  
27-31 May 2013, Poster

86. *Nedelcu L, Scarisoreanu ND, Banciu MG, Dinescu M*  
Terahertz time-domain spectroscopy of Ba(Mg<sub>1/3</sub>Ta<sub>2/3</sub>)O<sub>3</sub> thick films  
E-MRS Spring Meeting, Strasbourg, France  
27–31 May 2013, Poster
87. *Nedelcu L, Busuioc C, Banciu MG, Alexandru HV*  
Terahertz properties of barium tantalate-based microwave dielectrics  
International Balkan Workshop on Applied Physics (IBWAP) - 13<sup>th</sup> Edition, Constanta, Romania  
6-8 July 2013, Poster
88. *Negrea RF, Ghica C, Teodorescu VS, Maraloiu VA, Dragoi C, Pintilie I*  
Microstructural characterization of epitaxial perovskite multilayers  
E-MRS Spring Meeting 2013, Strasbourg, France  
27-31 May 2013, Poster
89. *Nistor LC, Nistor SV, Ghica D, Stefan M, Vlaicu I*  
Structural changes and crystallization of nanostructured ZnO during thermal decomposition of Zn-based precursors.  
The European Congress and Exhibition on Advanced Materials and Processes - EUROMAT 2013, Sevilla, Spain  
8-13 September 2013, Poster
90. *Nistor LC, Ghica C, Negrea R, Pintilie I, Nistor SV, Epurescu G*  
Aberration corrected STEM imaging and analysis of nano-structures  
The European Congress and Exhibition on Advanced Materials and Processes - EUROMAT 2013, Sevilla, Spain  
8-13 September 2013, Poster
91. *Nistor SV, Stefan M, Ghica D, Nistor LC*  
Characterization of cubic ZnS quantum dots with various Mn<sup>2+</sup> impurity ions doping levels by multifrequency electron paramagnetic resonance  
The European Congress and Exhibition on Advanced Materials and Processes - EUROMAT 2013, Sevilla, Spain  
8-13 September 2013, Talk
92. *Palade C, Lepadatu AM, Stavarache I, Teodorescu VS, Ciurea ML*  
Conduction mechanism versus annealing in SiO<sub>2</sub> films with Ge nanoparticles  
International Semiconductor Conference 2013, Sinaia, Romania  
14-16 October 2013, Talk
93. *Pintilie I*  
Particle and Photon Detectors - Radiation induced defects in Si based sensors  
HEPTech Industry Open Innovation Forum, Magurele, Romania  
8-9 October 2013, Talk

94. *Pintilie I, Radu R, Fretwurst E, Lindstroem G, Klanner R, Makarenko L, Barcz A, Kaminsky P, Nistor LC, Nistor SV, Ghica D*  
Update on irradiation experiments with electrons of different kinetic energies (between 1.5 MeV and 27 MeV) performed on n-type silicon  
23<sup>rd</sup> RD50-CERN Workshop, Geneva, Switzerland  
13-15 November 2013, Talk
95. *Pintilie L, Ibanescu G A, Hrib L, Chirila C, Iuga A, Pintilie I, Cernea M, Lowndes R, Negrea R, Ghica C, Preziosi D, Deniz H, Alexe M*  
Structural and electric properties of some ferroic thin films and multilayers  
COST workshop SIMUFER, Belfast, U. K.  
20-22 March 2013, Talk
96. *Plugaru N*  
Computational design and experiment in the search of new hard magnetic materials: Focus on itinerant electron magnetocrystalline anisotropy  
Seminar ICPE-CA, 29 Octombrie 2013
97. *Plugaru R, Plugaru N*  
First principles electronic structure of HfO<sub>2</sub> and La<sub>2</sub>O<sub>3</sub> doped with rare earth elements  
International Conference of Physical Chemistry - ROMPHYSICHEM 15 - Workshop 8 - Sol-gel science and applications, Bucharest, Romania  
11-13 September 2013, Talk
98. *Polosan S, Ciobotaru IC, Ciobotaru CC*  
Iridium dual emitter organometallic compound: thermal and structural analysis  
6<sup>th</sup> International Symposium on Flexible Organic Electronics (ISFOE13), Thessaloniki, Greece  
8-11 July 2013, Talk
99. *Polosan S, Ciobotaru IC, Ciobotaru CC*  
Dual emitter organometallic compounds: thermal and structural characteristics  
The 13th International Balkan Workshop on Applied Physics, Constanta, Romania  
4-6 July 2013, Talk
100. *Popescu AC, Popa AC, Stan GE, Husanu MA, Pasuk I, Popescu D, Mihailescu I*  
Protective haemocompatible Diamond-like Carbon thin films for metal surfaces in contact with corrosive body fluids  
4<sup>th</sup> International Conference from Nanoparticles and Nanomaterials to Nanodevices and Nanosystems (IC4N), Corfu Island, Greece  
16-20 June 2013, Talk
101. *Popescu M, Sava F, Velea A, Lőrinczi A, Șimăndan ID*  
Chalcogenide systems at the border of the glass formation domain: a key for understanding the switching phenomena  
6<sup>th</sup> International Conference - Amorphous and Nanostructured Chalcogenides, Brasov, Romania  
24-28 June 2013, Talk

102. *Popescu M, Sava F, Șimăndan I D, Lőrinczi A*  
Simulation of the structure and switching properties in chalcogenide systems  
The 25th International Conference on Amorphous and Nano-crystalline Semiconductors,  
Toronto, Canada  
18–23 August 2013, Talk
103. *Preda N, Enculescu M, Matei E, Florica C, Enculescu I*  
Biopolymers mediated chemical synthesis of ZnO nanostructures  
E-MRS 2013 Spring Meeting, Strasbourg, France  
27-31 May 2013, Poster
104. *Preda N, Enculescu M, Zgura I, Socol M, Matei E, Vasilache V, Florica C, Enculescu I*  
Superhydrophobic fabrics with UV-blocking properties by electroless deposition of ZnO on  
cotton fabrics  
E-MRS 2013 Spring Meeting, , Strasbourg, France  
27-31 May 2013, Poster
105. *Prodan AM, Andronescu E, Vasile BS, Beuran M, Marutescu L, Chifiriuc M, Barna E,  
Iconaru SL*  
Anti-biofilm activity of dextran coated iron oxide nanoparticles  
International Conference INnovation and Collaboration in Engineering Research Bucharest,  
Romania  
20-22 June 2013, Poster
106. *Radu M, Burtea C, Predoi D, Muller R, Dinischiotu A*  
Toxicological aspects of PANC-1 cells exposure to iron oxide dextran-covered nanoparticles  
FEBS Congress 2013 St. Petersburg, Russia  
6-11 July 2013, Poster
107. *Radu R, Fretwurst E, Klanner R, Lindstroem G, Pintilie I*  
Studies on n-type silicon after electron irradiation  
22<sup>nd</sup> RD50-CERN Workshop, New Mexico, USA  
3-5 June 2013, Talk
108. *Sandu SG, Miu L, Badica P, Noji T, Koike Y, Kuncser V*  
Fe local configuration and phase composition in FeSe<sub>0.3</sub>Te<sub>0.7</sub> single crystals studied by  
temperature dependent Mössbauer Spectroscopy  
International Balkan Workshop on Applied Physics, Constanta, Romania  
4-6 July 2013, Talk
109. *Sandu SG, Vopson M, Ghita I, Iuga A, Kuncser V*  
Ferromagnetic – Ferroelectric interfaces studied by Mossbauer Spectroscopy  
International Balkan Workshop on Applied Physics, Constanta, Romania  
4-6 July 2013, Poster
110. *Sandu T, R. Plugaru R, Plugaru N*  
On the variable hopping range conductivity in ZnO doped systems  
Le troisième colloque francophone pluridisciplinaire sur les matériaux, l'environnement et  
l'electronique", PLUMEE 2013, Bacau, Romania  
22 -25 May 2013, Talk

111. *Sandu V.*  
Magnetic pinning in nanostructured MgB<sub>2</sub> composites  
International Conference on Surfaces, Coatings and Nanostructured Materials  
(NANOSMATA<sub>Asia</sub>), Wuhan, China  
13-15 March 2013, Talk
112. *Sava F., Popescu M., Lőrinczi A., Velea A., Șimăndan I. D., Preda N., Matei E., Socol G., Mihailescu I. N.*  
Effect of thermal annealing on the structural and optical properties of Ag/As<sub>2</sub>S<sub>3</sub> multilayers  
6<sup>th</sup> International Conference - Amorphous and Nanostructured Chalcogenides, Brasov,  
Romania  
24-28.06.2013, Poster
113. *Scarisoareanu ND, Craciun F, Andrei A, Ion V, Birjega R, Nedelcu L, Banciu MG, Dinescu M*  
Pulsed laser deposition growth of lead-free (Ba<sub>1-x</sub>Ca<sub>x</sub>)(Ti<sub>1-y</sub>Zr<sub>y</sub>)O<sub>3</sub> thin films and their  
structural, optical and electrical properties  
E-MRS Spring Meeting, Strasbourg, France  
27–31 May 2013, Poster
114. *Schintei G, Sandu SG, Palade P, Filoti G, Trupina L, Lungu GA, Lungu CP, Kuncser V*  
Material migration processes in Fe-Cr(Al) thin films of interest for plasma facing components  
International Conference on the Applications of the Mossbauer Effect, Opatija, Croatia  
1-6 September 2013, Poster
115. *Secu CE, Bartha C, Secu M*  
Ceramization processes of RE-doped sol-gel derived oxyfluoride glasses  
The XVII International Sol-Gel Conference, Madrid, Spain  
25-30 August 2013, Poster
116. *Secu M*  
Luminescent nano- and microrods prepared by sol-gel template method  
The XVII International Sol-Gel Conference, Madrid, Spain  
25-30 August 2013, Poster
117. *Simandan ID, Sava F, Popescu M, Lőrinczi A*  
Complex Langmuir-Blodgett films based on barium stearate multilayers with carbon nanotubes  
and As<sub>2</sub>S<sub>3</sub>  
6<sup>th</sup> International Conference - Amorphous and Nanostructured Chalcogenides, Brasov,  
Romania  
24-28 June 2013, Poster
118. *Socol G, Socol M, Stefan N, Axente E, Popescu-Pelin G, Craciun D, Duta L, Mihailescu IN, Stanculescu A, Visan D, Galca AC, Jelinek M, Craciun V*  
CdS/CdTe/ZnTe thin-film solar cells fabricated by Pulsed Laser Deposition  
E-MRS Spring Meeting, Strasbourg, France  
27–31 May 2013, Poster
119. *Socol G, Socol M, Stefan N, Axente E, Popescu-Pelin G, Craciun D, Mihailescu CN, Mihailescu IN, Stanculescu A, Visan D, Jelinek M, Antohe S, Ion L, Galca AC, Craciun V*  
CdS/CdTe/ZnTe thin-film solar cells fabricated by Pulsed Laser Deposition  
E-MRS Fall Meeting, Warsaw, Poland  
16–20 September 2013, Poster

120. *Socol G, Sima F, Axente E, Ristoscu C, Stefan N, Socol M, Luculescu CR, Mihailescu IN*  
Enhancing the gas sensitivity of oxide thin films by surface structuring,  
SPRING 13 O: In Synthesis, processing and characterization of nanoscale multi functional  
oxide films, E-MRS Spring Meeting, Strasbourg, France  
27-31 May 2013, Poster
121. *Socol G, Sima L, Radulescu L, Sima F, Socol M, Axente E, Grumezescu V, Cristescu R.,  
Miroiu M., Antohe F, Breazu CS, Stanculescu A, Zgura I, Chiritoiu M*  
Release profile of proteins encapsulated in biodegradable calcium phosphates/poly(3-hydroxyl-  
butyrate-co-3-hydroxyvalerate) nanocomposite coatings  
SPRING 13 R: Nano-engineered bioactive interfaces, E-MRS Spring Meeting, Strasbourg,  
France  
27-31 May 2013, Poster
122. *Socol M, Vacareanu L, Grigoras M, Socol G, Mihailescu IN, Preda N, Stanculescu F, Jelinek M,  
Stanculescu A*  
Organic heterostructures based on arylenevinylene oligomers obtained by MAPLE  
SPRING 13 V: Laser materials interactions for micro and nano applications E-MRS Spring  
Meeting, Strasbourg, France  
27-31 May 2013, Poster
123. *Sopronyi M, Sima L, Radulescu L, Socol M, Nita C, Grumezescu V, Stanculescu A, Stefan N,  
Breazu CS, Zgura I, Chiritoiu M, Mihailescu IN, Socol G*  
Biodegradation study of polymeric coatings based on polyethylene glycol/poly(3-hydroxybuty-  
rate-co-3-hydroxyvalerate) blends  
SPRING 13 V: Laser materials interactions for micro and nano applications, E-MRS Spring  
Meeting, Strasbourg, France  
27-31 May 2013, Poster
124. *Stan GE, Galca AC, Trinca LM, Negrila CC, Nistor LC*  
Structural and optical properties of c-axis oriented aluminum nitride thin films prepared at low  
temperature by reactive RF-magnetron sputtering  
International Balkan Workshop on Applied Physics (IBWAP) - 13<sup>th</sup> Edition, Constanta,  
Romania  
6-8 July 2013, Poster
125. *Stan GE, Popa AC, Galca AC, Aldica G, Ferreira JMF*  
Strong bonding between sputtered bioglass thin films and Ti-substrate induced by atomic  
inter-diffusion post-deposition heat-treatments  
E-MRS Spring Meeting, Strasbourg, France  
27-31 May 2013, Poster
126. *Stan GE, Popa AC, Marques VMF, Lemos AF, Ferreira JMF*  
Structural properties and mechanical performance of bioglass films deposited onto Ti-  
substrates by magnetron sputtering  
E-MRS Spring Meeting, Strasbourg, France  
27-31 May 2013, Poster

127. *Stanculescu A, Socol M, Rasoga O, Mihailescu IN, Socol G, Enculescu M, Breazu C, Stanculescu F*  
Laser prepared ZnPc/NTCDA organic heterostructures on glass/AZO substrates  
SPRING 13 V: Laser materials interactions for micro and nano applications, E-MRS Spring Meeting, Strasbourg, France  
27-31 May 2013, Poster
128. *Stanculescu A, Socol G, Grigoras M, Ivan T, Vacareanu L, Socol M, Rasoga O, Mihailescu I N, Breazu C, Preda N, Stanculescu F*  
Laser prepared organic heterostructures based on star-shaped arylenevinylene compounds  
The 12th International Conference on Laser Ablation (COLA 2013), Ischia, Italy  
5-12 October 2013, Poster
129. *Stavarache I, Lepadatu AM, Maraloiu AV, Palade C, Teodorescu VS, Ciurea ML*  
Influence of annealing on Raman and electrical properties of Ge nanocrystals in amorphous SiO<sub>2</sub>  
E-MRS Spring Meeting, Congress Center, , Strasbourg, France  
27-31 May 2013, Talk
130. *Stefan N, Miroiu FM, Cristescu R., Visan A, Grumezescu V, Nita C, Socol M, Rasoga O, Sima L, Mihailescu IN, Socol G*  
Fabrication of biodegradable silk fibroin - poly(sebacic acid) diacetoxy terminated composite coatings for local release of proteins  
SPRING 13 V: Laser materials interactions for micro and nano applications , E-MRS Spring Meeting, Strasbourg, France  
27-31 May 2013, Poster
131. *Teodorescu VS, Ghica C, Maraloiu AV, Lepadatu AM, Stavarache I, Ciurea ML, Scarisoreanu ND, Andrei A, Dinescu M*  
Nanoscale fast diffusion in laser irradiated SiGe thin films  
NSTI-Nanotech 2013 Proceedings, vol.1, pp 109-112, Washington, USA  
12-16 May 2013, Talk
132. *Teodorescu VS, Maraloiu AV, Blanchin M-G, Yamada T, Sandu CS, Delaporte P, Zaharescu M*  
Structure and dielectric properties of low fluence excimer laser annealing of sol-gel HfO<sub>2</sub> thin films deposited on Si wafer  
36<sup>th</sup> edition International Semiconductor Conference, Sinaia, Proceedings CAS 2013, vol 1. pp 77- 80  
14-16 October 2013, Talk
133. *Teodorescu VS, Ghica C, Maraloiu AV, Lepadatu AM, Stavarache I, Ciurea ML, Dinescu M, Scarisoreanu ND, Andrei A*  
Fast diffusion of Ge in amorphous SiGe films during laser crystallization  
EMRS 2013, Symposium V "Laser materials interactions for micro and nano applications", Strasbourg, France  
27-31 May 2013, Poster
134. *Tolea F, Sofronie M, Crisan AD, Valeanu M*  
Influence of thermal treatments on the martensitic transition of Ni-Fe-Co-Ga melt spun ribbons Joint European Magnetic Symposia, Rhodes, Greece  
25-30 August 2013, Talk

135. *Tolea F, Kuncser V, Constantinescu SG, Tolea M, Grecu MN*  
Effect of iron doping and thermal treatment on magnetic properties of anatase TiO<sub>2</sub> nanopowders  
Joint European Magnetic Symposia, Rhodos, Greece  
25-30 August 2013, Talk
136. *Tolea F, Sofronie M, Crisan AD, Valeanu M*  
Influence of thermal treatments on the martensitic transition of Ni-Fe-Co-Ga melt spun ribbons  
Joint European Magnetic Symposia, Rhodos, Greece  
25-30 August 2013, Talk
137. *Visan A, Miroiu M, Cristescu R, Socol G, Stefan N, Dorcioman G, Sima F, Serban N, Nita C, Socol M, Sima L, Luculescu CR, Stanculescu A, Mihailescu IN*  
Characteristics and biodegradation properties of polycaprolactone –polyethylene glycol coatings for tissue engineering applications  
SPRING 13 V: Laser materials interactions for micro and nano applications, E-MRS Spring Meeting, Strasbourg, France  
27-31 May 2013, Poster
138. *Vlaicu AM, Mercioniu I, Ghica C, Teodorescu VS, Maraloiu AV, Negrea R, Stefan A, Manoliu V, Ionescu G, Mihailescu AD*  
Structural and morphological analysis of plasma jet synthesized thermal barrier coatings for aerospace applications  
Intermetallics 2013, Bad Staffelstein, Germany  
30 september– 4 October 2013, Poster
139. *Vlaicu ID, Olar R, Marinescu D, Badea M, Chifiriuc MC*  
New biologic active Cu(II) complexes with benzimidazole as one of the ligands: Synthesis, characterization and thermal behavior  
2<sup>nd</sup> Central and Eastern European Conference on Thermal Analysis and Calorimetry, CEEC-TAC2 2013, Vilnius, Lithuania  
27-30 August 2013, Poster
140. *Vlaicu ID, Badea M, Olar R, Marinescu D, Chifiriuc MC, Marutescu L, Lazar V*  
New cobalt(II) complexes with mixed ligands as antimicrobials  
2<sup>nd</sup> Central and Eastern European Conference on Thermal Analysis and Calorimetry, CEEC-TAC2 2013, Vilnius, Lithuania  
27-30 August 2013, Poster
141. *Zgura I, Frunza L, Moldovan R, Negrila C, Cotorobai F, Frunza S*  
Surface free energy of solids from contact angle measurement: model surfaces  
Conferinta Internationala de Chimie Fizica ROMPHYSICHEM 2013, Academia Romana, Bucharest, Romania  
11-13 September 2013, Poster

**Invited Lectures***Aldea A*

Topological properties of graphene and other 2D lattices  
New trends in the research of carbon based nanomaterials  
22-23 .04.2013

*Apostol NG, Stoflea LE, Lungu GA, Tache CA, Tanase LC, Chirila C, Pintilie L, Teodorescu CM*

Selective adsorption of polar organic molecules on ferroelectric  
Biomimetic sensing using nano-objects (BioSUN), Magurele, Romania  
17-19.06.2013

*Apostol NG*

X-ray photoelectron spectroscopy utilization for direct band bending measurements at metal-semiconductor interfaces, free ferroelectric surfaces, and metal-ferroelectric heterostructures  
New Trends in Nanophysics and Solar Energy Conversion, Magurele, Romania  
23-25.09.2013

*Apostol NG*

Band bending at ferroelectric surfaces and interfaces investigated by X-ray photoelectron spectroscopy  
TIM 2013 – International Physics Conference, Timisoara, Romania  
21-25.11.2013

*Badica P, Truccato M, Agostino A*

Solid-liquid-solid growth of oxide non-linear single crystal objects  
The 60th JSAP Spring Meeting 2013, Kanagawa Institute of Technology, Atsugi, Japan,  
27-30.03.2013

*Badica P, Aldica GV, Borodianska H, Sakka Y, Vasylykiv O*

Challenges and new approaches in reactive spark plasma sintering of selected ceramics: Case studies on nanostructuring versus functional properties  
JSAP-MRS Joint Symposia for 2013 JSAP Autumn Meeting, Doshisha University, Kyoto, Japan  
16-20.09.2013

*Ciurea ML*

Structure and electrical properties versus annealing of Ge nanoparticles embedded in SiO<sub>2</sub> matrix  
6-th Edition of the Conference on Amorphous and Nanostructured Chalcogenides 2013, Brasov, Romania  
24-28.06.2013

*Craciun V, Socol G, Galca AC*

Pulsed laser deposition of amorphous, transparent and conductive oxides  
E-MRS Spring Meeting, Strasbourg, France  
27-31.05.2013

*Filoti G*

Mössbauer parameters: unusual / atypical behavior versus classical one  
International Conference on the Applications of the Mossbauer Effect, Opatija, Croatia  
1-6.09.2013

*Galatanu M, Popescu B, Enculescu I, Tiseanu I, Galatanu A*

FAST as a new brazing route for refractory materials

IBWAP 2013, Constanta, Romania

4-6.07.2013

*Galca AC*

Spectroscopic ellipsometry: A useful non-destructive technique to probe the physical parameters of nanostructured materials

International Balkan Workshop on Applied Physics (IBWAP) - 13<sup>th</sup> Edition, Constanta, Romania

6-8.07.2013

*Kuncser V, Iacob N, Schinteie G, Palade P, Leca A, Filoti G*

Magnetic relaxation of nanoparticulate systems in relation to bio-medical applications

SCM 2013, Fifth Seeheim Conference on Magnetism, Frankfurt, Germany

29.09 – 3.10.2013

*Nedelcu L, Banciu MG*

Low-loss microwave dielectrics: synthesis, properties, and applications

In: International Balkan Workshop on Applied Physics (IBWAP) - 13<sup>th</sup> Edition, Constanta, Romania

6-8.07.2013

*Nistor SV*

Electron paramagnetic Resonance spectroscopy in the thermal analysis of nanocrystalline Zn-based compounds for nanoelectronics

The 2<sup>nd</sup> Central and Eastern European Conference on Thermal Analysis and Calorimetry (CEEC-TAC2), Vilnius, Lithuania

27-30.08.2013

*Pintilie I*

Bridging the gap between defect analyses and device characteristics

International Symposium on Semiconductors: Defects, Doping and Diffusion (IS2D3), Oslo, Norway

24-25.10.2013

*Pintilie L*

Electric properties of epitaxial ferroelectric films with perovskite structure and different metals as top electrodes

E-MRS Spring Meeting, Strasbourg, France

27–31.05.2013

*Pintilie L*

The (electrode) interface effect on the properties of thin films and multilayers with ferroelectric properties

International Conference from Nanoparticles and Nanomaterials to Nanodevices and Nanosystems (IC4N), Corfu, Greece

16-20.06.2013

*Pintilie L*

Interfaces in ferroelectric-based structures

ELETTRA Synchrotron Trieste, Italy

15.02.2013

*Pintilie L*

NIMP and the research in the field of ferroelectrics

University of Lyon, France

25.11.2013

*Schwandt J, Fretwurst E, Klanner R, Pintilie I, Zhang J*

Study of high-dose X-ray radiation damage of silicon sensors

Damage to VUV, EUV, and X-Ray Optics IV Conference, Prague, Czech Republic

15-18.04.2013

*Stanculescu A, Stanculescu F*

Pure and doped aromatic derivatives crystals growth and characterization

Collaborative Conference on Crystal Growth (3CG), Cancun, Mexic

10-13.06.2013

*Teodorescu CM*

Positron annihilation and materials science generation at ELI-NP

Towards Technical Design Reports of experiments with brilliant gamma-ray beams at ELI-NP, Magurele, Romania

25-26.06.2013

*Teodorescu CM*

X-ray photoelectron spectroscopy of ferroelectrics and metal/ferroelectrics interfaces

The 13th International Balkan Workshop on Applied Physics IBWAP 2013, Constanta, Romania

4-6.07.2013

*Teodorescu CM*

New SuperESCA Romanian Facility at Elettra

Elettra Science Advisory Committee, Trieste, Italy

17.09.2013

*Teodorescu CM*

Magnetic systems synthesized on semiconductor single crystals

New Trends in Nanophysics and Solar Energy Conversion, Magurele, Romania

23-25.09.2013

*Teodorescu CM*

Ferromagnetic ordering of metals in Si(001) and Ge(001)

TIM 2013 – International Physics Conference, Timisoara, Romania

21-25.11.2013

*Teodorescu CM*

Știința Suprafețelor și Interfețelor: implementarea acestei discipline in România în perioada 2007-2013

Lansarea Catalogului de Servicii si Produse INCDFM, Magurele, Romania

29.11.2013

*Vasylykiv O, Borodianska H, Badica P, Sakka Y, Xie SS, Tok AIY, Jan M*

Multilevel design of light boron-based composites for protection, ICMAT 2013

7<sup>th</sup> International Conference on Materials for Advanced Technologies, Suntec, Singapore

30.06-5.07.2013



# Selected Results

## Condensed Matter Physics at Mesoscale

## Resonant tunneling effects at the $\text{SiO}_2/4\text{H-SiC}$ interface

L. D. Filip, I. Pintilie, L. C. Nistor

in cooperation with

B. G. Svensson

Physics Department/Center for Materials Science and Nanotechnology, Oslo University, Norway

Power and high temperature electronics require a wide band gap, high values of breakdown field and stable native oxide semiconductor material such as silicon carbide (SiC). However, metal oxide semiconductor field effect transistors (MOSFETs) based on these materials present a series of issues, such as high density of states at the as-grown  $\text{SiC}/\text{SiO}_2$  interface. It was in the past decade that significant progress was obtained in the growth of quality oxides on SiC and also the passivation of the interface states via nitridation. For the case of the  $n$ -4H-SiC polytype, the fast responding states at the interface ( $D_{it}$ ) and in the oxide near the same interface ( $NIT^{fast}$ ) are greatly reduced while the slow near interface states ( $NIT^{slow}$ ) remain mostly unaffected. We have shown previously that the  $NIT^{fast}$  states do respond to the small a.c. signal and contribute to the frequency dependence of the capacitance-voltage characteristics (C-V) above 150 K [1]. C-V and TDRM measurements on MOS capacitors revealed the existence of the near interface states which do not saturate upon injection even after the passivation of the  $\text{SiO}_2/n$ -4H-SiC interface with N-implantation [1]. Below 150 K, C-V measurements on non-nitridated  $\text{SiO}_2/n$ -4H-SiC capacitors present abnormal minima while on the nitridated samples the minima disappeared [2,3].

These features can be observed in Fig.1.

In order to explain the apparition of the abnormal minima in the C-V characteristics of the non-nitridated samples, we propose a theoretical model suggesting a charge transfer between  $n$ -4H-SiC and  $NIT^{fast}$  oxide states via a tunneling process [4]. The capacitance minima appear in the C-V characteristics at the same voltage values for different measurements frequencies and various temperatures; therefore we can assume that the charge transfer into the

oxide region takes place from well-defined energy levels. To this end we will consider that neutral donor states are localized near the  $n$ -4H-SiC/ $\text{SiO}_2$  interface and are the source of the resonant tunneling electrons [4].

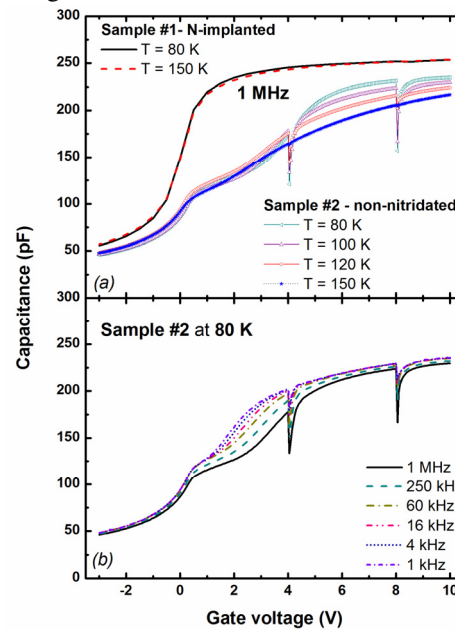


Fig. 1. C-V curves recorded from depletion to accumulation: a) for 1 MHz probe frequency on samples #1-N-implanted and #2-non-nitridated at different temperatures below 150K; b) at 80K, for different frequencies on non-nitridated sample.

Allowing a semi-Gaussian energy distribution for these states and two trapping levels ( $E_1$  and  $E_2$ ) located some distance  $w_b$  from the interface in the oxide layer, able to accommodate the incoming electrons, one can obtain the abnormal minima in the C-V characteristics (see Fig.2). As the applied gate voltage is increased, the neutral donor states and the two energy levels in the oxide layer will shift downwards with different energies such that at some point they will align allowing the electrons to tunnel resonantly from SiC into the oxide. The tunneling-injected negative charge will produce a sudden decrease in the surface potential at the semiconductor-oxide interface which will in

turn be transformed into a minimum in the C-V characteristics.

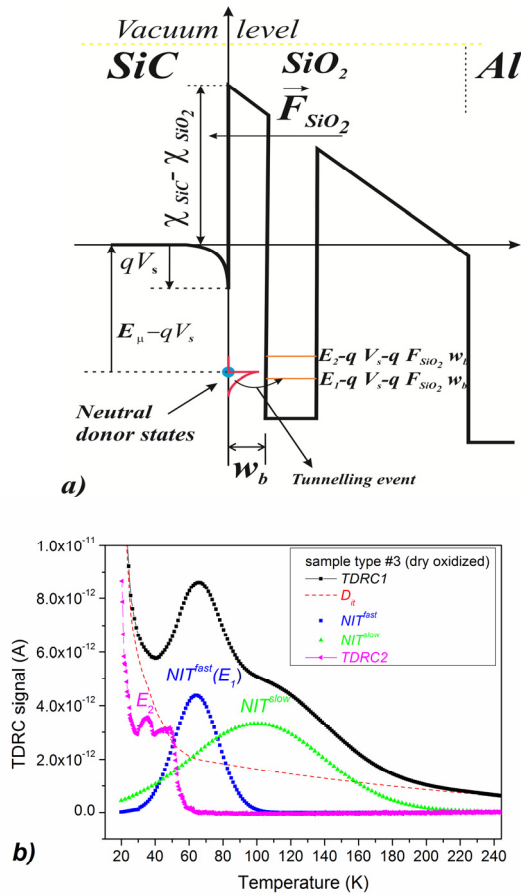


Fig. 2: a) Energy diagram for the proposed theoretical model; b) TDRC spectra showing the measured signals with contributions from  $E_1$  (ascribed to  $NIT^{fast}$ ),  $E_2$  and  $D_{it}$ . TDRC1 corresponds to a charging and discharging biases of  $V_{ch}=+30$  V and  $V_{disch}=-5$  V, respectively while TDRC2 to  $V_{ch}=+10$  V and  $V_{disch}=+3$  V (see Ref. 4 for more details).

As it can be seen good agreement can be obtained between the computed C-V diagrams for different temperatures (Fig. 3) and the measured ones. Using the described theoretical model it is possible to explain the apparition, the position and the depth of the abnormal minima in the C-V diagrams and it shows that given the right conditions (i.e. existence of donor-like states at the interface and available energy states in the SiO<sub>2</sub> region) such features should occur.

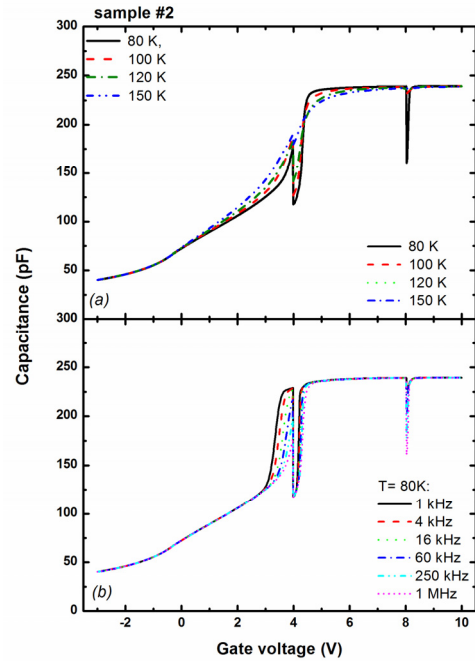


Fig. 3. Computed C-V diagrams for : a) different temperatures and 1 MHz probe frequency; b) 80 K and different probe frequencies.

NIMP researchers acknowledge financial support from the Romanian National Authority for Scientific Research through the CNCSIS Project “RP” Grant No. 1/28/2010.

## References

- [1] I. Pintilie, C. M. Teodorescu, F. Moscatelli, R. Nipoti, A. Poggi, S. Solmi, L. S. Lovlie, and B. G. Svensson, Journal of Applied Physics 108 (2), 2010, 024503 doi: 10.1063/1.3457906
- [2] I. Pintilie, C. M. Teodorescu, F. Moscatelli, R. Nipoti, A. Poggi, S. Solmi, L. S. Lovlie, and B. G. Svensson, Materials Science Forum Vols. 679-680,2011,346-349, Trans Tech Publications, Switzerland; doi:10.4028/www.scientific.net/MSF.679-680.346
- [3] L. D. Filip, I. Pintilie and B. G. Svensson, Materials Science Forum Vols. 740-742, 2013, 557-560, Trans Tech Publications, Switzerland doi:10.4028/www.scientific.net/MSF.740-742.557
- [4] L.D. Filip, I. Pintilie, L. C. Nistor, Thin Solid Films 545, 2013, 22–28; doi:10.1016/j.tsf.2013.03.083

## Conduction mechanisms in epitaxial ferroelectric films

Boni AG, Pintilie I, Pintilie L, Hrib LM, Chirila C, Pasuk I

in cooperation with

Preziosi D, Deniz H, Alexe M

Max Planck Institute of Microstructure Physics, Halle (Saale), Germany

Ferroelectric thin films are being studied for applications as DRAMs and non-volatile memories due to their high value of dielectric constant and to the presence of two stable states of polarization. Even if ferroelectrics films have a high resistivity, the electrical properties are affected by the leakage current. The mechanisms responsible for the leakage current of ferroelectric thin films has been intensive studied during the last decades. The extrinsic contributions to the macroscopic electrical properties, as composition variations or microstructural defects, can be reduced by growing epitaxial ferroelectric layers using pulse laser deposition (PLD). Electrical conduction is studied using capacitor-like structure based on perovskite ferroelectrics as PZT or BTO. This can be affected by the interfaces with electrodes.

The electrodes were from (La,Sr)MnO<sub>3</sub> (LSMO), known for its magnetic properties and for its perovskite structure appropriate for epitaxial growth[1]. The leakage current for LSMO-ferroelectric-LSMO structure was measured on 150K-400K temperature range, for different thicknesses of the ferroelectric layer. It has been found that leakage current depends on polarity, temperature and thicknesses, and simple conduction mechanisms as SCLC or thermionic emission cannot explain the experimental data.

For LSMO-BTO-LSMO a combination of thermionic injection and thermally activated hopping explain the voltage and temperature dependence of the current but fails to explain the thickness dependence. The following equation is suggested for the current density: [1]

$$J_{+/-} = F_1(E_a -/+ E_i) \exp\left(-\frac{q}{kT}\left(\phi_B^0 + W_a\right) - \sqrt{\frac{q(E_a -/+ E_i)}{4\pi\epsilon_0\epsilon_{op}}}\right)$$

Here  $E_a$  is the applied field,  $E_i$  is the imprint

field,  $(W_a + \phi_B^0)$  term takes into consideration both thermal activation energy for hopping and the height of potential barrier at the Schottky contact. The experimental and simulated I-V characteristics are shown in Fig. 1.

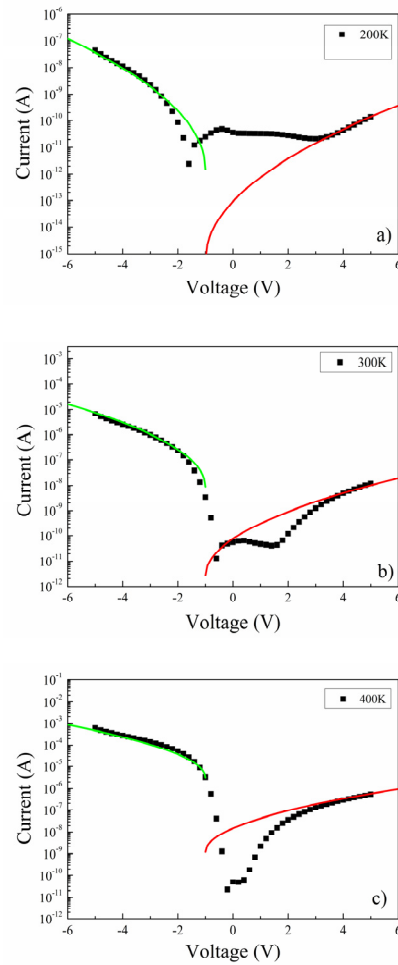


Fig.1 Experimental and simulated I-V characteristics at three temperatures for LSMO-BTO-LSMO structure

The leakage current measurements for LSMO-PZT-LSMO structures reveal a combination between thermionic injection at the interface of ferroelectric layer with electrodes and a bulk controlled drift-diffusion. Potential barriers estimated using Schottky-Simmons equation, are:

1. 0.45 eV for both polarities in the case of 25nm ferroelectric layer thickness;
2. 0.45eV for positive polarity and 0.75eV for negative polarity in the case of 50nm ferroelectric layer thickness;
3. 0.25eV for positive polarity and 0.8eV for negative polarity in the case of 100nm ferroelectric layer thickness;

In the case of (Pt, Cu, and SrRuO<sub>3</sub>)/Pb(Zr<sub>0.2</sub>Ti<sub>0.8</sub>)O<sub>3</sub>/SrRuO<sub>3</sub>/SrTiO<sub>3</sub>(001) heterostructure, the magnitude of the leakage current and the shape of the I–V characteristics are strongly influenced by the top electrode interface [2]. The lowest values of the leakage current are obtained for top Cu and the highest for top Pt (Fig. 2).

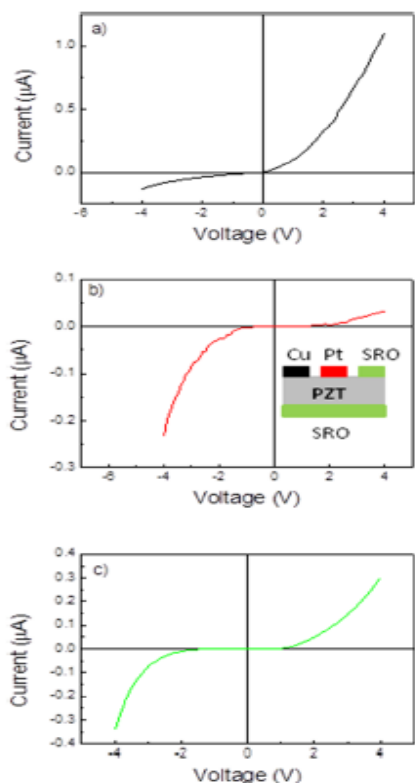


Fig. 2 I-V curves of the MFM structure based on PZT with different top metals: (a) Cu; (b) Pt and (c) SrRuO<sub>3</sub> (SRO).

The electrical properties of epitaxial metal-ferroelectric-metal (MFM) structure based on Pb(Zr<sub>0.2</sub>Ti<sub>0.8</sub>)O<sub>3</sub> can be simulated and modeled as a back-to-back connection of two Schottky diodes. In Fig. 3 are presented the results of simulations of the I-V curves, considering that the reverse current in a Schottky-type diode is controlled by thermionic

emission. The Schottky-Simmons equation was used for simulations.

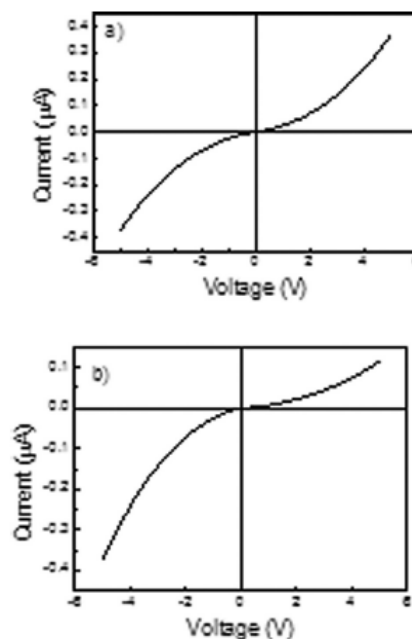


Fig. 3 Simulated I-V curves: (a) symmetric and (b) slightly asymmetric MFM structure

The calculate I-V characteristic resembles well the experimental curves obtained for top SRO and Pt. A slight asymmetry of the potential barriers at the electrode interfaces behaving as Schottky contacts may induce diode-like behavior (Fig. 3b), but this is not switchable with the orientation of the ferroelectric polarization. However, a switchable diode-like behavior can be present in the case of MFM structure based on BiFeO<sub>3</sub>. This can be related to the smaller band gap of BiFeO<sub>3</sub> compared to PZT.

NIMP researchers acknowledge financial support from PNII 72-153/2008, 12-101/2008, PCCE ID 76, RU-TE-2011-3-0016 and Core Program PN09-45.

## References

- [1] Boni AG, Pintilie I, Pintilie L, Preziosi D, Deniz H, Alexe M, Journal of Applied Physics, (2013), 113, 10.1063/1.4808335
- [2] Hrib LM, Boni AG, Chirila C, Pasuk I, Pintilie I, Pintilie L, Journal of Applied Physics, (2013), 113, 214108

## Pyroelectric effect in epitaxial PZT thin films

*M. Botea, A. Iuga and L. Pintilie*

The change with temperature of the spontaneous polarization in a ferroelectric material, known also as pyroelectric effect, is typically used to detect infrared radiation. The advantage of this type of detectors is that they can be successfully used at ambient temperature. [1,2] Pyroelectric detectors are used in applications like intruder alarms, motion sensors, non-contact temperature measurements, thermal imaging, etc. Usually the active element is a ferroelectric capacitor made from a bulk ceramic or a single crystal. The need for miniaturization and integration with semiconductor technology requires the change from bulk materials to thin films.

The development of the deposition methods enable now to control the film thickness, the composition, the epitaxial strain, allowing the growth of high quality epitaxial structures. The pyroelectric response of thin films is related to microstructure (granulation, domain structure, defects) and quality of the interfaces, which can be controlled during the growth process.

Lead zirconate titanate (PZT) is the best solution for applications required by new technology, due to the fact that the variation of the Zr/Ti ratio and the addition of dopants can lead to significant improvement of the physical properties of the material, including pyroelectric ones.

In order to obtain an epitaxial PZT thin film, we used pulsed laser deposition (PLD). The film was grown on SrTiO<sub>3</sub> (STO) substrate with (001) orientation. A SrRuO<sub>3</sub> (SRO) buffer layer, which is an excellent template for the epitaxial growth of high-quality ferroelectric perovskites, was used. This is acting also as a bottom electrode.

The quality of the films was tested by X-ray diffraction (XRD), (Fig.1) and transmission electron microscopy (TEM). Phi scan indicate that these structures are perfectly aligned in plane, showing cube on cube epitaxy.

Top electrodes were deposited by radio-frequency sputtering, using a metal shadow mask. The capacitance-voltage (C-V) and polarization-voltage (P-V) loops are shifted to positive voltages, suggesting an internal electric field which is preserving the polarization orientation.

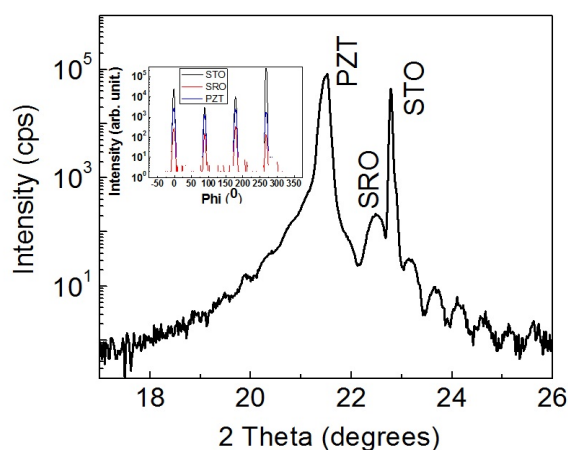


*Fig.1 X-ray diffraction of the PZT/SRO/STO structure. In the inset-Phi-scan showing the epitaxial relation between the deposited PZT/SRO layers on STO single crystal substrate with (001) orientation.*

The pyroelectric response is directly related to the substrate thermal properties, the thickness and the thermal properties of the layer, the orientation of the spontaneous polarization, domain structure, defect concentration, etc. A random orientation of polarization direction (as in case of polycrystalline materials) leads to a small pyroelectric response, especially under unpolled conditions. High crystalline quality and optimal domain orientation maximize the pyroelectric properties. [3]

Pyroelectric tests were performed in modulated light, using a laser diode with 800 nm wavelength, and a mechanical chopper having variable frequency. The pyroelectric signal was collected with the aid of a field effect transistor (voltage operation mode) and measured with a

lock-in amplifier. The pyroelectric coefficient was extracted from the  $\log S\text{-}\log\omega$  representation ( $S$ -pyroelectric signal measured in the voltage mode,  $\omega$ - pulsation of the incident radiation) and has a value over  $10^{-3} \text{ C/cm}^2\text{K}$ .

As can be seen from Fig.2, at low frequencies the pyroelectric signal is almost constant and then this decreases with the frequency, depending if the sample is uniformly heated or not.

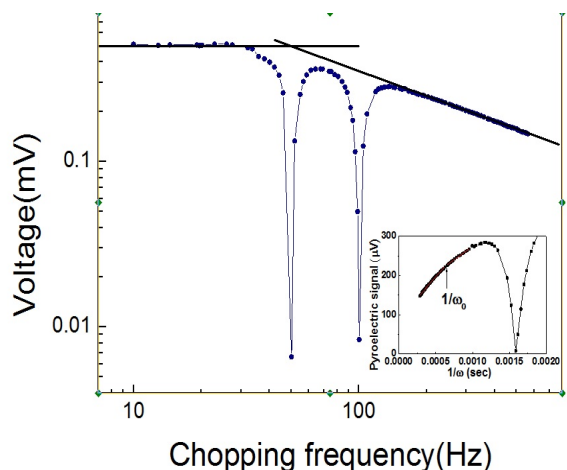


*Fig.2 The frequency dependence of the pyroelectric signal obtained from the Pt/PZT/SRO/STO. In the inset – the dependence of the pyroelectric signal on  $1/\omega$ .*

The high value obtained for the pyroelectric coefficient is due to the dominant presence of the  $90^\circ$  type domains. The rectangular grid observed with the piezoelectric force microscopy (PFM) is associated with the presence of these domains. (Fig.3)

Other contributions, less significant than the above mentioned, can be the compressive strain (which gives high values of polarization), the piezoelectric contributions caused by different expansion coefficients of the pyroelectric layer and the substrate, and non-uniform heating of the active layer. However, in the frequency range where the signal is almost constant, it can be considered that the sample is uniformly heated and the pyroelectric coefficient can be determined without errors.

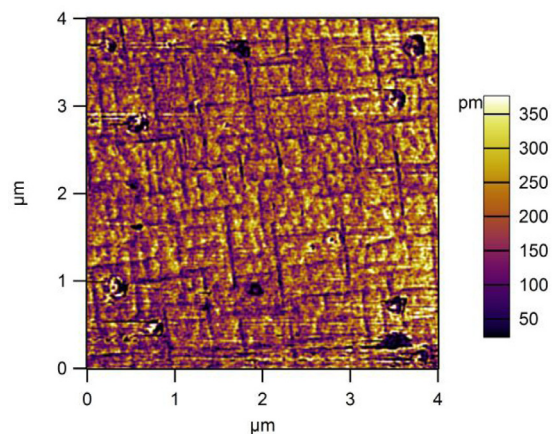


*Fig.3 The PFM image of the surfaces of the PZT layer*

In conclusion, the pyroelectric signal depends on the thickness and the thermal properties of the substrate. A suspended detector would eliminate the effect of the substrate, allowing a large temperature variation of the active pyroelectric layer, thus improving its response.

NIMP researchers acknowledge financial support from from the Romanian Ministry of Education through the Idea-Complex Research Grant PN-II-ID-PCCE-2011-2-0006 (contract nr. 3/2012).

#### References:

1. M.Botea, A.Iuga, and L.Pintilie, Applied Physics Letters, (2013), 103, 232902
2. C. W. Tipton, K. Kirchner, R. Godfrey, M. Cardenas, S. Aggarwal, H. Li, R. Ramesh, Applied Physics Letters, (2000), 77, 2388
3. R. P. Godfrey, T. Friessnegg, R. Ramesh, C. W. Tipton, R. C. Hoffman, D. N. Robertson, E. H. Poindexter, M. A. Quuada, B. Nielsen, D. J. Keeble, Integrated Ferroelectrics, (1999), 25, 135-147

## Interplay of charge density wave and superconductivity in the low dimensional metal $\text{Tl}_x\text{V}_6\text{S}_8$

C.F. Miclea, C. Miclea

in cooperation with

H.D. Hochheimer, B. Martin

Department of Physics, Colorado State University, Fort Collins, CO 8052, USA

T. Ohtani

Laboratory for Solid State Chemistry, Okayama University of Science, Okayama, Japan

The interdependence between different ground states in solid state physics is of great interest both theoretically and experimentally. Here we focus on the interplay between superconductivity (SC) and charge density wave (CDW) instability in  $\text{Tl}_x\text{V}_6\text{S}_8$ , a metallic system with reduced electronic dimensionality. This whole report is based on the reference [1].

$\text{TlV}_6\text{S}_8$  is a metallic system with a quasi-one-dimensional (1D) structure based on hexagonal cells of the  $\text{Nb}_3\text{X}_4$ -type (P63 space group). Resistivity and susceptibility measurements indicate a decrease in electronic density of states (DOS) [2, 3]. This coupled with a first-order structural phase transition and corroborated with the nesting conditions revealed by band structure calculations, indicate the formation of a CDW phase in this compound. At a significantly lower temperature  $\text{TlV}_6\text{S}_8$  adopts a SC ground state.

Polycrystals of  $\text{Tl}_x\text{V}_6\text{S}_8$  ( $x=0.1, 0.15, 0.25, 0.47, 0.63$  and  $1$ ) were prepared by vapor deposition and investigated by resistivity, magnetic susceptibility and specific heat measurements. For selected compositions resistivity measurements under hydrostatic pressure,  $p$ , were carried out.

The CDW anomaly is present in all samples (fig. 1) with a clear thermal hysteresis (inset figure 1) which varies with the composition indicating a first-order phase transition. The temperature of the CDW phase transition shows a slight dependence on Tl concentration; it is continuously reduced upon increasing  $x$  up  $0.63$  and then enhanced again at  $x = 1$ . The most pronounced CDW anomaly observed for half Tl filling,  $x = 0.47$ , corresponds to an increase in resistivity of about 36%. Remarkably, this is the

only composition, which does not display any signature of superconductivity down to the lowest temperature of our investigation.

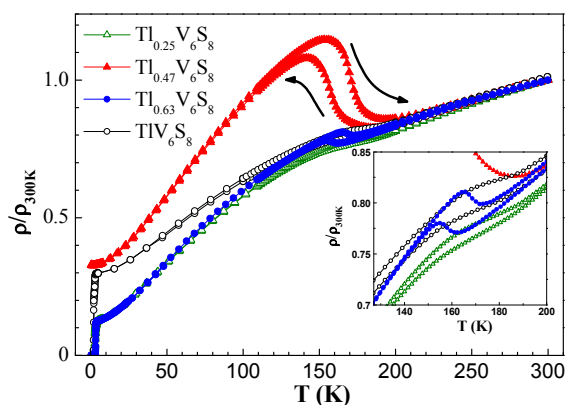


Fig.1 Normalized resistivity vs. temperature for different Tl concentrations. The inset emphasizes the hysteretic behavior (from ref. [1]).

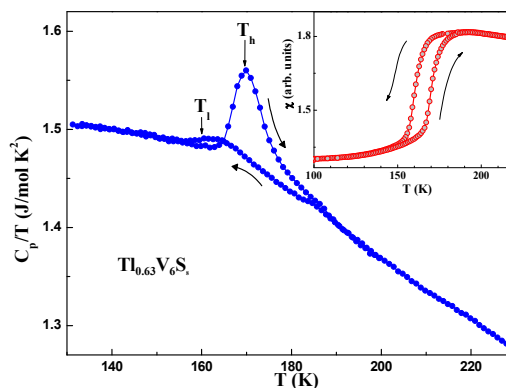


Fig.2 CDW transition revealed by specific heat. Inset: Susceptibility across the CDW transition (from ref. [1]).

The susceptibility and specific heat measurements, exemplified for  $x=0.63$  in fig. 2, are also hysteretic and reveal a transition temperature in excellent agreement with the resistivity. The susceptibility indicates an effective drop of the DOS by  $0.83 \times 10^{17}$  states  $\text{J}^{-1}\text{mol}^{-1}$  (roughly 30%) upon opening the CDW

gap. This is significantly higher than the drop revealed by resistivity. It is likely that the V chains have different contributions to the CDW and SC. A similar picture emerged from electron diffractions measurements on the isostructural  $\text{In}_x\text{Nb}_3\text{Te}_4$  [4] where two of the three Nb zigzag chains are responsible for the CDW and the third for SC. Electrical resistivity would therefore be less affected if CDW gaps open more on two of the channels and less (or not at all) on the third. This is also corroborated by the rather weak interdependence of superconductivity and CDW as revealed by our pressure studies.

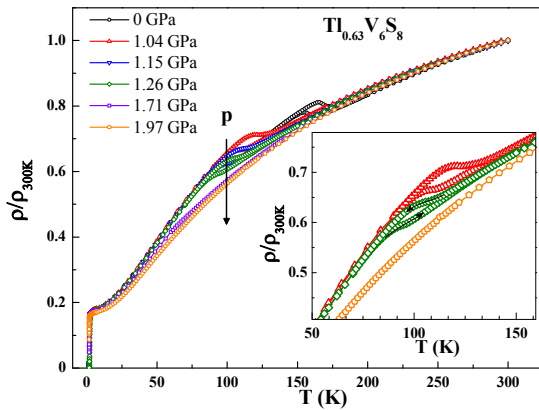


Fig. 3 Normalized resistivity vs. temperature at different pressures for  $\text{Tl}_{0.63}\text{V}_6\text{S}_8$  (from ref. [1]).

The transition from the CDW gaped state into the SC phase is also revealed by specific heat. For  $x=0.63$ , we estimate a Debye temperature of  $\Theta_D = 246$  K and an electron-phonon coupling constant  $\lambda = 0.61$ , same as for the metallic V. Taking into account the effect of anisotropy on the thermodynamic properties of superconductors [5], we find a very large value for mean-squared anisotropy,  $\langle a^2 \rangle = 0.24$  and a normalized energy gap  $\Delta_0/(k_B T_c) = 1.14$  lower than the 1.76 value expected from the BCS theory. For details see Ref. [1]. Our specific heat results suggest that this compound is a highly anisotropic weak coupled superconductor. However, the value of the electronic specific heat term in the normal state above the SC transition is large,  $\gamma = 447$  mJ/(mol K<sup>2</sup>) and might be an indication of strong electronic correlations.

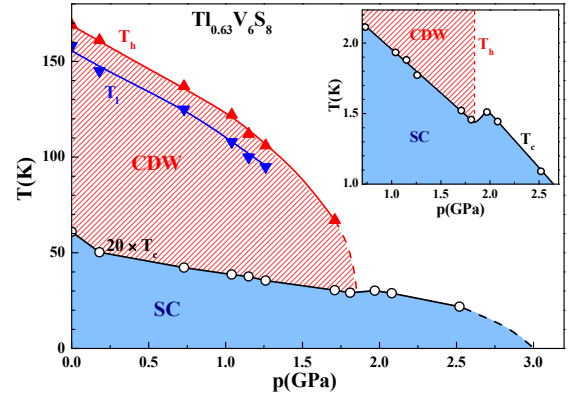


Fig. 4 Phase diagram for  $\text{Tl}_{0.63}\text{V}_6\text{S}_8$ . At the critical pressure,  $p_c$ , CDW is suppressed and concomitantly  $T_c$  is enhanced (inset). The dashed lines are guides for the eye (from ref. [1]).

The study of resistivity under pressure (fig. 3) reveals a rapid suppression of CDW transition temperature upon increasing  $p$  for all samples investigated. The pressure is also detrimental to the SC phase with  $T_c$  being reduced with increasing  $p$ . Nevertheless, as the CDW gap is closed at a critical pressure  $p_c = (1.85 \pm 0.12)$  GPa, the increase of the density of states leads also to a small enhancement of  $T_c$  of roughly 120 mK (see the inset in fig. 4) suggesting that SC and CDW compete for parts of the Fermi-surface.

## References

- [1] C. F. Miclea, H. D. Hochheimer, B. Martin, C. Miclea and T. Ohtani, *New Journal of Physics* **15**, 083008 (2013).
- [2] T. Ohtani, Y. Miyoshi, Y. Fujii, T. Koyakumar, T. Kusano and K. Minami, *Solid State Commun.* **120**, 95 (2001).
- [3] W. Bensch, J. Abart and E. Amberger, *Solid State Commun.* **58**, 631 (1986).
- [4] T. Ohtani, Y. Yokota and H. Sawada, *Japan. J., Appl. Phys.* **38**, L142 (1999).
- [5] J. R. Clem, *Ann. Phys. NY* **40**, 268 (1966).

## Relationship between optical properties, density and cations concentration in amorphous oxide semiconductors

A.C. Galca, L.M. Trinca

in cooperation with

G. Socol, V. Craciun

National Institute for Lasers, Plasma and Radiation Physics, Magurele, Romania

Investigation of the dependence between the cation concentration and optical properties of amorphous-like  $\text{In}_{x-w}\text{Ga}_w\text{Zn}_{1-x}\text{O}_{1+0.5x-\delta}$  (a-IGZO) thin films were performed in order to prove the stoichiometry control necessity when designing a device for transparent electronics, such as TFTs (depicted in Fig.1).

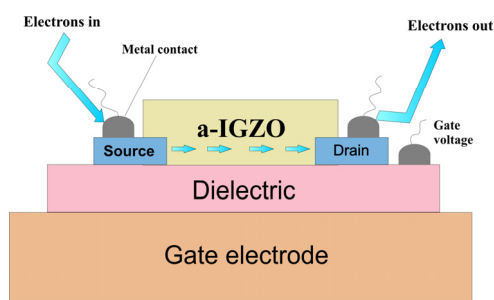


Fig.1 Schematic representation of a Thin Film Transistor with a-IGZO channel.

Aiming to find a correlation between optical properties, density and cation concentration of given amorphous oxide semiconductors, Spectroscopic Ellipsometry (SE) and X-Ray Reflectivity (XRR) were employed. These two techniques have the major advantage of being non-invasive, hence non-destructive characterization methods.

The natural trends that regard the physical properties of such materials were studied. Their properties are strongly related to the constituent atoms/ions concentration. Ternary or quaternary compound properties should be derived firstly from those of each binary compound. By mixing ZnO which has a hexagonal wurtzite structure,  $\text{In}_2\text{O}_3$  with cubic bixbyite structure and  $\text{Ga}_2\text{O}_3$  with monoclinic structure, the  $\text{In}_{x-w}\text{Ga}_w\text{Zn}_{1-x}\text{O}_{1+0.5x-\delta}$  will have an amorphous-like structure for a wide range of concentrations.

Besides its amorphous nature which assures the desired electrical and mechanical properties,

IGZO has the advantage of being highly transparent in the visible spectrum (Fig. 2a), which recommends this material for transparent electronics as channel gate instead of a-Si which is opaque or a-SiC which is less optical dense but it has poorer electric properties than a-Si.

This semiconductor can be easily degenerated by overbalancing one cation with respect to the others, becoming in this way an transparent conductive oxide (TCO). Fig.2(b) shows the imaginary part of dielectric constant of the TCOs proposed in literature.

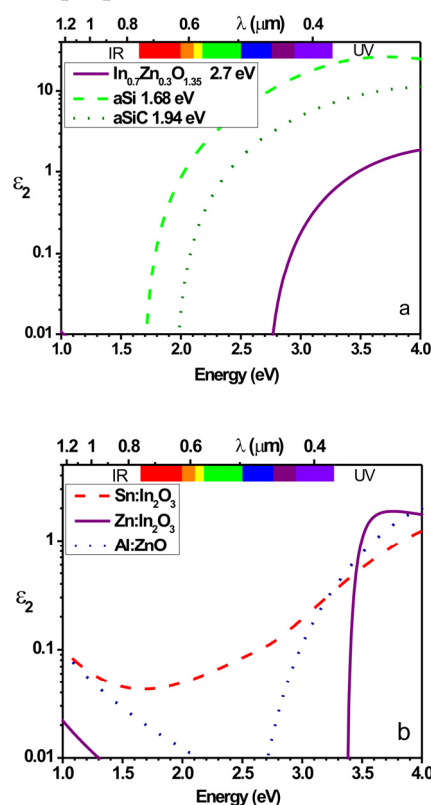


Fig.2 -adapted from ref [1] - (a) Imaginary part of dielectric function of aIZO, aSi and aSiC; (b) Imaginary part of dielectric function of ITO, IZO and AZO.

By comparing the binary semiconductors, there is an evident correlation between the

average atomic number  $\bar{Z}$  and the band gap, lattice constant and optical properties (Eq.1).

$$\bar{Z} \propto a \propto \varepsilon_{\infty} \propto n \propto \frac{1}{E_g} \quad (1)$$

For  $A_{1-x}B_xC$  ternary compounds, the equation that express better the material properties as a function of composition is Eq.(2):

$$T(x) = T_{AC} + \beta x + \gamma x^2 \quad (2)$$

where:

$$\beta = T_{BC} - T_{AC} \quad (3)$$

and  $\gamma$  is a bowing parameter which is used in the case of deviation from a linear relationship.

For  $In_xZn_{1-x}O_{1+0.5x-\delta}$  has been observed a clear relationship between band gap and cation concentration for  $x_{In} \in \{0.3 - 0.6\}$ :

$$E_g^{In_xZn_{1-x}O}(x) \approx 2.77 - 0.57x \quad (4)$$

The SE and XRR thickness results obtained for different stoichiometries of a-IGZO thin films indicate similar values within 10% (Fig.3). The discrepancy is due to different size area measured by the mentioned techniques as well as due to abrupt hill like thickness lateral profile specific to the deposition method (PLD).

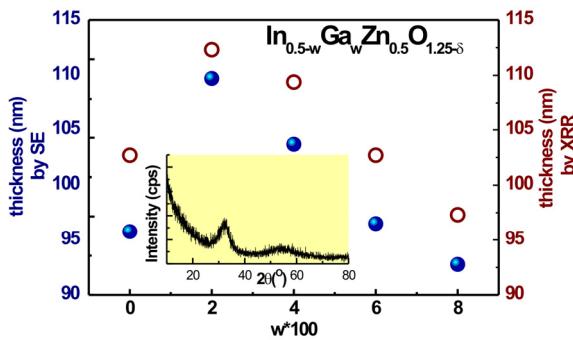


Fig.3 -adapted from ref [1] - Thin film thicknesses determined by SE and XRR. Inset: XRD pattern of a-IGZO ( $w=0.02$ ) thin film deposited on glass.

When replacing a heavier atom (e.g. In) with a lighter one (e.g. Ga), the refractive index and the mass density are decreasing as shown in Fig.4a, in accordance with Eqs.1&3. The two parameters do not follow a perfect linear behavior, most probably due to the inhomogeneity in composition and influence of the extended defects which might be different from sample to sample.

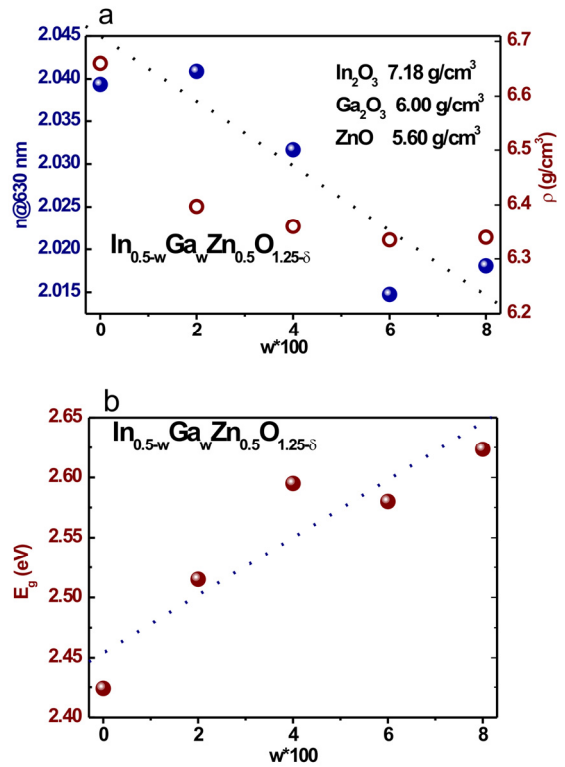


Fig.4 -adapted from ref [1]- (a) Thin film refractive index determined by SE and mass density derived from XRR measurements. In inset are written the bulk crystalline compounds densities. (b) Band gap vs. Ga concentration in a-IGZO thin films.

According to Eq.1 the band gap will increase while decreasing the average atomic number (increasing the Ga concentration). This dependence is proved experimentally in Fig. 4(b).

In conclusion, the optical properties of ternary and quaternary semiconductors (e.g. a-IGZO) can be optimized as a function of experimenter necessity by adjusting material composition.

NIMP researchers acknowledge financial support from RU-TE-2011-3-0016.

### Reference

- [1] A.C. Galca, G. Socol, L.M. Trinca, V. Craciun Applied Surface Science 281 2013, 96-99; doi:10.1016/j.apsusc.2013.01.176

## Thermal transformation and non-isothermal crystallization kinetics of doped glass

*C. Bartha, C. Plapcianu, P. Palade*

in cooperation with

*M. Elisa and B. Sava*

National Institute of Research and Development for Optoelectronics, Magurele, Romania

Glasses with photonic properties have been attracting a great attention due to their expected significant role in the next generation of multimedia systems. Phosphate glasses are excellent host materials for active rare earth (RE) ions due to advantageous local structure effect and high RE ion solubility. Such RE-doped phosphate glasses demonstrate high UV transmission, low linear and nonlinear refractive index, low viscosity and low melting temperatures [1-3]. An essential condition to obtain desired properties refers to the rigorous control of processing parameters, and this is done only by knowing and understanding the formation mechanism of the involved materials.

Detailed kinetic understanding of the nucleation and crystallization process is therefore fundamental to propose new processing conditions for a controlled crystallization, morphology and microstructure of the material.

The crystallization kinetics of Eu-doped phosphate glass with molar composition of 20.42 Li<sub>2</sub>O-10.25 Al<sub>2</sub>O<sub>3</sub>-58.49 P<sub>2</sub>O<sub>5</sub>-7.23 BaO-1.44 La<sub>2</sub>O<sub>3</sub>-2.16 Eu<sub>2</sub>O<sub>3</sub> and particle size lower than 30 μm has been studied by differential thermal analysis (DSC) under non-isothermal conditions. The kinetic parameters of the crystallization process were comparatively determined by different models.

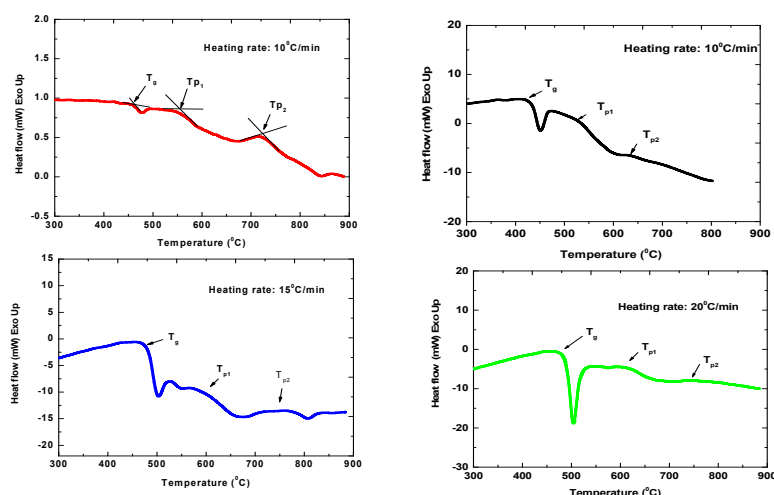


*Figure 1: DSC curves obtained in synthetic air, at four different heating rates, as follow: 2, 10, 15 and 20°C/min (particle size < 30μm) [2].*

Crystalline phases formed during the thermal treatment of glass were identified by X-ray diffraction. Differential scanning calorimeter measurements at four heating rates, from room temperature up to 900°C using synthetic air (Fig.1) have revealed that the step changes in heat flow signals are associated with the presence of three important effects: the first one,

corresponding to the glass transition effect appearing at  $T_g$ , is followed by two exothermic peaks. The first peak, which is more pronounced, is associated to a first crystallization process (taking place at  $T_{p1}$ ), while, the second one, of lower intensity, corresponds to a second crystallization process (at  $T_{p2}$ ) [2].

The kinetic parameters of the crystallization process were comparatively determined using both Friedman (Fig.2) and Ozawa-Flynn-Wall analysis (Fig.3).

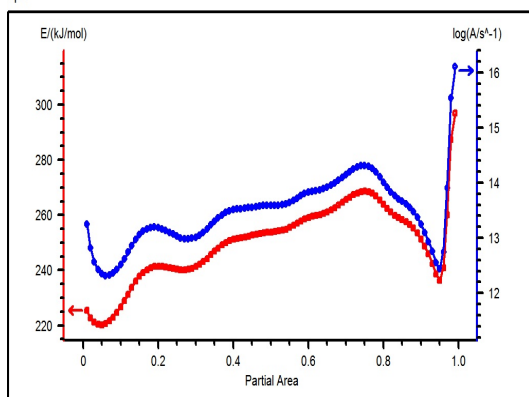


Figure 2 : Energy plot of Friedman analysis [2].

According to the Friedman analysis (see Fig.2), the maximum of the activation energy for this first crystallization peak is obtained for a conversion rate of 75% ( $265.52 \pm 4$  KJ/mol). From the energy plot (which takes into account all the values obtained from Friedman lines) it is obvious that the crystallization process occurs as a multistep-reactions (four maxima on  $E_a$  curve). Similar values are also obtained by applying Ozawa-Flynn-Wall free-model (Fig. 3).

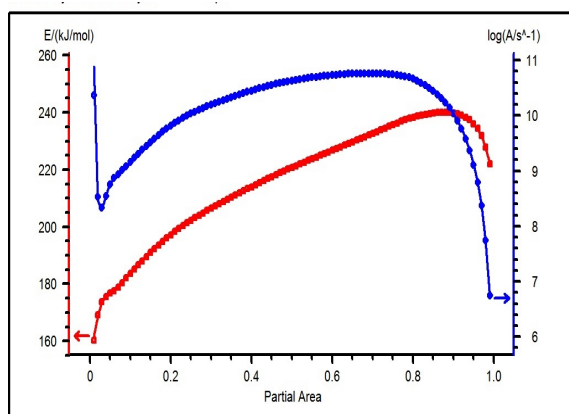


Figure 3 : Energy plot of Ozawa-Flynn-Wall analysis [2].

Hence, the maximum value of the obtained activation energy at a conversion rate of 90% is, according to the Ozawa-Flynn-Wall analysis, of  $239.91 \pm 2$  KJ/mol, in good agreement with

Friedman's data. In both model-free evaluations,  $E_a$  values are very similar and consistent with each other. The comparative kinetics of processes met in glass is very important because is offering essential information regarding the transformation mechanisms by the two parameters (activation energy and pre-exponential factor) and is widely investigated. In our case, the values of activation energies calculated from the above mentioned methods show variation in different stages of transformations. The observed decrease in the activation energy with temperature demonstrates that the rate constant of crystallization is in fact determined by the rates of two processes: (i) nucleation and (ii) diffusion. The pre-exponential factor (known as the frequency factor) gives the number of attempts per second made by the nuclei to overcome the energy barrier and reflects the information about the number of nucleation sites. It has a decreasing trend for the two peaks of crystallizations. Thus, it is possible to assert that at temperatures corresponding to the first crystallization peak, the number of crystallization nuclei is initially increasing and then followed by an intense crystal growth process. This is evidenced by the increased values of the activation energy and pre-exponential factor for the highest crystallization fraction of 70-90 %.

## References

- [1] I. Feraru, I.C. Vasiliu, R. Iordanescu, M. Elisa and C. Bartha, Engineering and Applied Electrochemistry, 49(6), 493–499. (2013)
- [2] B. Sava, C. Bartha, M. Elisa, R. Iordanescu, I. Feraru, C. Plapcianu, R. Patrascu, Ceramics International (Manuscript Number: CERI-D-14-00545)
- [3] C.E. Secu, C. Bartha, S. Polosanu, M. Secu, Journal of Luminescence, Volume 146, p.543 (2013)

## Te and SiC co-doped MgB<sub>2</sub> obtained by ex-situ Spark Plasma Sintering technique

G. Aldica, S. Popa, M. Enculescu, P. Badica

The literature indicates that C-based compounds [1] are very effective additions to improve the functional characteristics of MgB<sub>2</sub> superconductors. These compounds usually replace B with C in the MgB<sub>2</sub> crystal lattice. It has been shown that SiC is very efficient and is preferable to carbon [2]. This is because SiC has a double action through chemical substitution, and morphology composite details [1,3,4]. The two effects of SiC addition have been shown to influence pinning and connectivity, both important in controlling critical current density,  $J_c$ . Following the idea of a double action, we hypothesize that the use of two or more additions with different and specific functions can provide means to further improve the practical superconducting characteristics. Several articles have addressed this approach. Ma et al. [5, 6] added Cu and SiC, Kimishima et al. [7] added Cu, Nb, Ag or Pt and SiC, Zhang et al. [8] added C and SiC, Flukiger et al. [9] added B<sub>4</sub>C and SiC. All these articles showed enhancement of  $J_c$  in low, intermediate or high magnetic fields and in different temperature ranges, depending also on the processing route. It should be noted that the indicated articles used *in-situ* approaches starting from mixtures of Mg and B. Additions were also introduced to the starting mixture.

In this work [10] we show that an *ex-situ* route for double co-doping of a commercial MgB<sub>2</sub> powder with SiC and Te can enhance  $J_c$  in high fields at up to 30 K, as well as  $H_{irr}$ . Recently we have shown [11] that *ex-situ* spark plasma sintering (SPS) of MgB<sub>2</sub> with added Te produces bulk materials with higher  $J_c$  and  $H_{irr}$  than the pristine sample. SPS applies a uniaxial pressure and a pulsed electrical current to a graphite die system loaded with a powder. The use of a pulsed current induces specific non-thermal activation effects [12]. Most of these effects strongly influence grain boundaries. SPS also produces nano-grained high density bulk

materials of difficult to consolidate materials. Nano-grained high density MgB<sub>2</sub> is highly desirable. A low grain size means a high density of grain boundaries and it has been established that the grain boundaries in MgB<sub>2</sub> are excellent vortex pinning sites enhancing the critical current density [13]. Modification of the boundaries, introduction of defects, and control of the grain size by SPS and the use of additives are of practical interest.

Samples with added SiC show, as expected, a decrease in critical temperature  $T_c$  (Fig. 1). This indicates C substitution for B in the crystal lattice of MgB<sub>2</sub>, an effect which is accompanied by a decrease in the *a*-axis lattice parameter, while the *c*-axis parameter remains almost constant. Tellurium has no significant influence on  $T_c$  or the lattice parameters.

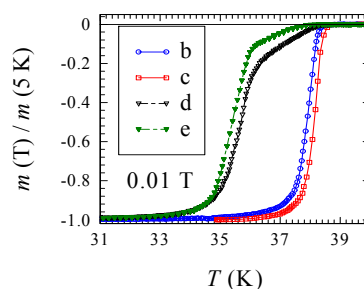
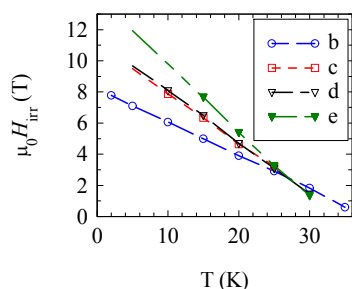


Fig. 1. Normalized magnetization vs. temperature for an applied magnetic field  $\mu_0 H_{dc} = 0.01$  T. Samples are: (b) pristine; (c)  $x_{Te} = 0.01$  (d)  $x_{SiC} = 0.025$ ; (e)  $x_{Te} = 0.01 + x_{SiC} = 0.025$ .

The amount of Te in the samples was selected based on results of ref. [11]. Sample c (MgB<sub>2</sub>(Te)<sub>0.01</sub>) had higher  $J_c(5-30$  K) (Fig. 3) and  $H_{irr}$  (Fig. 2) values than the pristine MgB<sub>2</sub> sample b. SiC was added (sample d, MgB<sub>2</sub>(SiC)<sub>0.025</sub>) at half of the amount of C<sub>60</sub> added in sample (MgB<sub>2</sub>)(C)<sub>x=0.05</sub> [14], which showed significant enhancement of  $J_c(5-30$  K) in high fields.

Addition of SiC to our samples slightly decreased  $T_c$  (Fig. 1) and improved  $J_c(5-30$  K) in high fields (Fig. 3), above the values for pristine MgB<sub>2</sub> sample b.



**Fig. 2.** Irreversibility field vs. temperature ( $100 \text{ A cm}^{-2}$  criterion).

When the indicated amounts of Te and SiC were co-added (sample e,  $\text{MgB}_2(\text{SiC})_{0.01}\text{Te}_{0.01}$ ) the values of  $J_c(5\text{--}30 \text{ K})$  in high fields (e.g. above 4 T at 5 K and 3 T at 20 K) (Fig. 3) and  $H_{\text{irr}}$  (Fig. 2) were higher than for all the single-compound-added or pristine samples.

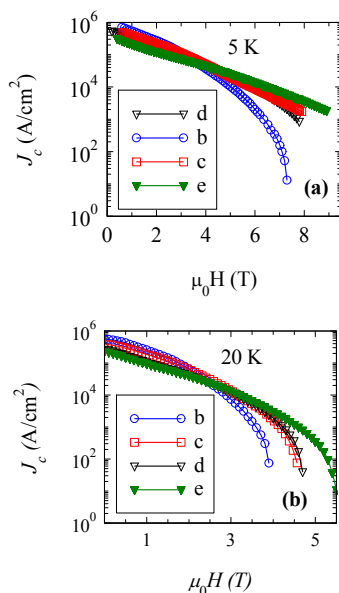


**Fig. 3.** Magnetic field  $H$  dependence of the critical current density  $J_c$  at (a)- 5 K and (b)- 20 K.

This is remarkable considering that SiC is considered one of the most efficient additions to  $\text{MgB}_2$  to enhance  $J_c$  in high fields and at high temperatures. The results indicate the possibility of further increasing the value of  $J_c$  in high fields and at high temperatures, while preserving a good level of  $T_c$ . Co-added sample e has a  $J_c(20 \text{ K})$  of  $10^3 \text{ A cm}^{-2}$  at 4.6 T. The co-addition of Te and SiC can enhance flux pinning, resulting in higher  $J_c(5\text{--}30 \text{ K})$  and  $H_{\text{irr}}$  values than for a pristine  $\text{MgB}_2$  sample and for samples with Te or SiC added separately. The contributions of Si and Te to  $\delta T_c$  pinning are collaborative rather

than additive. The data indicate that the number of boundaries derived from the average crystallite size of  $\text{MgB}_2$  cannot explain the  $\delta T_c$  flux pinning behavior of our samples. Other morphological details, such as the uniformity of the Si and Te distributions vs. impurity phases, have to be considered.

## References

- [1] Kim JH, Oh S, Heo YU, Hata S, Kumakura H, Matsumoto A, et al. 2012 *NPG Asia Mater.* **4** 1.
- [2] Yeoh WK, Dou SX 2007 *Physica C* **456** 170.
- [3] Birajdar B, Peranio N, Eibl O 2008 *Supercond. Sci. Technol.* **21** 073001.
- [4] Birajdar B, Eibl O 2009 *J. Appl. Phys.* **105** 033903.
- [5] Ma Z, Liu Y, Hu W, Gao Z, Yu L, Dong Z 2009 *Scripta Mater.* **61** 836.
- [6] Ma Z, Liu Y, Yu L, Zhao Q 2008 *J. Appl. Phys.* **104** 113917.
- [7] Kimishima Y, Okuda T, Uehara M, Kuramoto T 2007 *Physica C* **463–465** 286.
- [8] Zhang X, Ma Y, Wang D, Gao Z, Wang L, Qi Y, Awaji S, Watanabe K, Zheng D 2009 *IEEE Trans. Appl. Supercond.* **19** 2694.
- [9] Flukiger R, Lezza P, Cesaretti M, Senatore M, Gladyshevskii R 2007 *IEEE Trans. Appl. Supercond.* **17** 2846.
- [10] Aldica G, Popa S, Enculescu M, Badica P 2013 *Scripta Mater.* **68** 428.
- [11] Aldica G, Popa S, Enculescu M, Badica P 2012 *Scripta Mater.* **66** 570.
- [12] Munir ZA, Anselmi-Tamburini U, Ohyanagi M 2006 *J. Mater. Sci.* **41** 763.
- [13] Larbalestier DC, Cooley LD, Rike MO, Polyanskii AA, Jiang J, Patnaik S, et al. 2001 *Nature* **410** 186.
- [14] Miu L, Aldica G, Badica P, Ivan I, Miu D, Jakob G 2010 *Supercond. Sci. Technol.* **23** 095002.

The authors acknowledge “Nucleu”-PN09-450103 and Idei Complexe 9/2010.

## Effect of tritiation on the superconducting properties of MgB<sub>2</sub>

V. Sandu, G. Aldica, M. Baibarac

Harnessing the fusion energy seems to be not that far off and the big projects like ITER in Cadarache, France, are on the way to demonstrate the sustainability of the fusion reactions as source of energy. Among the problems related to materials which still waiting to be solved, we mention two capital issues: the release of neutrons and tritium (<sup>3</sup>H) uptake which have severe effects on the structural components. Neutron capture leads to the formation of radioactive isotopes, some of them with very long life time. Meanwhile, tritium penetrates fast into the crystalline lattice of the metal components where it creates damaged structures. The confining magnets which is located in the nearest vicinity of the fusion plasma, hence submitted to a high flux of neutrons and tritium. MgB<sub>2</sub> might successfully compete with the NbTi and Nb<sub>3</sub>Sn because the activity of the transmutation products is evaluated to decrease to a safe level in several tens of years whereas the radionuclide <sup>94</sup>Nb has a half-time of almost 2×10<sup>4</sup> years.

This is the first report on the effect of tritium on superconductivity of MgB<sub>2</sub> [1,2]. Hydrogen is not able to substitute for boron or magnesium in ordinary condition of temperature and pressure. There are, however, differences between hydrogen and tritium. First, the tritium permeation rate in metals is faster than for hydrogen at moderate temperatures [3] due to the decrease of the zero point energy for the interstitial tritium. Second, the decay of tritium releases He atoms which generate self interstitials, which favour open volume defects. In the case of the MgB<sub>2</sub>, these structural defects might have beneficial influence on the current carrying capacity.

We investigated high density, polycrystalline MgB<sub>2</sub> superconducting ceramics which were fabricated by spark plasma sintering technique [4] and further submitted to tritiation for 2 and 216 hours, respectively.

The dc magnetic susceptibility data measured at a constant field of 5·10<sup>-4</sup> T after 370 days from tritiation with an accuracy of 0.1 K for temperature are presented in the figure 1.

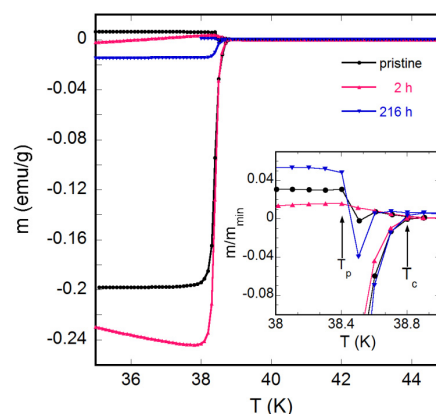


Fig. 1. Temperature dependence of the dc-magnetization for the pristine and tritiated MgB<sub>2</sub>. Inset: a zoom of the relative magnetization.

The critical temperature of the tritiated samples is not constant in time but it slowly decreases while the critical temperature of the pristine sample  $T_{\text{cref}}$  shows no change. Specifically,  $T_c$  is slightly higher  $T_c = 39.1$  K after 7 days since the tritium uptake, decreases to  $T_{\text{cref}} = 38.8$  K after 370 days and to 38.5 K after 445 days. The slight increase of the critical temperature immediately after tritiation shows that there is no substitutionally doping but, merely, tritium enters interstitially the boron layer as it was reported for hydrogen [5].

As the magnetic field increases, the superconductivity in the tritiated samples proves to be more robust than in the virgin sample. The upper critical field  $B_{c2}$  shows a significant enhancement for the tritiated samples (figure 2). While  $B_{c2}$  is almost identical for both tritiated samples, the irreversibility field,  $B_{\text{irr}}$ , shows that long time tritiation leads to a consistent enhancement of  $B_{\text{irr}}$ .

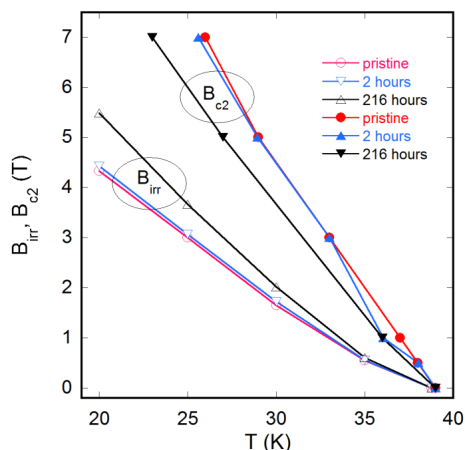


Fig. 2. Temperature dependence of the upper critical field  $B_{c2}$  (solid symbols) and irreversibility field  $B_{irr}$  (empty symbols) of the pristine and tritiated  $MgB_2$ .

The most striking difference between samples with different tritium loading is visible in the field  $B$  dependence of the critical current density (figure 3).

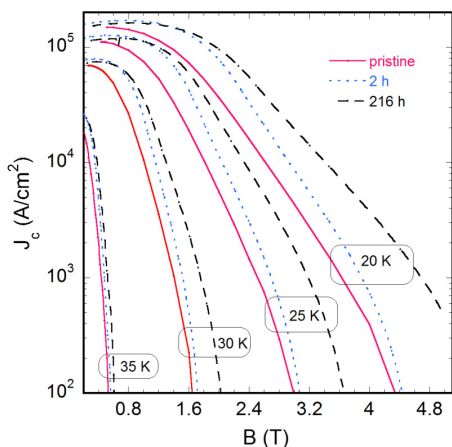


Fig. 3. Field  $B$  dependence of the critical current density  $J_c$  for the  $MgB_2$  samples submitted to tritium upload for 2 and 216 hours.

The difference is striking at high applied fields. It shows that long time tritiation leads to a consistent enhancement of the irreversibility. Equal  $B_{c2}$  suggests that incorporation of tritium into the boron ring as interstitial is limited, occurs at the beginning of the tritiation process and reaches saturation. The rest of tritium accumulates at pre-existent defects. In time, tritium starts to disintegrate with the production of  $^3He$  atoms which have a strong tendency to migrate and make clusters which are valuable pinning centres.

Raman spectra, which were measured after 370 days, shows that all samples display the broad  $E_{2g}$  band, which is the unique Raman active mode for pure  $MgB_2$  and two additional peaks which are sampling the phonon density of state but would have to be silent in the pure  $MgB_2$ . This means that disorder breaks the selection rules and makes these modes active. These peaks are weak in the pristine sample but their contribution to the total Raman spectrum is consistent and continuously increases as the tritium upload time increases, therefore their FWHM is associated to the strength of the pinning, hence, with the critical current density.

In conclusion, the structural disorder created by both tritium uptake and its decay product,  $^3He$ , has no detrimental effect on the superconducting properties of dense  $MgB_2$  ceramics. Even more,  $T_c$  is slightly higher immediately after tritiation, 39.1 K, but slowly decays to the same value as the untritiated sample, 38.8 K, after 370 days.

The results suggests that  $MgB_2$  have obvious advantages over the low temperature superconductors as a potential material for superconducting cables which are considered to work under tritium environment and neutron flux like in fusion plants. The positive effect of neutrons in improving the pinning has already been demonstrated. Now, we have shown that tritium has not only beneficial effects on the transport properties but, even more, the basic superconducting properties are not depressed like in the case of low temperature superconductors.

## References

- [1] V Sandu *et al.*, Supercond. Sci. Technol. 26(4) 045014 (2013)
- [2] V. Sandu *et al.*, J. Supercond. Nov. Magn. 25 1799 (2012)
- [3] J. L. Mainschein, F. E. McMurphy, V. L. Duval, Fus. Technol. 14 701 (1988)
- [4] V. Sandu *et al.*, J. Appl. Phys. 110 123921 (2011)
- [5] Y. Nakamori, S. Orimo, T. Ekino, H. Fujii, J. Alloys Comp. 335 L21 (2002)

## Interaction of epitaxial single atomic Au layer with Ge(001) substrate deduced from photoelectron spectroscopy experiments and first-principles calculations

*D.G. Popescu, M.A. Husanu*

There is an increased effervescence concerning the incidence of a 1D signature in the electronic properties of systems resulted through noble metal growth on Si(001) and Ge(001) surfaces. Thus, understanding the mechanisms that govern Au aggregation at dimerized surfaces is of great importance in deciding the 1D or 2D character of these systems. In this context, we show for the first time that when deposited at high temperature on Ge(001) surface, Au reacts with the substrate and covalent bonding occurs. We identify for the first time the signature of Ge-bonded Au in the X-ray photoelectron spectra (XPS) [1,2].

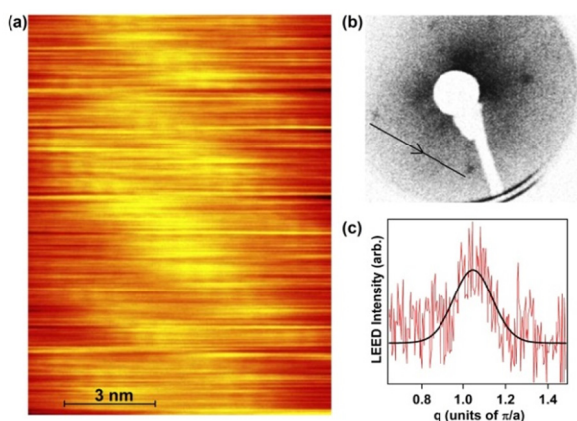


**Fig. 1** STM image of the Au-covered Ge(001) surface (a) and LEED patterns recorded on 1 ML Au-covered Ge surface (b); the spot profile analysis (c). [1].

This study presents the structure and electronic properties of the system resulted by epitaxial growth of a single atomic Au layer on heated Ge(001) surface featured by  $(2 \times 1)$  reconstruction [1,2]. The deposition at  $\sim 750$  K results in well-ordered Au surface featured by ripples separated by four times the theoretical distance between two neighbouring Au atoms [1]. Valence-band photoemission studies revealed the metallic character of Au/Ge(001) system [1,2]. Correlating X-ray photoelectron spectroscopy results with first principles calculations [1,2] we derive the

implications on the covalent bonding of Au on the Ge dimer surface.

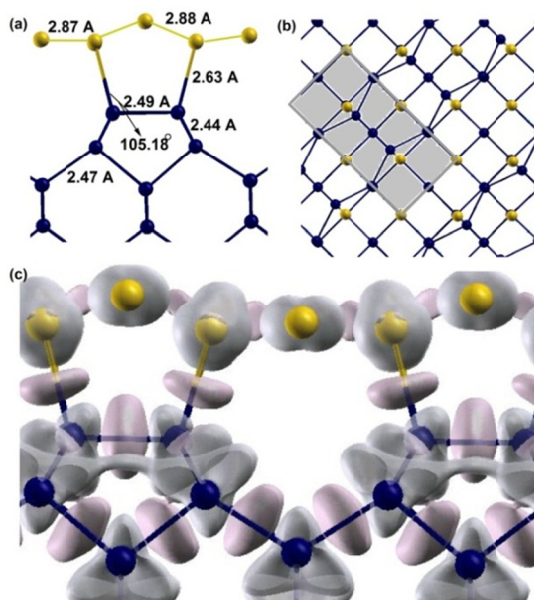


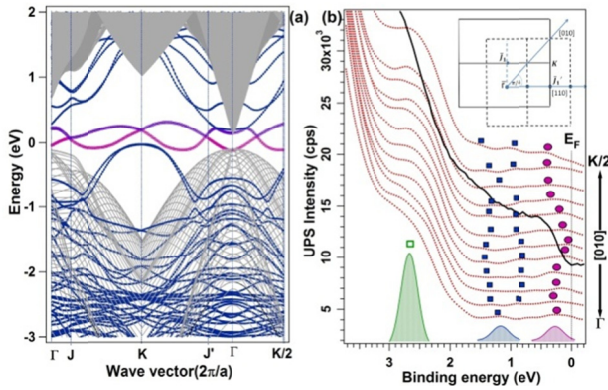
**Fig. 2** Side view of the relaxed Ge slab covered with 1 ML Au and its structural parameters (a); the top view of the relaxed structure with the surface unit cell of the  $p(1 \times 2)$  reconstruction in shaded grey (b); the  $0.002 \text{ e}\text{\AA}^{-3}$  deformation density isosurface of the relaxed 1 ML Au covered Ge(001) surface (c). [1]

An uniform coverage of the surface has occurred as suggested by the STM image recorded on the Au-covered Ge(001) surface and the LEED pattern (Fig. 1a,b). The uniform coverage was also tested by means of numerical simulations, the structural parameters being presented in Fig. 2(a) and the top-view of the relaxed Au-layer on top of Ge-surface in 2(b).

In this context, the theoretical band structure calculated along several important directions of the surface Brillouin zone is presented in Fig. 3(a) and the energy distribution curves recorded along  $[010]$  directions near the Fermi level in (b). We identified four electronic states in the interval ranging from 0 to  $-3$  eV ( $\bullet, \blacksquare, \square$ ), indicating that the resonance noted with ( $\bullet$ ) originates in the competing contribution of Ge – Ge symmetric dimers and Au – Ge

bonding. As a result of non-vanishing density of states at  $E_F$  induced by both the dimers electronic states and Au – Ge covalent bond states the Au-covered slab is metallic.

*Fig. 3 Calculated band structure of the relaxed Ge slab covered with Au (a). With grey colour the bulk*



*Ge states projected on the (001) surface are traced. The blue lines are electronic states associated to the slab and with violet and magenta colours those of the dimer “up” and “down”. In (b), the ARUPS spectra are shown along [010] direction. With (●,■,□) are noted the electronic resonances. In inset of the (b) figure the 2-domain SBZ is depicted. [1]*

The charge sharing of atoms leads to covalent bond formation which can be seen in the XPS spectra as additional components in both Ge 3d and Au 4f core spectra (Fig. 4), shifted towards higher binding energies with respect their bulk components. The Au atoms stabilize the Ge dimers (Fig. 5) and form covalent bond with the Ge atoms (Fig. 2). In Fig. 5 some details of bond structure of Ge (001) slab are shown [2]. The Ge-enriched surface stays semiconducting, no additional electronic states due to self-doping being visible [2].

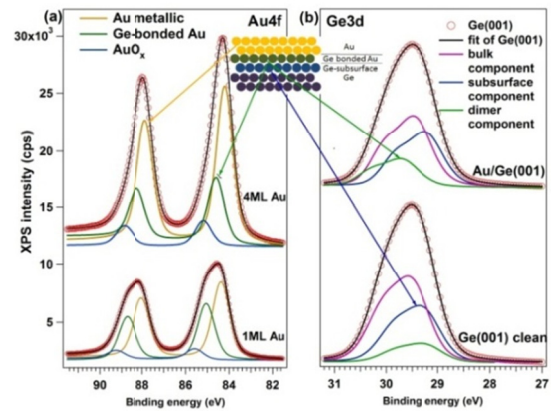


*Fig. 4 XPS spectra of Au 4f core level of 1 ML Au and 4 ML Au on clean Ge(001) surface (a); Ge 3d spectra of clean Ge surface and 1 ML Au covered Ge(001) surface. [1]*

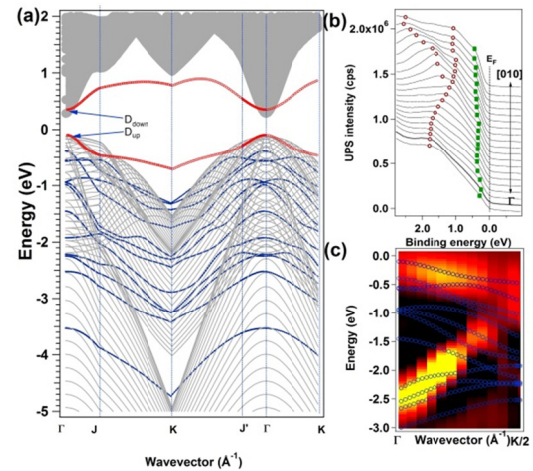


*Fig. 5 (a) Band structure of the Ge(001) slab (thick lines) along important directions in SBZ superimposed over the projected bulk band structure on (001) surface (grey lines). In (b) the EDC along  $\Gamma - K$  direction and in (c) the second derivative of the photoelectron intensity with respect the binding energy and the calculated bands. [2].*

#### References:

- [1] D.G. Popescu, M.A. Husanu, Phys. Status Solidi-Rapid Res. Lett. 7, 274 (2013).
- [2] D.G. Popescu, M.A. Husanu, Thin Solid Films 552, 241 (2014).

## Dependence of the strain diffraction line broadening on $(hkl)$ and sample direction in textured polycrystals

*N. C. Popa and G.A. Lungu*

In the recent paper [1] we presented a new phenomenological model describing the dependence of the strain diffraction line breadth on directions in both, crystal and sample. This is an extension of the older model used today in the most popular Rietveld programs, known as Popa or Stephens model [2], [3] which describes the dependence of strain line broadening only on the direction in crystal. For processing simultaneously the diffraction patterns recorded in multiple sample directions with the old model, a number of sets of independent strain broadening parameters should be used which increases irrationally the number of refinable parameters.

The derivation of the model starts from a statistical analysis of the strains and stresses in polycrystalline samples [4]. From this analysis it results that the strain in the point  $\mathbf{r}$  in the crystallite  $k$  of orientation  $g$  can be written as a sum of three independent strain types: type I, at macroscopic scale having two components, the mean and intergranular strain, type II, mesoscopic, and type III at microscopic scale:

$$\varepsilon_i(\mathbf{R}_k + \mathbf{r}, g) = [\bar{\varepsilon}_i + \Delta\varepsilon_i(g)] + \Delta\varepsilon_i(\mathbf{R}_k, g) + \Delta\varepsilon_i(\mathbf{R}_k + \mathbf{r}, g) \quad (1)$$

For simplicity, the last two terms are together called microscopic. The average of these terms over  $k$  and over  $\mathbf{r}$ , respectively, are zero but the same averages on the products of two such terms are different from zero. Similar behaviour have averages over Euler angles involving intergranular strain. As a consequence the microscopic terms contribute only to the peak breadth, not to the peak shift.

The quantity „seen” in diffraction is the strain along the reciprocal lattice vector. Denoting by  $\mathbf{h}$  its unit vector and by  $a_i$  the direction cosines in an orthogonal crystal reference system this quantity and its square are:

$$\varepsilon_{\mathbf{h}}(\mathbf{R}_k + \mathbf{r}, g) = \sum_{i=1}^6 E_i \rho_i \varepsilon_i(\mathbf{R}_k + \mathbf{r}, g) \quad (2) \quad (3)$$

$$\varepsilon_{\mathbf{h}}^2(\mathbf{R}_k + \mathbf{r}, g) = \sum_{i=1}^6 \sum_{j=1}^6 E_i E_j \rho_i \rho_j \tau_{ij}(\mathbf{R}_k + \mathbf{r}, g)$$

$$\tau_{ij}(\mathbf{R}_k + \mathbf{r}, g) = \varepsilon_i(\mathbf{R}_k + \mathbf{r}, g) \varepsilon_j(\mathbf{R}_k + \mathbf{r}, g)$$

where  $(E_i) = (a_1^2, a_2^2, a_3^2, a_2 a_3, a_1 a_3, a_1 a_2)$ , and  $(\rho_1, \dots, \rho_6) = (1, 1, 1, 2, 2, 2)$ .

The peak shift and variance from which the breadth is calculated are obtained by substituting expression (1) into (2) and (3) and performing three averages. The first two are over  $\mathbf{r}$  in one crystallite and over  $k$  for the crystallites of a given orientation  $g$ . The third average is performed only over those crystallites orientations  $g^+$  for which  $\mathbf{h}$  is parallel to  $\mathbf{y}$ , the unit vector of the scattering vector; this means that only the crystallites in Bragg reflection are considered. From this reason the intergranular strain contributes to both, peak shift and peak broadening, but the last contribution is negligible small compared to those of microstrains. And then, the strain peak variance is:

$$V_{\mathbf{h}}^m(\mathbf{y}) = \sum_{i=1}^6 \sum_{j=1}^6 E_i E_j \frac{\rho_i \rho_j}{2\pi P_{\mathbf{h}}(\mathbf{y})_{\pm\mathbf{h}|\mathbf{y}}} \int d\omega \Delta_{ij}(g^{\pm}) f(g^{\pm}) \quad (4)$$

Here  $f(g)$  is the orientation distribution function (texture) while  $P_{\mathbf{h}}(\mathbf{y})$  is the reduced texture pole distribution used together with the average of integrals over  $g^+$  and  $g^-$  because the peaks of  $+\mathbf{h}$  and  $-\mathbf{h}$  are indistinguishable. The functions  $\Delta_{ij}(g)$  are elements of correlation matrix of microstrains. If  $V_k$  is the volume of crystallite  $k$  and  $N_g$  is number of crystallites of orientation  $g$  these are:

$$\Delta_{ij}(g) = \frac{1}{N_g} \sum_{k=1}^{N_g} \Delta\varepsilon_i(\mathbf{R}_k, g) \Delta\varepsilon_j(\mathbf{R}_k, g) + \frac{1}{N_g} \sum_{k=1}^{N_g} \frac{1}{V_k} \int d\mathbf{r} \Delta\varepsilon_i(\mathbf{R}_k + \mathbf{r}, g) \Delta\varepsilon_j(\mathbf{R}_k + \mathbf{r}, g) \quad (5)$$

The variance of microstrains  $V_{\mathbf{h}}(\mathbf{y})$  is susceptible to an analysis by generalized spherical harmonics similar to those developed by Popa & Balzar [5] for the peak shift caused by

macrostrain. According to this approach, for microstrains variance the functions to be expanded in generalized spherical harmonics should be the elements of the matrix  $\Delta_{ij}(g)$  calculated by (5) from the strain tensor defined in the crystal reference system, weighted by ODF:

$$\Delta_{ij}(g)f(g) = \sum_{l=0}^{\infty} \sum_{m=-l}^l \sum_{n=-l}^l \left[ c_{ijl}^{mn} \exp(im\varphi_2) \right. \\ \left. P_l^{mn}(\Phi_0) \exp(in\varphi_1) \right]$$

Inserting this expression into equation (4) the variance becomes:

$$V_h(\mathbf{y})P_h(\mathbf{y}) = \sum_{l=0}^{\infty} [2/(2l+1)] I_l(\mathbf{h}, \mathbf{y}) (l=2k) \quad (6)$$

$$I_l(\mathbf{h}, \mathbf{y}) = \sum_{i=1}^6 \sum_{j=1}^6 E_i E_j \rho_i \rho_j t_{ijl}(\mathbf{h}, \mathbf{y}) \quad (7)$$

$$t_{ijl}(\mathbf{h}, \mathbf{y}) = \sum_{\mu=1}^{2l+1} \sum_{\nu=1}^{2l+1} \alpha_{ijl}^{\mu\nu} C_l^{\mu}(\Phi, \beta) S_l^{\nu}(\Psi, \gamma) \quad (8)$$

Here  $C_l^{\mu}$ ,  $S_l^{\nu}$  are spherical harmonics in crystal and sample reference system fulfilling selection rules in accordance with the specific symmetries, the pairs  $(\Phi, \beta)$  and  $(\Psi, \gamma)$  being the polar and azimuthal angles of  $\mathbf{h}$  and  $\mathbf{y}$ , respectively. It is expected that the selection rules for the coefficients  $\alpha_{ijl}^{\mu\nu}$  be much complicated than those found in [5] for the problem of the strain peak shift. Once the selection rules found, the coefficients  $\alpha_{ijl}^{\mu\nu}$  can be refined in a least square or in a Rietveld program and further, the distributions  $\Delta_{ij}(g)$  calculated. In contrast with the strain, these distributions are not of practical interest. In this case it is possible to find a "short" representation of the variance, requiring a smaller number of parameters, overcoming in this way those much complicated selection rules. This can be accomplished by passing in (8) from the pair  $(\Phi, \beta)$  to the direction cosines  $(a_1, a_2, a_3)$ . As a result, in place of (7) and (8) we have:

$$I_l(\mathbf{h}, \mathbf{y}) = \sum_{\mu=1}^{M_{l+4}} E_{\mu l}(\mathbf{y}) J_{\mu, l+4}(a_1, a_2, a_3) \quad (8)$$

$$E_{\mu l}(\mathbf{y}) = \eta_{\mu l}^0 P_l^0(\Psi) + \sum_{n=1}^l \left( \begin{array}{c} \eta_{\mu l}^n \cos n\gamma \\ + \zeta_{\mu l}^n \sin n\gamma \end{array} \right) P_l^n(\Psi) \quad (9)$$

In equation (8)  $J_{\mu, l+4}(a_1, a_2, a_3)$  are homogenous polynomials of degree  $l+4$  invariant to the operations of the crystal Laue group and  $M_{l+4}$  is the number of these polynomials. The polynomials up to degree six are listed in Tables 17 to 21 from paper [5] for all Laue classes.

In practice (6) is truncated at  $l=2$ . The term  $l=0$  is just the model [2,3] Popa/Stephens. Finally, here are two examples. Presuming the crystal and sample Laue group to be  $m\bar{3}m$  and  $mmm$ , respectively, the strain variance becomes:

$$V_h(\mathbf{y})P_h(\mathbf{y}) = \eta_{10}^0 (a_1^4 + a_2^4 + a_3^4) \\ + \eta_{20}^0 (a_1^2 a_2^2 + a_1^2 a_3^2 + a_2^2 a_3^2) \\ + [\eta_{12}^0 P_2^0(\Psi) + \eta_{12}^2 \cos 2\gamma P_2^2(\Psi)] (a_1^6 + a_2^6 + a_3^6) \quad (10) \\ + [\eta_{22}^0 P_2^0(\Psi) + \eta_{22}^2 \cos 2\gamma P_2^2(\Psi)] \\ \times (a_1^4 a_2^2 + a_2^4 a_3^2 + a_3^4 a_1^2 + a_1^4 a_3^2 + a_2^4 a_1^2 + a_3^4 a_2^2) \\ + [\eta_{32}^0 P_2^0(\Psi) + \eta_{32}^2 \cos 2\gamma P_2^2(\Psi)] a_1^2 a_2^2 a_3^2$$

The first two terms are the old model [2,3] of the strain broadening; the last three are due to the developments reported in this paper. For crystal and sample Laue groups  $m\bar{3}$  and  $mmm$ , respectively, the 4<sup>th</sup> term in (10) splits in two distinct terms (see Table 21 from [5]) and then two supplementary refinable parameters are added.

## References

- [1] N. C. Popa & G. A. Lungu, *J. Appl. Cryst.*, (2013), **46**, 391-395.
- [2] N. C. Popa, *J. Appl. Cryst.* (1998), **31**, 176-180.
- [3] P. W. Stephens, *J. Appl. Cryst.* (1999), **32**, 281-289.
- [4] N. C. Popa, (2008) Chapter 12, p. 332-375 in *Powder Diffraction, Theory and Practice*, eds. R. E. Dinnebier and S. J. L. Billinge, RSC, Cambridge
- [5] N. C. Popa & D. Balzar, *J. Appl. Cryst.* (2001), **34**, 187-195

## Ferromagnetic thin layers stabilized on Ge(001) single crystals

*G.A. Lungu, N.G. Apostol, L.E. Ștoflea, R.M. Costescu, D.G. Popescu, L.C. Tănase, I.C. Bucur, N. Răduțoiu, F. Vasiliu, I. Mercioniu, V. Kuncser, C.M. Teodorescu*

This work is stimulated by the tremendous applicative potential of diluted magnetic semiconductors (DMS), where magnetic entities (atoms, ions, small clusters) may become mutually magnetically ordered by indirect exchange, intermediated by the charge carriers in semiconductors. More specifically, the possibility is investigated to obtain DMS starting with the Ge(001), which is isomorphic with the high technological important Si(001) surface, and by simple evaporation of magnetic atoms (Fe or Mn) at various temperatures [1,2].

The experiments are performed in a ultrahigh vacuum cluster system (base pressure: below  $2 \times 10^{-10}$  mbar), equipped with a molecular beam epitaxy (MBE), a scanning tunneling microscopy (STM) facility, and a X-ray photoelectron spectroscopy (XPS) chamber (manufacturer: Specs). In-situ experiments are XPS and STM, then samples are capped with protective Cu or Au layers (2-3 nm thick) and ex-situ measurements are performed, such as magnetic measurements by magneto-optical Kerr effect (MOKE) using a setup provided by AMACC Anderberg and Mod er Accelerator, and superconducting quantum interference device measurements (Quantum Design). Cross sectional high resolution transmission electron microscopy (HRTEM) is performed by using a JEOL JEM ARM 200F electron microscope.

Ferromagnetic  $\text{Fe}_x\text{Ge}_{1-x}$  with  $x = 2\%–9\%$  are obtained by Fe deposition onto Ge(001) at high temperatures (500 °C). Low energy electron diffraction (LEED) investigation evidenced the preservation of the  $(1 \times 1)$  surface structure of Ge(001) with Fe deposition. X-ray photoelectron spectroscopy (XPS) at Ge 3d and Fe 2p core levels evidenced strong Fe diffusion into the Ge substrate and formation of Ge-rich compounds, from  $\text{FeGe}_3$  to approximately  $\text{FeGe}_2$ , depending on the amount of Fe deposited. Room temperature magneto-optical Kerr effect

(MOKE) evidenced ferromagnetic ordering at room temperature, with about 0.1 Bohr magnetons per Fe atom, and also a clear uniaxial magnetic anisotropy with the in-plane [110] easy magnetization axis (Fig. 1). This compound is a good candidate for promising applications in the field of semiconductor spintronics [1].

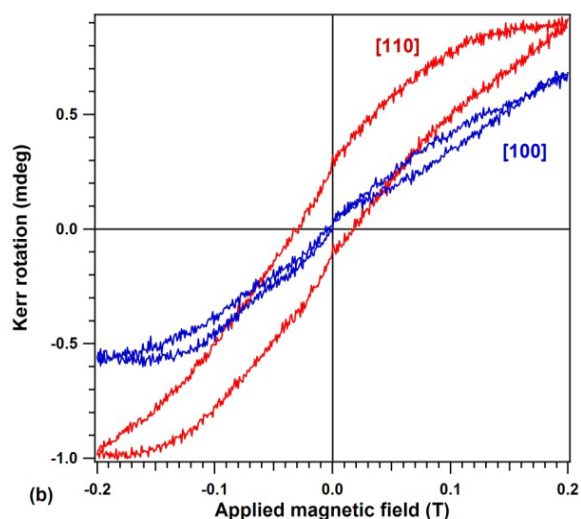


*Fig. 1. MOKE hysteresis loop for 12 ML Fe deposited on Ge(001) at 500 °C, with the linear polarization vector of the incident light in the plane defined by the [001] and [100] direction (blue curve), and in the plane defined by the [001] and [110] direction (red curve).*

In Ref. [2], we report the synthesis of a room temperature ferromagnetic Mn-Ge system obtained by simple deposition of manganese on Ge(001), heated at relatively high temperature (starting with 250°C). Samples deposited at relatively elevated temperature (starting with 350°C) exhibited the formation of  $\sim 5–8$  nm diameter  $\text{Mn}_5\text{Ge}_3$  and  $\text{Mn}_{11}\text{Ge}_8$  agglomerates by HRTEM (Fig. 2), while XPS identified at least two Mn-containing phases: the agglomerates, together with a Ge-rich  $\text{MnGe}_{2.5}$  phase, or manganese diluted into the Ge(001) crystal. Low energy electron diffraction (LEED) revealed the persistence of long range order with  $(1 \times 2) - (2 \times 1)$  reconstruction of Ge(001) after a relatively

high amount of Mn (100 nm) deposited on the single crystal substrate (Fig. 3). STM probed the existence of dimer rows on the surface, slightly elongated as compared with Ge–Ge dimers on Ge(001), as represented in Fig. 4.

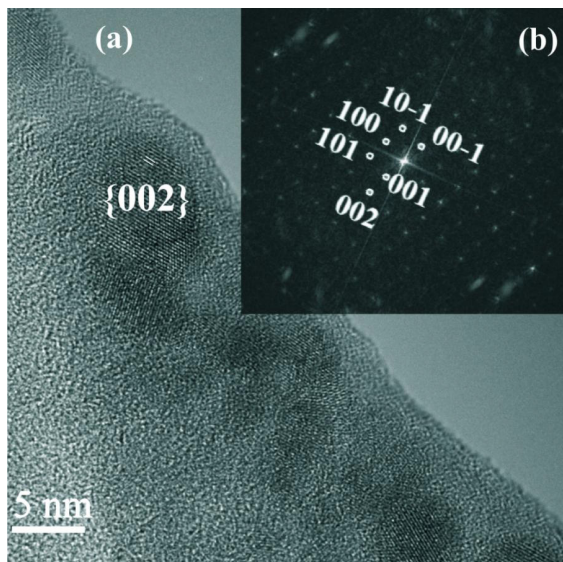


**Fig. 2.** (a) Cross section HRTEM image of an area of MBE MnGe layer deposited at 350 °C; (b) the associated FFT pattern showing the presence of Mn<sub>5</sub>Ge<sub>3</sub> (electron beam direction [010]).

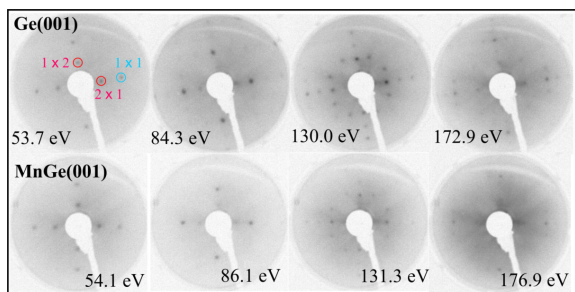


**Fig. 3.** Low energy electron diffraction (LEED) patterns for Ge(001) on the panels above, and for 100 nm Mn deposited on Ge(001) at 350 °C (panels below).

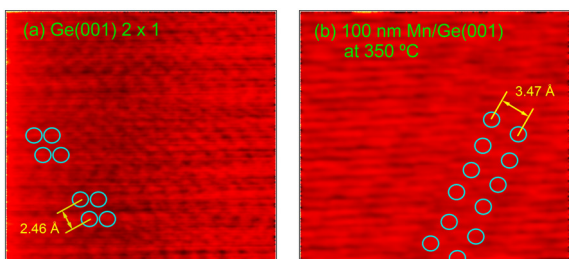


**Fig. 4.** Scanning tunneling microscopy (STM) images obtained at a tip voltage of +150 mV (empty-states images), on (a) clean Ge(001) and (b) after the deposition of 100 nm Mn at 350 °C. The scanned area is 3×3 nm<sup>2</sup> in both cases.

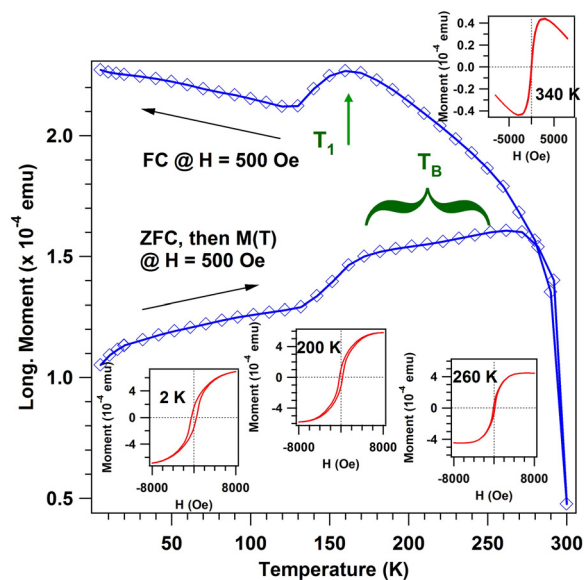


**Fig. 5.** SQUID measurement of the Mn-Ge(001) sample obtained by deposition of 100 nm Mn on Ge(001) held at 350 °C. The main graph with blue symbols and lines represent zero field cooled - field-cooled magnetisation. The inserts represent magnetisation hysteresis at the specified temperatures.

The Mn-Ge films exhibited a clear ferromagnetism at room temperature, opening the possibility of forming a magnetic phase behind a nearly ideally terminated Ge surface, which could find applications in integration of magnetic functionalities on semiconductor bases. SQUID (Fig. 5) probed the co-existence of a superparamagnetic phase with one ferromagnetic phase. Based also on the XPS and MOKE data, the hypothesis that the room temperature ferromagnetic phase might be the one with manganese diluted into the Ge crystal is formulated and discussed in Ref. [2], whereas the superparamagnetic component is attributed to the observed clusters by HRTEM.

## References

- [1] G.A. Lungu, N.G. Apostol, L.E. Ștofleă, R.M. Costescu, D.G. Popescu, C.M. Teodorescu, *Materials* **6**, 612-625 (2013).
- [2] G.A. Lungu, L.E. Ștofleă, L.C. Tănase, I.C. Bucur, N. Răduțoiu, F. Vasiliu, I. Mercioniu, V. Kuncser, C.M. Teodorescu, *Materials* **6**, 106-129 (2014).

## Band bending effects in ferroelectric single crystal layers investigated by photoelectron spectroscopy

*N.G. Apostol, L.E. Ștoflea, G.A. Lungu, L.C. Tănase, I.C. Bucur, C.A. Tache, C. Chirilă,  
L. Trupină, R.F. Negrea, C. Ghica, L. Pintilie, C.M. Teodorescu*

This group of papers [1-4] represent a pioneering work in the area of determination of band bending in ferroelectrics and in metal-ferroelectric contacts by X-ray photoelectron spectroscopy (XPS). Fig. 1 represents band bending occurring at metal-semiconductor interfaces with different work functions, whereas Fig. 2 demonstrates that such band bendings are visible from core level spectroscopy [1], which is crucial when metals are deposited on semiconductors, since the valence band of the semiconductor is weak, attenuated and mixed with the metal valence states.

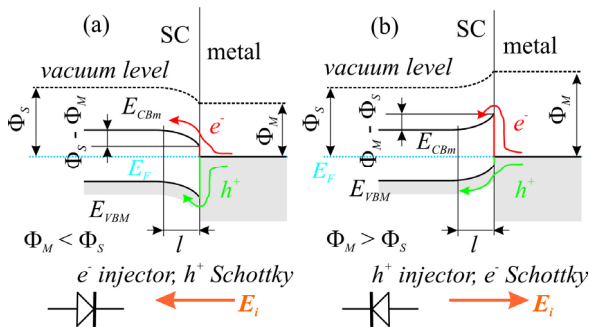


**Fig. 1.** Band bending at metal-semiconductor contacts, with work function of the metal lower (a) or higher (b) than that of the semiconductor.

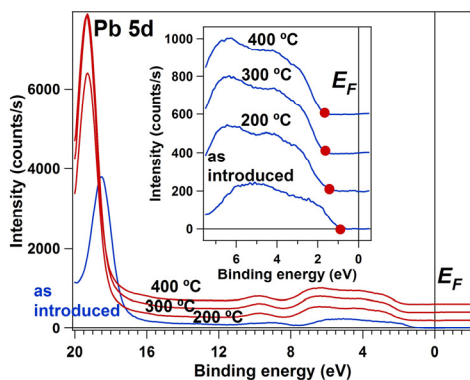


**Fig. 2.** Evidence of band bending by photoemission spectroscopy. The Pb 5d core level shifts rigidly with the valence band offset when the sample is progressively n-doped by heating (producing oxygen vacancies).

The case of ferroelectrics is of particular importance, since free ferroelectric surfaces with out-of-plane polarization exhibit also a surface band bending (Fig. 3).

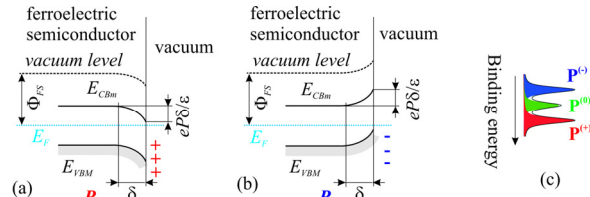


**Fig. 3.** Band bending at ferroelectric surfaces with polarization oriented outwards (a) or inwards (b). (c) represents the corresponding core level components.

Samples are deposited by pulsed laser deposition, and the XPS experiments together with metal deposition are performed in a ultrahigh vacuum cluster system (base pressure: below  $2 \times 10^{-10}$  mbar), equipped with a molecular beam epitaxy (MBE) and a XPS chamber (Specs). Piezo-response force microscopy (PFM) is performed with an Asylum Research setup, while cross sectional high resolution transmission electron microscopy (HRTEM) is performed by using a JEOL JEM ARM 200F electron microscope.

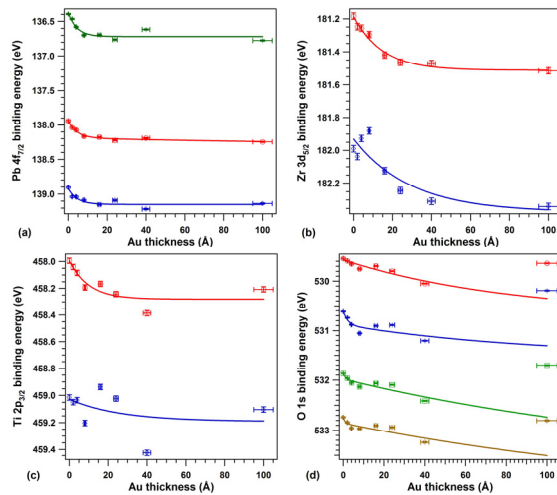


**Fig. 4.** Evolution of different components of core levels from PZT(001) with Au deposition: (a) Pb 4f<sub>7/2</sub>; (b) Zr 3d<sub>5/2</sub>; (c) Ti 2p<sub>3/2</sub>; (d) O 1s.

It is demonstrated that, when Au is deposited on (001) lead zirco-titanate (PZT), the band bending exhibits the expected Schottky effect, by  $\Phi_{PZT} - \Phi_{Au} \approx 0.45$  eV downwards (Fig. 4), which also implies a slight *p* doping of the PZT layer. All core levels exhibit two main components,

attributed to  $P^{(+)}$  poled areas (lower intensity) and to areas with no out-of-plane polarization, a situation which is visible also from PFM (Fig. 5). Therefore, a compositional and polarization model may be developed, represented in Fig. 6 [2]. It is also shown that these states are highly dependent on the history of the PZT film [3].

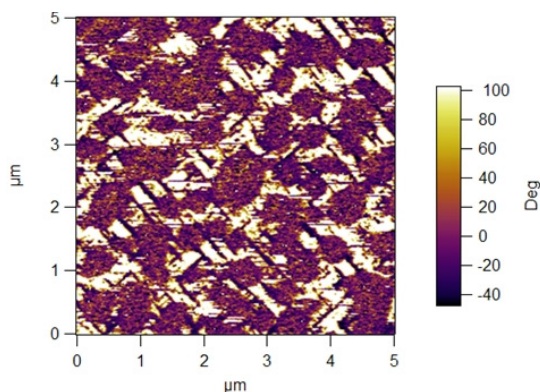


Fig. 5. Phase PFM of clean PZT(001) surface.

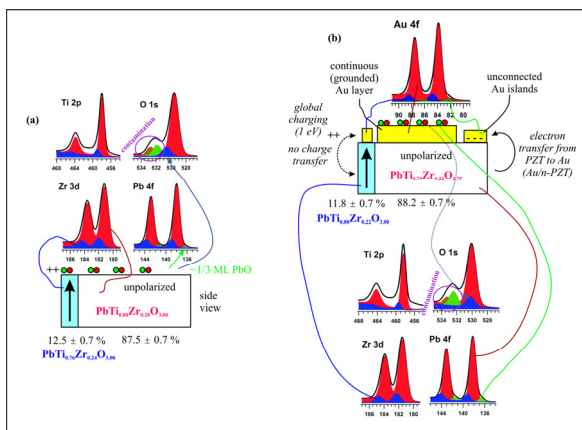


Fig. 6. Compositional model for (a) a clean PZT surface and (b) an Au/PZT surface, together with the attribution of several components observed in XPS.

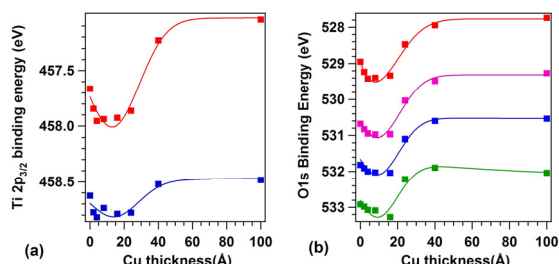


Fig. 7. Evolution of core levels from PZT(001) with Cu deposition: (a)  $Ti\ 2p_{3/2}$ ; (b)  $O\ 1s$ .

For Cu/PZT, band bending combined with another effect, which is the charge compensation at the interface by electrons provided by the grounded metal layer, which results in a non uniform dependence of the binding energies on the effective thickness of the Cu layer (Fig. 7)

[4]. For a critical amount of Cu, the initial Cu clusters (Fig. 8) coalesce and, therefore, mobile charge carriers (electrons) are provided such as to compensate the surface band bending due to the ferroelectric polarization. For larger Cu thicknesses, just the Schottky effect, as if the ferroelectric were not out-of-plane polarized. This evolution is schematized in Fig. 9.

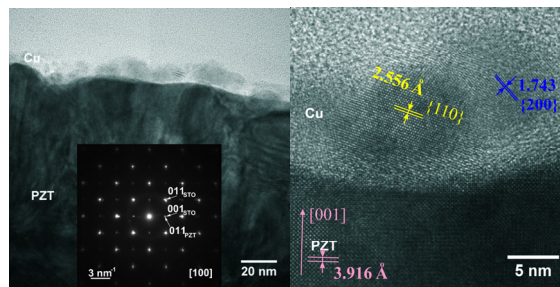


Fig. 8. Cross sectional (a) TEM and (b) HRTEM images of Cu/PZT(001).

This effect was not visible for Au/PZT(001), since Au deposited at room temperature forms unconnected clusters, unable to provide additional electrons, such as to screen the out-of-plane polarization.

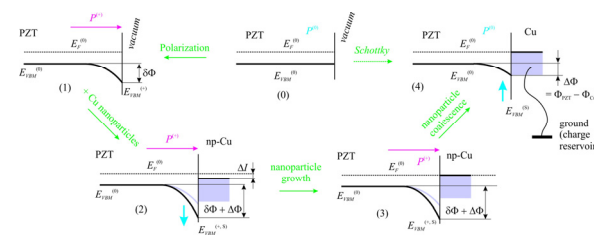


Fig. 9. Band bending model proposed to explain the core level behavior from Fig. 8.

References

[1] N.G. Apostol, L.E. Ștoflea, G.A. Lungu, C.A. Tache, L. Pintilie, C.M. Teodorescu, Mater. Sci. Eng. B 178, 1317-1322 (2013).  
 [2] N.G. Apostol, L.E. Ștoflea, G.A. Lungu, C. Chirilă, L. Trupină, R.F. Negrea, C. Ghica, L. Pintilie, C.M. Teodorescu, Appl. Surf. Sci. 273, 415-425 (2013).  
 [3] N.G. Apostol, L.E. Ștoflea, G.A. Lungu, L.C. Tănase, C. Chirilă, L. Frunză, L. Pintilie, C.M. Teodorescu, Thin Solid Films 545, 13-21 (2013).  
 [4] L.E. Ștoflea, N.G. Apostol, C. Chirilă, L. Trupină, R. Negrea, L. Pintilie, C.M. Teodorescu, J. Mater. Sci. 49, 3337-3351 (2014).

## Ga and As competition for thiolate formation at p-GaAs(1 1 1) surfaces

C.C. Negrila, M.F. Lazarescu

in cooperation with

M. Enache, L. Preda, M. Anastasescu, A.M. Toader, S. Ionescu, V. Lazarescu

Romanian Academy-Institute of Physical Chemistry "Ilie Murgulescu" Bucharest, Romania

The aim of the present work is to investigate the influence exerted by the chemical nature of the surface atoms on the 4,4'-thio-bis-benzene-thiolate formed at p-GaAs(111) surfaces. Understanding the chemical bonding between thiols and GaAs is undoubtedly related with the possibility to control the chemical and the electronic properties of the GaAs surface for specific applications, since its poor chemical stability and high density of surface/interface states are considered major impediments for functional performances of the GaAs-based devices [1]. We chose X-ray photoelectron spectroscopy (XPS) to monitor the chemical composition of the surface, atomic force microscopy (AFM) to examine the surface morphology and electrochemical impedance spectroscopy (EIS) to explore the electrochemical behavior of the thiolate films and their effects on the electronic properties of the semiconductor electrodes.

The p-GaAs(1 1 1) electrodes used in this study were prepared from Zn doped ( $p = 1-2 \cdot 10^{19} \text{ cm}^{-3}$ ) wafers mounted on Teflon holders with the rear part and the edges sealed by epoxy resin. Ohmic contacts to the sample were made by alloying with Ti-Pt-Au (18.5:7.5:74) using magnetron sputtering deposition and thermal annealing techniques. The 4,4-thio-bis-benzene-thiolate (TBBT) self-assembled layers were formed from anhydrous ethanol solutions, usually of 2 mM concentration. The electrochemical measurements were performed in the dark, in a three-compartment electrochemical cell of conventional design, using an IM-6 Zahner frequency analyzer between 0.3 Hz and 300 kHz. Spectra were fitted using Z-View software (Scribner Associates Inc., Southern Pines, NC). All potentials refer to the saturated calomel electrode (SCE). The impedance spectra

revealed important differences between the electrical responses of the two types of electrodes. The thiolate film exerts clearly passivation effects only at the As terminated surface whereas at the Ga-terminated surface it rather facilitates the interfacial charge transfer (Fig.1).

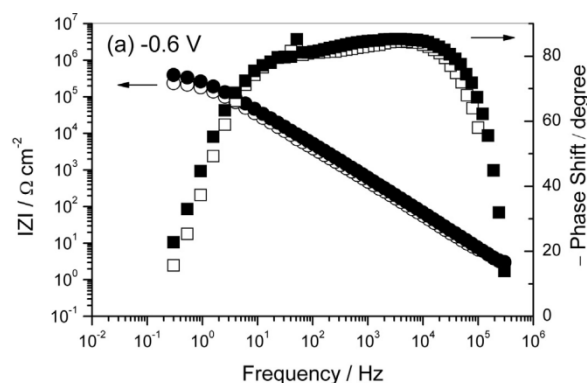


Fig.1 Bode plots of the impedance spectra for TBBT/p-GaAs(1 1 1)A (open symbols) and TBBT/p-GaAs(111)B (filled symbols) at  $-0.6 \text{ V}$

The AFM experiments were carried out in the intermittent contact mode, using an EasyScan2 model from Nanosurf AG. The images suggest that thiolate species are more compact packed than at TBBT/p-GaAs(111)A, giving rise to a more uniform and smoother overlayer (Fig.2).

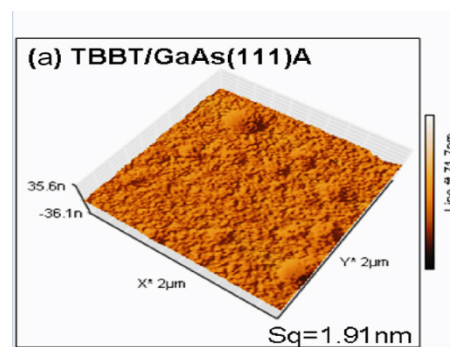


Fig.2 AFM image of TBBT-covered p-GaAs(111)A

XPS spectra were obtained with a SPECS spectrometer equipped with a monochromatized

Al  $K\alpha$  anode radiation ( $E_x = 1486.6$  eV) source operated at 400 W. The survey and region spectra were acquired at pass energy of 100 eV and 20 eV, respectively. The spectra were charge corrected assuming the C-1s (C-C) peak occurs at 285.0 eV. The XPS investigations carried out on p-GaAs(111)A and p-GaAs(111)B electrodes modified with 4,4'-thio-bis-benzene-thiolate plead for the involvement of both As and Ga atoms in the chemisorption bond, no matter the nature of the terminal atom, in good agreement with other recent reports. The presence of both types of bonding, As-S and Ga-S, at GaAs(111) surfaces makes no doubt that As and Ga atoms do compete for thiolate formation, no matter the nature of the terminal atom (Fig. 3).

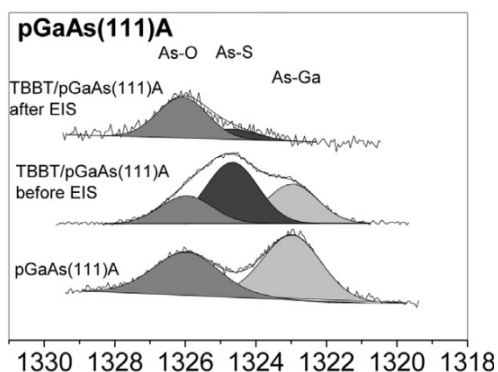


Fig.3. XPS spectra of As-2p core-level region for the bare-GaAs(111)A surfaces exposed to air after etching and TBBT covered-p-GaAs(111) electrodes

The thiolate layer formed at the two (111) surfaces exhibits, distinct chemical and electrochemical stability due to the balance between the chemical and packing forces operating within the ad-layer, that should be sensitive to the terminal atom nature. The S2p core level spectra show that  $S_{\text{not-bound}}/S_{\text{bound}}$  peak area ratio is approximately 2 at both types of TBBT-covered p-GaAs(111) surfaces, suggesting that only one of the thiol heads is involved in the thiolate bonding (Fig.4).

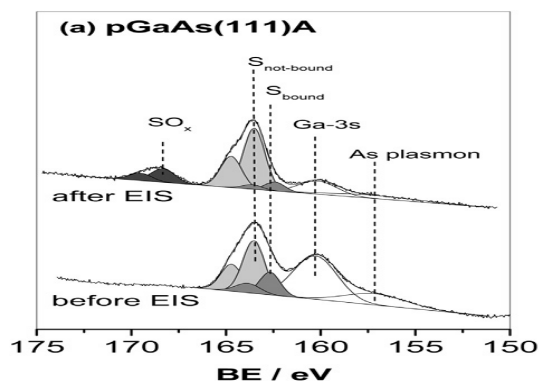


Fig.4. XPS spectra of S2p region

The presence of Ga-O and As-O species suggests that thiolate cannot bind to all As and/or Ga atoms in the surface, leaving a significant fraction of surface atoms uncovered and thus available for oxygen bonding. It is important to note that TBBT formed at As-terminated surface completely blocks the further oxidation of As atoms and inhibits that of the Ga atoms whereas thiolate formed at the Ga terminated surface allows the further oxidation of the Ga atoms and As atoms. The poorer self-organization of the thiolate layer formed at Ga terminated substrate is responsible for both the lower protection against the oxidation in air and the potential-induced defects within the thiolate layer. From our EIS and XPS studies one may conclude that TBBT monolayer is better organized on GaAs(111)-As than on GaAs(111)-Ga. Given that TBBT on GaAs(111)A electrode provides an uniform binding interface, stable electrochemically, it may candidate as adsorption platform for metallic ions[2] as an alternative to the self-assembled monolayers of mercaptoalkanoic acids in order to build new assemblies of high potential technological interest for optoelectronic and sensor applications.

## References

- [1] V. Lazarescu et al. *Electrochim. Acta* 55, 8293, (2010)
- [2] M. Brust et al. *Langmuir* 13, 560, (1997)

## Spectral and transport properties of the line-centered square lattice

*M. Niță, B. Ostabie, and A. Aldea*

The interest in the line centered square lattice, known as the 2D Lieb lattice (Fig.1), come from the specific properties induced by its topology. The lattice is characterized by a unit cell containing three atoms and the energy spectrum shows a three band structure with electron-hole symmetry, one of the branches being flat and macroscopically degenerate. Except for the presence of the flat band, the Lieb lattice shows similarities with the honeycomb lattice in what concerns both spectral and transport properties. For instance, besides the presence of the Dirac cone, the energy spectrum in the presence of the magnetic field shows also a double Hofstadter picture, with the typical  $\sqrt{B}$  dependence of the relativistic Landau bands [1]. One has to note that the line centered square lattice are found in nature as  $Cu - O_2$  planes in cuprate superconductors [2] and also can be engineered as an optical lattice [3,4].

We address the properties of the *finite* (mesoscopic) Lieb lattice with emphasis on some features of the flat band and of the edge states, which are specific to this lattice. We adopt the spinless tight-binding approach, introducing creation  $\{a_{nm}^\dagger, b_{nm}^\dagger, c_{nm}^\dagger\}$  and annihilation  $\{a_{nm}, b_{nm}, c_{nm}\}$  operators of the localized states  $|A_{nm}\rangle, |B_{nm}\rangle, |C_{nm}\rangle$ , where  $(nm)$  stands for the cell index and the letters  $A, B, C$  identify the type of the atom, therefore the Hamiltonian of the Lieb lattice in perpendicular magnetic field reads:

$$\begin{aligned}
 H = & \sum_{n,m} E^a a_{n,m}^\dagger a_{n,m} + E^b b_{n,m}^\dagger b_{n,m} + E^c c_{n,m}^\dagger c_{n,m} \\
 & + t_x e^{-im\phi} a_{n,m}^\dagger b_{n,m} + t_x e^{im\phi} a_{n,m}^\dagger b_{n-1,m} \\
 & + t_y a_{n,m}^\dagger c_{n,m} + t_y a_{n,m}^\dagger c_{n,m-1} + t_x e^{-im\phi} b_{n-1,m}^\dagger a_{n,m} \\
 & + t_x e^{im\phi} b_{n,m}^\dagger a_{n,m} + t_y c_{n,m}^\dagger a_{n,m} + t_y c_{n,m-1}^\dagger a_{n,m}.
 \end{aligned}$$

where  $\phi$  is the flux through the unit cell of the Lieb lattice measured in quantum flux units; we mention that the vector potential has been chosen as  $\vec{A} = (-By, 0, 0)$ .

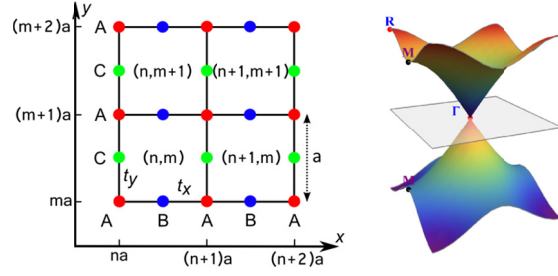


*Fig.1: The Lieb lattice: the unit cell contains three atoms A, B, and C; indices  $(n, m)$  identify the cell;  $t_x, t_y$  are the hopping integrals along the directions  $O_x$  and  $O_y$ , respectively;  $a$  is the lattice constant (left). The energy spectrum of the infinite Lieb lattice in the case  $E^a = E^b = E^c = 0$ , when the three bands (two dispersive and one flat) get into contact at  $\Gamma = (\pi, \pi)$ . At low energy, the dispersion is linear giving rise to Dirac cones (right).*

The perpendicular magnetic field applied on a finite (mesoscopic) Lieb plaquette opens a gap around the flat band, and we show the presence in this gap of a new class of edge states with alternating chirality (which we call twisted edge states see Fig.2(a, b)).

We calculate analytically the orthogonal eigenfunctions of the finite Lieb system corresponding to the three spectral branches in the low energy range, both for periodic and vanishing boundary conditions. In this way we find also the degeneracy of the zero-energy band, which, in the periodic case, equals the total numbers of unit cells  $N_{cell}$  (except when both  $N_{cell}^x$  and  $N_{cell}^y$  are even numbers, in which case the degeneracy increases to  $N_{cell} + 2$ ), while in the case of the closed boundaries the degeneracy is  $N_{cell} + 1$ . A toy model composed of only two unit cell helps to understand the behavior in the presence of a perpendicular magnetic field.

The quantum transport of the 2D Lieb plaquette shows some similarities with the case of graphene, however, it also reveals particular properties. The Hall conductance as a function of the Fermi energy at a given quantizing

magnetic field was obtained in [3] by calculating the Chern numbers, and has the general behavior of the Hall resistance ( $R_H$ ) from Fig.2(c). The Hall resistance was obtained with Landauer-Büttiker formalism: starting from the extremities of the spectrum,  $R_H$  shows  $h/e^2$  steps in the Bloch-Landau region, then change the sign, and show again  $h/e^2$  steps in the Dirac-Landau region. The change of sign is associated with the opposite chirality of the edge states in the two regions and occurs around the saddle points ( $M$  points in Fig.1 right) of the spectrum.

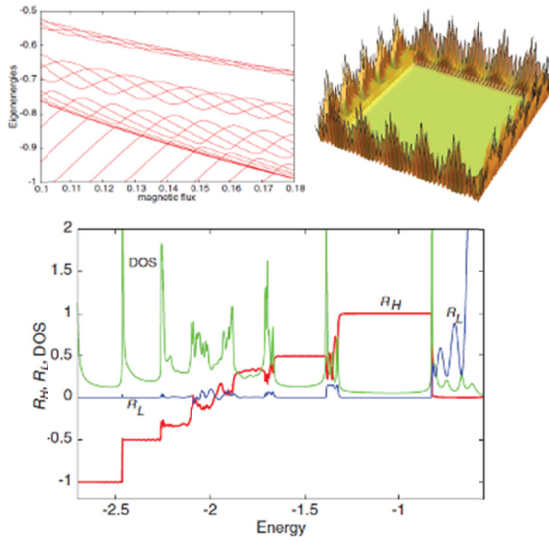


Fig.2: The eigenenergies in the range of twisted edge states vs. magnetic flux  $\phi$ . They have an oscillatory behavior when the magnetic flux is varied, and form bunches with four states in each bunch (a).

$|\psi|^2$  for a twisted edge state (b). The Hall resistance  $R_H$ , longitudinal resistance  $R_L$ , and the density of states DOS for a finite Lieb lattice (c). In the energy range  $E \in [-0.8, -0.6]$ , the transport properties are due to the twisted edge states, and we get zero Hall resistance  $R_H = 0$ , and oscillations of the longitudinal resistance with characteristic minima at  $R_L = 1/4$ . The density of states exhibits maxima at the transition between the Hall plateaus, and the energy values where the twisted edge states appear. The dimension of the plaquette is  $10 \times 30$  unit cells, the magnetic flux is  $\phi = 0.12$ , the resistance is in units  $h/e^2$ , DOS in arbitrary units, and the energy in units of  $t$ .

The density of states (shown in Fig.2(c)) is calculated as  $DOS = -\frac{1}{\pi} \text{Tr}[ImG^+(E)]$ , where  $G^+(E)$  is the retarded Green function for the mesoscopic plaquette connected to the leads.

In our recent paper [5], we analyzed the contribution to transport of the twisted edge states. In Fig.2(c) in the energy range  $E \in [-0.8, -0.6]$ , where one observes that the twisted edge states found in this range do not support the Hall resistance ( $R_H = 0$ ), however, they contribute to the longitudinal resistance, which exhibits an oscillating behavior and also can be correlated with the oscillations of the density of states (calculated in the presence of the leads). This behavior stems from the symmetry  $T_{\alpha, \alpha+1} = T_{\alpha+1, \alpha}$  of the transmittances (where  $\alpha$  indexes the leads), which occurs despite the presence of the magnetic field.

## References

- [1] R. Rammal, J. Phys. France **46**, 1345 (1985).
- [2] E. H. Lieb, Phys. Rev. Lett. **62**, 1201 (1989).
- [3] N. Goldman, D. F. Urban, and D. Bercioux, Phys. Rev. A **83**, 063061 (2011).
- [4] V. Apaja, M. Hyrkas, and M. Manninen, Phys. Rev. A **82**, 041402(R) (2010).
- [5] M. Nita, B. Ostahie, and A. Aldea, Phys. Rev. B **87**, 125428 (2013).

## Casimir effect demonstrated by Raman Spectroscopy on Trilayer Graphene Intercalated into Stiff Layered Structures of Surfactant

Mihaela Baibarac, Ioan Baltog, Lucian Mihut, Iuliana Pasuk,

in cooperation with

S. Lefrant

Institut des Materiaux “Jean Rouxel”, Nantes, France

Graphene, the latest discovered carbon allotrope, has focused a great interest of many scientists because it is an ideal material for the study of the basic properties of two-dimensional nanostructures and a promising candidate for different application in electronic devices [1]. Graphenes can be found in structure of single-layer, bi-layer and multi-layer, each of them revealing specific properties. For example, the single layer graphene (SLG) is a zero-gap semiconductor or a semimetal while the bi-layer graphene (BLG) is known as semi-conductor with tunable energy gap [2]. Recently, three-layer graphene (TLG) became subject of many studies. Due to the interlayer coupling featured by energy transfer between adjacent layers, the electronic band gap structure both of BLG and TLG differs from the SLG. An interesting recent experimental finding regards the dependence of the electrical transport properties on the stacking order. It is well known that the Raman spectroscopy is one of the most powerful method used in the characterization of carbon based materials. The Raman spectrum of graphene is dominated by two main bands, one at  $\sim 1585\text{cm}^{-1}$  and another at  $\sim 2700\text{cm}^{-1}$ , the former called G band and the latter known under various notations as 2D band. G band originates from the  $E_{2g}$  in-plan phonon at the C point of Brillouin zone where the longitudinal optical (LO) and transverse optical (TO) branches touch each other. Due to the phonons from the vicinity of C point, in the high energy side of the G band is observed a band at  $\sim 1620\text{cm}^{-1}$ , called  $D_0$ , which is induced by disorder. Located around of  $\sim 1350\text{cm}^{-1}$  under excitation light of  $514.5\text{nm}$  there is another band labeled D, which is associated with TO branch near K point of Brillouin zone. It is activated by

the disorder into graphene sheet and presents a dispersive behavior of  $\sim 50\text{cm}^{-1}/\text{eV}$  [3]. The physical properties of graphene are mainly determined by edges, which play a crucial role in the functionalization with different chemical groups.

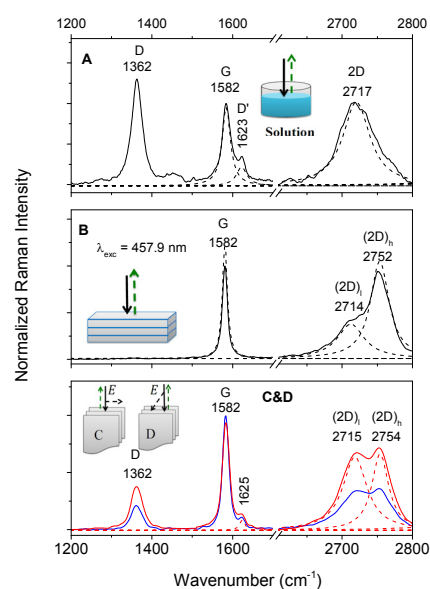


Fig. 1 – Raman spectra at  $\lambda_{\text{exc}} = 457.9\text{ nm}$  of TLG in different morphological forms: (A)–dispersed with surfactant (SDS) in aqueous solution; (B)–intercalated in stiff layered structure of (top graphene layer view); (C&D) –intercalated in stiff layered structure (graphene edge view).

One of the most important results regards D band which unambiguously is associated with the edge of graphene. Studies of polarized Raman scattering have shown that the intensity of this band passes through a maximum and minimum when the electric field of the excitation light is oriented along the graphene layer or perpendicular to it, respectively. Figure 1 is quite illustrative. By comparative studies of Raman scattering on TLG intercalated into stiff layered structures of surfactant (Figure 2) we

demonstrate that the profile of the 2D band contains two components separated by  $\sim 40\text{cm}^{-1}$ , which equals the energy of a phonon associated with  $E_{2g}$  interplanar vibration mode.

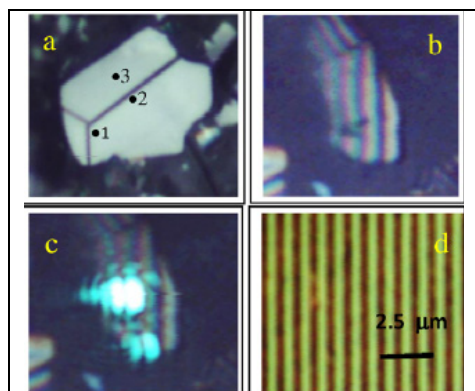
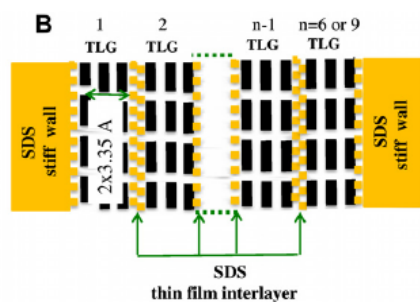


Fig. 2 –View of layered structure of SDS intercalated with TLG  
d) image of diffraction grating (1200grooves/mm)



Scheme of the layered structure

Figure 1 shows the Raman spectra under excitation light of 457.9nm for TLG in three morphological forms: A) TLG dispersed with SDS in aqueous solution; B) stiff layered structure excited perpendicular to the layer; and C&D) stiff layered structure excited with light polarized along (C) and perpendicular (D) to the edges layers. Figure 1A discloses significant details regarding the Raman spectrum of graphene: an intense D band of lorentzian profile peaking at  $1362\text{cm}^{-1}$ , a G band at  $1582\text{cm}^{-1}$  flanked by a D' band at  $1623\text{cm}^{-1}$  whose intensity is approximately one third of the G band and 2D band at  $2717\text{cm}^{-1}$  that fits a lorentzian profile. Figure 1B is different since it shows the well-known Raman spectrum of graphene layer excited perpendicular on this, which consists from two intense bands G and

2D, the latter disclosing clearly two components at  $2714$  and  $2752\text{cm}^{-1}$ . In Figure 1 C&D is relevant the presence of the D band, it demonstrating the contribution of the graphene edges in the formation of Raman spectrum, it appears when the edges of graphene are submitted directly to optical excitation. According to expectations, the relative intensity of D band depends on the polarization of the excitation light, the highest intensity is obtained when the polarization is along the layers and approximately half when the polarization is perpendicular to the layers. The replica of second-order of D band is the 2D band whose intensity varies in the same way when the polarization of the exciting light is rotated with 90 degrees. The 2D band discloses two lorentzian components, separated by  $\sim 40\text{cm}^{-1}$ , which result from the action of interplanar forces, of Casimir nature [4]. The value of  $\sim 40\text{cm}^{-1}$  is close to the energy value associated with  $E_{2g}$  interplanar layer shear mode evidenced so far only by neutron spectrometry. A new result regards the opposite variation of the intensities of D and 2D band with the increase of the wavelength of the excitation light. This originates is due to the different origin of the D and 2D bands; the former is dependent on disorder including also the graphene edges while the latter results from in a double resonant mechanism combined with a Casimir effect. One demonstrates that the magnitude of Casimir force, which activates interlayer vibration modes, depends on the carrier density on the graphene sheets which can be varied both by the intensity and the wavelength of the excitation laser light.

## References

- [1] K.S. Novoselov, A.K. Geim, et al. Science **306**, 666 (2004).
- [2] Y. Zhang, et al. Nature, **459**, 820 (2009)
- [3] L.M. Malard, et al. Phys Rep;**473**, 51 (2009).
- [4] M. Baibarac, I. Baltog, L. Mihyt, I. Pasuk, S. Lefrant, Carbon, **51**,134, (2013).

## Silver photodiffusion in a-As<sub>2</sub>S<sub>3</sub> thin films

M. Popescu, A. Lőrinczi, F. Sava, A. Velea, I. D. Simandan

in cooperation with

G. Socol, I. N. Mihailescu, N. Stefan

National Institute for Laser, Plasma and Radiation Physics, Bucharest-Magurele, Romania

The silver diffusion mechanism in chalcogenide glasses (ChG) is important both from application and fundamental points of view. Chalcogenide multi-layers are important for information recording and other applications in optics or optoelectronics [1].

We report here the results of a transmission experiment using two laser beams, evidencing the silver's photodiffusion in a silver-chalcogenide thin film heterostructure in bottom-up geometry [2].

The optical transmission results are supported by X-ray diffraction (XRD) measurements as well. These new data follow our earlier results regarding Ag-diffusion rate and a suggested four-step diffusion mechanism for the Ag-As<sub>2</sub>S<sub>3</sub> interface region [3].

A heterostructure of As<sub>2</sub>S<sub>3</sub> on Ag deposited onto glass substrate by vacuum evaporation has been prepared. The first layer on the substrate is the silver layer with a thickness of ~100 nm. The thickness of the As<sub>2</sub>S<sub>3</sub> layer was ~1 μm.

The photodiffusion or photodissolution of the silver in the amorphous chalcogenide thin film has been monitored in transmission geometry, as shown in Fig.1 in top view below:

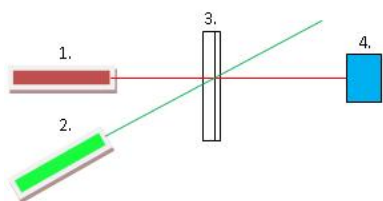


Fig. 1. Two-laser setup for monitoring the photodiffusion of silver in a-As<sub>2</sub>S<sub>3</sub> film.

The two layer sandwich (3.) was illuminated from the chalcogenide layer's side by two continuous laser diodes: (1.) a red one ( $\lambda=635$  nm,  $P=100$ mW), placed at normal incidence against the sample, used to continuously monitor the transmission of the thin-film structure for the

changes induced during the illumination with (2.), a green laser diode (GLD) light, ( $\lambda=532$  nm,  $P=100$ mW), under an angle of  $\sim 30^\circ$  relative to the normal incidence. It has been tested previously that red laser diode light alone does not produce measurable changes in the optical transmission of the Ag-ChG heterostructure.

The optical power transmitted by the heterostructure was recorded by the power meter (4.) for a series of illuminating times (Fig. 2).

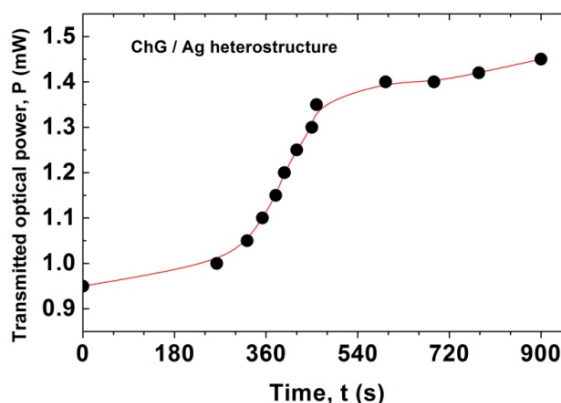


Fig. 2. Real-time measurement of the transmitted optical power through the heterostructure.

In order to follow the structural changes in the chalcogenide-silver sandwich film samples for several illumination times with GLD light, XRD diagrams were recorded with a Bruker D8 Advance diffractometer, as presented in Fig. 3.

The evolution of the thickness of the metallic silver layer (first layer of the sandwich) was followed through the (111) diffraction peak of silver. With increasing illumination times, the peak of silver decreases and finally almost vanishes.

It is interesting to note a correlated process with the gradual dissolution of the Ag layer, namely the gradual degradation of the first sharp diffraction peak (FSDP).

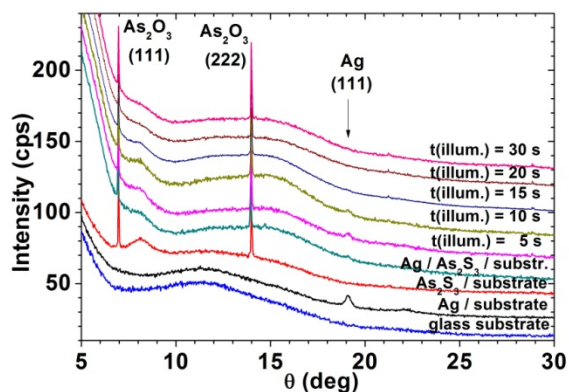


Fig. 3. X-ray diffraction measurement of the heterostructure, after various GLD illuminating times.

In order to gain additional insight, we performed a study of the behaviour of a series of stacked silver-chalcogenide interfaces upon illumination with broadband halogen lamp [4]. Four double layers of Ag/As<sub>2</sub>S<sub>3</sub> were prepared on glass substrate by pulsed laser deposition (PLD), using a KrF\* laser source, model COMPexPro 205, Lambda Physics-Coherent. This time the first layer on the substrate was As<sub>2</sub>S<sub>3</sub>. The depositions were carried out at room temperature. The power of the illuminating light beam was 100W, and the area of illumination was 1cm<sup>2</sup>. The temperature did not exceed 35°C during illumination.

Figure 4 shows the X-ray reflectivity (XRR) diagrams of the multilayer sample, which changes during illumination. For all illumination times an oscillating character of X-ray reflectivity is observed. This is due to the multilayer structure of deposited films (Kossel fringes). For 18,100 s illumination time the intensities of the fringes between 0.5° (2θ) and 1.3° (2θ) are much lower (~20 times) than those of the initial state, as a consequence of silver diffusion in chalcogenide layers.

We have applied a Fast Fourier Transformation (FFT) to the XRR diagrams. Thus we obtained for initial state the thickness of one bilayer (87.7nm) and the thickness of the multilayer (4×87.7nm = 350.8nm). The thickness of the multilayer after 5h of illumination is a little bit more expanded (~4.8%) than initial sample (from 87.7nm to 91.9nm for one bilayer). This effect can be ascribed to the expansion of the sample during the photo-diffusion of silver and,

also, photoexpansion effect in the chalcogenide layers, characteristic phenomena in As<sub>2</sub>S<sub>3</sub> [1]. In conclusion, after five hours of illumination, silver has diffused into As<sub>2</sub>S<sub>3</sub> layers, but the multilayer structure was maintained.

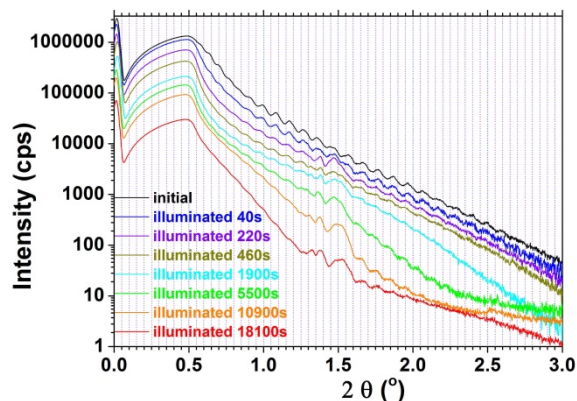


Fig. 4. Modification of the XRR diagram of the multilayer sample during illumination.

## References

- [1] M. Popescu, Non-Crystalline Chalcogenides, Kluwer Academic Publishers, Dordrecht, 2000.
- [2] F. Sava, M. Popescu, A. Lorinczi, Alin Velea, Physica Status Solidi (B); 250; 5; 999 - 1003 (2013)
- [3] A. Lórinzi, M. Popescu, F. Sava, A. Velea, I.-D. Simandan, Phys. Status Solidi C 8, No. 9, 2617 (2011).
- [4] F. Sava, A. Velea, M. Popescu, A. Lorinczi, I.D. Simandan, A.M. Vlaicu, G. Socol, I.N. Mihailescu, N. Stefan, Journal of Non-Crystalline Solids; 377; 159 – 161 (2013)

The authors kindly acknowledge the financial support of the Ministry of Education, Research, Youth and Sports (Romania) in the frame of the contracts 45N/1.03.2009 and PNII-IDEI No. 673/2009.



# Nanoscale Physics

## Magnetic behaviour of functionalized magnetite nanoparticles for various applications

*C. Bartha, P. Palade, G. Filoti, V. Teodorescu, A. Galatanu, V. Kuncser,*  
in cooperation with  
*D. Culita, L. Patron*

Ilie Murgulescu Institute of Physical Chemistry, Bucharest, Romania

*S. Suneritz*

Institut de Recherche Interdisciplinaire, Universite Lille 1, France

Recently, multifunctional nanomaterials have attracted a great attention not only for their fundamental scientific interest but also for technological and biological applications such as magnetic carriers for drug delivery systems, cell sorting, contrast-enhancement agent for MRI, therapeutic agent in cancer treatment, biosensors, etc. Results obtained on magnetite successfully functionalized with different molecules are briefly resumed, as follows: magnetite functionalized with *o*-vanillin (reported here as sample DC1) and 5-formylsalicylic acid (reported here as sample DC2) [1], but also for magnetite functionalized with dopamine or different dopamine derivatives (reported here as MF-MPs, from multifunctional nanoparticles) [2]. The investigations, involving chemical and physical methods, provided relevant features involving cell parameters and grain sizes, or the intermingling ratio between magnetite and functionalizing molecules, as deduced from magnetic measurements. A large amount of interesting data concerning various surface and local interaction mechanisms was supplied by detailed Mossbauer measurements. The new outputs were explained in terms of material processing and intimate mixing of the involved molecules. The XRD profiles of initial (naked) magnetite, as well as of DC1 and DC2 samples, discussed in terms of the corresponding Rietveld refinements obtained via the MAUD software (Lutterotti et al. 1992) show that for both functionalized samples the lattice parameter of magnetite is slightly larger than in the initial sample (naked nanoparticles). This fact suggests the inclusion of some ions

belonging to every functionalizing organic ligand in the unit cell of the initial magnetite, in larger numbers mainly at the particle surface. The HRTEM analysis (Fig. 1) provides the evidence for amorphous layers at surface of nanoparticles of average size of about 20 nm, as well as similar crystalline orientations for many adjacent nanoparticles.

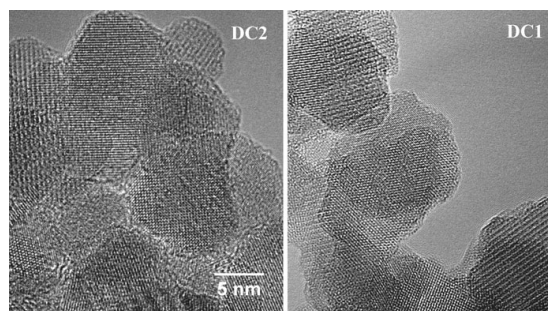


Figure 1: HRTEM images of the functionalized magnetite samples DC1 and DC2 [1].

Hysteresis loops of the three samples investigated (naked nanoparticles, and DC1 and DC2 samples) are shown in Fig. 2.

The saturation magnetization value for the naked nanoparticles is  $55.37 \text{ emu g}^{-1}$  much smaller than those reported for bulk magnetite ranging from  $88$  to  $94 \text{ emu g}^{-1}$ . The above observed lower magnetization is naturally related to the nanosized character of the grains with defected surface positions. The fraction of the functionalizing molecules has been also estimated in the two cases starting from the magnetic data. Accordingly, in average one functional molecule at about 1.9 magnetite molecules and one functional molecule at about 4.7 magnetite molecules correspond to samples DC1 and DC 2, respectively.

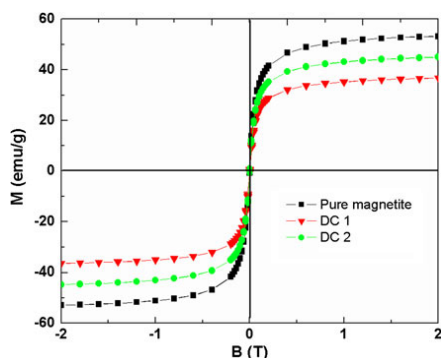


Figure 2: The hysteresis curves at room temperature for: pure magnetite, DC1, and DC2 samples [1].

The presence of well-defined sextets in the room temperature Mossbauer spectra proved the existing magnetic state of the samples, the three fitting sextets being assigned to tetrahedral, octahedral and specific surface Fe positions, with the relative amount of the surface position as significant parameter for the derivation of the above fraction of functionalized molecules.

The phase composition, local structure and magnetic interactions, as well as the magnetic relaxation phenomena in naked and MF-MPs systems were studied by magnetic measurements and temperature dependent  $^{57}\text{Fe}$  Mossbauer spectroscopy (Fig. 3). These nanoparticles of average size of about 25 nm show higher saturation magnetization (84 emu/g for naked MPs and 80 emu/g in case of MF-MPs) than in the previous case, proving a ratio 0.06 between the weight of the surfactant shell with respect to the magnetite core.

More distorted Fe positions at the particle surface were evidenced by Mossbauer spectroscopy as well as a narrow relative size dispersion of nanoparticles of 4-6%, together with an anisotropy constant of one order of magnitude lower than of bulk magnetite.

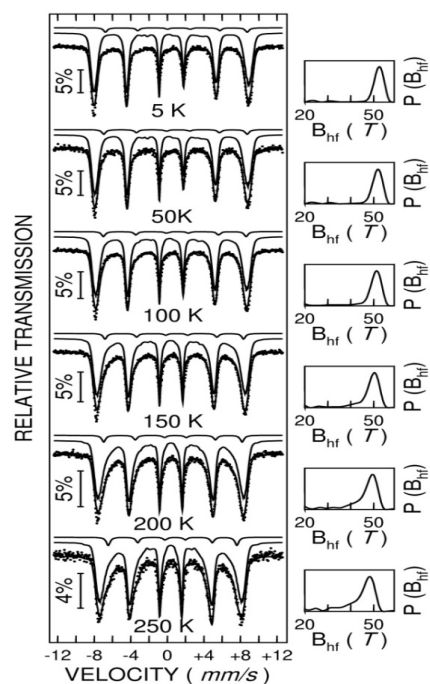
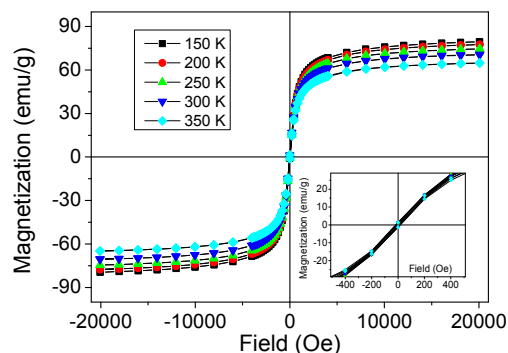


Figure 3: Magnetic hysteresis loops (up) and Mossbauer spectra (down) of the MF-NPS system [2].

## References

- [1] D. Culita, L. Patron, O. Oprea, C. Bartha, P. Palade, V. Teodorescu and G. Filoti, *Journal of Nanoparticle Research* (2013) 15:1916
- [2] M. Mazur, A. Barras, V. Kuncser, A. Galatanu et al. *Nanoscale*, (2013), 5, 2692-2702

## Magnetic relaxation of dispersed Fe-based magnetic nanoparticles

*G. Schinteie, P. Palade, C. Bartha, G. Filoti, V. Kuncser,*

in cooperation with

*L. Vekas*

Laboratory of Magnetic Fluids, Centre for Fundamental and Advanced Technical Research,  
Romanian Academy-Timisoara Division, Timisoara, Romania

*N. Iacob, F. Dumitrache, I. Morjan*

National Institute for Lasers, Plasma and Radiation Physics, Bucharest-Magurele, Romania

Iron based magnetic nanoparticles are intensively studied due to their novel applications in microelectronics (magnetic recording and magneto-optics, data storage devices), biomedicine (magnetic resonance imaging, magnetic carriers for drug delivery, a.c. magnetic field-assisted cancer therapy) or catalysis. Relevant results related to the magnetic properties and the local interaction mechanisms specific to two Fe based magnetic nanoparticulate systems were recently reported, as carefully analyzed under adequate magnetic relaxation regimes.

In the first case, three ferrofluid (FF) samples with different volume fractions ( $\eta$ ) ranging from 0.04 to 0.2, consisting of magnetite nanoparticles (NPs) coated with oleic acid and dispersed in non-polar organic solvent were studied by X-ray diffraction, SQUID magnetometry and temperature dependent Mössbauer spectroscopy.

Magnetic nanoparticles dispersed in a liquid media (ferrofluid) may support either Neel or Brownian type of relaxation mechanisms, each one with a specific dependence of the relaxation time versus temperature [1]. By freezing the ferrofluid at low temperatures, the Brownian relaxation is suppressed and the only mechanism in work is the Neel relaxation with a relaxation characteristic time given by the equation:  $\tau_N = \tau_0 \exp(KV/kT)$  (1), where  $\tau_0$  is a material dependent time constant of order of  $10^{-12}$ - $10^{-8}$  s,  $KV$  is the anisotropy energy of a nanoparticle of uniaxial anisotropy constant  $K$  and volume  $V$ ,  $T$  is the absolute temperature and  $k$  the Boltzmann constant.

From zero-field-cooled (ZFC) - field-cooled (FC) magnetisation curves measured on all

magnetite NPs dispersed in the transformer oil, in a small applied magnetic field of 80 Oe, it was observed an increment of the blocking temperatures  $T_B$  (specific to Neel relaxation mechanisms) with the volume fraction. This suggests an increasing interparticle interaction (counted by an effective anisotropy energy barrier per NP). Two different de-freezing mechanisms (in one step, for lower volume fractions and in two steps, for larger volume fractions) have been also evidenced by the evolution of the ZFC-FC curves. In order to further evidence the interparticle interactions in such kind of FF systems, magnetization measurements in applied external field were performed, as well as hysteresis loops at different temperatures (Figure 1).

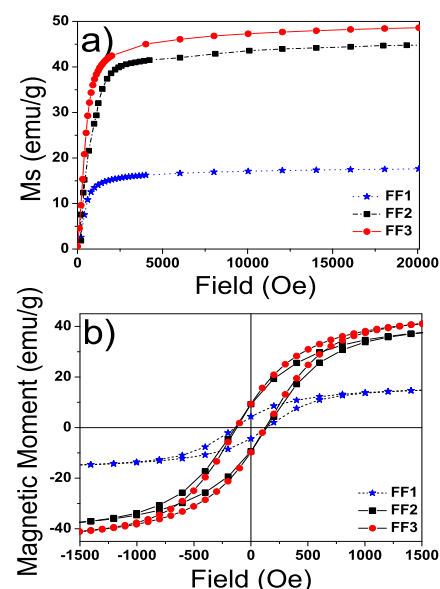


*Figure 1. The  $M(H)$  curves acquired at 10 K in an applied fields up to 20 kOe (a) and the hysteresis loops for all analyzed samples at at lowest temperatures (10 K)*

According to the Stoner –Wolhart model, the ratio,  $\zeta$ , between the remanence ( $M_R$ ) and

the saturation magnetization ( $M_s$ ) at low temperature, for an assembly of non-interacting NPs with randomly oriented uniaxial easy axes of magnetization, must be about 0.5. Deviations from this value are related to the presence of interparticle interactions [2] which are dipolar in nature. In our case, values for  $\zeta$  close to 0.3 have to be mentioned. They suggest on one hand, the presence of the interparticle interactions in all the analyzed samples, and on the other hand, their antiferromagnetic type.

New criteria for the quantitative estimation of the interparticle interactions by different methods are explained. If antiferromagnetic dipolar interactions manifest among nanoparticles (equivalently to the presence of an internal field), a negative magnetization of the sample will be expected at the lowest temperature, after the ZFC procedure. By increasing slightly the applied magnetic field, the magnetization will become zero, exactly at an applied field opposite and equal in magnitude to the internal field,  $H_i$ . Such  $M(H)$  curves are shown in figure 2, leading to values for  $H_i$  of about 18 Oe in case of FF1 and about 45 Oe in case of FF2 and FF3 samples.

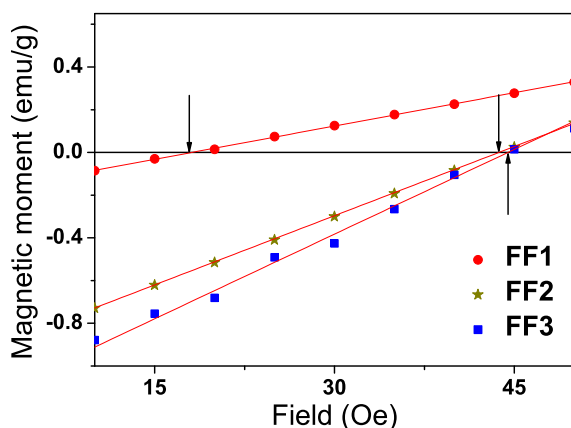


Figure 2.  $M(H)$  curves at 2 K in increasing applied fields up to 60 Oe. The arrows indicate the estimation of the applied field equating the internal field

These results support clearly the presence of dipolar interactions of antiferromagnetic type which are much stronger in samples with high volume fraction (FF2 and FF3) as compared with sample FF1, in close agreement with the

evolution of the blocking temperatures observed from ZFC-FC curves [3]. Temperature dependent Mössbauer spectroscopy gives direct confirmation for the dependence of the anisotropy energy versus the volume fraction and as a local microscopic technique provides evidence that the additional energy in dense ferrofluids is due to stronger dipolar interactions among nanoparticles

The second system consisting in iron carbon nanocomposites (obtained by laser pyrolysis in specific configurations) was investigated by X ray diffraction, magnetic measurements and Mossbauer spectroscopy, for a complex characterization regarding Fe phase composition, local magnetic interactions and magnetic relaxation. Magnetic relaxation phenomena was studied by following the evolution of the Mössbauer spectra as a function of temperature while the Fe phase composition was obtained from the low temperature Mössbauer spectra in the static regime

Three types of nanoparticles were identified in the investigated samples, as obtained by using specific parameters of the laser pyrolysis process (the diameter of the central nozzle in the concentric configuration and the relative flow of the reactive gases). These are metallic Fe, Fe carbide and Fe oxide. In particular, their relative content, average size, anisotropy constant and magnetic relaxation mechanism are strongly depending on the processing parameters [4].

## References

- [1]. R.E. Rosenweig 2002 J. Magn. Magn. Mater 252 370
- [2]. Hadjipanayis G, Sellmyer D J and Brandt B 1981 Phys.Rev. B 23(7) 3349
- [3]. G Schinteie, P Palade, L Vekas, N Iacob, C Bartha and V Kuncser; Journal of Physics: Applied Physics, Volume 46(39), 395501 (2013)
- [4]. G. Schinteie, V. Kuncser, P. Palade, F. Dumitrache, R. Alexandrescu, I. Morjan and G.Filoti; JALCOM, 564, pp. 27-34 (2013)

## Template assisted sol-gel synthesis of Eosin Y-SiO<sub>2</sub> hybrid nano- and microrods

C.E. Secu, R.F. Negrea, C. Bartha, M. Secu, M. Sima

in cooperation with

M. Dinescu and V. Damian

National Institute for Lasers, Plasma and Radiation, Bucharest-Magurele, ROMANIA

Since the first successful attempt to incorporate organic dyes within sol-gel glasses in 1984 many efforts have been devoted for finding new materials, improving and understanding the mechanisms with the aim developing successful applications as laser materials, nonlinear optical materials, optical memories, light concentrators in solar cells and electrooptical materials ([1] and references therein). Recently the incorporation of dyes in small particles has opened a promising field toward the development of new luminescent biolabel and nanometer-sized fluorescent hybrid silica particles for fluorescence imaging [2].

Sol-gel chemistry has provided a new route for preparing nanostructures by conducting sol-gel synthesis within the pores of a polycarbonate template membrane [3,4]. By using this method we prepared Eosin Y-SiO<sub>2</sub> hybrid nano- and microrods in which luminescent Eosin-y dye is entrapped [4]. Silica xerogels were prepared from organometallic tetraethylorthosilicate (TEOS) precursor in the presence of trifluoroacetic acid (TFA) as catalyst [5]; Eosin-y dye was added in the sol phase. The capillary force drives the sol into the pores of the membrane; then it is withdrawn, dried and dissolved and finally xerogel rods are obtained [3].

The Eosin Y-SiO<sub>2</sub> hybrid rods retain the morphology of the parent template membrane pores as it can be seen from scanning electron microscopy (SEM) images showing rods-type structures of about 30 $\mu$ m length with 200 and 1200nm diameter (Fig. 1). This indicate that xerogel formation mechanism is not influenced by the physical constraints imposed by the reduce nano-dimensionality of the pores membrane.

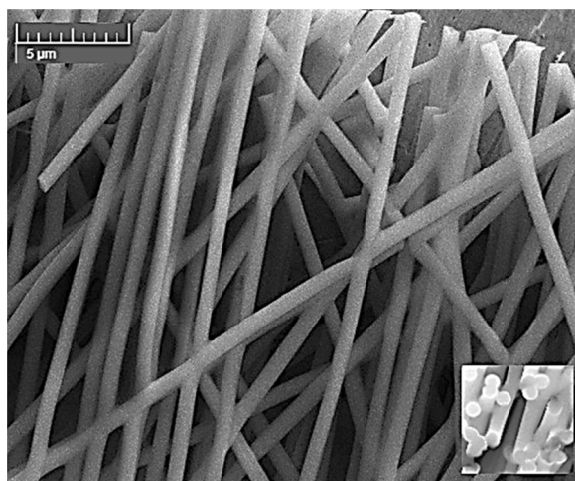
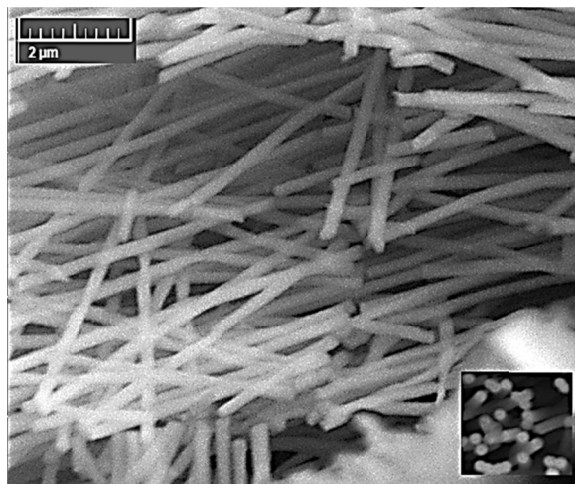


*Fig. 1: SEM images of the Eosin Y-SiO<sub>2</sub> hybrid nano- and microrods; the inset show the heads of the rods*

The Eosin Y-SiO<sub>2</sub> hybrid rods have luminescent properties and this can be seen in the Figures 2 and 3 where correlated optical microscopy and the luminescence microscopy images are presented.

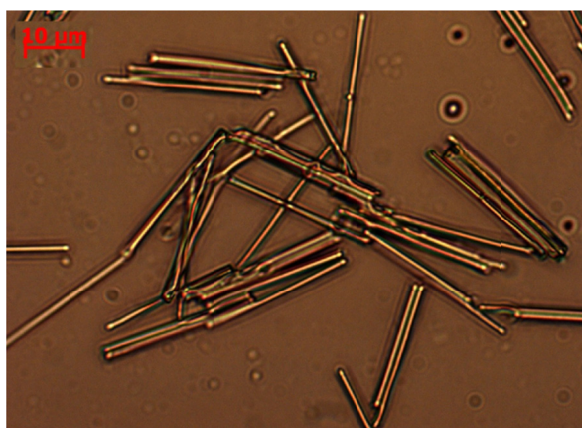


*Fig. 2: Optical microscopy images of the Eosin Y-SiO<sub>2</sub> hybrid microrods.*

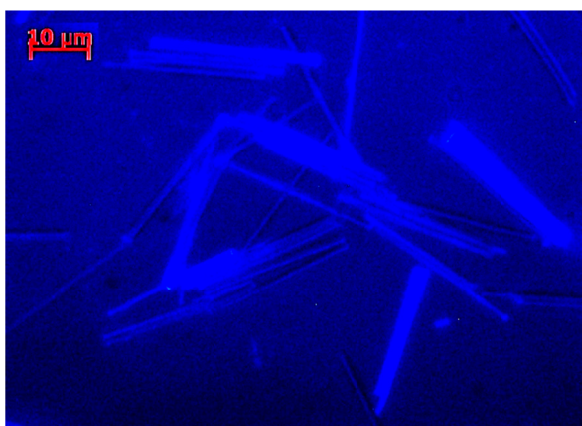


*Fig. 3: Luminescence microscopy images of the Eosin Y-SiO<sub>2</sub> hybrid microrods.*

For the description of the luminescence properties of the Eosin Y-SiO<sub>2</sub> hybrid rods in comparison with the bulk we have used optical absorption and photoluminescence spectroscopy (Figure 4). Photoluminescence spectra show a broad peak at around 545nm in bulk and rods samples; the spectra are due to transition between singlet and tripled states of the Eosin-y dye molecule [6]. We noticed a very good agreement between the main absorption peak and luminescence peak in the Eosin Y-SiO<sub>2</sub> hybrid bulk (at 517 nm and 545 nm) and in the Eosin-Y water solution at (515 nm and 545 nm) [7]. Therefore we assign the luminescence spectra to the Eosin-Y dye molecule in the xerogel porous network and surrounded by a solvation shell given mainly by the residual water. As Eosin-Y molecule size (of about 1nm) is much smaller than xerogel pore size of about few nm, the optical properties (i.e. the energies

of the excited states) are not influenced by the interaction with the silica “rigid cage”, as for other dyes [7].

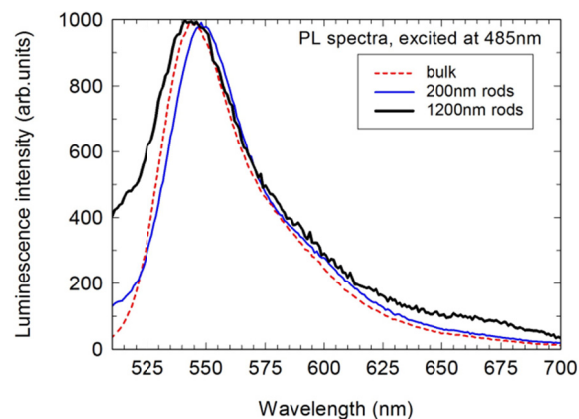


*Fig. 4: Normalised photoluminescence spectra of Eosin Y-SiO<sub>2</sub> hybrid nano- and microrods by comparison to the Eosin Y-SiO<sub>2</sub> hybrid bulk.*

Combination of the wide range of achievable materials and relatively easiness of the sol-gel method with the template preparation method allow exploiting the advantages of the light-guiding properties of the rods to sustain the next generation of optoelectronic nanodevices.

## References

- [1] K. Binnemans Chem. Rev. 109 (2009) 4283-374.
- [2] C. Philippot, F. Dubois, M. Maurin, B. Boury, A. Prat, A. Ibanez, J. Mater. Chem. 22 (2012) 11370-11378.
- [3] M. Secu, C.E. Secu, M. Sima, Journal of Nanoparticles Research 14 (4) 772 (2012)
- [4] M. Secu, C.E. Secu, M. Sima, R.F. Negrea, C. Bartha, M. Dinescu and V. Damian, J. Luminesc 143 (2013) p.89-92
- [5] Fujihara S., Mochizuki C., Kimura T., J. Non-Crystalline Sol. 244 (1999) 267-274
- [6] A. Penzkofer, Chem Phys 177 (1993) 203-216.
- [7] V. Balzani, P.Ceroni, S. Gestermann, M. Gorka, C. Kauffmann, F. Vögtle, Tetrahedron 58 (2002) 629-637.

## Spectroelectrochemical properties of the single walled carbon nanotubes functionalized with polydiphenylamine doped with heteropolyanions and its applications in the supercapacitors field

*I. Smaranda, M. Baibarac, I. Baltog, S. Frunza,*

in cooperation with

*A. Magrez<sup>1</sup>, D. Schur<sup>2</sup>, S.Yu Zaginaichenko<sup>2</sup>, J.Y. Mevellec<sup>3</sup>, S. Lefrant<sup>3</sup>*

<sup>1</sup> Ecole Polytechnique Federale Lausanne, Institute of Condensed Matter Physics,  
Lausanne, Switzerland

<sup>2</sup> Institute of Hydrogen and Solar Energy, Institute for Problems of Materials Science of Ukrainian  
Academy of Sciences, Kiev, Ukraine

<sup>3</sup>Institut des Materiaux "Jean Rouxel", Nantes, France

The functionalization of carbon nanotubes with polyoxometallates was shown to be a potentially useful method for the preparation of new active materials with applications in the supercapacitors field. In the context of the applications of polyoxometallate-functionalized carbon nanotubes and the applications of conducting polymers doped with heteropolyanions of  $\text{H}_3\text{PMo}_{12}\text{O}_{40}$  in the energy storage, we note that the synthesis of these materials has received special attention over the last 2 years. Until now, two methods have been used to prepare composite materials based on carbon nanotubes, conducting polymers and polyoxometallates: the chemical polymerization of a monomer in the presence of heteropolyacids and carbon nanotubes and a combined chemical-electrochemical method.

The chemical polymerization of monomer molecules in the presence of carbon nanotubes and the  $\text{H}_3\text{PMo}_{12}\text{O}_{40}$  heteropoly-acid results in three types of composites: i) carbon nanotubes as whole units functionalized with the conducting polymers doped with heteropolyanions of  $\text{H}_3\text{PMo}_{12}\text{O}_{40}$ , ii) tube fragments with shorter lengths, like closed-shell fullerenes functionalized with polymers in the doped state and iii) blends based on polymers in the un-doped state and carbon nanotubes doped with heteropoly-anions. Composites based on polydiphenylamine (PDPA) doped with heteropolyanions of  $\text{H}_3\text{PW}_{12}\text{O}_{40}$  and single-walled carbon nanotubes (SWNTs) were prepared by electrochemical polymerization of diphenylamine (DPA) on carbon nanotube films deposited onto Pt electrodes. HRTEM studies

reveal that the electrochemical polymerization leads to the filling the spaces between tubes which compose the bundles, creating a monolithic film on the Pt electrode. The resulting composites were tested as active materials in supercapacitors. The characterization of symmetric solid-state supercapacitors was performed for electrodes prepared from i) SWNTs functionalized with PDPA doped with  $\text{H}_3\text{PW}_{12}\text{O}_{40}$  heteropolyanions, ii) SWNTs electrochemically decorated with  $\text{H}_3\text{PW}_{12}\text{O}_{40}$  heteropolyanions, and iii) PDPA doped with  $\text{H}_3\text{PW}_{12}\text{O}_{40}$  heteropolyanions. Preliminary results indicate high discharge capacitance values of up to  $157.2 \text{ mF/cm}^2$  for SWNTs functionalized with PDPA doped with  $\text{H}_3\text{PW}_{12}\text{O}_{40}$  heteropolyanions. The discharge capacitance of this material is superior to those recorded for SWNTs electrochemically decorated with  $\text{H}_3\text{PW}_{12}\text{O}_{40}$  heteropolyanions ( $\sim 18.2 \text{ mF/cm}^2$ ) and PDPA doped with  $\text{H}_3\text{PW}_{12}\text{O}_{40}$  heteropolyanions ( $\sim 62.1 \text{ mF/cm}^2$ ).

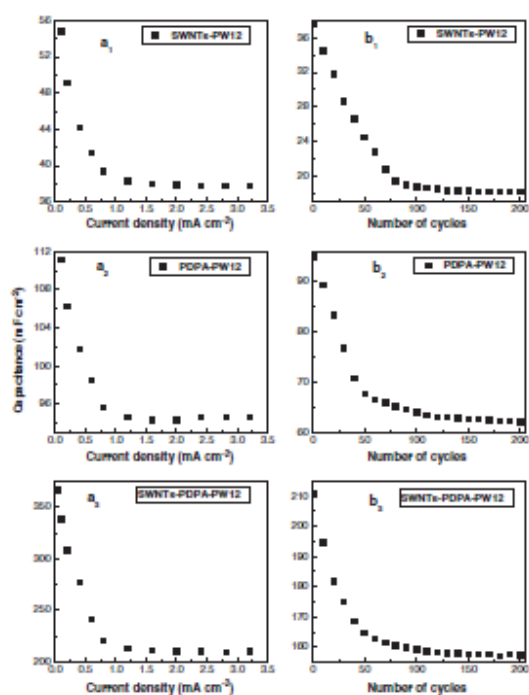


*Fig.1 Performances of symmetrical solid-state supercapacitors. a) The dependence of the capacitance at different current densities using different active electrode materials: a<sub>1</sub>) SWNTs electrochemically decorated with H<sub>3</sub>PW<sub>12</sub>O<sub>40</sub> heteropolyanions; a<sub>2</sub>) PDPA doped with H<sub>3</sub>PW<sub>12</sub>O<sub>40</sub> heteropolyanions; and a<sub>3</sub>) SWNTs covalently functionalized with PDPA doped with H<sub>3</sub>PW<sub>12</sub>O<sub>40</sub> heteropolyanions. b) The evolution of capacitance at successive charge–discharge cycles performed in the potential range 0–0.8 V using different active electrode materials: b<sub>1</sub>) SWNTs electrochemically decorated with H<sub>3</sub>PW<sub>12</sub>O<sub>40</sub> heteropolyanions; b<sub>2</sub>) PDPA doped with H<sub>3</sub>PW<sub>12</sub>O<sub>40</sub> heteropolyanions; and b<sub>3</sub>) SWNTs covalently functionalized with PDPA doped with H<sub>3</sub>PW<sub>12</sub>O<sub>40</sub> heteropolyanions.*

This work reports for the first time new results concerning the influence of H<sub>3</sub>PW<sub>12</sub>O<sub>40</sub> on the electrochemical functionalization of carbon nanotubes with conducting polymers of the type polydiphenylamine. The electrochemical functionalization of SWNTs with PDPA doped with H<sub>3</sub>PW<sub>12</sub>O<sub>40</sub> heteropolyanions not needs other chemical or annealing treatments as in the case of other active materials such as composites of the type activated carbon–ruthenium oxide and multi-walled carbon nanotubes functionalized with ruthenium oxide. We demonstrate for the first time that single-walled carbon nanotubes (SWNTs) functionalized with PDPA doped with

the H<sub>3</sub>PW<sub>12</sub>O<sub>40</sub> heteropolyanions can be used as active electrode materials in supercapacitors field. [1] The value of the discharge capacitance of cells having as active material SWNTs functionalized with PDPA doped with H<sub>3</sub>PW<sub>12</sub>O<sub>40</sub> heteropolyanions (52.5 F/g) is superior to that reported for the activated carbon – ruthenium oxide nanoparticles composites (38.7 F/g) and smaller in comparison with the specific capacitance of ruthenium oxide functionalized MWNTs (80 F/g) (Fig. 1). Taking into account the high cost of ruthenium oxide, we think that an optimization of the supercapacitors based on active materials of the type SWNTs functionalized with PDPA doped with H<sub>3</sub>PW<sub>12</sub>O<sub>40</sub> heteropolyanions will lead in the future to a more attractive cost/performance ratio.

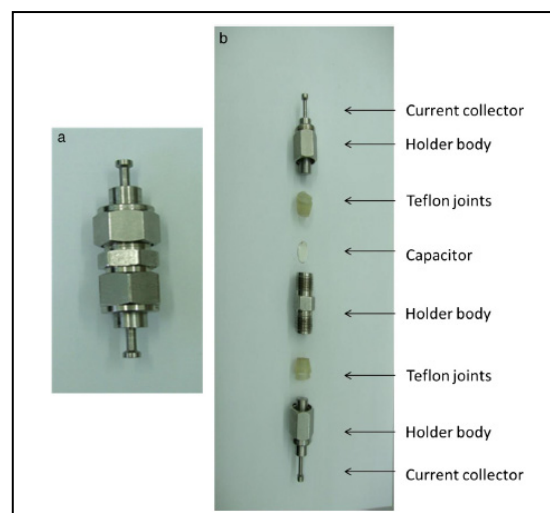


*Fig. 2 The overview of the Swagelok cell (a) and its main components (b).*

Symmetric solid-state supercapacitors were assembled in Swagelok cells as is shown in Fig. 2.

## References

- [1] M. Baibarac, I. Baltog, S. Frunza, A. Magrez, D. Schur, S.Yu. Zaginaichenko; *Diamond & Related Materials*, **32**, 72 (2013).
- [2] I. Smaranda; M. Baibarac, I. Baltog, J-Y Mevellec, S. Lefrant. *Journal of Solid State Chemistry* **197**, 352 (2013).

## EPR probing of the crystallization and growth mechanism of nanostructured ZnO doped with Mn<sup>2+</sup>

*M. Stefan, S. V. Nistor, D. Ghica*

Strains induced by both surface and lattice disorder in semiconductor nanocrystals (NCs) for electro-optical applications strongly affect the electronic processes and characteristics such as light yield, energy transfer to dopants, scintillation decay time, conductivity etc. In one of the very few investigations on the origin and distribution of strain in NCs [1] it was hypothesized that lattice disorder strongly depends on the nanoparticle size.

From correlated electron paramagnetic resonance (EPR) and X-ray diffraction (XRD) investigations on Mn<sup>2+</sup> doped ZnO NCs synthesized by different procedures we were able to confirm this hypothesis, by establishing an empirical relationship between the local strain/lattice disorder and the average crystallite size of the NCs [2].

The investigated Mn<sup>2+</sup> doped ZnO samples were prepared by colloidal synthesis or thermal decomposition of precursors such as Zn(OH)<sub>2</sub> and hydrozincite Zn<sub>5</sub>(CO<sub>3</sub>)<sub>2</sub>(OH)<sub>6</sub> (ZCB) [3,4]. The EPR measurements were carried out in the Center for advanced ESR techniques (<http://cetresav.infim.ro>).

In semiconductor NCs the lattice disorder leads to variations in the local crystal fields acting on the activating impurity ions, such as Mn<sup>2+</sup>, affecting their spectral properties. The resulting local strain induces a broadening of the EPR lines, which can be quantified by Gaussian distributions of the axial zero-field-splitting parameter  $D$  values [4,5], with standard deviation  $\sigma(D)$ . In the following  $\sigma(D)$ , expressed as % $D$ , is referred to as the broadening parameter.

As determined by EPR, all ZnO samples consist of a mixture of various proportions of ZnO NCs and disordered ZnO. The two phases are reflected in the EPR spectra by the presence of two Mn<sup>2+</sup> centers with similar EPR parameter values and different broadening parameters [4].

Their concentrations are proportional with the amount of the corresponding ZnO phase in the sample. The Mn<sup>2+</sup>-d center in disordered ZnO has  $\sigma(D) = 42\%$ , while for the Mn<sup>2+</sup>-c center in ZnO NCs  $\sigma(D)$  varies with the average crystallite size  $d$ . As shown in Fig.1, in the case of a ZnO sample prepared by the thermal decomposition of ZCB in air at three different temperatures,  $\sigma(D)$  of the Mn<sup>2+</sup>-c centers decreases with the annealing temperature and the increase of  $d$ .

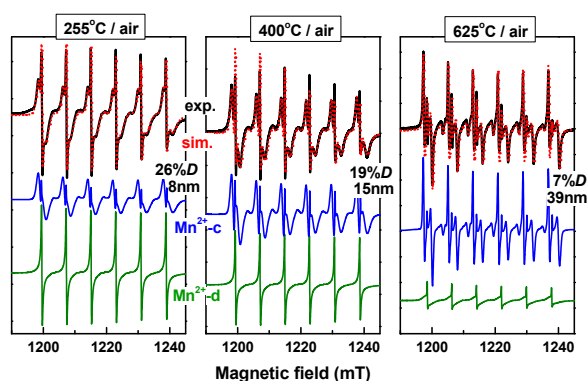


**Figure 1.** Experimental (black) and simulated (red) EPR spectra of the Mn<sup>2+</sup> ions in ZnO NCs resulted from ZCB annealed in air at (a) 255 °C, (b) 400 °C, and (c) 625 °C. The simulated spectrum is the sum of the Mn<sup>2+</sup>-c (blue) and Mn<sup>2+</sup>-d (green) calculated spectra.

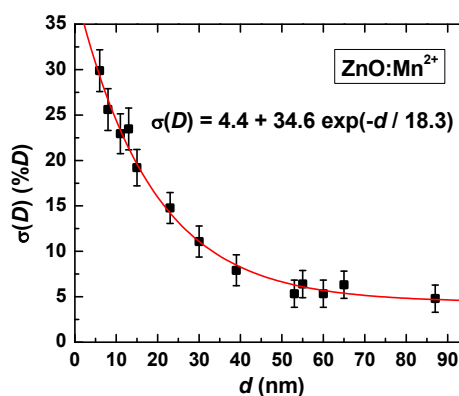


**Figure 2.** The broadening parameter  $\sigma(D)$  of the Mn<sup>2+</sup> ions EPR spectra in ZnO NCs of different origins vs the average crystallite size  $d$  determined by XRD.

The variation of  $\sigma(D)$  for the Mn<sup>2+</sup>-c centers in the different ZnO NCs samples with the

average crystallite size  $d$  follows a uniform exponential decay-like behavior (Fig. 2), independent of the samples preparation history. Thus, all other possible strain sources are bypassed by the contribution of the dominant size related strain. As the  $\sigma(D)$  broadening parameter is a measure of the local strain, reflecting a certain degree of lattice disorder, this empirical relationship demonstrates a direct link between the lattice disorder and the average crystallite size.

Another important consequence is that the average crystallite size of the ZnO NCs can be estimated directly from the EPR spectrum of the  $Mn^{2+}$  dopant. This result was further used to determine by EPR the crystallization mechanism of the nanostructured ZnO prepared by the thermal decomposition of ZCB annealed in air in the temperature range 225°C -245°C [2]. By further annealing the disordered ZnO formed during this first step one obtains a population of ZnO NCs of increasing size interspersed in a ZnO disordered matrix [4].

Four samples of nanostructured ZnO thus prepared were submitted to isothermal annealing at 300°C, 400°C and 500°C and to isochronal annealing at temperatures between 255°C and 625°C. The EPR spectra were recorded at room temperature after each annealing step. From the relative intensities of the EPR lines of the two  $Mn^{2+}$  centers one could calculate the proportion of NCs in the ZnO sample, further called crystallized fraction. Fig. 3 displays the variation of the crystallized fraction  $f$  vs the NCs volume  $d^3$  for the ZnO samples submitted to different annealing procedures.

Two growth stages can be identified for the ZnO NCs, namely one of free growth, up to a volume fraction of NCs of ~75 %, followed by a second stage, where the larger NCs grow at the expense of the smaller ones, the driving force being the reduction of the total grain boundary energy. The growth of the ZnO NCs at lower temperatures was found to take place by a structural relaxation mechanism, consisting in the rearrangement of atoms at interfaces, driven

by the reduction of the surface induced strain, with activation energy of ~23 kJ/mol. At higher temperatures, in the second growth stage, atom diffusion at grain boundaries, with activation energy of ~79 kJ/mol, was found to contribute to the NCs growth as well.

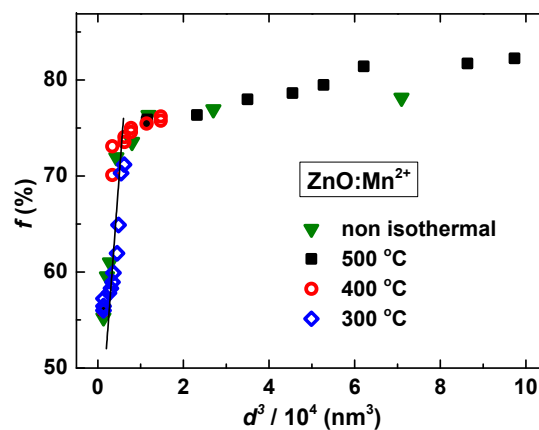


**Figure 3.** Variation of the crystallized fraction  $f$  with the average crystallite volume  $d^3$  for ZnO samples annealed either isothermally at 300 °C, 400 °C and 500 °C or isochronally at different temperatures.

It is worth mentioning that structural features, such as the presence of the disordered phase and strain in the ZnO NCs, were easily observed and quantitatively evaluated by EPR, while they could not be observed by XRD. We emphasize thus the quality and sensitivity of the structural information available when EPR is employed for the characterization of nanostructures.

## References

- [1] B. Gilbert, F. Huang, L. Zhang, C. Goodell, H. Zhang, J.F. Banfield, *Nano Lett.* **6**, 605 (2006) and references cited there in
- [2] M. Stefan, S.V. Nistor, D. Ghica, *Cryst. Growth Des.* **13**, 1350 (2013)
- [3] S.V. Nistor, D. Ghica, M. Stefan, I. Vlaicu, J. N. Barascu; C. Bartha, *J. Alloys Comp.* **548**, 222 (2013)
- [4] S.V. Nistor, L.C. Nistor, M. Stefan, D. Ghica, Gh. Aldica, J.N. Barascu, *Cryst. Growth Des.* **11**, 5030 (2011)
- [5] M. Stefan, S.V. Nistor, N.J. Barascu, *J. Magn. Res.* **210**, 200 (2011)

## New Zn-nanocompounds resulting from the thermal decomposition of the disordered $\text{Zn}(\text{OH})_2$ shell of $\text{cZnS}$ core-shell quantum dots

S. V. Nistor, D. Ghica, M. Stefan, L. C. Nistor

Cubic zinc sulphide ( $\text{cZnS}$ ) nanocrystals of a few nanometer average diameter, called quantum dots (QDs), doped with transition metal ions, represent one of the most investigated II-VI nanosemiconductors. This high interest is due to its outstanding optical properties and low toxicity, of special interest for optoelectronic and bio-medical applications [1]. The optical emission properties of the  $\text{cZnS}$  QDs doped with  $\text{Mn}^{2+}$  ions were found to change by the presence of a surface layer/shell, inferred from the preparation procedure to be  $\text{Zn}(\text{OH})_2$  [2].

Monitoring the structure, thermal stability and decomposition products of such a disordered  $\sim 1$  nm thick surface layer/shell by the usual X-ray diffraction (XRD) and high resolution transmission electron microscopy (HRTEM) structural techniques is extremely difficult, as one needs to distinguish the  $\text{Zn}(\text{OH})_2$  from other possible compounds such as  $\text{ZnO}$ ,  $\text{ZnCO}_3$  or  $\text{Zn}_5(\text{CO}_3)_2(\text{OH})_6$ , with the last two resulting from atmospheric corrosion.

We have shown that electron paramagnetic resonance (EPR) can determine with high sensitivity the presence, composition and structure of such nanolayers, by using low concentrations of  $\text{Mn}^{2+}$  impurity ions as local atomic probes. This is possible by the accurate determination of the spin Hamiltonian (SH) parameters, using the specially developed multifrequency spectra analysis procedure [3, 4]. The success of this approach is also conditioned by the existence of accurate reference SH parameter values for the  $\text{Mn}^{2+}$  ions in the corresponding bulk material [5].

In the present investigations [6] multifrequency EPR measurements were carried out in the Center for Advanced ESR Techniques (<http://cetresav.infim.ro>), at room temperature (RT), on  $\text{cZnS}$  QDs doped with 2000 ppm  $\text{Mn}^{2+}$  ions, prepared by colloidal synthesis at  $\text{pH} = 6.5$  and  $\text{pH} = 8$ . According to the XRD

and HRTEM studies, both types of samples exhibited a mesoporous structure of strongly aggregated QDs with an average core size distribution centered at 3.1 nm and 1.9 nm, respectively [6]. The samples prepared at  $\text{pH} = 6.5$  exhibited only the narrower six-line component spectrum (Fig. 1a), attributed from its SH parameters (Table 1) to  $\text{Mn}^{2+}$  ions localized in the core of the QDs at  $\text{Zn}^{2+}$  cation sites next to an extended stacking defect, called  $\text{Mn}^{2+}(\text{I})$  centers [4]. The samples prepared at  $\text{pH} = 8$  exhibited an additional broader six-line component spectrum with a larger hyperfine splitting  $A$  (Fig. 1b) from the so-called surface  $\text{Mn}^{2+}(\text{II})$  centers [2].

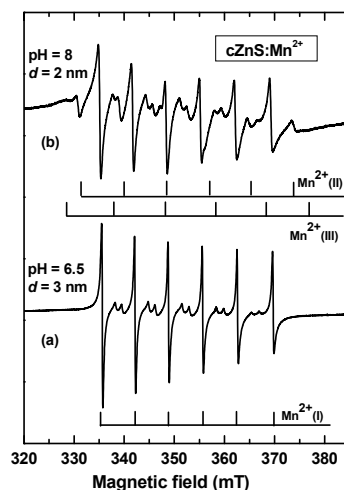


Figure 1. The X-band EPR spectra at RT of  $\text{cZnS:Mn}^{2+}$  QDs prepared by colloidal synthesis: (a) at low  $\text{pH} = 6.5$ , and (b) at high  $\text{pH} = 8$ .

Their SH parameters (Table 1), practically identical with those of the  $\text{Mn}^{2+}$  ions in crystalline  $\epsilon\text{-Zn}(\text{OH})_2$  [5], indicate that the shell of the  $\text{cZnS}$  QDs grown at  $\text{pH} = 8$  has an orthorhombic  $\epsilon\text{-Zn}(\text{OH})_2$  structure [6]. There is a second set of lines in the EPR spectrum of this sample (Fig. 1b) from other surface centers called  $\text{Mn}^{2+}(\text{II})$ , with smaller hyperfine splitting [4]. Their origin will be discussed later.

**Table I.** The SH parameters of the  $Mn^{2+}$  centers in as-grown and annealed  $cZnS$  QDs. The  $A$  and  $D$  parameters are given in  $10^4 \text{ cm}^{-1}$  units.

SH param	$Mn^{2+}$ (I)	$Mn^{2+}$ (III)	$Mn^{2+}$ (II)	$(Mn^{2+} - ZnO)_p$	$(Mn^{2+} - ZnO)_s$
$g$	2.0022	2.0009	2.0012	2.0012	2.0012
$A$	-63.7	-86.8	-80.5	-76.4	-73.5
$ D $	41	75-105	60-90	150-270	242
$\sigma(D)$ [%D]	43	53	63	42	42

The HRTEM images (Fig. 2) of the samples prepared at  $pH = 8$  display strongly aggregated  $cZnS$  QDs of 2-3 nm diameter, separated by disordered regions/layers of 0.3 to 1.9 nm variable thickness. Such layers correspond to the  $\epsilon$ - $Zn(OH)_2$  shell with partially disordered structure hosting the  $Mn^{2+}$ (III) centers observed by EPR [2,6].

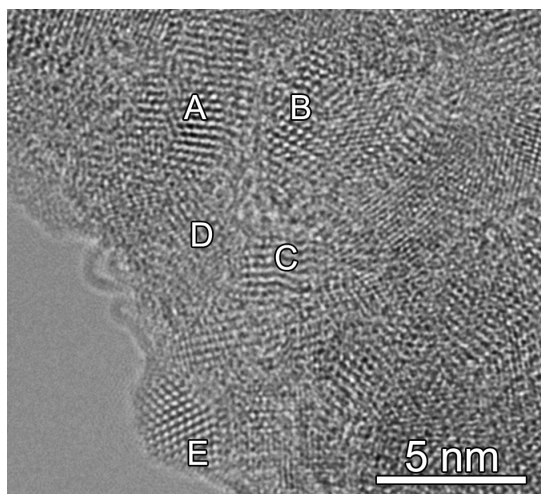


**Figure 2.** HRTEM image of  $cZnS:Mn^{2+}$  QDs prepared at high  $pH$ . Letters A-E mark the core of individual QDs separated, according to the EPR analysis, by disordered layers of  $Zn(OH)_2$ .

The temperature induced changes in the  $\epsilon$ - $Zn(OH)_2$  shell were further investigated by EPR pulse annealing experiments [6], in which the measuring ampoules with the investigated sample was annealed in a temperature stabilized ( $\pm 1$  °C) furnace at temperatures which increased in equal steps of 10 °C up to 200 °C and of 50 °C for higher temperatures. After each pulse annealing step the sample ampoule was cooled down to RT, where its X- and Q-band EPR spectra were recorded. According to the resulting sequence of EPR spectra (Fig. 3), the surface

$Mn^{2+}$ (III) centers transform above 80 °C into the  $Mn^{2+}$ (II) centers and above 250 °C into the  $(Mn^{2+}-ZnO)_p$  and finally  $(Mn^{2+}-ZnO)_s$  centers. The analysis of their hyperfine  $A$  parameter (Table 1) point out to a sequential decomposition by dehydration of the disordered  $\epsilon$ - $Zn(OH)_2$  shell into  $ZnO$ , with formation of intermediate  $Zn_2O(OH)_2$  and  $Zn_4O_3(OH)_2$  nanocompounds [6]. This process is entirely different from the one step decomposition of bulk  $\epsilon$ - $Zn(OH)_2$  around 120 °C [5].

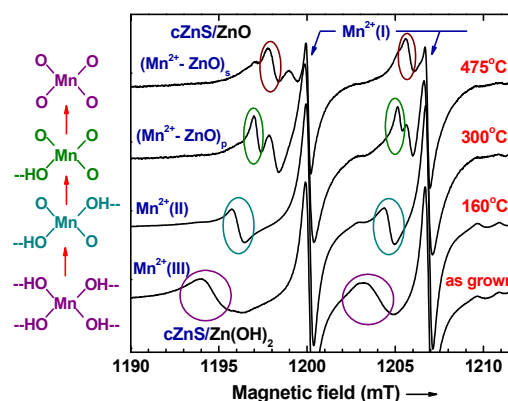


**Figure 3.** Significant Q-band EPR spectra of pulse annealed  $cZnS:Mn^{2+}$  QDs grown at  $pH=8$ , presenting the lowest two hyperfine transitions of the  $Mn^{2+}$  ions in the decaying  $Zn(OH)_2$  shell.

After annealing at 350°C the shrinking of the  $Zn(OH)_2$  shell to a few atomic layers, by loss of the  $H_2O$  molecules tetrahedrally coordinating the  $Mn^{2+}$  ions (Fig. 3 - left side), was also evidenced by HRTEM [6].

## References

- [1] H. Hu, W. Zhang, *Opt. Mat.* **28**, 536 (2006)
- [2] M. Stefan, S. V. Nistor, D. Ghica, C. D. Mateescu, M. Nikl, R. Kucherko, *Phys. Rev. B* **83**, 045301 (2011)
- [3] M. Stefan, S. V. Nistor, N. J. Barascu, *J. Magn. Res.* **210**, 200 (2011)
- [4] S. V. Nistor, M. Stefan, L. C. Nistor, E. Goovaerts, G. Van Tendeloo, *Phys. Rev. B* **81**, 035366 (2010)
- [5] S.V. Nistor, D. Ghica, M. Stefan, I. Vlaicu, J. N. Barascu; C. Bartha, *J. Alloys Comp.* **548**, 222 (2013)
- [6] S. V. Nistor, D. Ghica, M. Stefan, L. C. Nistor, *J. Phys. Chem. C*, **117**, 2217 (2013)

## Single bath electrodeposition of samarium oxide/zinc oxide nanostructured films with intense, broad luminescence

*Elena Matei, Monica Enculescu, Ionut Enculescu*

Electrochemical deposition of semiconductors represents an interesting approach for the preparation of different electronic or optoelectronic devices. This technique shows the promises of low infrastructure cost and high scalability, these two characteristics making it appealing for cheap, high yield production such is the case of solar photovoltaics or solid state lighting

Zinc oxide is a direct band-gap semiconductor extremely interesting for optoelectronic applications. Its band gap of approximately 3.3 eV is well suited for ultraviolet light emitting devices such as LED's or lasers. Electrochemical deposition of zinc oxide was intensively studied during the last decade. Extremely interesting is the fact that by appropriately tuning the deposition conditions one succeeds in tailoring the properties of the film such as morphology or optical properties. Doping can also be achieved for a wide range of impurities, such as, for example, dopants with magnetic or optic properties.

Electrochemical deposition of rare earth metals or rare earth compounds became increasingly important during the last years due to the special high interest in the field of magnetic films (e.g. deposition of CoSm alloys) but also in protective coatings (e.g. deposition of ceria or samaria thin films). Of major interest is considered the deposition of rare earth metal doped zinc oxide, since its potential in light emitting optoelectronic devices [1].

Zinc oxide electrodeposition from baths containing nitrate ions is a rather well known phenomenon. For several tens of millimoles of zinc nitrate, the typical morphology consists in hexagonal prisms with base size ranging from several hundred nanometers to micrometers (Fig. 1). Rather well crystallized, the ZnO structures obtained in this way present properties determined by the deposition conditions e.g.

morphology or photoluminescence spectra strongly depends on deposition rate.

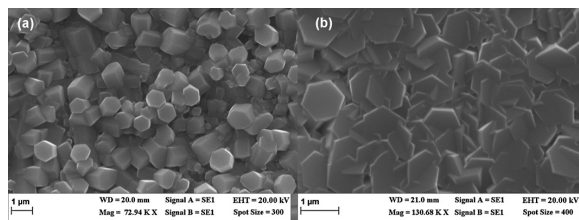


*Fig. 1. ZnO layers deposited from solution containing 50 mM Zn(NO<sub>3</sub>)<sub>2</sub> and 100 mM KNO<sub>3</sub> at (a) -750 mV and (b) -1000 mV.*

Porous samarium compound layers are obtained even only samarium ions were present in the solution or potassium nitrate is added, as revealed by the scanning electron microscopy studies (Fig. 2). Macroscopically, the deposited layers are extremely brittle with a strong tendency to exfoliation. The samples prepared from the bath containing only samarium chloride present a more compact aspect in comparison to the samples deposited from the bath containing also the nitrate ions. If in the first case there is only one reduction mechanism which may take place, in the second case is probable that both water reduction and nitrate reduction occur at the working electrode.

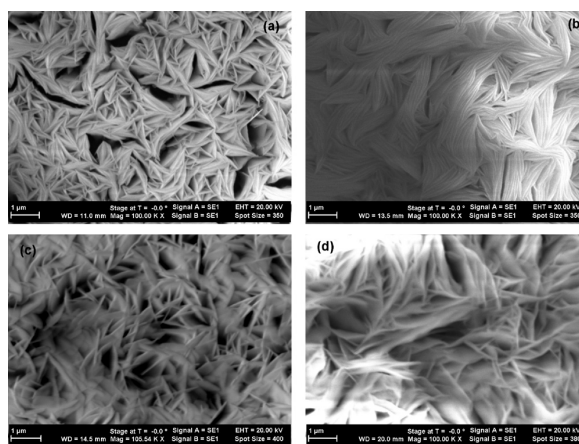


*Fig. 2. Scanning electron images of samples deposited from the bath containing: SmCl<sub>3</sub> at (a) -750 mV, (b) -1000 mV and 60 mM SmCl<sub>3</sub>, 100 mM KNO<sub>3</sub> at (c) -750 mV, (d) -1000 mV.*

Electrodeposition from the bath which contains both zinc and samarium ions leads to the most interesting and also complex results, the formation of a bilayer system. This phenomenon takes place for bath composition and electrodeposition potential higher than a certain threshold, for lower values only zinc oxide layers being obtained. The morphology measurements show typical hexagonal prism morphology for the zinc oxide layer and a nanoporous/nanowalls amorphous like structure for the samarium oxide film (Fig. 3). The samarium oxide films look more compact for the cases when the deposition took place at lower overpotential values i.e. at lower growth rates.

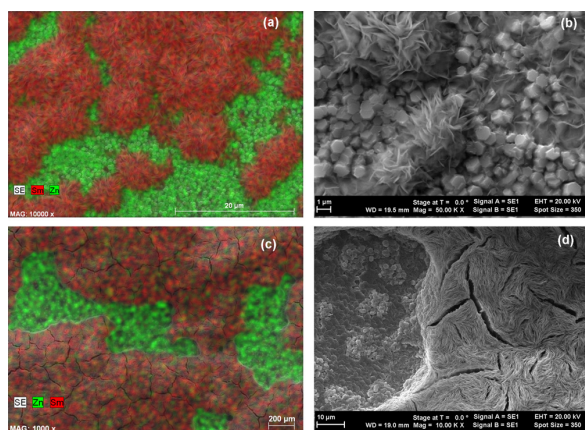


Fig. 3. (a) EDX mapping and (b) SEM image of a sample deposited from bath containing 60 mM  $\text{SmCl}_3$  and 50 mM  $\text{Zn}(\text{NO}_3)_2$  at  $-900$  mV for 10 min (c) EDX mapping and (d) SEM image of a sample deposited from bath containing 60 mM  $\text{SmCl}_3$  and 50 mM  $\text{Zn}(\text{NO}_3)_2$  at  $-900$  mV for 60 min.

X-ray diffraction studies confirmed the presence of  $\text{ZnO}$ ,  $\text{Sm}_2\text{O}_3$  and  $\text{SmOH}_3$  in bilayer. Optical properties of the double layered film show several characteristic features. The optical reflection spectra show the characteristic peaks corresponding to optical transitions of Sm (3+) ions and the band to band characteristic transition of zinc oxide. Photoluminescence measurements of the material show an enhanced emission when compared to pure zinc oxide but with the same typical emission spectrum, slightly blue shifted (Fig. 4). The increase in intensity makes the samples extremely emissive.

Very interesting is the dependence of emitting intensity as a function of deposition time (Fig. 4(b)) leading to the conclusion that we do not have a typical proportional dependence with the amount of material deposited. Cathodoluminescence emission was very weak for the samples where thick layers of samaria were deposited. This is a consequence of the presence of the samaria layer with wider band gap which acts as a window for the photon excitation while blocking the electron excitation. Cathodoluminescence scans on incompletely covered samples and on samples with thin layers of samaria covering the  $\text{ZnO}$  show enhanced emission near the edges of samaria islands. The origin of this intense light emission is, in our assumption, a defect rich interface layer in zinc oxide near the border with the samarium oxide. The system has potential applications in solid state lightning or thin film based displays.

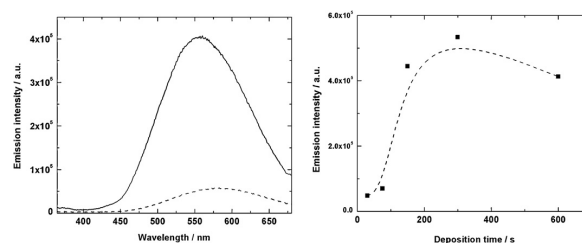


Fig. 4. (a) PL emission of samples prepared using bath containing:  $\text{Zn}^{2+}$  ions (dashed line) and 60 mM  $\text{SmCl}_3$ , 50 mM  $\text{Zn}(\text{NO}_3)_2$  and 100 mM  $\text{KNO}_3$  (continuous line) at  $-1100$  mV; (b) luminescence intensity as a function of deposition time for samples obtained from bath with 60 mM  $\text{SmCl}_3$ , 50 mM  $\text{Zn}(\text{NO}_3)_2$  and 100 mM  $\text{KNO}_3$  at  $-1000$  mV.

NIMP researchers acknowledge financial support of SCOPUS programme (Swiss National Science Foundation) no. IZ 73Z0 127968 and IDEI programme (UEFISCDI) contract TE 37/2011.

## References

- [1] Elena Matei, Monica Enculescu, Ionut Enculescu, *Electrochimica Acta* 95 (2013) 170–178.

## Transmission electron microscopy study of Ge nanoparticles formed in GeSiO films by annealing in Hydrogen

V. S. Teodorescu, V.A. Maraloiu, I. Stavarache, A.-M. Lepadatu, M. L. Ciurea

We present a detailed transmission electron microscopy (TEM) study of GeSiO films containing embedded Ge nanoparticles. We aim to explain the presence of the Ge-III phase in the samples annealed in H<sub>2</sub> and to elucidate if this phase is induced or not by preparation of TEM specimen, using ion milling or the micro-fragment extraction method. For this, all the TEM specimens used in the present study are prepared by the conventional cross-section method [1]

The GeSiO films with thickness of about 2.5 μm were deposited by RF magnetron co-sputtering of SiO<sub>2</sub> and Ge on quartz substrate [2], with an atomic Ge concentration of about 40%. Germanium nanoparticles are formed by Ge segregation in SiO<sub>2</sub> matrix during the thermal annealing performed in H<sub>2</sub> at 2 atm and 500°C for 2 h. A secondary annealing was performed in N<sub>2</sub> at 1 atm and 800°C for 2 h.

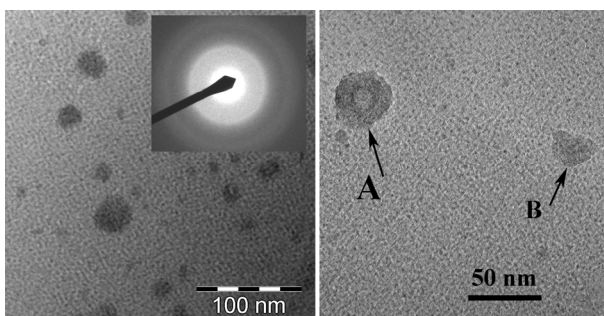


Fig.1. TEM images showing large spherical nanoparticles in a thick area of the XTEM specimen (left). The inset SAED pattern shows an amorphous structure. Multibeam TEM image (right) in the thinnest part of the specimen, showing particles with modified contrast (A) and modified morphology (B).

The low magnification cross-section (XTEM) observation of the film reveals the presence of quite big Ge nanoparticles with round or irregular shape distributed in all the film volume and a uniform network of nanoparticles forming the film matrix (see Fig.1).

The big Ge nanoparticles appear in dark contrast with different morphologies, their sizes varying between 20 and 50 nm. The round ones show more contrast and are similar to the

particles showing tetragonal phase previously observed [1]. Many of the big Ge nanoparticles are amorphous but some of them show traces of crystallinity.

In the thinnest areas of the XTEM specimen, the contrast of the big Ge nanoparticles changes showing an inner ring, while some of them appear with a modified shape due to the ion thinning process (see Fig. 2).

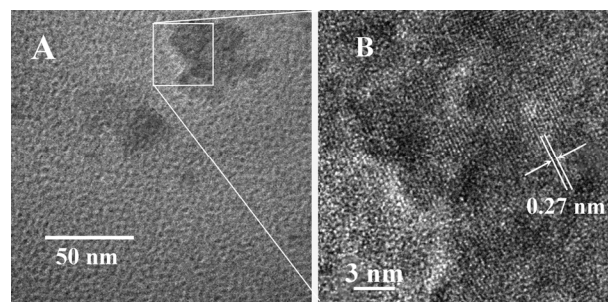


Fig 2. Multibeam image of an Ge big nanoparticle with irregular shape (A). The HRTEM detail (B) shows the presence of the 0.27 nm lattice fringes, corresponding to the (201) reflection of Ge-III phase.

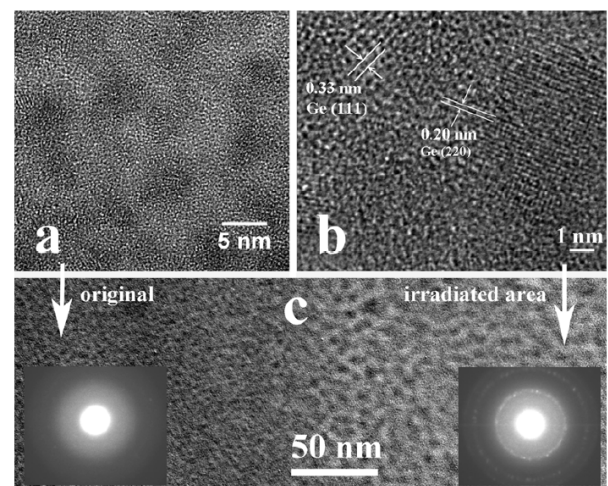


Fig. 3. (a). HRTEM image of the small Ge nanoparticles. (b). HRTEM image showing the cubic Ge crystallization. (c). Low-magnification TEM image showing modification of the specimen structure, after several minutes of HRTEM observation.

The network of the amorphous small Ge nanoparticles with sizes between 3 and 5 nm can be observed at high magnification (Fig 3.). Some of them, with sizes between 5 and 15 nm, are formed by aggregation of several small

nanoparticles, as the images contrast suggests. The main part of Ge content of the film segregates in these small amorphous nanometric particles and only few percents of Ge content form the big Ge nanoparticles.

The effect of the electron irradiation can be easily seen by imaging the specimen areas where the high resolution imaging was performed before (see Fig. 3c). Fig. 3c also shows the ripening effect of the electron irradiation. In the electron irradiated area, the Ge nanocrystallites are crystallized in the diamond cubic structure as revealed by the high resolution image shown in Fig. 3b. At this stage, the HRTEM images become stable under the electron beam.

The presence of the two types of Ge nanoparticles after annealing in hydrogen suggests two types of segregation mechanisms by which the big Ge nanoparticles and the uniform network of amorphous small Ge nanoparticles are formed.

In the first mechanism, the Ge segregation processes in the GeSiO films begin in the nano-regions where the initial concentration of Ge species has a maximum fluctuation value. These nano-regions contain more Ge species compared to the rest of the film and probably also an amorphous cluster of  $\text{GeO}_x$ , which is reduced easily in the beginning of the annealing and act as initial nuclei for the Ge segregation and growth of the big Ge nanoparticles. This stress field is lower than the value necessary to stabilize the high pressure form of Ge. However, the growth of the tetragonal high pressure (Ge-III/ST12) phase is possible due to the structure of the initial Ge clusters in the deposited GeSiO film, which is different from the structure of a Ge cluster formed by thermal nucleation.

The second mechanism, comes after the first one, when the big nanoparticles are formed and the Ge content in the film matrix is more uniform. It is an uniform nucleation of Ge amorphous clusters in all the film volume, leading to the formation of the small Ge nanoparticle network. The annealing in  $\text{H}_2$  at 2 atm and 500 °C is not sufficient to crystallize this network of small Ge nanoparticles.

In order to establish the evolution of the GeSiO film structure during subsequent annealing, the samples were heated at 800°C in

nitrogen atmosphere. This evolution is illustrated in Fig. 4 which shows the film structure after the first and the second annealing, in the region near the interface with the quartz substrate. After the 800°C annealing, the two types of morphology for the Ge nanoparticles disappear and all the Ge crystallites have the same morphology. The Ge crystallites have the diamond cubic structure (Ge-I) and sizes between 20 and 50 nm (Fig. 4). These Ge nanoparticles have mainly (111) facets and their observation near the [110] orientation revealed inside defects as stacking faults and nanotwins.

The prolonged high-resolution observations of the big Ge-III structures induce the amorphisation of the metastable phase and finally the crystallization of the amorphous Ge nanoparticles in the stable cubic Ge-I structure. The subsequent annealing of the film at 800°C in  $\text{N}_2$  relaxes the structure and the high diffusivity of Ge atoms at this temperature leads to the crystallization and growth of the network of small amorphous Ge nanoparticles. The density of the crystallized Ge particles is much smaller due to the Ostwald ripening process working during the crystal growth. The metastable Ge-III phase is transformed into the cubic phase by the 800 °C annealing.

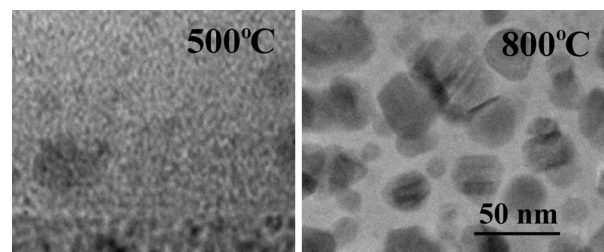


*Fig.4. (a). Low magnification TEM images comparing the film structure near the interface with the quartz substrate, after the first annealing at 500°C in  $\text{H}_2$  and after the second annealing in  $\text{N}_2$  at 800°C.*

## References

- [1] I. Stavarache et al., J. Nanopart. Res. **13**, 221 (2011)
- [2] V. S. Teodorescu et al., Digest of Nanomaterials and Biostructures **8**, 1771-1780, 2013

## Controlling Ge nanocrystals formation at fixed position in (Ge/SiO<sub>2</sub>) multilayer structures

Magdalena Lidia Ciurea, Valentin Serban Teodorescu, Ana-Maria Lepadatu, Ionel Stavarache

in cooperation with

T. Stoica, D. Buca

Peter Grünberg Institut, Forschungszentrum Jülich, Jülich, Germany

Controlling the formation of Ge nanocrystals (NCs) at precise location in oxide matrix represents a strong motivation for preparation of nanomaterials and nanostructures based on Ge NCs for non-volatile memory devices and photodetectors [1].

By controlling the diffusion-crystallization process of Ge in SiO<sub>2</sub> layers through the annealing conditions we succeeded in obtaining Ge NCs at fixed positions in (Ge/SiO<sub>2</sub>) multilayer structures. More, these multilayer structures show bright IR photoluminescence (PL) at low temperatures.

Structures with two pairs of Ge/SiO<sub>2</sub> were deposited by magnetron sputtering on clean Si substrates, and then were annealed in a rapid thermal annealing (RTA) equipment [2]. The structures were capped with a SiO<sub>2</sub> layer, so that the deposited structure is SiO<sub>2</sub>/2x(Ge/SiO<sub>2</sub>)/Si. The annealing in N<sub>2</sub> at different temperatures of 650, 700 and 800 °C was performed for nanostructuring.

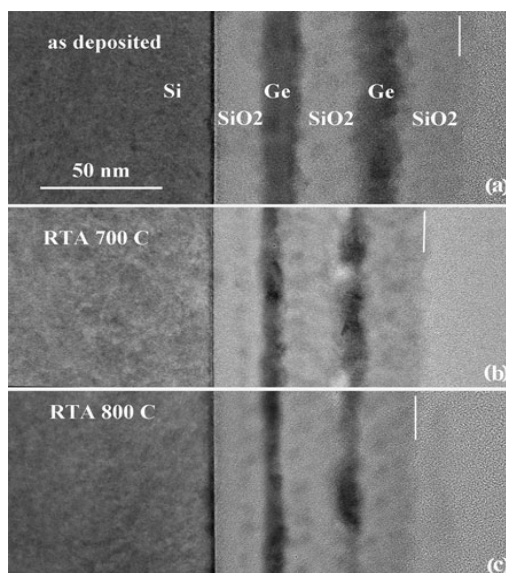


Fig. 1 XTEM images on: (a) as deposited and (b) 700 °C and (c) 800 °C annealed structures.

TEM, Raman spectroscopy and infrared PL were employed for the study of these structures. The cross-section TEM (XTEM) images (Fig. 1) show the as-deposited multilayer structure with thickness of 100 nm, together with the 700 and 800 °C annealed ones. One can see that both annealed

structures are contracted with about 15% in respect to the as deposited one, having similar thicknesses. Only a very small amount of Ge diffuses into the SiO<sub>2</sub> layers (Fig. 1). The Ge nanoparticles from the SiO<sub>2</sub> layers which border the Ge layers are some of them crystallized, some not. The HRTEM (Fig. 2) performed on the 700 °C annealed structures shows that the annealing was efficient in producing Ge NCs which remain in the fixed (as deposited) positions, but the Ge NCs forming these layers are not uniformly distributed.

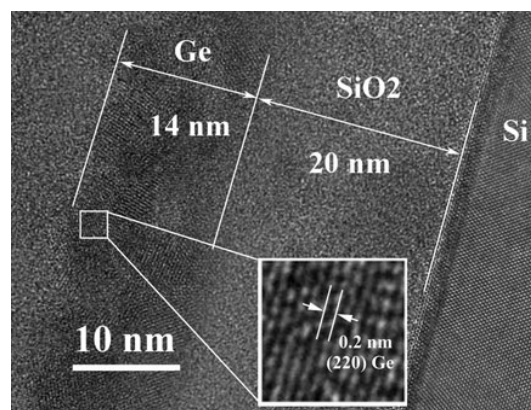


Fig. 2 HRTEM image, near Si substrate of 700 °C annealed structure.

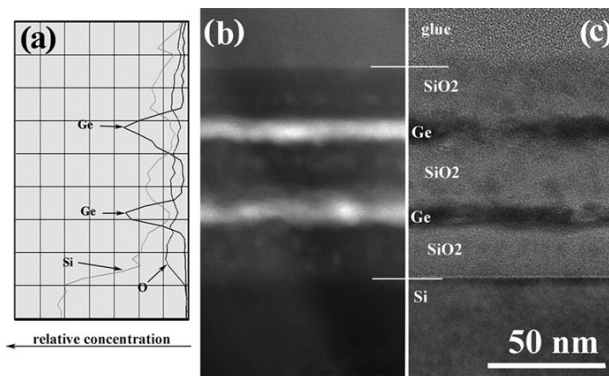


Fig. 3 Scan-line EDX analysis (a), ADF-STEM image showing the Ge layers in Z contrast (b) and TEM image (c), all measured on the same area of the specimen (700 °C annealing).

In the TEM image from Fig. 3(b), Ge appears in dark contrast, while in the ADF-STEM one (Fig. 3(c)), in white contrast. The relative concentrations of elements are presented in Fig. 3(a) evidencing the

concentration maxima of Ge in the initial location of Ge layers where O and Si have minimum concentrations. This means that the crystallization precedes the diffusion. So, the only process which takes place in the RTA annealing/heating is the direct light absorption limiting the Ge diffusion and favouring its crystallization.

In the Raman spectra (Fig. 4) the Ge NCs peak ( $297.7 - 298.4 \text{ cm}^{-1}$ ) increases and sharpens with the annealing temperature and is red-shifted in respect to bulk Ge ( $299.8 \text{ cm}^{-1}$ ). This shift is given by the phonon confinement in Ge NCs [3]. The Ge NCs peak presents a tail at lower energies. By modeling the Raman spectra of  $800 \text{ }^\circ\text{C}$  annealed structures it results that the structures are formed of strain-free Ge NCs with an average diameter of  $9.5 \text{ nm}$  (which contribute to the main peak) and of small ones with  $3 \text{ nm}$  diameter contributing to the low energy tail (together with the amorphous phase). For  $650$  and  $700 \text{ }^\circ\text{C}$  annealing, the Ge NCs have smaller diameters of  $8$  and  $8.5 \text{ nm}$ , respectively.

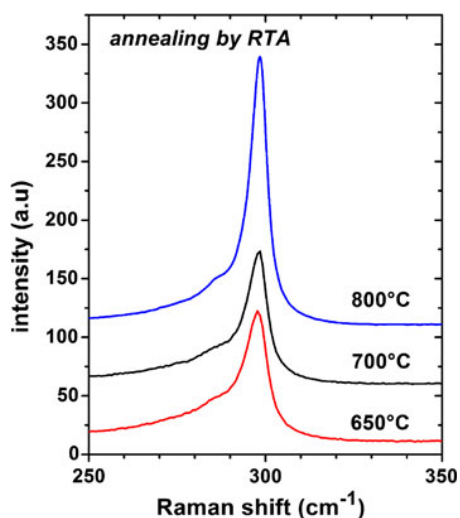


Fig. 4 Raman spectra of annealed structures.

We show for the first time that the structures annealed at  $650$  and  $700 \text{ }^\circ\text{C}$  present a bright PL at low temperature (with maximum at  $50 \text{ K}$ ) with an intense IR emission at about  $1000 \text{ meV}$  (Fig. 5). The PL spectra have two main sharp peaks very close to each other, being positioned at  $1004$  and  $1008 \text{ meV}$ . Two other broad peaks, one positioned at  $991 \text{ meV}$  and the other one at  $1004 \text{ meV}$  are observed. The spectra deconvolution shows that the full width at half maximum is of  $2 \text{ meV}$  for sharp peaks and of  $20$  and  $11 \text{ meV}$  for the broad peaks at  $991$  and  $1004 \text{ meV}$ , respectively. By comparing

these PL spectra with the ones measured on bulk Ge, we observe that they are similar, but the PL spectra measured on the  $\text{SiO}_2/2x(\text{Ge/SiO}_2)/\text{Si}$  structures are shifted to higher energy, demonstrating that the quantum confinement effect plays an important role in radiative recombination processes. The mechanism which explains the IR PL emission is that of radiative recombination of carriers through traps located at the surface of Ge NCs.

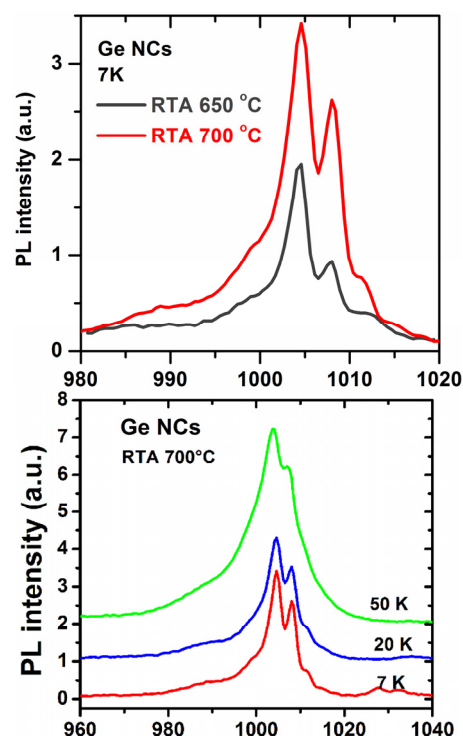


Fig. 5 IR PL spectra measured on structures annealed at  $650$  and  $700 \text{ }^\circ\text{C}$ .

In conclusion, the Ge NCs formation in relation to Ge diffusion process in  $\text{SiO}_2/2x(\text{Ge/SiO}_2)/\text{Si}$  multilayer structures was studied and for the first time we showed that the faster Ge NC formation has a positive feedback in reducing the Ge diffusion, leading to fixed positioned layers formed of dense Ge NCs. Also, for the first time the bright IR PL at about  $1000 \text{ meV}$  was evidenced in these structures at low temperatures.

## References

- [1] S.K. Ray, S. Maikap, W. Banerjee, S. Das, *J. Phys. D Appl. Phys.* **46**, 153001 (2013).
- [2] A. M. Lepadatu, T. Stoica, I. Stavarache, V. S. Teodorescu, D. Buca, M. L. Ciurea, *J. Nanopart. Res.* **15**, 1981 (2013).
- [3] I. Stavarache, A. M. Lepadatu, T. Stoica, M. L. Ciurea, *Appl. Surf. Sci.* **285B**, 175 (2013).



# Potential Applications

## Multi-layer haemocompatible diamond-like carbon coatings obtained by combined radio-frequency plasma enhanced chemical vapor deposition and magnetron sputtering

A.C. Popa, G.E. Stan, M.A. Husanu, I. Pasuk

in cooperation with

I.D. Popescu

“Victor Babes” National Institute of Pathology, Bucharest, Romania  
and

A.C. Popescu, I.N. Mihailescu

National Institute for Lasers, Plasma and Radiation Physics, Magurele-Bucharest, Romania

Radio-frequency Plasma Enhanced Chemical Vapour Deposition method was used to synthesize adherent and haemocompatible diamond-like carbon (DLC) with different  $sp^3/sp^2$  ratios onto medical grade titanium (Ti) substrates, by changing the methane concentration in the deposition chamber. Three different dilutions of methane in argon (20%, 60% and 100%) were used, by keeping the total pressure at 15 Pa. The samples are further denoted as D20, D60 and D100, respectively.

The sustainability of a biocompatible film, to be applied as biofunctional coating layer of implantological elements used to remedy various cardiologic, orthopaedic or dental medical conditions, is essentially conditioned by the adherence to substrate [1].

The improvement of the adherence has been attempted by interposing a functional buffer layer with graded composition  $Ti_xTiC_{1-x}$  ( $x=0-1$ ) synthesized by Magnetron co-Sputtering. The  $Ti_xTiC_{1-x}$  transition stratum aimed to reduce the interface discontinuity between the two different materials (Ti and DLC), and improve significantly the adhesion strength. The functionally graded interlayer acted as an anchor, contributing to the adaptation at the interface area. This way, high bonding strength (pull-out tests - ASTM D4541 - 09e1) values in the 58 – 67 MPa range have been achieved [2].

Raman Spectroscopy, X-ray Photoelectron Spectroscopy (XPS), and Surface Energy measurements were employed for the physical-chemical characterization of the DLC films.

In order to better predict the behaviour of materials *in vivo* we designed a range of *in vitro* tests to investigate the events that take place on the implant coating surface when put in contact with blood. Consequently, the biological response of the DLC films was assayed by a state-of-the-art biological analysis method (SELDI: Surface Enhanced Laser Desorption/Ionization – Time of Flight Mass Spectroscopy), in conjunction with other dedicated testing techniques: Western blot and partial thromboplastin time (aPTT).

The increase in the  $sp^3$ -C content with the increase of the methane concentration in the working atmosphere has been confirmed both by Raman and XPS [2]. The surface energy had an inverse evolutionary trend [2]. The highest concentration of  $sp^3$ -C (~80%), corresponding also to a lower DLC surface energy (28.7 mJ/m<sup>2</sup>), has been obtained for D100.

The partial thromboplastin time of the DLC functionalized implants increased with the decrease of surface energy values (Fig. 1). The clotting process can usually be initiated by surface adsorption and contact activation of coagulation factors of the endogenic clotting system. Unlike bare Ti, the contact with the DLC coated surface suppressed the activation of the endogenic clotting system (Fig. 1).

The adherence of platelets to the materials plays a key role in platelet activation and subsequently in blood clotting activation. Platelet adherence was studied by Western blot analysis of beta actin, a structural protein present in all cells. As seen in the platelet adhesion

experiment, the DLC films create conditions for a weaker platelet-surface interaction, which *in vivo* can conduct to a lower platelet activation and subsequently a prolonged time of coagulation (Fig. 2). One can assert that this effect derives from the fact that all cells have a negatively charged cellular membrane which tends to interact/adhere to hydrophilic surfaces, rather than to hydrophobic ones.

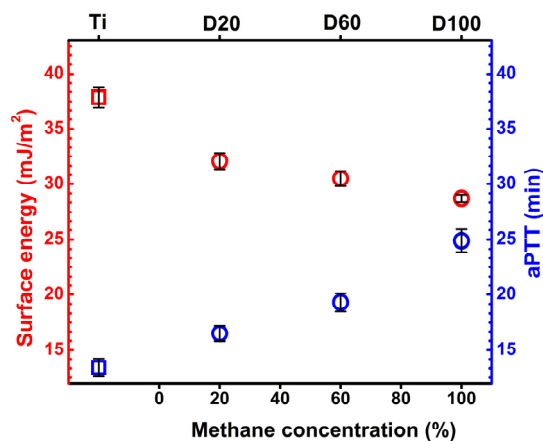


Fig. 1 Dependence of the surface energy and aPTT values on the methane concentration.

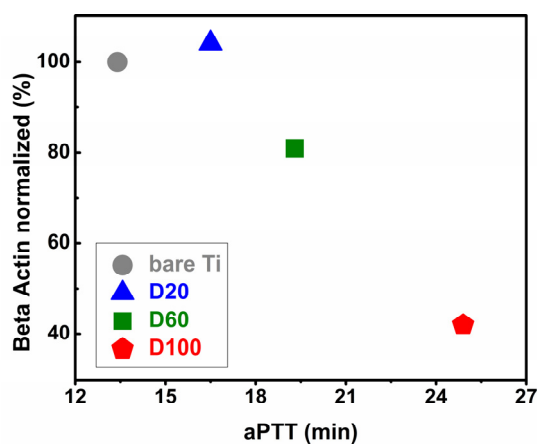


Fig. 2 The DLC films and Ti bare control aPTT values plotted against the normalized beta-actin values.

In this work, the interaction of blood with the surface was investigated also by SELDI-ToF mass spectroscopy which generates a profile of protein adsorption at interface with materials, as seen in Fig. 3. As one can observe, serum albumin was adsorbed in greater quantities on all DLC surfaces than on the bare Ti control surface (Albumin molecular weight  $\approx$  66483 Da).

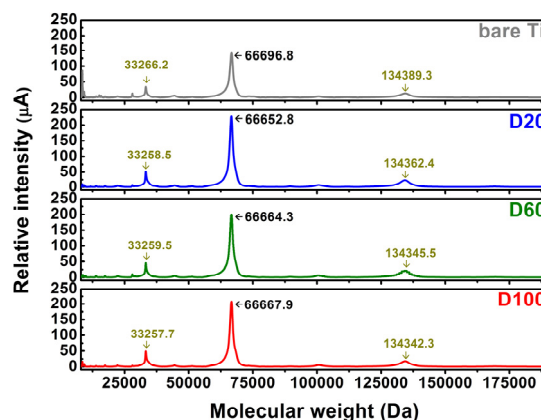


Fig. 3 SELDI-ToF complete spectra of proteins adsorbed on DLC films and bare Ti control from fresh blood plasma.

Albumin represents roughly 50–60 % of plasma proteins and is not glycosylated like other proteins in blood. Albumin is a protein which has hydrophobic moieties, being a blood carrier for many hydrophobic molecules. Since our DLC surfaces tend to be more hydrophobic it is expected to find more adsorbed albumin than on Ti, as it was confirmed by mass spectroscopy spectra. The vast majority of proteins in blood are glycosylated which makes them more hydrophilic and more susceptible to polar interactions. The quantity of albumin adsorbed on the surface shields the surface of the sample, making it difficult for the different proteins and coagulation factors to reach the sample and activate the coagulation cascade.

The data support a cause-effect relationship between  $sp^3$ -C content, surface energy data and coagulation time, as well as between platelet-surface adherence properties and protein adsorption profiles.

## References

- [1] R.K. Roy, K.R. Lee, J Biomed Mater Res B 83 (2007) 72–84; DOI: 10.1002/jbm.b.30768.
- [2] A.C. Popa, G.E. Stan, M.A. Husanu, I. Pasuk, I.D. Popescu, A.C. Popescu, I.N. Mihailescu, J Mater Sci–Mater Med 24 (2013) 2695–2707; DOI: 10.1007/s10856-013-5026-y.

## Synthesis and Antimicrobial Activity of Silver-Doped Hydroxyapatite Nanoparticles

*Carmen Steluta Ciobanu, Simona Liliana Iconaru, Cristina Liana Popa, Daniela Predoi*

in cooperation with

*P. Le Coustumer*

Universite Bordeaux, Pessac, France

*M.C. Chifriuc*

University of Bucharest, Department of Botany and Microbiology, Romania

In last years, the progress made in the area of engineered nanomaterials allowed us to have spectacular inside knowledge about materials at an atomic and molecular scale. Biomaterials could be defined as “implantable materials that perform their function in contact with living tissues” [1]. This is a new interdisciplinary branch set to achieve new and improved materials with biological properties for use in clinical applications.

The aim of this study was to evaluate Ag:HAp-NPs for their antimicrobial activities against Gram-positive and Gram-negative bacteria and fungal strains. The preparation of Ag doped hydroxyapatite by coprecipitation method at 100°C has several advantages over other techniques [2]. In our previous studies [2] we presented preliminary results regarding the synthesis, characterization, and antibacterial properties on hydroxyapatite (HAp) and silver doped hydroxyapatite (Ag:HAp) with  $x_{Ag} = 0.2$ . In this study we present complex studies on silver doped hydroxyapatite samples for different silver concentration:  $0 \leq x_{Ag} \leq 0.4$ .

The designed unit formula of the doped HAp is  $Ca_{10-x}Ag_x(PO_4)_6(OH)_2$ , with  $0 \leq x_{Ag} \leq 0.4$ . The XRD patterns, presented in Fig. 1, show the characteristic peaks of hydroxyapatite for each sample, according to ICDD-PDF no. 9-432, represented at the bottom of the figure, as reference. No other crystalline phases were detected beside this phase (Fig. 1). The XRD of HAp and Ag:HAp also demonstrates that powders made by co-precipitation at 100°C exhibit the apatite characteristics with good crystal structure and no new phase or impurity is found. It can be seen from the HRTEM image of Ag:HAp (Fig. 2A) that the crystalline phase of hydroxyapatite with well-resolved lattice fringes

can be observed. The distances between the adjacent lattice fringes (2.72 Å) agree well with the  $d_{300}$  spacing of the literature values (2.872 Å) (ICDD-PDF no. 9-432). Fig. 2B shows a selected area electron diffraction (SAED) pattern recorded from an area containing a large number of ellipsometric nanoparticles. No extra reflections are observed and we can therefore conclude that the product consists of pure HAp ellipsometric nanoparticles. These results are well consistent with the XRD, and revealed that the doping components have no influence on the surface morphology of the samples.

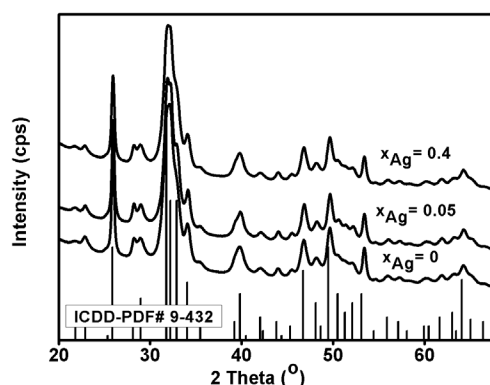


Fig. 1. Comparative representation of the experimental XRD patterns of the Ag:HAp samples synthesized with  $x_{Ag}=0$ ,  $x_{Ag}=0.05$ , and  $x_{Ag}=0.4$ , and the characteristic lines of hydroxyapatite (ICDD-PDF no. 9-432).

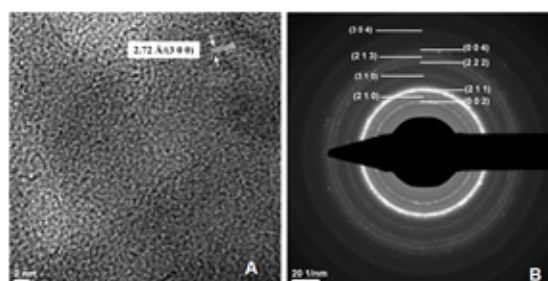


Fig. 2. HRTEM image and SAED analysis of Ag:HAp with  $x_{Ag}=0.5$ .

The antimicrobial activity of Ag:HAp ( $0 \leq x_{Ag} \leq 0.1$ ) nanoparticles was tested using strains belonging to the most commonly encountered

pathogens: *E. coli* ATCC 25922, *E. coli* 714, *K. pneumoniae* 2968, *B. subtilis*, and *C. krusei* 963. The results of microbiological assays of Ag:HAP ( $0 \leq x_{Ag} \leq 0.1$ ) nanoparticles are shown in Figures 3(A)–3(E).

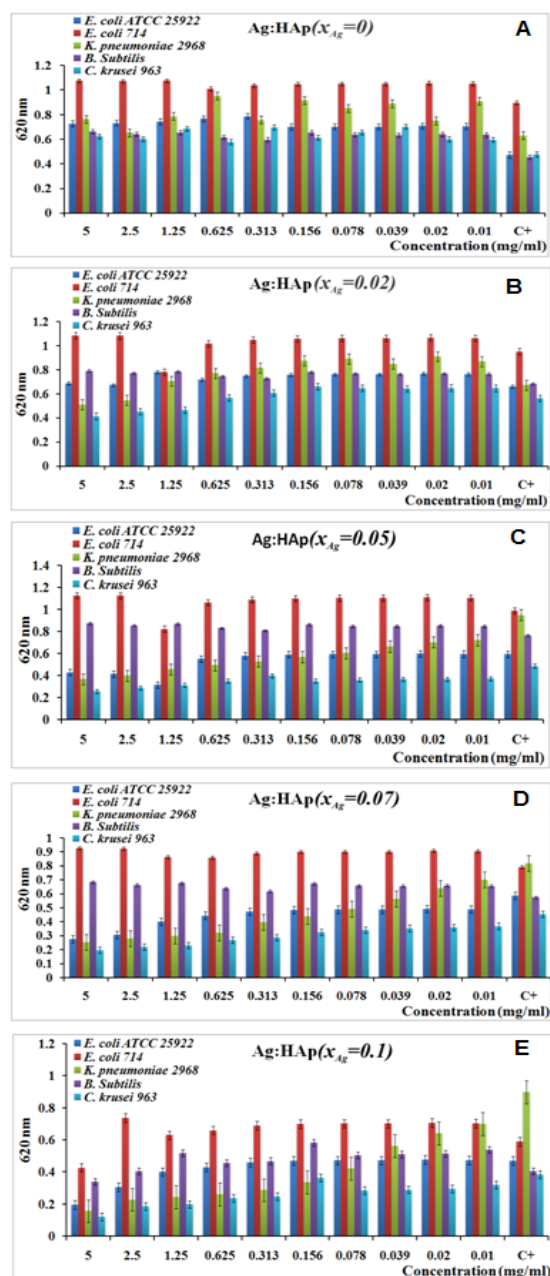


Fig.3. A-E: Antibacterial activity of Ag:HAP-NPs ( $x_{Ag} = 0, 0.02, 0.05, 0.07, \text{ and } 0.1$ ) on *E. coli* ATCC 25922, *E. coli* 714, *K. pneumoniae* 2968, *B. subtilis* and *C. krusei* strains.

The Ag:HAP ( $x_{Ag}=0$ ) nanoparticles exhibited no inhibitory effect on the microbial growth as compared to the positive growth control (C+) (Figure 3(A)). The Ag:HAP nanoparticles with  $x_{Ag}=0.02$  exhibited an inhibitory effect on the growth of *K. pneumoniae* at the first two tested

concentrations and of *C. krusei* 963 at the first three tested concentrations (Figure 3(B)). The Ag:HAP nanoparticles with higher concentrations of Ag ( $x_{Ag} = 0.05; 0.07$  and  $0.1$ ) showed an improved antimicrobial activity against the same two pathogens, *K. pneumoniae* and *C. krusei*, but maintained for the entire range of the tested concentrations, from 5 to 0.01 mg/mL (Figures 3(C), 3(D), and 3(E)). These results are clearly demonstrating that the antimicrobial effect of the silver doped nanoparticles is dependent on the structure of the microbial cell wall [3-5].

The results obtained in this study demonstrated that silver doped hydroxyapatite nanoparticles may offer an effective alternative to antibiotic treatments, exhibiting a specific spectrum of antimicrobial activity, and also inhibiting the initial step of microbial biofilm development, but not the preformed biofilms, which proved to be more resistant and difficult to eradicate.

## References

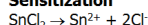
- [1] C. S. Ciobanu, S. L. Iconaru, E. Gyorgy et al., *Chemistry Central Journal*, vol. 6, article 17, 2012.
- [2] C. S. Ciobanu, F. Massuyeau, L. V. Constantin, and D. Predoi, *Nanoscale Research Letters*, vol. 6, article no. 613, 2011.
- [3] Carmen Steluta Ciobanu, Simona Liliana Iconaru, Mariana Carmen Chifriuc, Adrian Costescu, Philippe Le Coustumer, and Daniela Predoi, *BioMed Research International Volume 2013*, Article ID 916218, 10 pages
- [4] A. Costescu, C. S. Ciobanu, S. L. Iconaru, R. V. Ghita, C. M. Chifriuc, L. G. Marutescu, and D. Predoi, *Journal of Nanomaterials Volume 2013*, Article ID 194854, 9 pages
- [5] C.S. Ciobanu, S.L. Iconaru, I. Pasuk, B.S. Vasile, A.R. Lupu, A. Hermenean, A. Dinischiotu, D. Predoi, *Materials Science and Engineering C xxx (2013) xxx-xxx*, <http://dx.doi.org/10.1016/j.msec.2012.12.042>

## Superhydrophobic ZnO arrays prepared by electroless deposition

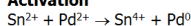
*N. Preda, M. Enculescu, I. Zgura, M. Socol, E. Matei, I. Enculescu*

The surface-wetting behavior of ZnO nanostructures has recently attracted attention. In our studies the low-dimensional ZnO particles were synthesized by a simple and inexpensive solution chemistry approach, electroless deposition (ELD) on polymer sphere arrays [1] or cotton textiles [2]. As it can be seen in Fig. 1, the ELD is based on the activation of the surface which is intended to be covered with a layer of catalyst material. A priori, a rough surface, like polymer sphere arrays can favor a uniform attachment of the catalysis colloids comparatively with a smooth surface, like spin-coated polymer. We used polymethyl methacrylate (PMMA) in order to obtain both surfaces types.

### Sensitization



### Activation



### Deposition

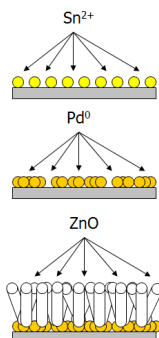
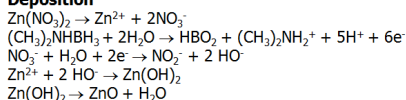


*Fig. 1: ELD steps: sensitization, activation and deposition involved in ZnO synthesis*

The samples morphology was observed by scanning electron microscopy - SEM (Fig. 2). It can be clearly seen that in the case of ZnO deposition on glass substrate (Fig. 2A) or spin-coated PMMA (Fig. 2B), the surfaces are not entirely covered by hexagonal prisms while in the case of ZnO deposition on PMMA sphere arrays (Fig. 2D) continuous prisms arrays are observed. In Fig. 2C is shown the PMMA sphere array used as substrate for ZnO deposition. The SEM images sustain the hypothesis that a rough surface favors a uniform attachment of the palladium colloids promoting the site-selectively nucleation of ZnO crystallites on the area covered with catalysis colloids.

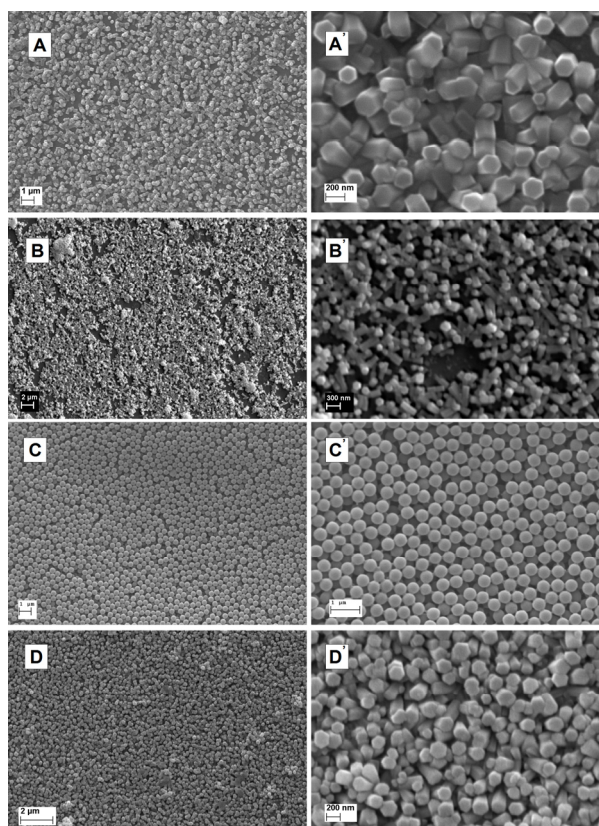


*Fig. 2: ZnO film deposited on glass substrate (A, A'), ZnO film deposited on PMMA spin-coated (B, B'), PMMA sphere array (C, C') and ZnO film deposited on PMMA array (D, D') samples.*

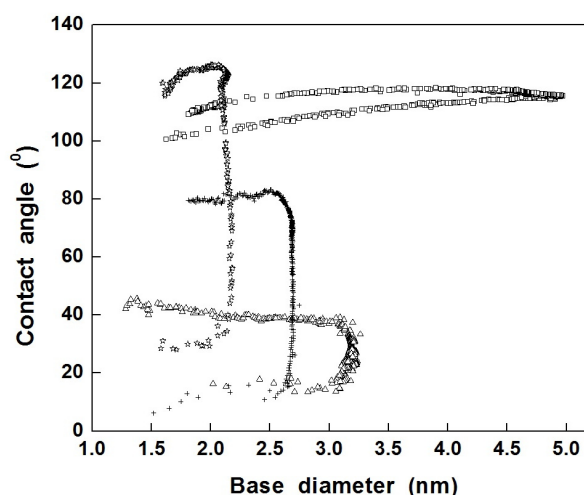


*Fig. 3: Advancing and receding contact angles for PMMA sphere array (triangle), ZnO film deposited on glass substrate (cross), ZnO film deposited on PMMA spin-coated film (circle) and ZnO film deposited on PMMA sphere array (square) samples.*

The importance of the substrate surface roughness on the wetting properties of ZnO film was put in evidence by the contact angle (CA) measurements (Fig. 3): the CA hysteresis value for ZnO deposited on spin-coated polymer is  $90^\circ$  (advancing CA =  $121^\circ$  and receding CA =  $31^\circ$ ) and the CA hysteresis value for ZnO deposited on polymer array is  $4^\circ$  (advancing CA =  $115^\circ$  and receding CA =  $111^\circ$ ). So, ZnO surface presents an inversion of a hydrophilic-hydrophobic behavior with a small value for CA hysteresis.

In the case of cotton textiles, after ZnO deposition the fabrics surfaces present a water repellent effect (Fig. 4).

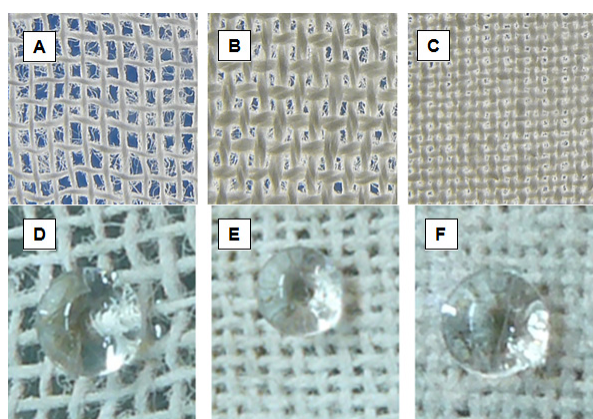


*Fig. 4: Optical images of the cotton fabrics with different mesh density before and after ZnO deposition: sparse (A, D); medium (B, E) and dense (C, F).*

From the CA measurements it is observed that after being covered with ZnO, the fabrics surface shows hydrophobic and even superhydrophobic behaviour (CA values even beyond  $150^\circ$ ) suggesting that a uniform coating of cotton fibers with ZnO crystallites arrays leads to superhydrophobicity (Fig. 5 A-C).

An explanation for the hydrophobicity or superhydrophobicity behavior of ZnO arrays can be linked to the fact that the deposited ZnO on both polymer arrays or cotton textiles consist of a large number of small hexagonal prisms which include a huge amount of air bubbles. The ZnO prisms action cumulates with the effect of the air present in the space between crystallites to more efficiently support the droplet weight. In this way, the numerous gaps between these ZnO

crystallites are filled with air acting as a support “buffer” for the water droplet with contact to the surface in a few small nanometric sites only.

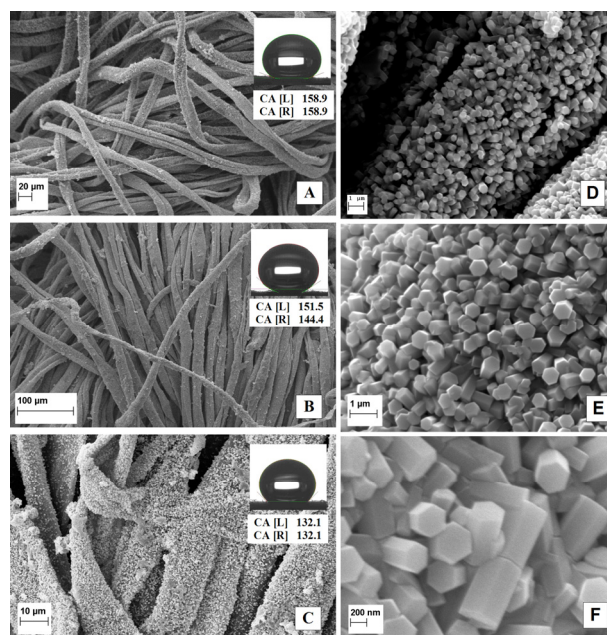


*Fig. 5: SEM images of ZnO-coated fabrics with different mesh density (A, B, C). In the inset are shown the optical photographs of the water droplets shape on the ZnO-coated fabrics surfaces and the corresponding water CA. Higher magnification images of ZnO-coated fabrics (E, F, G)*

Such ZnO arrays can have potential applications in various areas where properties such as self-cleaning or superhydrophobicity are required, ranging from smart protective surfaces to optoelectronics and medical fields. The main advantages of ZnO ELD compared to other ZnO deposition techniques are related to its scalability and low cost, being an efficient and suitable method for industrial preparation.

## References

- [1] N. Preda, M. Enculescu, I. Enculescu, *Soft Mater.* 11, 457, 2013
- [2] N. Preda, M. Enculescu, I. Zgura, M. Socol, E. Matei, V. Vasilache, I. Enculescu, *Mater. Chem. Phys.* 138, 253, 2013

## Unusual magnetic configurations of Ni-Cu alloy nanowires

*E. Matei, I. Enculescu, A. Ghica, A. Leca and V. Kuncser,*

in cooperation with

ME. Toimil-Molaes (*Gesellschaft fuer Schwerionenforschung, Darmstadt, Germany*)

Nanowires with controlled dimension and composition represent suitable model systems to investigate the magnetic properties of one-dimensional systems, presenting also interesting applications in sensoristics and not. Among the various methods to synthesize such magnetic nanowires, the template approach is frequently employed, allowing a simultaneous and precise control of both morphology and composition of nanowires. Arrays of high aspect ratio (30  $\mu\text{m}$  long and 70 nm diameter) nanowires of Ni-Cu alloys have been synthesized by potentiostatic electrochemical deposition in etched ion track membranes. The nickel-to-copper ratio in the nanowires was controlled via the deposition potential and electrochemical bath composition. A complex study concerning the nanowire properties including morphology, composition and magnetic behavior was reported, including a discussion of their close interdependence [1]. Morphology, composition and structural aspects were analyzed by scanning electron microscopy (SEM), energy dispersive X-ray spectroscopy (EDX) and X-ray diffractometry (XRD) with Cu  $K_{\alpha}$  radiation, after dissolving the templates. On the same nanowires, transmission electron microscopy (TEM) investigations have been performed together with elemental mapping via energy filtered transmission electron microscopy. Magnetic measurements were realized by SQUID magnetometry.

Four samples of different Fe to Ni content (S1 to S4, with S1 indexing the lowest Ni content) have been considered with a relationship between processing conditions and structural, morphologic and compositional aspects presented in fig. 1.

The elemental distribution inside nanowires (e.g. as presented in Fig. 2) proves the elemental segregation of either Ni or Cu in low Ni content nanowires (e.g. sample S1) and a good compositional homogeneity in samples of higher Ni content (e.g. S3).

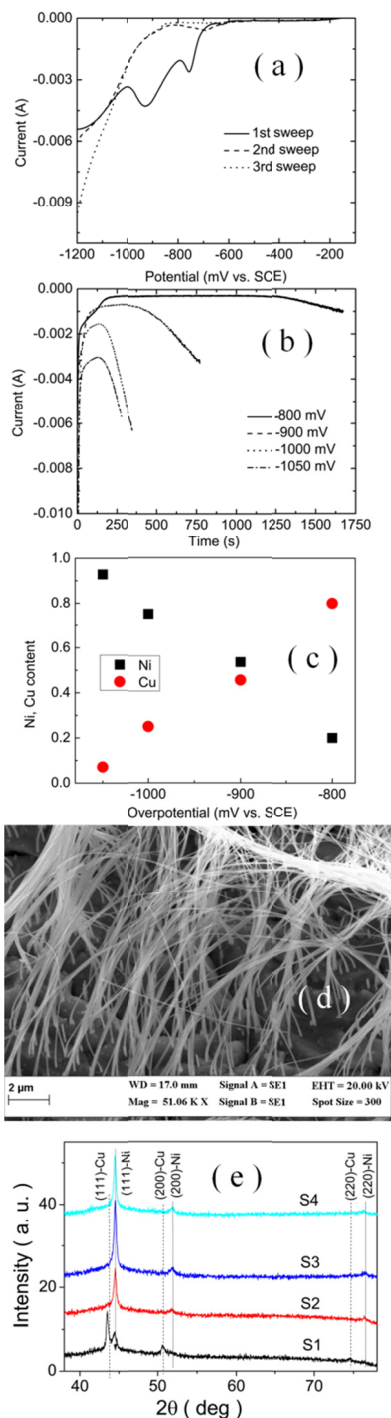


**Fig. 1:** Electrochemical polarization (a) and chrono-amperometric (b) curves during potentiostatic deposition of nanowires. (c) Cu and Ni content vs. deposition potential (increasing Ni content from S1 to S4). Representative SEM image (d) and XRD ( $\lambda=0.154$  nm) patterns (e) of samples.

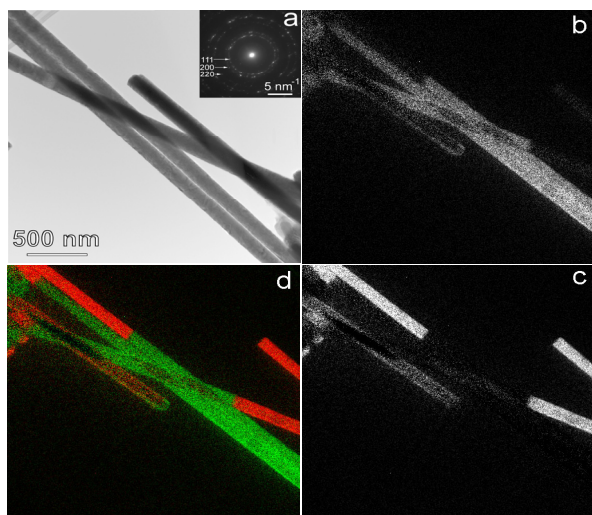


**Fig. 2:** (a) TEM image of the CuNi nanowires in sample S1 and corresponding SAED pattern inserted; (b) EFTEM image showing the Ni  $L_{3,2}$  elemental map; (c) EFTEM image showing the Cu  $L_{3,2}$  elemental map; (d) composite image in false colors showing the Cu and Ni distribution in the nanowires (Red – copper; Green - nickel) [1].

The compositional dependent magnetic configuration was analyzed starting from the geometry dependent magnetization reversal and suitable estimations with respect to the average magnetic moment, anisotropy constants and energies, exchange length parameters, interactions between nanowires, switching fields and angular apertures of easy axis distributions (Fig. 3). The estimated average magnetic moment of the alloys does not follow the typical linear decrease versus the Cu content, due to lower average densities of the wires (gas evolution at higher deposition potential) and the heterogeneous composition (at the highest Cu content). Estimations of reference material parameters give support for nanowires consisting of a chain of polycrystals of high aspect ratio and non-cooperative magnetic response. Due to the predominance of the shape anisotropy over the magnetocrystalline anisotropy in any crystallite, the magnetic reversal in each wire takes place at an almost unique switching field, similar as for a magnetic monodomain wire. The specific geometry dependent hysteresis loops seem to be explained via an easy axis distribution (EAD), involving angular distributed anisotropy axes. While the angular dispersion of the nanowires

inside the polymer is physically better than few degrees, the observed angular distribution of the spin directions was related, in agreement with previous micromagnetic calculations [2], to a flower like spin structure, depending on the alloy composition.

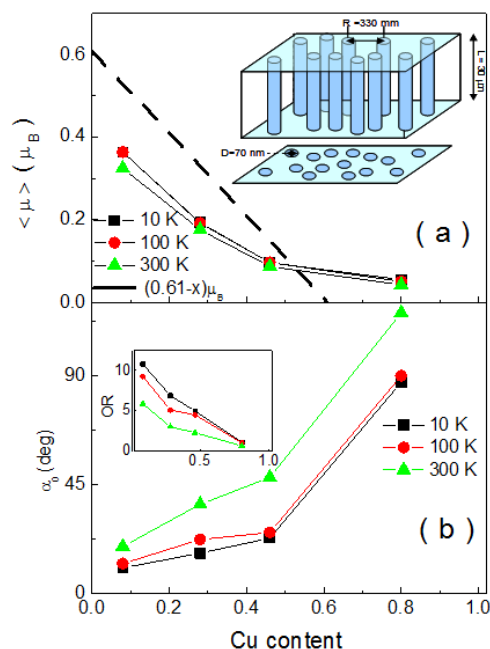


**Fig.3** The average magnetic moment (a) and apertures of the angular distribution of easy axis (b) versus the Cu content. Inset: values of the orientation ratios

The angular aperture of the distribution, as estimated by using the orientation ratio, OR, defined as the ratio between the remanent magnetization in parallel and perpendicular geometry increases at higher Cu content, due to a more competitive contribution of the magneto-crystalline anisotropy.

## References

- [1] E. Matei, I. Enculescu, ME Toimil-Molares, A. Leca, C. Ghica and V. Kuncser, 2013 *Journal of Nanoparticle Research* 15(8) 1863
- [2] CA. Ross, M. Hwang, M. Shima et al 2002, *Phys Rev B* 65:144417

## Reduced graphene-based surfaces with enhanced optical properties

*C.M. Teodorescu*

in cooperation with

*M. Iliuț, C. Leordean, V. Cănpăan, A.M. Găbudean, T. Șimon, S. Aștilean*

Babes-Bolyai University, Cluj-Napoca, Romania

The improvement of fluorescence properties for derivatives of graphene, particularly for graphene oxide (GO), is a challenging topic and very few achievements were reported up to now. An easy method, proven in this work, to enhance the fluorescence of highly reduced graphene oxide (rGO) is to induce non-covalent binding to a molecular fluorophore, namely the riboflavin (Rb). While the fluorescence of Rb is quenched, the Rb-decorated rGO exhibits strong blue fluorescence and significantly increased fluorescence lifetime. The data reported in Ref. [1] represent a promising start towards tailoring the optical properties of rGOs, for practical applications in optics and photonics.

A new green method for the synthesis of reduced graphene oxide-gold nanoparticle (rGO-AuNP) hybrids in aqueous solution that exploits the ability of ascorbic acid (AA) to operate as an effective dual agent for both GO and gold ion reduction is reported in Ref. [2]. Through careful investigation of the production of rGO-AuNP hybrids stabilized with polyvinyl-pyrrolidone (PVP), several versatile routes were derived with the aim of controlling the size, shape and distribution of AuNPs anchored onto the graphene sheets as well as the GO reduction. Particularly, when rGO is used as a platform for Au ion nucleation, a relative sparse distribution of AuNPs of size ranging from 20 nm to 50 nm is noticed. In contrast, when gold ions are added to the solution prior to any GO reduction, the density of large AuNPs is rather low relative to the uniformly packed small sized AuNPs (3–12 nm). The progress of GO reduction is explained by considering the contribution of the catalytic activity of AuNPs, besides the reducing activity of AA. Finally, a plausible mechanism for the nucleation and distribution of AuNPs onto the graphenic surface is assumed, highlighting the significance of oxygen moieties. The green

method developed here is promising for the fabrication of gold-graphene nanocomposites with tunable surface “decoration”, suitable for surface-enhanced Raman spectroscopy (SERS) [2].

GO was synthesized according to Hummers and Offeman’s method. Four samples were analyzed in the study concerning rGO-AuNP. Samples S1 and S2 are produced by first adding ascorbic acid (AA) to the GO capped by polyvinyl-pyrrolidone (PVP), heating (80 °C) to reduce the GO, then adding chloroauric acid (HAuCl<sub>4</sub>), with S1 heated during HAuCl<sub>4</sub> addition and S2 cooled down (0 °C) previously. Samples S3 and S4 were first treated by HAuCl<sub>4</sub> and only subsequently reduced by AA, again with S3 kept warm and S4 cooled prior to AA addition.

X-ray photoelectron spectroscopy (XPS) measurements are performed in the National Institute of Materials Physics (NIMP), by using monochromated Al K<sub>α1</sub> radiation and a Phoibos 150 mm radius electron energy analyzer operated with 20 eV pass energy. Other analyses, not performed in NIMP, included: X-ray diffraction, UV-Vis-IR absorption, Fourier Transform Infrared spectroscopy, Raman spectroscopy, atomic force microscopy, steady state fluorescence and fluorescence lifetime measurements, and zeta potential measurements.

C 1s XPS spectra are represented in Fig. 1. The component representing reduced C from graphene (C=C) occurs at 284.3 eV in all samples, with the exception of S2, where it occurred at 284.0 eV. The component indexed with C–OH occurs at energies varying between 285.3 and 285.7 eV, C–O–C occurs between 286.6 and 287.6 eV, while O–C–O occurs at 287.7–287.8 eV for S1–S4 and at 289.5 eV for GO. Sample S3 has also shown a low binding

energy C 1s peak, at 282.5 eV, which may be attributed to carbides.

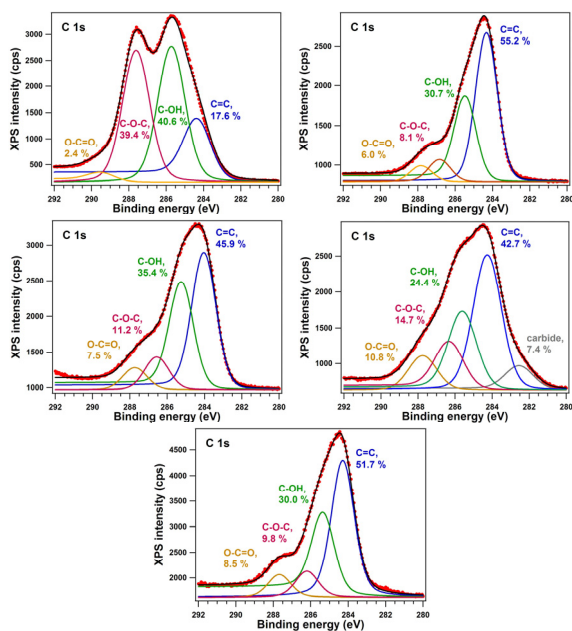


Fig. 1. C 1s XPS data for GO and for the samples S1–S4, together with deconvolutions into four components (see text for details).

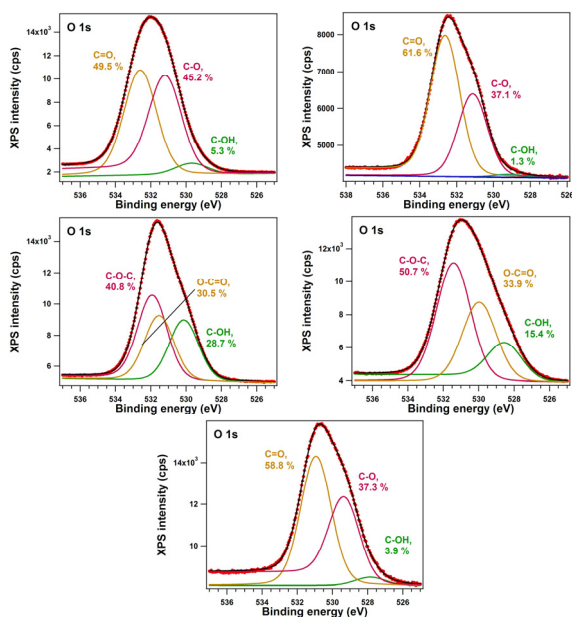


Fig. 2. O 1s XPS data for GO and for the samples S1–S4, together with deconvolutions into three components.

The reduction process in samples S1–S4 is straightforward from the aspect of the C 1s spectra: the relative percentage of the C=C component goes from 17.6% in GO to about 50% in the other samples. The ratio of the C=C component to the C 1s spectrum and the total O 1s signal (Fig. 2), weighted by the XPS atomic sensitivity factors yields 12.5% for GO, 80.7%

for S1, 31.2% for S2, 29.3% for S3, and 45.0% for S4 [2].

Fig. 3 represents Au 4f spectra and one remarks the occurrence of a quite low binding energy component, visible as a shoulder in the enlarged spectra (red curves). According to other recent data [3], this component is attributed to negative Au nanoparticles, whose ionization energies are far below the Fermi energy of the metal Au. The charge state modification of Au may be connected to the strong Surface Enhanced Raman Spectroscopy (SERS) enhancement obtained for samples S3 and S4 [2].

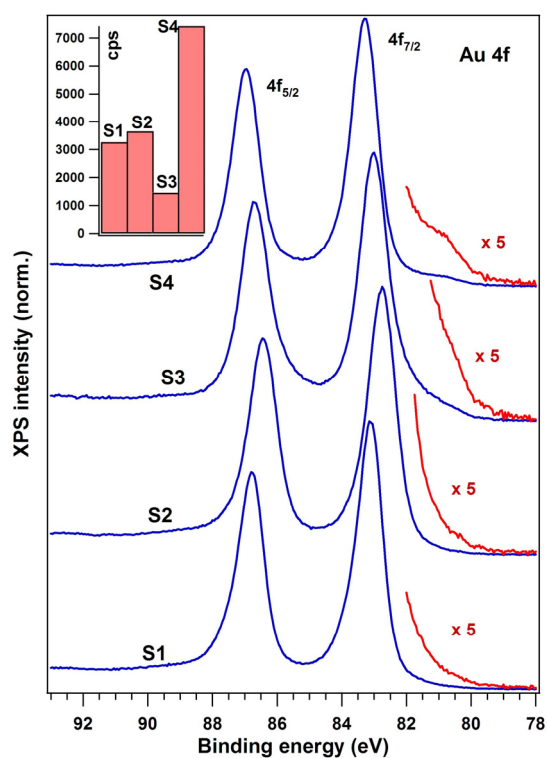


Fig. 3. Au 4f XPS data for rGO-AuNP samples.

## References

- [1] M. Iliuț, A.-M. Găbudean, C. Leordean, T. Șimon, C.M. Teodorescu, S. Aștilean, Chem. Phys. Lett. 526, 127-131 (2013).
- [2] M. Iliuț, C. Leordean, V. Căncă, C.M. Teodorescu, S. Aștilean, J. Mater. Chem. C 1, 4094-4104 (2013).
- [3] N.G. Apostol, L.E. Ștoflea, G.A. Lungu, C. Chirilă, L. Trupină, R.F. Negrea, C. Ghica, L. Pintilie, C.M. Teodorescu, Appl. Surf. Sci. 273, 415-425 (2013).

## Structural characterization and wetting properties of textile materials and model surfaces

*L. Frunza, I. Zgura, S. Frunza, C.P. Ganea, V.F. Cotorobai, M. Enculescu, E. Matei,  
N. Preda, C.C. Negrila and O. Rasoga*

ZnO is deposited on textile materials in order to develop super hydrophobic, UV-blocking, self-cleaning and antibacterial properties on the surface. Up to now, the most used textiles for such studies were cotton fabrics while the synthetic textiles were less deposited with ZnO. It then became important to have more information about the functionalization of the synthetic textiles with semiconductor particles, especially with ZnO. We covered then textile materials made from polyester (PES), polyamide (PA), poly(lactic acid) (PLA) and hemp (H) with ZnO layers [1] by electroless method which has been already proven [2] to have some clear advantages. These textiles show interaction with the modifying groups leading to new behavior.

Characterization methods considered both the original and the deposited fabrics as well. Thus, the structure and surface morphology were studied by X-ray diffraction, by optical and electron microscopy, while the deposition changes were measured by FT-IR spectroscopy:

- Direct visualization of the samples was applied to assess the mesh size (Fig. 1).

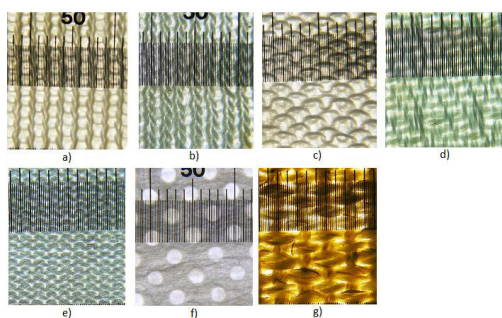


*Fig. 1. Images by optical microscopy of the samples: (a) PES1; (b) PES2; (c) PES3; (d) PES4; (e) PA; (f) PLA; (g) H. The color has no relevance.*

- Scanning Electron Microscope (SEM) micrographs (typical images are given in Fig. 2) were taken with a Zeiss Evo 50 XVP instrument.

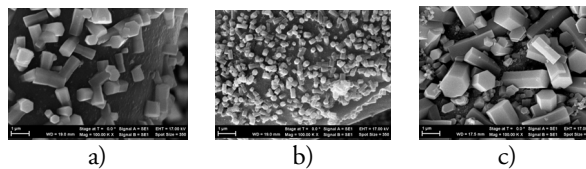


*Fig. 2. SEM images of ZnO deposited samples:  
a) PES1; b) PLA; c) H.*

- X-ray energy dispersive spectroscopy (EDAX) leads to the elemental analysis of the surface composition, confirming the presence of the deposited ZnO particles.

- X-ray diffraction (XRD) done with a D8 Advance (Bruker-AXS) equipment allowed phase identification, see one pattern in Fig. 3. The qualitative aspects were obtained by Rietveld refining.

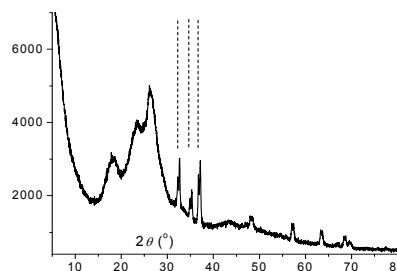


*Fig. 3. XRD patterns of ZnO/PES2 sample.  
Characteristic peak triplet of hexagonal ZnO is marked.*

- Fourier Transform Infrared Spectroscopy (FTIR) was applied in attenuated total reflection (ATR) mode with a Scanning Microscope Spotlight 400 (Perkin Elmer) coupled with a Spectrum 100 FTIR spectrometer. These investigations show that the groups responsible for IR vibrations unless the OH groups are not directly reacting with ZnO particles.

- Wetting properties were important features to evaluate the modification of the surface. Static (equilibrium) contact angles were measured at room temperature with Drop Shape Analyzer DSA 100 (Krüss). At least 5 different points were tested on each sample. An example of drop images appears in Fig. 4.

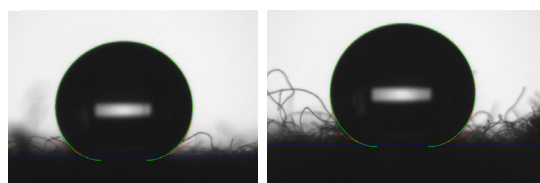


Fig. 4. Water droplets in contact with the surface of  
a) PES1; b) ZnO/PES1 samples.

The raw materials are all, hydrophobic, with  $CA > 90^\circ$ . CA increases by the surface treatment, with a few degrees in the case of PES samples, up to  $20^\circ$  for PLA and even more for H sample. Their behavior was approximated by the Cassie-Baxter equation in the form  $\cos \theta_c = f \cos \theta_0 - (1-f)$  where  $\theta_c$  is the contact angle formed on the treated fabric and  $\theta_0$  is the contact angle formed on untreated fabric. Though the  $f$  parameter is positive in our cases, the equation should be applied with caution.

The same textile materials from PES, PA, PLA and H were then covered with SiOx nanoparticles [3] applying a vacuum deposition at small angle previously developed for other materials [4]. The SiOx layer was expected to modify the wetting properties and to lead to flame retardant properties. The oxide layer was amorphous as shown by SEM (Fig. 5) and XRD investigations.

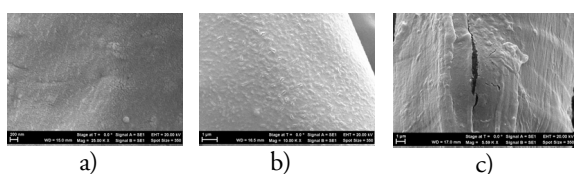


Fig. 5. SEM images of SiOx deposited upon:  
a) PES2; b) PLA; c) H samples.

Thermogravimetric (TG) studies show different onset temperature of the highest peak, higher for the deposited samples than for the raw ones, indicating the interaction between the deposited layer and the substrate. CA generally decreases by SiOx functionalization, with a few degrees up to several tens of degrees: The materials become more hydrophilic.

Contact angle measurements were in addition used to evaluate the surface free energy of a model surface (smooth and dehydroxylated fused quartz) using some particular organics as probe

liquids [5]. The contact angle values were further processed applying either the approach of Owens-Wendt with geometric mean

$$\gamma_L(1 + \cos \theta) = 2\sqrt{\gamma_s^d \gamma_L^d} + 2\sqrt{\gamma_s^p \gamma_L^p} - \Pi e_L$$

or the Wu's approach of harmonic mean

$$\gamma_L(1 + \cos \theta) = 4 \left( \frac{\gamma_s^d \gamma_L^d}{\gamma_s^d + \gamma_L^d} + \frac{\gamma_s^p \gamma_L^p}{\gamma_s^p + \gamma_L^p} \right) - \Pi e_L$$

of nonpolar ( $d$ ) and polar ( $p$ ) interactions.

The liquids were chosen thus to fulfill Della Volpe and Siboni's criterium: water (W), glycerol (Gly), nematic phase 5 (NP5), ethylene glycol (EG), dimethylsulfoxide (DMSO). The values obtained for the components of surface free energy of amorphous surface were discussed in comparison with the results obtained in literature for crystalline quartz or for other silica forms as bulk or films (Table 1).

Table 1. Dispersive  $\gamma_s^d$  and polar  $\gamma_s^p$  parts (in mN/m) of surface tension of fused quartz

Treat. temp. ( $^\circ\text{C}$ )	Owens-Wendt/ least squares		Owens-Wendt/ average		Wu/ least squares	
	$\gamma_s^d$	$\gamma_s^p$	$\gamma_s^d$	$\gamma_s^p$	$\gamma_s^d$	$\gamma_s^p$
240	12.0	61.2	12.4	60.3	23.7	46.7
1000	16.0	46.9	16.0	49.5	25.3	37.5

The study has shown a decrease of the polar component of the surface tension by increase of the pretreatment temperature. It can be used to interpret a part of the data obtained for silica containing layers onto other materials, more complicated.

## References

- [1] L. Frunza, N. Preda, E. Matei, S. Frunza, *et al.* J. Polymer Sci., B Polymer Phys. 2013, 51, 1427–1437.
- [2] N. Preda, M. Enculescu, I. Enculescu, *Soft Mater.* 2013, 11, 457–464.
- [3] L. Frunza, I. Zgura, M. Enculescu, S. Frunza, *et al.*, J. Optoelectron. Adv. Mater. 2014, 16, 176–181.
- [4] S. Frunza, R. Moldovan, T. Beica, D. Stoenescu, *et al.*, Liq. Cryst. 1993, 14, 293–296.
- [5] I. Zgura, R. Moldovan, C.C. Negriila, S. Frunza, *et al.*, J. Optoelectron. Adv. Mater. 2013, 15, 627–634.

## NO<sub>2</sub> sensing mechanism of ZnO-Eu<sub>2</sub>O<sub>3</sub> binary oxide under humid air conditions

A. Stănoiu, C.E. Simion

in cooperation with

S. Somăcescu

“Ilie Murgulescu” Institute of Physical Chemistry, Romania Academy, Bucharest-Romania

ZnO<sub>x</sub>Eu<sub>2</sub>O<sub>3</sub> (x=5 wt. %) sensitive materials were prepared by hydrothermal route using cetyltrimethylammonium bromide (CTAB). The binary oxide ZnO<sub>x</sub>Eu<sub>2</sub>O<sub>3</sub> exhibited an increase in sensor signals assisted by changes in the electron affinity when exposed to NO<sub>2</sub> in humid background.

Before exploring the insights of the NO<sub>2</sub> sensing mechanism by using simultaneous electrical resistance and work function measurements, sensor signal dependence as a function of operating temperature for a certain NO<sub>2</sub> concentration has been performed [1].

Thus, in Figure 1 it can be seen that the optimum NO<sub>2</sub> detection takes place at 200°C and therefore all the subsequent investigations were performed at this temperature.

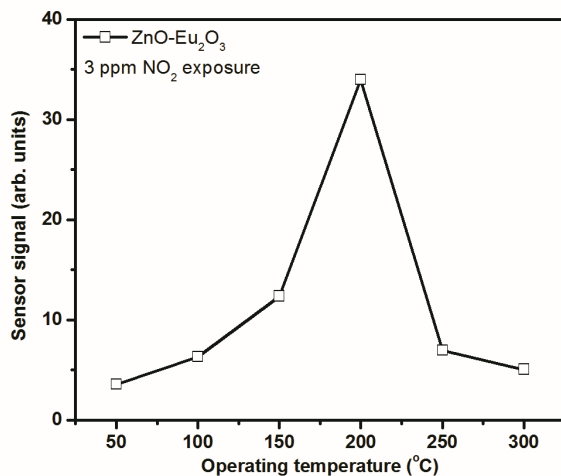


Fig.1 Sensor signal as a function of operating temperature when exposed to 3 ppm of NO<sub>2</sub>.

An interesting phenomenon which could be observed when ZnO-Eu<sub>2</sub>O<sub>3</sub> materials were exposed to different NO<sub>2</sub> concentrations under RH background is presented in Figure 2. One should note that the presence of relative humidity does not hinder the NO<sub>2</sub> detection, on contrary induces an increase in the sensor signal over the whole range of concentrations. Additionally, the sensor signal dependence on

NO<sub>2</sub> concentration indicates the power law behaviour [2].

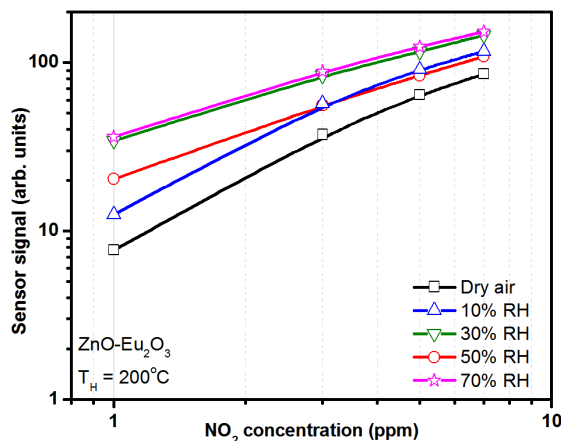
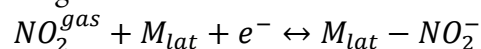
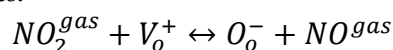


Fig.2 Log-log representation of the sensor signal dependence on NO<sub>2</sub> exposure (1,3,5,7 ppm) in dry and humid air conditions.

Simple evaluation of the electrical resistance only brings information about the changes in the charge carrier concentration induced by the gas-surface interactions. Simultaneous electrical resistance and work function changes provide insights about surface species which may not have influence over the conduction process. Thus, one can clearly discriminate between ionosorption (e.g. changing the electrical resistance of the material) and localized chemisorptions (e.g. terminal OH groups leading to dipolar species, no change in the electrical resistance). It is known that the work function can be described as a sum of the surface band bending ( $q\Delta V_s$ ) and electron affinity ( $\Delta\chi$ ) changes:  $\Delta\phi = q\Delta V_s + \Delta\chi$ . Under dry air conditions NO<sub>2</sub> might undergo direct ionosorption process, possibly on cations of Eu<sup>3+</sup> according with:



or a dissociative adsorption of NO<sub>2</sub> on ZnO-Eu<sub>2</sub>O<sub>3</sub> surface might take place on the oxygen vacancies:



In this respect, the appearance of negative charge over the surface induces an increase of surface band bending and work function without any change in electron affinity [3] (see Fig. 3).

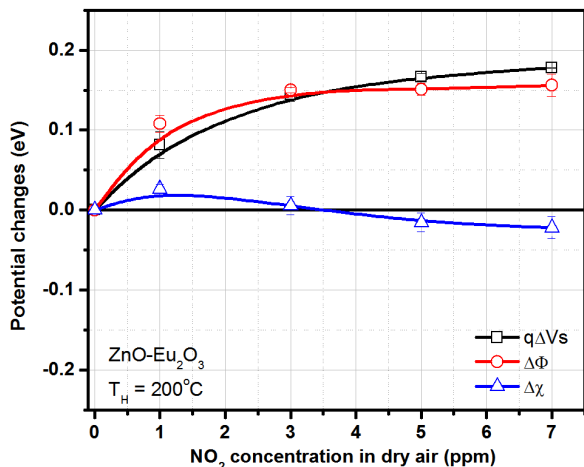
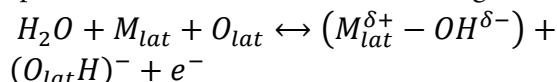


Fig.3 Potential changes with respect to the changes in NO<sub>2</sub> exposure in dry air background.

Water vapour interaction with different metal oxide surfaces can be summarized as follow: physisorbed molecular water or hydroxyl (OH) groups on the surface. If one assumes the homolytic dissociation of water then, hydroxyl groups are formed on the surface according with:



In the above equation, terminal hydroxyl groups (e.g.  $(M_{lat}^{\delta+} - OH^{\delta-})$ ) are responsible for the changes in electron affinity, since the rooted ones (e.g.  $(O_{lat}H)^-$ ) induce changes only in the free charge carrier concentration, being responsible for the overall variation of the electrical resistance of the material.

Figure 4 a shows that the increase of the NO<sub>2</sub> concentration leads to an increase in surface band bending ( $q\Delta V_s$ ) explained by the ionosorption of NO<sub>2</sub> on the surface of ZnO-Eu<sub>2</sub>O<sub>3</sub>.

In Figure 4 b one can see that a further increase in NO<sub>2</sub> concentration (>1ppm) is accompanied by a decrease in the electronic affinity independent on the RH level.

The decrease in the electron affinity is related to a decrease in the coverage with terminal hydroxyl groups and is accompanied by a net

charge transfer from the host material to the ionosorbed NO<sub>2</sub> species. Thus, more electrons are subtracted from the material, leading to an increase in NO<sub>2</sub> sensitivity under humid air conditions.

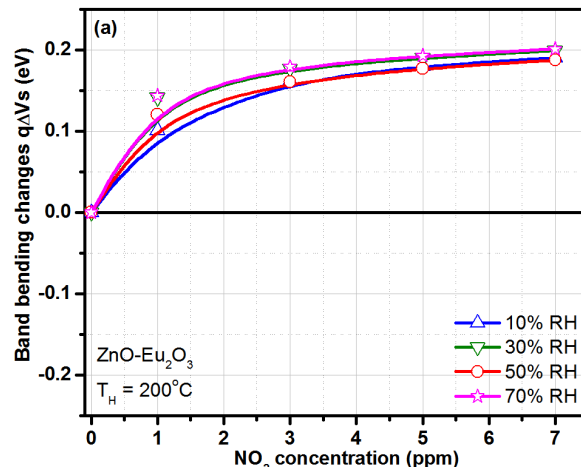


Fig. 4a Band bending changes with respect to different NO<sub>2</sub> concentrations in RH.

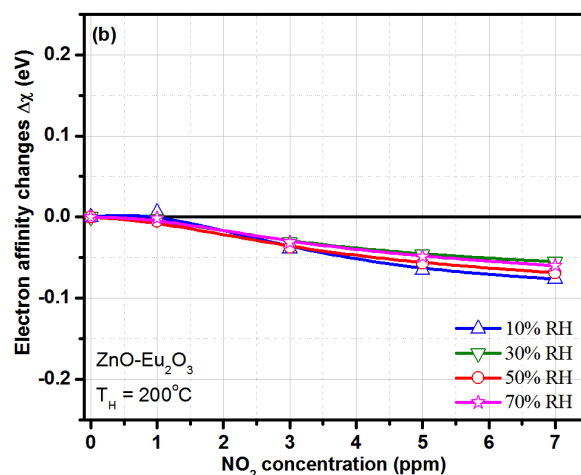


Fig. 4b Electron affinity changes with respect to different NO<sub>2</sub> concentrations in RH.

These results recommend ZnO-Eu<sub>2</sub>O<sub>3</sub> as promising material towards NO<sub>2</sub> detection under real operating conditions (e.g. in the presence of variable relative humidity).

### References

- [1] A. Stănoiu, C.E. Simion, S. Somăcescu, Sens. Actuators B. 2013;186;687-694.
- [2] N. Yamazoe, K. Shimano, Sens. Actuators B. 2008;128;566-573.
- [3] M. Ivanovskaya, P. Bogdanov, G. Faila, G. Sberveglieri, Sens. Actuators B. 2000; 68; 344-350.



# Patents and Patent Requests

## PATENTS

*W. Kappel, M. Codescu, E. Patroi, N. Stancu, E. Manta, M. Valeanu, V. Kuncser, F. Tolea, M. Sofronie*

Nanocomposite isotrope permanent magnet and his obtaining procedure  
Patent Number RO125435 ( 29 March 2013)

*L. Pintilie, I. Pintilie, A. Iuga, C. Dragoi*

Method of forming ferro-electric Schottky diode  
Patent Number: RO128455-A2 (30 May 2013)

*E. Andronescu, R. Ghita, C. D. Ghitulica, S. L. Iconaru, D. Predoi, R. Trusca, F. Ungureanu*

Superparamagnetic iron oxide synthesis in polysaccharides  
Patent Number: RO128484-A2 (28 June 2013)

## PATENT REQUESTS

*C. Cotîrlan-Simioniuc, M. F. Lazarescu*

Detection system with nanostructured surfaces for biosensors and imagistics having a resolution better than diffraction limit  
A00244 /25.03.2013.

*S. Frunza, T. Beica, I. Zgura, L. Frunza, A. Nuta, A. Sorescu, C. Zaharia, I. Bunea*

Device and method for detection of the interactions antigen viral-specific antibody by the estimation of contact angle  
A 2010 01004/RO 126242 B1/2013

# Events

## Workshop “New trends in the research of carbon based nanomaterials”

*April 22-23, 2013*

National Institute of Materials Physics (NIMP, Romania) has been host of the workshop with the title “New trends in the research of carbon based nanomaterials”, from the 22<sup>nd</sup> until the 23<sup>rd</sup> of April 2013.

This workshop was designed to present some new latest results obtained in the field of carbon based materials. The invited lectures will be focalized on graphene, graphene oxide, carbon nanotubes, diamond and carbon nanowalls as well as on their use in different composite materials.

The main topics under discussion were:

- i) preparation and functionalization of graphene as well as their use in the different applications;
- ii) synthesis and optical properties of carbon nanowalls and their applications;
- iii) the preparation of diamond nanowires for applications in the biosensors field;
- iv) the use of composites based on carbon nanotubes and different organic host matrices for applications in the field of biosensors and the energy storage.

The organizers acknowledge the financial support of "Culture and Physics at Magurele" Foundation.

Chairs:

Dr. Mihaela Baibarac, National Institute of Materials Physics, Romania

Prof. Sabine Szunerits, Univ Lille I, France

### April 22, 2013

9:00-9:15 Opening workshop,

General Director of National Institute of Materials Physics, Romania

#### **Session: Carbon nanoparticles**

9:15-10:00 Preparation, functionalization and applications of graphene,

Professor Rabah Boukherroub, Univ Lille I, France

10:00–10:45 Ionic transport and field-effect conductance in voltage-controlled carbon nanotubes,

Professor Titus Beu, University Babes-Bolyai, Romania

11:00-11:45 Diamond nanowires: the new jewel for biosensing,

Professor Sabine Szunerits, Univ Lille I, France

11:45-12:30 Carbon nanowalls: plasma synthesis, properties and applications,

Professor Gheorghe Dinescu, National Institute for Laser, Plasma and Radiation Physics, Romania

#### **Session: Graphene - chemical and physical properties and applications**

14:00-14:45 Graphene materials for dye sensitized solar cells,

Professor Ladislav Kavan, J. Heyrovsky Institute of Physical Chemistry, Czech Republic

- 14:45-15:30 Topological properties of graphene and other 2D lattices,  
Professor Alexandru Aldea, National Institute of Materials Physics, Romania
- 15:45-16:30 Chemistry and processing of graphene towards the fabrication of multifunctional materials,  
Professor Dimitrios Tasis, University of Pastras, Greece
- 16:30-17:15 Carbon-based nanoelectronics,  
Professor Daniela Dragoman, Faculty of Physics, Bucharest University, Romania

#### April 23, 2013

##### Session: **Applications of composite materials based on carbon nanoparticles and organic host matrix**

- 9:00-9:45 Organic and hybrid organic-inorganic electronics 12 years after the Nobel Prize – a chemist approach,  
Professor Adam Pron, Faculty of Chemistry, Warsaw University of Technology, Poland
- 9:45-10:30 Polymer nanocomposites, from fundamentals to applications,  
Professor Luca Valentini, University of Perugia, Italy
- 10:45-11:30 Carbon nanomaterials: from nanoscale object towards macroscopic materials,  
Professor Wolfgang Maser, Institut Carbochimica, Zaragoza, Spain
- 11:30-12:45 Biosensors based on carbon nanotubes – interface design and application,  
Professor Camelia Bala, Faculty of Chemistry, Bucharest University
- 14:00-14:45 Carbon nanotube nanostructures: Resonance and anti-Stokes Raman effects,  
Professor Serge Lefrant, Institut des Materiaux „Jean Rouxel”, Nantes, France
- 14:45-15:30 Composite materials based on carbon nanotubes and conjugated polymers for applications in the energy storage  
Dr. Mihaela Baibarac, National Institute of Materials Physics, Romania

#### Workshop "**Biomimetic sensing using nano-objects (BioSuN)**", *June 17 – 19, 2013*

##### Monday 17<sup>th</sup> of June

- 9.00 - 9.20 Opening remarks – General Director of National Institute of Materials Physics
- 9.20 - 10.00 Maria Eugenia Toimil Molares
- 10.00 - 10.40 Horia Iovu **Advanced Polymer Nanocomposites**
- 11.10 - 11.50 Hubert Bruckl - **Nano-engineered materials for sensor applications**
- 11.50 - 12.30 Stefan Schuz **Sensors on the basis of insect olfaction - Prospects of different approaches**
- 14.30 - 15.10 J.E. ten Elshof **Core-shell and segmented metal oxide-metal composite nanowires for photocatalytic generation of hydrogen**
- 15.10 - 15.50 Adrian Dinescu **Nanoscale structuring using electron beam lithography**
- 15.50 - 16.30 Peter Gnauk - **Helium Ion Microscopy. Extending the frontiers of nanotechnology**
- 16.30 - 17.10 Cristian Zet **Sensors using magnetic nanowires as sensing elements**
- 17.30 - 18.45 Visit of the Institute

**Tuesday 18<sup>th</sup> of June**

- 9.00 - 10.00 Wolfgang Knoll **Biosensing with nano-objects: optical or by electronics?**  
10.00 - 10.40 Paolo Pelossi **Olfactory code and odorant-binding proteins for an artificial nose**  
11.10 - 11.50 Mircea Dragoman **Graphene Nanoelectronics**  
11.50 - 12.30 Patrick Guerin  
14.30 - 15.10 Christoph Nowak  
15.10 - 15.50 Ionut Enculescu **Nanowire based electronic devices**  
15.50 - 16.30 Maria Adriana Acasandrei and Iulia Diana Savu - **Toxicity studies of nanostructured materials**  
16.30 - 17.00 Daniel Herea **Magnetic particles in medicine. Some practical applications**  
17.00 - 17.30 Sorin Zgura

**Monitoring session EFDA (materials section)**

A monitoring session EFDA (materials section) has been organized by INCDFM between 26.06–03.07.2013. At the event have participated 79 researchers from abroad, including the EUROATOM/EFDA officer for materials (Dr. Sehila Gonzales) as well as the three scientific reporters of the section (Dr. Sergei Dudarev, Dr. Michael Rieth, Dr. Jean Luis Boutard).

# International Cooperation

## INTERNATIONAL COOPERATION PROJECTS

### *2 FP7 projects*

*Pintilie L.*

**FP7 project Large-scale integrating project Interfacing Oxides (IFOX)**

**NMP-2009-2.2-1**

Coordinator: Theo Rasing (Radboud University, Nijmegen)

Scientific coordinator: Georg Schmidt (Martin-Luther-Universität, Halle-Wittenberg)

Partners: Radboud University Nijmegen (NL), Martin-Luther-Universität Halle Wittenberg (DE), Max Planck Gesellschaft zur Foerderung der Wissenschaften E.V. (MPI-HALLE) (DE), University of Glasgow (UK), Centro Ricerche Fiat SCPA (IT), Universiteit Antwerpen (BE), Paul Scherrer Institut (CH), National Institute of Materials Physics (NIMP) (RO), IBM Research GMBH (CH), Universitat Konstanz (DE), Institute for Nanostructured Materials Bologna (IT), Intel Performance Learning Solutions Limited (IE), Forschungszentrum Jülich GmbH (DE), Twente Solid State Technology (NL), Georg August Universitaet Goettingen (DE), Holy Trinity College Dublin (IE), Organic Spintronics srl (IT), Universiteit Twente (NL)

<http://www.ifofox-project.eu/>

2010-2014

*Mercioniu I.*

**Development of a sintering centre and know-how exchange for non-equilibrium sintering methods of advanced ceramic composite materials (SINTERCER)**

**FP7 EU-Research Potential – Capacities – REGPOT-CT-2013-316232-SINTERCER**

Coordinator: The Institute of Advanced Manufacturing Technology, Krakow, Poland

Partners: Politecnico di Torino (POLITO), Torino, Italy, Institute of Ceramics and Glass (ICV-CSIC), Madrid, Spain, University of Rostock (UR), Rostock, Germany, National Institute of Materials Physics (NIMP), Bucharest – Magurele, Romania, Aalto University School of Chemical Technology, Espoo, Finland, RHP-Technology GmbH & Co. KG (RHP), Seibersdorf, Austria, Universidade de Aveiro(UA), Aveiro, Portugal, University of Science and Technology (AGH), Cracow, Poland, Institute of Metallurgy and Materials Science of Polish Academy of Sciences (IMIM), Cracow, Poland

<http://www.ios.krakow.pl/sintercer/>

### *2 projects Romanian Swiss Research Program RSRP*

*Baibarac M.*

**Electrochemical functionalization of carbon nanotubes with heteropolyanions and conjugated polymers and the elucidation of interactions at the carbon nanotubes/ heteropolyacid/ conjugated polymer interface**

Partners: Ecole Polytechnique Fédérale de Lausanne, Switzerland and Institute for Problems of Materials Science of National Academy of Science of Ukraine

*Crisan O.*

**Novel FePt-based hard magnetic materials for sustainable energy applications**

**Project 6 / 2012-2015**

Partener: Swiss Federal Laboratories for Materials Science and Technology, EMPA Thun Switzerland

---

### *3 CEA projects*

*Pintilie L.*

**IFA-CEA**

**RF Components Laboratory, CEA-LET Grenoble, France**

Investigation of metal-ferroelectric interface at macro- and nanoscale

Contract no. C1 09/2010

Duration 2010-2013

*Predoi D.*

**Institut de Chimie Séparative de Marcoule - UMR 5257**

Development and characterization of solid apatite matrices capable of storing inorganic pollutants: structure and adsorption processes.

IFA-CEA Project No. C2-06/2011

Duration: 2012-2015

*Teodorescu C.M.*

**Service de Physique et Chimie des Surfaces et Interfaces, Institut Rayonnement Matière Saclay, Commissariat à l'Energie Atomique, France**

Ferroelectric and diluted magnetic semiconductor based multiferroic heterostructures for energy applications

IFA-CEA Project No. C1-08/2010

Duration: 2010-2013

### *Other European projects*

*Baibarac M.*

**SCOPES Project No. IZ74Z0\_137458/2012**

Implementation in East Europe of new methods of synthesis and functionalization of carbon nanotubes for applications in the energy storage and sensors field

2011- 2014

*Enculescu I.*

**EUROCORE (ESF) Project**

Insect Odorant-Binding Proteins on Conductive Polymer Nanofibers Based Biosensor to Diagnose Crop Disease

2011-2014

*Teodorescu C. M.*

**ANR-ANCS (RO-FR) PN-II-ID-JRP-2011- 2 Project**

**Service de Physique et Chimie des Surfaces et Interfaces, Institut Rayonnement Matière Saclay, Commissariat à l'Energie Atomique, France**

Chemical switching of surface ferroelectric topology

2013-2015

*2 Erasmus projects*

*Predoi D.*

**Institut des Sciences de la Terre d'Orléans, UMR 6113 CNRS – Université d'Orléans**

Biogeochemistry of iron in surface environments

ERASMUS

2009-2013

*Predoi D.*

**Universite Bordeaux 1**

Surface properties of iron oxide nano-particles for biomedical applications

ERASMUS

2009-2013

*1 Brancusi project*

*Crisan O.*

**Programme Hubert Curien PHC « Brancusi ANCS-CNRS**

**Universite du Maine, Le Mans, Franta**

Hard magnetic nanocrystalline materials obtained from amorphous precursors

*Partnership IUCN Dubna*

*Kuncser V.*

Complex characterization of multilayered magnetic films by neutron scattering and complementary techniques

Protocol Romania - IUCN:: 4134-4-2012/2014

2012-2014

*Partnership Japan Society for the Promotion of Science*

*Plugaru N.*

Modeling the Properties of Porous Silicon -Based Systems from First Principles Electronic Structure.

2012-2014

*1 COST action*

*Pintilie L.*

**COST action SIMUFER (COST MP0904)**

**Single- and multiphase ferroics and multiferroics with restricted geometries**

Action Coordinator: Prof. Liliana Mitoseriu

[http://www.cost.eu/domains\\_actions/mpns/Actions/MP0904](http://www.cost.eu/domains_actions/mpns/Actions/MP0904)

2010-2014

---

*7 EURATOM projects**Badica P.*

Laboratory preparation and characterization of nanostructured ODSFS samples produced by plasma arc sintering  
BS-M8

*Galatanu A*

Production by powder metallurgy procedures of W-FGM-steel components  
BS-M3

*Galatanu A*

Welding and brazing W-W and W-steel by SPS  
BS-M3A

*Galatanu A.*

Complex composite materials W-SiC  
BS-M3B

*Kuncser V.*

Complex characterization of films based on Be, W, C for fuel retention  
BS-M5

*Mihalache V.*

Optimizing of chemical composition and preparation process of ODSFS based on precipitation hardened FeCr  
BS-M7

*Sarbu C.*

HRTEM, X-EDS and EELS characterization of some W alloys with self-passivating properties and of W-based composite materials  
BS-M2  
EFDA WP13-MAT-HHFM-01/02/PS

*Projects for ELETTRA (Trieste) Synchrotron**Teodorescu C. M.*

Elettra proposal No. 20135077:  
Imaging ferroelectric domains in BaTiO<sub>3</sub> and Pb(Zr,Ti)O<sub>3</sub> single crystal layers with binding energy contrast. Depth profiling of depolarization charge. Experimental band structure of areas with well defined ferroelectric polarization.

*Pintilie L.*

Elettra proposal No. 20130333:  
High-speed field effect devices based on graphene on epitaxial ferroelectric oxides: in-situ investigation of ferroelectric-graphene interface formation and properties by XPS and XAS combined with STM.  
Duration: 2013-2015

## AGREEMENTS

*Badica P/Sandu V*

STM/STS studies concerning local electromagnetic structure of some nanostructured superconducting and magnetic materials (STMNANO) Copbil 629/2013

*China*

*Baibarac M*

Etudes des propriétés optiques et électriques de nano-matériaux composites à base de nanotubes de carbone et polymère conjugué

*France*

*Stănculescu A.*

Accord de coopération scientifique dans le domaine des films minces notamment sur les thématiques suivantes: structures multicouches organiques à basse dimension et composantes organiques et hybrides

*France*

*Secu M*

Optical and structural properties of rare-earth doped glasses and oxyfluoride glass ceramics prepared by sol-gel technique with applications in optoelectronics and photonics

*Germany*

*Secu M*

Preparation and investigation of optical and structural properties of vitreous oxide materials with applications in optoelectronics and photonics

*Letonia*

## BILATERAL COOPERATION PROJECTS

*Cernea M.*

**Institute for Science and Technology of Ceramics (ISTEC), Faenza, Italy**

Lead free piezoelectric materials processed by wet chemical routes (MPPC)

2010-2013

*Ciurea M. L.*

**Cankaya University, Ankara, Turkey**

Modelling and simulation: transport phenomena in nanostructures (0D, 1D and 2D)

2008-2013

*Ciurea M. L.*

**Belarusian State University, Minsk, Byelarus**

Hall investigations on irradiated Si and SiGe bulk materials

2010-2013

*Crisan A.*

**Nanoelectronics Research Institute of AIST Tsukuba, Japan**

Comprehensive Agreement on Joint Scientific Cooperation in the field of Science and Technology of Advanced Materials

2007-2013

*Crisan O.*

**Programme Hubert Curien PHC “Brancusi”: ANCS – CNRS**

**Universite du Maine, Le Mans, Franta**

Hard magnetic nanocrystalline materials obtained from amorphous precursors

2013-2014

*Ghica C.*

**Institut de Physique et Chimie des Matériaux de Strasbourg, France**

Effet de la réduction de taille, de la forme et des caractéristiques des interfaces sur la structure et les propriétés des matériaux nanostructurés

Convention Bilatérale de Coopération et d’Echange, 2012-2016

*Kuncser V.*

**University of Duisburg, Germany**

Interphase mechanisms in thin layer compounds and composites

2007-2013

*Maraloiu V. A. and Teodorescu V. S.*

**Institut Lumière Matière – Université Claude Bernard, Lyon, France**

Biocalisation et biotransformation de nanoparticules à coeur d’oxydes magnétiques.

Fonctionnalisation de substrats par irradiation laser à faible fluence

Convention Bilatérale de Coopération et d’Echange, 2013

*Moldoveanu V.*

**Science Institute Dunhaga 3, 107 Reykjavik, Iceland**

Time-dependent transport in interacting open systems: theory & modeling

Permanent

*Moldoveanu V.*

**Physics Department, Bilkent University, Ankara, Turkey**

Correlated transport in parallel quantum dots

Permanent

*Pasuk I.*

**University of Cyprus, Nicosia, Cyprus**

Cuprates thin films

Permanent

*Predoi D.*

**Le Havre University France**

Ultrasonic characterization of bio-ceramics powders and ferro-fluids

2007-2013

*Predoi D.*

**University of Bordeaux I, France**

Magnesium based nanocomposites for hydrogen storage and Fe oxide colloids

2005-2013

*Stan G.E.*

**University of Aveiro, Department of Materials and Ceramic Engineering, CICERO, Aveiro, Portugal**

Development of a new generation of highly biocompatible dental titanium implants functionalized by sputtering techniques with novel bioactive glass materials

2012-2014

*Collaboration with foreign institutions*

*Pintilie L., Pintilie I.*

**University of Oulu, Finland**

Ferroelectric measurements

*Pintilie L.*

**Universitatea Tehnica Darmstadt, Germania**

Specimen exchange common publications

*Pintilie I.*

**Universitatea din Oslo**

Specimen exchange, working stages

# Funding



**NIMP Funding**

Core Programme	4.481.854 Euro
Ideas	1.277.633 Euro
Human Ressources	478.157 Euro
Partnerships	613.663 Euro
Capacities	122.380 Euro
International Projects	377.962 Euro
Economic Contracts	146.959 Euro
<b>TOTAL</b>	<b>7.498.608 Euro</b>

